Dynamics of petroleum generation, migration, accumulation and leakage: a 3D basin modelling study of the glacially influenced Southwestern Barents Sea

vorgelegt von
Diplom–Geochemiker
Enmanuel Alexis Rodrigues Duran
aus Caracas–Venezuela

von der Fakultät VI – Planen Bauen Umwelt
der Technischen Universität Berlin
zur Erlangung des akademischen Grades

Doktor der Naturwissenschaften
Dr. rer. nat

genehmigte Dissertation

Promotionsausschuss:
Vorsitzender: Prof. Dr. Gerhard Franz
Gutachter: Prof. Dr. Brian Horsfield
Gutachter: Prof. Dr. Ralf Littke

Tag der wissenschaftlichen Aussprache: 08. Dezember 2014

Berlin, 2015

Fakultät VI - Planen, Bauen, Umwelt
der Technischen Universität Berlin
Author: Enmanuel Alexis Rodrigues Duran
Die Arbeiten im Rahmen dieser Dissertation wurden am **Helmholtz Zentrum Potsdam, Deutsches GeoForschungsZentrum (GFZ)** in der Sektion 4.3 Organische Geochemie (Prof. Dr. Brian Horsfield) durchgeführt.

Diese Dissertation wurde mit Microsoft Word 2010 erstellt. Sie ist ebenfalls als elektronische Version (PDF) über das digitale Repositorium (System OPUS) der Technischen Universität Berlin erhältlich.
Webadresse: **http://opus.kobv.de/tuberlin**

Berlin, 2015

To my lovely mother

Mercedes Duran

To my father

Manuel Rodrigues

To my niece and my sister

Sophia and Sonia

To my brothers

Alejandro and Johan

Table of contents

Statement of original authorship 17

Preface 19

Publications 21

Acknowledgements 23

Abstract 24

Zusammenfassung 26

1 Introduction 28

1.1 Scientific interest and objectives 28

1.2 Theoretical background 31

1.2.1 Methane on the move (MOM) 31

1.2.2 Petroleum origin and occurrence 33

1.2.3 Petroleum system 37

1.2.4 Petroleum system elements and processes 38

1.2.5 Petroleum systems modelling 41

1.2.6 Glaciers and glaciations 43

1.3 Study areas 48

1.3.1 Exploration history 48

1.3.2 General description of the study areas 49

1.3.3 Geological evolution 52

1.3.4 Uplift and erosion 57

1.3.5 Glacial history 60

1.3.6 Petroleum plays in the Barents Sea 62

2 Data and methods 69
2.1 Petroleum system model building workflow and input 69
2.1.1 Lithology and petroleum system elements definition 73
2.1.2 Kinetic models 74
2.1.3 Definition of the boundary conditions 75
2.2 Geochemical data 85
3 Synthesis of the main results 86
3.1 Hammerfest Basin (papers 1 and 2) 86
3.1.1 Model calibration and sensitivity analysis (paper 1) 86
3.1.2 Petroleum generation, migration, accumulation and leakage 95
3.1.3 Main discussion from basin modelling (focus in gas leakage) 108
3.1.4 Geochemical – basin modelling correlation (paper 2) 110
3.1.5 Main discussion geochemistry and basin modelling correlation 123
3.2 Loppa High model (paper 3 – ready for submission) 127
3.2.1 Model calibration 127
3.2.2 Petroleum generation, migration and accumulation 133
3.2.3 Main discussion from basin modelling in the Loppa High 145
4 Conclusions 148
5 Summary and future work 151
6 References 161
Appendices 183

List of Figures

Figure 1.1 General evolution scheme of organic matter maturation (Modified from Tissot and Welte, 1984). 34

Figure 1.2 Sketch for a typical conventional petroleum system (McCarthy et al., 2011)……. 37

Figure 1.3 Sketch of the migration and trapping processes in a petroleum system…….....40

Figure 1.4 Different glacier images. The Arctic Glacier (left; image from Red Orbit - Your universe online, 2011) and the Wolverine Glacier (right; image from USGS, 2014)…….. 43

Figure 1.5 The Southwestern Barents Sea. The colored squares represent the areas for which the models were built. Red square corresponds to model 1 presented in papers 1 and 2; and blue square corresponds to model 2 presented in paper 3 (AFC: Asterias Fault Complex; BFC: Bjørnøyrenna Fault Complex; MFC: Måsøy Fault Complex; ND: Nordvarg Dome; NFC: Nyslepp Fault Complex; RLFC: Ringvassøy–Loppa Fault Complex; SD: Samson Dome; SvD: Svalis Dome; SLHFC: Southern Loppa High Fault Complex; TFFC: Troms–Finnmark Fault Complex). 50

Figure 1.6 General lithostratigraphy of the Barents Sea (adapted from Nøttvedt et al., 1993; Ohm et al., 2008). The potential source rocks (SR) and reservoirs (R) that have been proposed and found in the area, as well as the general overview of the geological and tectonic events are also shown. 56

Figure 1.7 Geographical distribution of the petroleum plays in the Southwestern Barents Sea (adapted from Norwegian Petroleum Directorate, 2011).....68

Figure 2.1 Identification of the structural maps (left) provided by Lundin Norway AS and their 3D view for the study area of model 1 (right).....70

Figure 2.2 Quality control of the temperature data and vitrinite reflectance measurements for several groups of wells in the two modelled areas; based in the linear regressions…. 72

Figure 2.3 Activation energy (left) and generation curves (right) of the PhaseKinetics models used for the Upper Jurassic Hekkingen Formation (top) and the Triassic Snadd and Kobbe formations (bottom). Note that secondary cracking is also considered after approximately 150 °C (generation curves). 75

Figure 2.4 Heat flow history trends (left) and maps (right) used for model 1 (bottom) and model 2 (top). The dots shown in the trends correspond to the time for which a heat flow map was created with that specific value. 77

Figure 2.5 Definition of the sediment–water interface temperature (SWIT) trend, based on the time–latitude correlation of surface temperatures of Wygrala (1989) for the period before glaciation (left). Upper–boundary thermal and/or SWIT for the glacial–interglacial periods (right). 79

Figure 2.6 Erosion map (top) created for the two erosion events considered in model 1. The same erosion trend was used for both events, but with different magnitudes (2:3 relationship; explanation in text). The magnitudes for the three erosion scenarios (maximum, medium and minimum) considered in the sensitivity analysis are also shown (bottom). The iso–erosion lines in the maps were used for the creation of the map by interpolation. 81

Figure 2.7 Erosion maps created for the three erosion phases considered in model 2. The magnitudes for the three erosion scenarios (maximum, medium and minimum) considered in the sensitivity analysis are also shown. The iso–erosion lines are shown which were used for the creation of the map by interpolation. 82

Figure 2.8 Definition of the ice–sheet evolution. *Top:* Glaciation history through five ice megacycles including isostatic response. The MC1 also includes the Weichselian period. *Bottom:* Ice thickness specification. Three ice–sheet thicknesses were considered in order to evaluate the sensitivity of the model output. For the Weichselian period (between 0.12 and 0.01 Ma) no thickness variation was considered since this

period has been well constrained and several models give an estimate of the thickness…….....84

Figure 3.1 Temperature calibration results for wells around three of the main fields in the Hammerfest Basin; Snøhvit (left), Askeladd (middle) and Albatross (right). The comparison of the three erosion scenarios is displayed vertically while the comparison of the three heat flow scenarios is inside each plot: continuous line represents minimum heat flow; dotted line represents medium heat flow and segmented line represents maximum heat flow. The gray lines correspond to the best calibration zone.....88

Figure 3.2 Temperature calibration results for wells around three of the main fields in the Hammerfest Basin; Snøhvit (left), Askeladd (middle) and Albatross (right). The comparison of the three heat flow scenarios is displayed vertically while the comparison of the three erosion scenarios is inside each plot: continuous line represents maximum erosion; dotted line represents medium erosion and segmented line represents minimum erosion. The gray lines correspond to the best calibration zone. 89

Figure 3.3 Vitrinite reflectance calibration results for wells around three of the main fields in the Hammerfest Basin; Snøhvit (left), Askeladd (middle) and Albatross (right). The comparison of the three erosion scenarios is displayed vertically while the comparison of the three heat flow scenarios is inside each plot: continuous line represents minimum heat flow; dotted line represents medium heat flow and segmented line represents maximum heat flow. The gray lines correspond to the best calibration zone…….....90

Figure 3.4 Vitrinite reflectance calibration results for wells around three of the main fields in the Hammerfest Basin; Snøhvit (left), Askeladd (middle) and Albatross (right). The comparison of the three heat flow scenarios is displayed vertically while the comparison of the three erosion scenarios is inside each plot: continuous line represents maximum erosion; dotted line represents medium erosion and segmented line represents minimum erosion. The gray lines correspond to the best calibration zone.....91

Figure 3.5 Modeled present–day transformation ratio at the top of each source rock: the Upper Jurassic Hekkingen Formation and the Triassic Snadd and Kobbe formations.

The circle corresponds to the pseudo–well taken in order to have an extraction with the information presented in Figure 3.6. 96

Figure 3.6 Burial history of the three main source rocks (top): Hekkingen, Snadd and Kobbe formations. The vitrinite reflectance is shown as an overly. Maturity evolution of each source rock based on the transformation ratios (Bottom). Both plots were taken from a pseudo–well northwest of the modeled area. Please look at Figure 3.5 for reference of the well location. 97

Figure 3.7 Total cumulative mass (in Gigatonnes) of oil and gas generated by the three source rocks considered in this model together (top left), and separately (top right and bottom)…. 98

Figure 3.8 Accumulation history for oil and gas in the main reservoir, the Stø Formation (left). Porosity and permeability history for both seal rocks, corresponding to Fuglen and Hekkingen formations. 100

Figure 3.9 *Top left:* Predicted hydrocarbon accumulations (Snøhvit, Albatross, Askeladd and Goliat fields and Tornerose Discovery) in the Stø Formation at present–day (top left). Minor untested accumulations predicted with this model in the area are also shown (blue circles and ellipses). The inlets in the figure list the gas–oil ratios reported in the Norwegian Petroleum Directorate (2012) and calculated in the model for each field and discovery. *Top right:* Map view of the Hammerfest Basin and the fields on it as reported by the Norwegian Petroleum Directorate. *Bottom:* Comparison of the original recoverable oil and gas volumes reported in the Norwegian Petroleum Directorate (2012) with the volumes calculated in the model. The volumes of oil and gas predicted for the time before glaciations (1.10 Ma) are also shown (bottom right)……. 102

Figure 3.10 Migration pathways and drainage areas for the Askeladd, Albatross, Snøhvit, Goliat fields and the Tornerose discovery. The background shows the depth map of the Stø Formation. The maturity map at present–day of the Kobbe Formation with the five drainage areas is shown for reference (bottom right). 103

Figure 3.11 Correlation of modeled glacial history, predicted reservoir pressure conditions and gas masses trapped and leaked. a) Glacial history together with the depth variation of the Stø Formation reservoir. b) Oscillating reservoir (Stø Formation) pressure conditions (pore, hydrostatic and excess hydraulic pressures). c) Calculated gas mass in the Stø Formation during the last 1.2 Ma. Note that the main events of gas decrease occur in the transition from maximum glaciation to the interglacial period. d) Gas loss expressed as outflow at model top. 106

Figure 3.12 3D view at 0.95 Ma (end of the 1st glaciation) showing the Stø Formation, the shallowest layer at that time (brown layer) and the displacement vectors of hydrocarbons (red arrows); which indicate the migration of hydrocarbons from the deep reservoir unit to the shallowest layer. 107

Figure 3.13 a) Correlation of gas–dryness ($C_1/(C_2 + C_3)$) with the methane isotopic composition. b) Correlation of wetness percentage with the methane isotopic composition. Description of gas–dryness and wetness percentage can be found in the text (section 3.1.4). The data for the Goliat field and the Tornerose discovery is shown in two separate areas corresponding to the stratigraphic levels where the fluids were encountered, which are: the Tubåen, Snadd and Kobbe formations for the Goliat field, and the Stø and Snadd formations for the Tornerose discovery. The interpretation overlays stem from pIGI software and this correspond to an IGI's syntheses of the references given in the software. 111

Figure 3.14 Maturity interpretation using gas isotopic composition. The interpretation overlays of this figure stem as well from pIGI software. 113

Figure 3.15 Light hydrocarbons (C_7) oil–correlation and oil–transformation star diagrams (Halpern, 1995). The results for the Goliat field (yellow and pink lines) were taken from the work of Ohm et al. (2008). 114

Figure 3.16 Light hydrocarbons star diagrams using the Thompson (1983) parameters. The different parameters correspond to: A=Benzene/*n*–hexane; B=Toluene/*n*–heptane; X=(*m*–xylene + *p*–xylene)/*n*–octane; C=(*n*–hexane + *n*–heptane)/(cyclohexane + methyl-cyclohexane); I=(2– + 3–methyl-hexane)/(1*cis*3 + 1*trans*3 + 1*trans*2–dimethyl-

cyclopentanes); S=*n*–hexane/2,2–dimethyl-butane; F=*n*–heptane/methyl-cyclohexane; R=*n*–heptane/2–methyl-hexane; U=cyclohexane/methyl-cyclohexane..... 115

Figure 3.17 Correlation of the heptane and *iso*–heptane ratios according to Thompson (1983)…… 116

Figure 3.18 Paleo–environment interpretation using the correlation of pristane/*n*–C_{17} versus phytane/*n*–C_{18} 117

Figure 3.19 Paleo–environment interpretation using the C_{27}, C_{28}, C_{29} steranes percentage (top) and the correlation of the dibenzothiophene/phenantrane ratio versus pristine/phytane ratio (bottom)..... 118

Figure 3.20 Maturity interpretation based on six biomarkers and aromatics, which are: (1) C_{32} 22S homohopane relative to C_{32} 22R homohopane ratio; (2) 18α 22,29,30 Trisnorhopane (Ts) relative to 17α 22,29,30 Trisnorhopane (Tm); (3) C_{27} diasteranes [13β, 17α (20S, 20R) diacholestanes and 13α, 17β (20S, 20R) diacholestanes] relative to C_{29} steranes [5α, 14α, 17α (20S, 20R) regular steranes and 5α, 14β, 17β (20S, 20R) isosteranes] ratio; (4) Isomerization index for C_{29} regular steranes (5α, 14α, 17α 20S regular steranes and 5α, 14α, 17α 20R regular steranes); (5) Racemization index for C_{29} steranes or ββ/(ββ+αα) ratio [5α, 14β, 17β (20S, 20R) C_{29} isosteranes relative to 5α, 14α, 17α (20S, 20R) C_{29} regular steranes], (6) mono–aromatic steroids ratio; and (7) tri–aromatic steroids ratio. *Bottom right:* Approximate ranges of biomarker maturity ratios against vitrinite reflectance (Peters et al., 2005). Here the terms west, east, northwest, northeast, central, Beta and North for the Albatross, Askeladd and Snøhvit fields are used. This nomenclature is based on the location of the samples as observed in the fields at the Norwegian Petroleum Directorate website (FactMaps). 120

Figure 3.21 Correlation of the Ts/ (Ts + Tm) and diasteranes/steranes ratios. 121

Figure 3.22 Correlation of two age–related biomarker ratios, the extended tricyclic terpane ratio (ETR) and the C_{28}/C_{29} steranes ratio..... 122

Figure 3.23 Vitrinite reflectance calibration with comparison of the three erosion scenarios. Continuous line represents maximum erosion, dotted line represents medium

erosion and segmented line represents minimum erosion. The gray lines correspond to the best calibration zone. 129

Figure 3.24 Temperature calibration with comparison of the three erosion scenarios. Continuous line represents maximum erosion, dotted line represents medium erosion and segmented line represents minimum erosion. 130

Figure 3.25 Vitrinite reflectance calibration with comparison of the three heat flow scenarios. Continuous line represents minimum heat flow, dotted line represents medium heat flow and segmented line represents maximum heat flow. The gray lines correspond to the best calibration zone. 131

Figure 3.26 Temperature calibration with comparison of the three heat flow scenarios. Continuous line represents minimum heat flow, dotted line represents medium heat flow and segmented line represents maximum heat flow. 132

Figure 3.27 Maturity at present–day of the Hekkingen (top), Snadd (middle) and Kobbe (bottom) formations based on vitrinite reflectance (VR, left) and transformation ratio (TR, right). The lower boundary is 0.5% VR, meaning that areas in gray have maturity levels below this value. The black dots observed in the maps to the right correspond to the areas where an extraction has been done in order to obtain the maturity evolution shown in Figure 3.28. 134

Figure 3.28 Maturity evolution based on transformation ratios for the five areas marked with black dots (A – E) in Figure 3.27. 135

Figure 3.29 Evaluation of the Kolmule Formation maturity. Present–day vitrinite reflectance map (left) and vitrinite reflectance evolution through time for the two locations shown in the map 137

Figure 3.30 3D view of the three source rocks using the expulsion onset as an overly……. 138

Figure 3.31 Present–day migration pathways of gas (red) and oil (green) for the two reservoir units: the Stø and Tubåen formations. 139

Figure 3.32 Aerial model view with the drainage areas and the location of the three zones selected for further detailed analysis in Figure 3.33 to Figure 3.35. 140

Figure 3.33 Drainage areas and hydrocarbon accumulations in the southwestern part of the modelled area (see Figure 3.32 for reference) for the interglacial period, the maximum glaciation, the glacial retreat or deglaciation and the present–day. 142

Figure 3.34 Drainage areas and hydrocarbon accumulations in the western part of the modelled area (see Figure 3.32 for reference) for the interglacial period, the maximum glaciation, the glacial retreat or deglaciation and the present–day. 143

Figure 3.35 Drainage areas and hydrocarbon accumulations in the northeastern part of the modelled area (see Figure 3.32 for reference) for the interglacial period, the maximum glaciation, the glacial retreat or deglaciation and the present–day. 144

List of tables

Table 1.1 Some of the physical properties of ice (Knight, 1999). 47

Table 1.2 Main characteristics of the petroleum plays in the Southwestern Barents Sea, compilation from the Norwegian Petroleum Directorate (2011). 66

Table 2.1 Age assignment of each stratigraphic unit and also of the erosion events. .. 70

Table 2.2 Description of the lithology used for each of the layers (including the ice–sheet) and the respective properties. 71

Table 2.3 Petroleum system elements definition and source rock properties. 71

Table 2.4 Description of the samples provided by Applied Petroleum Technology AS (Nr.: Number of samples; SLHFC: Southern Loppa High Fault Complex; HS: Headspace; Fm.: Formation; fms.: formations) 85

Table 3.1 Comparison of the masses generated, expelled and accumulated in the reservoir with respect to the different heat flow scenarios. The values shown in brackets correspond to the detailed masses of each source rock, i.e. Kobbe + Snadd + Hekkingen formations. The value outside is then the sum of these three masses (Heat flow 1=minimum; heat flow 2=medium; heat flow 3=maximum; Gt = Gigatonnes, SD = Standard deviation). 93

Table 3.2 Comparison of the masses generated, expelled, accumulated and leaked from the reservoir with respect to the different erosion scenarios (a=maximum erosion; b=medium erosion; c=minimum erosion; Gt=Gigatonnes; SD=Standard deviation)……..... 94

Table 3.3 Comparison of the masses accumulated in reservoir and lost/leaked from it with respect to the different ice thickness scenarios (Gt=Gigatonnes; SD=Standard deviation)…..... 94

Table 3.4 Contribution from each source rock to the main accumulations present in the Hammerfest Basin (mass %) based on results from the 3D basin model. 104

Statement of original authorship

I, **Enmanuel Alexis Rodrigues Duran**, hereby state that the work contained in this dissertation or any parts thereof has not previously been submitted to the Fakultät VI – Planen, Bauem, Umwelt at the Technical University of Berlin or any other institution except where explicitly acknowledged.

To the best of my knowledge and belief, the thesis does not contain any previously published material or any material which has been written by another person except where due reference is made.

Hiermit erkläre ich, ***Enmanuel Alexis Rodrigues Duran****, dass diese Arbeit oder darin enthaltene Teile bisher von mir weder an der Fakultät VI - Planen, Bauen, Umwelt der Technischen Universität Berlin noch einer anderen wissenschaftlichen Einrichtung zum Zwecke der Promotion eingereicht wurde.*

Ferner erkläre ich, dass ich diese Arbeit selbständig verfasst und keine anderen als die darin angegebenen Quellen und Hilfsmittel benutzt habe.

Enmanuel Alexis Rodrigues Duran

Berlin, August 2014

Preface

The Methane on the Move (MOM) project started at the German Research Centre for Geosciences – Potsdam (GeoForschungsZentrum Potsdam) in 2007 with the main objective of evaluating the possible impact of thermogenic methane leakage to the atmosphere on paleo– and present–global climate change. This PhD study began then as part of this project in July 2009 having as a focus the petroliferous basins of the glacially influenced Barents Sea. The results of this work were sub–divided into three parts and compiled in the form of three scientific publications, the first two are published in Marine and Petroleum Geology and Organic Geochemistry and the third one is ready for submission (the three articles are at the end of this dissertation in the Appendix).

For the initial stage of this study, regional maps of the Southwestern Barents Sea were kindly provided by Lundin Norway AS. The maps were then edited and restricted to the first area of interest corresponding to the Hammerfest Basin. This was chosen as a first study area due to the fact of being the most explored basin in the Southwestern Barents Sea and therefore the area with the largest amount of data available from exploration wells, useful for model calibration. This initial stage also included the acquisition of all necessary literature which was used to understand the geological evolution of the area, the petroleum systems, the glacial processes and the glaciation, the uplift and erosion events, the lithological variations, etc… Data necessary for the model input and calibration was also acquired; which corresponds to temperature, vitrinite reflectance, and source rock properties such as total organic carbon and hydrogen index. The first model was then built and calibrated. Sensitivity analyses were run at the same time. Once calibration was achieved, the interpretation of the best calibrated model output started including source rock maturity, hydrocarbon migration and accumulation, volumetric in terms of masses of petroleum generated, migrated, accumulated and leaked. Finally the first publication was prepared. This stage also included the contribution in conferences and internal seminars at GFZ.

During the second stage a geochemical dataset was provided by Applied Petroleum Technology Norway, AS. This included fluid data from the main fields (Snøhvit, Askeladd, Albatross and Goliat) and discoveries (Tornerose) in the Hammerfest Basin. The specific data available corresponds to gas isotopes, light hydrocarbons, biomarkers and aromatics. Thus, the geochemical interpretation of the available data, basically in relation with the origin of the hydrocarbons in the reservoirs, maturity and age of the source rocks that have generated these hydrocarbons and the influence of secondary processes was performed. With this it was assured to have a better understanding of the petroleum systems in the Hammerfest Basin. This part was then followed by a correlation study between the observed trends from geochemical interpretation and the results from basin modelling. As far as is known from the area, no correlations of this type have been attempted before. The second paper was then prepared using the results from this second stage. Contributions in conferences and internal seminars were also part of this stage.

The final stage of this PhD corresponds to the building of the second and last model. Once again the regional maps provided by Lundin were edited and restricted to the second area of interest corresponding to the Loppa High. Other areas were also included to the west and east of the High. The idea was to build a second model beside the one already built (in the Hammerfest Bain), with the aim of evaluating the petroleum system dynamics of this zone which has a different structural pattern and different basin configurations, in the same way as was done for the first modelled area. Calibration data was also acquired and used for model calibration. For this part new assumptions and interpretations were done mainly regarding the differentiation of the erosional patterns and magnitudes and the establishment of erosion boundaries. Sensitivity analyses were also performed. The calibration was achieved and the best calibrated model was used for further evaluation and interpretation. Preparation of the third article was started considering the modelling results from this final stage. Initially it was planned to build a series of models covering the entire Southwestern Barents Sea and therefore reach a complete understanding of the petroleum system dynamics in the entire area. However, due to time and data limitation this proved unfeasible.

Publications

In the scope of this dissertation the following articles, conferences contributions and internal seminars were published and/or presented:

Publications as requirement for this dissertation

Paper 1 *– Rodrigues Duran, E., di Primio, R., Anka, Z., Stoddart, D., Horsfield, B. (2013). 3D– Basin modelling of the Hammerfest Basin (southwestern Barents Sea): A quantitative assessment of petroleum generation, migration and leakage. Marine and Petroleum Geology 45, 281–303.*

Paper 2 *– Rodrigues Duran, E., di Primio, R., Anka, Z., Stoddart, D., Horsfield, B. (2013). Petroleum system analysis of the Hammerfest Basin (southwestern Barents Sea): Comparison of basin modelling and geochemical data. Organic Geochemistry 63, 105–121.*

Paper 3 *– Rodrigues Duran, E., di Primio, R., Anka, Z., Stoddart, D., Horsfield, B. (2014). Petroleum systems evaluation of the Loppa High and surrounding areas in the Southwestern Barents Sea through 3D basin modelling (Ready for submission)*

Contributions in conferences and internal seminars

- **Rodrigues Duran, E.**, di Primio, R., Anka, Z. (2012). Organic geochemical interpretation and basin modelling in the Southwestern Barents Sea. Internal seminar. GeoForschungsZentrum Potsdam. 20. June 2012, Potsdam–Germany.
- Anka, Z., **Rodrigues Duran, E.**, Ostanin, I., di Primio, R., Stoddart, D., Horsfield, B. (2012). Release of thermogenic–methane in the Hammerfest Basin after the Last Glacial Maximum. Indications from numerical modelling and 3D seismic reflection data. European Geosciences Union General Assembly (EGU). 22.–27. April 2012, Vienna–Austria.
- Ostanin, I., **Rodrigues Duran, E.**, Nickel, J., Anka, Z., di Primio, R., Magelsdorf K., Horsfield, B. (2012). Effects of glaciations on thermogenic methane release in the SW Barents Sea: an interdisciplinary approach. Regionale

Klimaänderung (REKLIM) workshop. 19.–21. March 2012, Lüneburg–Germany.

- **Rodrigues Duran, E.**, di Primio, R., Anka, Z., Stoddart, D., Horsfield, B. (2011). Basin modelling of the Hammerfest Basin and Loppa High (Southwestern Barents Sea); investigating the leakage of hydrocarbons in a glacially influenced marine environment. International Meeting on Organic Geochemistry (IMOG). 18.–23. September 2011, Interlakken–Switzerland.
- **Rodrigues Duran, E.**, di Primio, R., Anka, Z., Stoddart, D., Horsfield, B. (2011). Leakage of hydrocarbons in a glacially influenced marine environment: Hammerfest Basin (Southwestern Barents Sea). European Geosciences Union General Assembly (EGU). 03.–08. April 2011, Vienna–Austria.
- **Rodrigues Duran, E.**, di Primio, R., Anka, Z., Stoddart, D., Horsfield, B. (2011). Assessing the leakage of hydrocarbons in the glacially influenced Hammerfest Basin (Southwestern Barents Sea) using basin modelling. Regionale Klimaänderungen (REKLIM) workshop. 29.–30. March 2011, Bremerhaven–Germany.
- **Rodrigues Duran, E.**, di Primio, R., Anka, Z. (2011). Leakage of hydrocarbons in a glacially influenced marine environment. Basin modelling of the southwestern Barents Sea. Internal seminar. GeoForschungsZentrum Potsdam. 26. January 2011, Potsdam–Germany.
- **Rodrigues Duran, E.**, di Primio, R., Anka, Z., Stoddart, D., Horsfield, B. (2011). Leakage of hydrocarbons in a glacially influenced marine environment: Basin modelling of the south–western Barents Sea (Hammerfest Basin). Norwegian Meeting on Organic Geochemistry (NMOG). 08.–10. September 2010, Oslo–Norway.

Acknowledgements

I would like to begin by thanking my supervisors Prof. Dr. Rolando di Primio and Dr. Zahie Anka. You were the mainstay in the initiation, development and completion of this doctoral study. Always supported me with your best advises and great scientific knowledge.

Thanks to Prof. Dr. Brian Horsfield who also supported me and my scientific research in the organic geochemistry department at the German Research Centre for Geosciences (GFZ-Potsdam). Thanks for your ideas and the motivation to finish my PhD with success and great scientific basis.

Thanks to MoM project and all the scientists involved on it because with the creation of this project it was possible as well the initiation of this PhD. Thanks also to Lundin Norway AS for providing the surface maps used in the models building. Thanks are due to Nigel Mills and APT Norway for providing access to the geochemical data.

Thanks to all my friends and colleagues from GFZ who always were there helping me, sharing knowledge, and allowing me to have a great time, between them: my excellent roommates Ilya Ostanin, Dr. Alexander Hartwig and Dr. Jingquiang Tan; as well as Jacqui, Dr. Julia Nickel, Dr. Philipp Kuhn, Niko, Mareike Noah, Maren Brehme, Dr. Robert Ondrak, Dr. Kai Magelsdorf and Claudia Engelhardt. Very special thanks to my dear Gaby Marcano, you were there for me as a great friend and almost like a sister; and to Alejandro Berbesi, my good friend and brother even since Venezuelan times at the university, you have always shown me the heart of a valuable and excellent scientist.

Thanks to all my very good friends from Venezuela, my Berlin friends (especially Heidi, Amalia and Otto) and my friends in Harstad and Statoil (especially Maru and Björn), who always have been following with enthusiasm the development of my PhD studies and this thesis.

Thanks to my beautiful family, you were and have been my main strength and motivation to start and finish this PhD. My mother “Mercedes” always there with the most beautiful words of encouragement. My sister “Sonia” showing me her great love and showing me that it will always be possible to reach my goals. My father and brothers and my wonderful niece and princess Sophia, your smile is a source of life.

Finally but not least, thanks to my dear God, you are always there in every step.

Abstract

The 3D basin modelling of the Southwestern Barents Sea was planned with the aim of addressing the masses of petroleum generated, migrated, accumulated and lost during the basin evolution. The first model was constructed for the Hammerfest Basin considering three source rocks, which correspond to the Upper Jurassic Hekkingen Formation and the Triassic Snadd and Kobbe formations. The highest maturities for the three source rocks were reached in the western and northwestern margin of the basin. The model reproduced satisfactorily the hydrocarbon phases and distribution of the main fields and discoveries. Two events of petroleum re-distribution occurred in the basin: the first corresponds to the oil re-distribution (during the Oligocene–Miocene); the second corresponds to the gas leakage (during the Pliocene–Pleistocene) in connection to the glacial–interglacial cycles. At least 0.247 Gt of thermogenic gas leaked from the main reservoir and reached the sediment interface. The analysis of the volumetric proportions of oil and gas contributions to each field and discovery, suggest that the gas contribution stems mainly from Triassic source rocks, while the oil phases contain variable proportions from both the Jurassic Hekkingen Formation and the Triassic source rocks. Available fluid geochemical data from the main fields in the Hammerfest Basin allowed testing these results. The interpretation of gas isotopes and maturity related biomarker ratios confirms the maturity trends derived from basin modelling; and light hydrocarbons indicate the influence of secondary processes. However, age related biomarker ratios did not provide a clear separation when evaluating a contribution from Jurassic versus Triassic source rocks.

The 3D basin modelling was extended to include the Loppa High as well as some other important frontier exploration areas; taking into account the same source rocks. Calibrated model predictions indicate that the three source rocks are overmature in the western margin and also have high maturities in the deepest parts of the Maud Basin to the east. However, in the Bjarmeland platform, only the Triassic source rocks have entered the oil window. Recent generation has been observed in the eastern part around the Bjarmeland Platform and generative potential is still available at present–day. The timing of generation in the western part is different in comparison to the east, with the

Abstract

Kobbe Formation starting to generate during the Late Triassic–Early Jurassic, the Snadd Formation during Late Jurassic–Early Cretaceous and the Hekkingen Formation during Middle Cretaceous. The three source rocks do not have any generative potential left; therefore, it is necessary to rely on younger source rocks. Additional results indicate that the main drainage directions do not change drastically during the evolution of the area, not even during the glacial–interglacial cycles. The model output shows changes in the sizes of the relative oil versus gas quantities in the modelled accumulations during the glacial cycles.

Zusammenfassung

Die Zielsetzung der vorliegende 3D Beckenmodellierungsstudie ist ein besseres Verständnis der Kohlenwasserstoffsysteme der Südwestlichen Barentssee. Dies beinhaltet eine Beschreibung der generierten Mengen an Kohlenwasserstoffen, deren Migration und Akkumulation sowie die Abschätzung des Verlusts aus potentiellen Reservoiren im Verlauf der Evolution des Sedimentbeckens.

Hierzu wurde zunächst ein Modell für das Gebiet des Hammerfest Sedimentbeckens erstellt, welches drei Muttergesteine beinhaltet: die Oberjurassische Hekkingen Formation, sowie die Triassische Snadd und Kobbe Formation. Die höchste Reife dieser Muttergesteine wurde für den westlichen und nordwestlichen Beckenrand vorhergesagt. Das Modell ist somit in der Lage die Kohlenwasserstoffe und deren Verteilung für schon bekannte Felder und Ressourcen zufriedenstellend zu reproduzieren. Basierend auf diesem Model konnte gezeigt werden, dass in dem Untersuchungsgebiet im Wesentlichen zwei Phasen der Re-migration die rezente Verteilung zur Folge hatten; die Umverteilung des Öls während des Oligozäns-Miozäns und ein Verlust der Gasphase während des Pliozäns-Pleistozäns in Zusammenhang mit den glazial-interglazialen Zyklen. Hierbei gelangten mindestens 0.247 Gt thermogenes Gas aus der Hauptlagerstätte an die Sedimentoberfläche. Die volumetrische Analyse der Öl- und Gaszusammensetzung der einzelnen Felder und weiterer neuer Entdeckungen weist darauf hin, dass das vorhandene Gas hauptsächlich von Triassischen Muttergesteinen stammt, wohingegen das Öl in variablen Anteilen von der Jurassischen Hekkingen Formation als auch den Triassischen Muttergesteinen gespeist wurde. Diese Ergebnisse konnten unter Zuhilfenahme von geochemischen Daten von Fluidanalysen der Hauptfelder des Hammerfest Sedimentbeckens überprüft werden. Die Interpretation von Gasisotopendaten und Reifeparametern bestätigt die Reifetrends welche bereits durch die Beckenmodellierung erhalten wurden. Die Daten der kurzkettigen Kohlenwasserstoffe zeigen den Einfluss sekundärer Prozesse an. Die Analyse der altersabhängigen Biomarker konnte keine eindeutige Abgrenzung zwischen Jurassischen und Triassischen Muttergesteinen aufzeigen.

Zusammenfassung

Unter Berücksichtigung der gleichen Muttergesteine wurde das 3D Beckenmodell auf die Loppa High Region und weitere Explorationsgebiete erweitert. Die kalibrierten Ergebnisse des Modells zeigen, dass die drei Muttergesteine am westlichen Rand des Beckens überreif sind. Des Weiteren weisen sie eine hohe Reife in den tiefsten Teilen des Maud Sedimentbeckens gen Osten des Modells auf. Im Bereich der Bjarmeland Plattform hat nur das Triassische Muttergestein das Ölfenster erreicht. Die derzeitige Generierung von Kohlenwasserstoffen kann im östlichen Teil der Bjarmeland Plattform beobachtet werden, wobei heutzutage noch immer ein Generierungspotential vorhanden ist. Im westlichen Teil des Modells begann die Kohlenwasserstoffgenerierung der Kobbe Formation bereits im Obertrias – Unterjura. Die Snadd Formation erreichte das Ölfenster im Oberjura – Unterkreide und die Hekkingen Formation während der oberen Unterkreide. In diesem Gebiet ist das Generierungspotential der drei Muttergesteine erschöpft. Aus diesem Grund ist es notwendig sich auf jüngere Muttergesteine zu konzentrieren. Weitere Ergebnisse zeigen, dass sich die Hauptmigrationsrichtungen während der Evolution des Gebiets nicht drastisch geändert haben, auch nicht während der glazial-interglazialen Zyklen. Das Modellierungsergebnis zeigt, dass die Gas- zu Ölverhältnisse der modellierten Akkumulationen mit den glazialen Zyklen in Zusammenhang stehen.

1. Introduction

1.1 Scientific interest and objectives

Several studies, related with the investigation of the sources and behavior of the greenhouse gases and their accumulation in the atmosphere, have been performed during the recent past (Blunier et al., 1995; Raynaud et al., 1998; Petit et al., 1999; Raynaud et al., 2000; Weissert, 2000; Kvenvolden and Rogers, 2005). It has been corroborated that the accumulation of greenhouse gases in the atmosphere has certainly influenced the overall increase of global temperature and therefore has affected present climate. Abrupt climate changes in the past were discovered during the last few decades and on a hemispheric scale. The fact of having encountered the way of recognizing past changes in climate is of real importance for predicting possible changes in future climate (Raynaud et al., 2000).

Methane is one of the most important greenhouse gases and its atmospheric concentration has increased considerably after the Last Glacial Maximum (LGM; O'Connor et al., 2010). Petit et al. (1999) have also observed using greenhouse gas records that the main trends of the CO_2 and methane concentration changes is quite well connected with glacial cycles. The major transitions from the lowest to the highest values are associated to the glacial–interglacial transitions (the highest CO_2 and methane contents are found during the interglacials and the lowest during the glacial maxima). On the other hand, the global mean atmospheric abundance of methane is determined by the interplay between emissions and sinks. Methane emissions are very diverse and cover a wide range of natural and anthropogenic sources (O'Connor et al., 2010). One of the natural sources corresponds to methane degassing from sedimentary basins. This type of methane flux has been recognized as a potentially significant source of methane to the atmosphere and may therefore have an influence in the global climate, affecting the atmospheric composition on geologically long or short periods of time, depending on the evolution of a basin (Kroeger et al., 2011; Etiope, 2012; Berbesi et al., 2014). During periods of glaciation, ice–sheet growth and retreat can be one of the mechanisms triggering the flux or leakage of methane from sedimentary basins located in high latitudes, due to pressure release during the retreat phase of the capping ice–

sheets (Kennett et al., 2000; Cavanagh et al., 2006; Kroeger et al., 2011; Etiope, 2012; Ostanin et al., 2013).

Moreover, several pieces of evidence exist around the globe that can actually prove the natural gas leakage to the atmosphere as coming from the subsurface. Some of these evidences are related to features, which can be recognized on the Earth's surface and on the seafloor, they include for instance macroseepage such as mud volcanoes and pockmarks; and a not so obvious emission of methane that can occur through pervasive microseepage, driven by diffusion or separate phase flow (Hovland and Judd, 1988; Lammers et al., 1995; Milkov, 2000; Etiope and Klusman, 2002; Milkov, 2004; Hovland et al., 2005; Archer, 2007; Etiope et al., 2008a; Etiope et al., 2008b; Etiope and Klusman, 2010; Plaza-Faverola et al., 2011). Etiope and Klusman (2002, 2010) have tried to evaluate the extension of micro and macroseepage worldwide and improve the estimation of the global positive fluxes or emission rates of methane at present–day to the atmosphere, from different hydrocarbon–prone sedimentary basins. The estimated global fluxes correspond to: a) >7 Mt/y from diffuse microseepage; b) around 2Mt/y in mud volcanoes; and c) between 18 and 48 Mt/y in submarine hydrocarbon–areas seeps. These authors established based on these estimates that submarine seeps, mud volcanoes and microseepage occurring in petroleum–prone basins represent the largest geologic source of methane.

The Barents Sea is a petroleum province located in the Arctic Ocean, covering a total area of 1.3 million km^2 with water depths in general between 200 and 500 m. The southern part of the Barents Sea is in general open for petroleum activities and the interest for exploration in the area has been growing through the last few years. In the area 390 billion Sm^3 of gas and 210 million Sm^3 of oil have been proven by the end of December 2012 (Goa and Bjørøen, 2013). The Barents Sea also represents a sedimentary area strongly affected during the recent past by severe glaciations with the development of several phases of glacial growth and retreat since approximately the last 2.50 Myr (Jansen and Sjoholm, 1991; Vorren et al., 1991; Eidvin et al., 1993; Mørk and Duncan, 1993; Solheim et al., 1996; Svendsen et al., 1999; Siegert and Marsiat, 2001; Knies et al., 2009).

In order to assess all these mechanisms and topics of scientific interest, and to have an idea of the possible paleo contribution of methane from petroleum–prone sedimentary basins, it is therefore important that a study is performed with the combination of different tools and techniques. This PhD was defined, therefore, with the aim of investigating the dynamics of the petroleum systems in the glacially influenced Southwestern Barents Sea by using 3D basin modelling. To achieve this general goal the following steps were covered:

- 3D basin modelling for two specific areas of interest, the Hammerfest Basin and the Loppa High, using the software PetroMod v.11. This allows to reconstruct the burial and thermal history of the basin, evaluate the effects of glaciation and deglaciation, assess the maturity of the source rocks, quantify the amount of hydrocarbons generated and expelled, reconstruct hydrocarbon migration and address the volumes of hydrocarbons trapped in the reservoir and the proportion leaked to the surface.

- Perform an organic geochemical data interpretation to evaluate: the origin of the petroleum (oil and gas) that have been found in different fields and discoveries in the Hammerfest Basin, the possible influence of secondary processes (biodegradation and water washing), and the source rocks maturity and age.

- Finally a correlation of the results from basin modelling with the organic geochemical data interpretation was planned and performed.

The next part of this introduction (***section 1.2***), corresponds to the definition of a general background that will help to understand in more detail: 1) the scientific questions and reasons for the establishment of this PhD study; 2) the understanding of a petroleum system, which is an elemental key of the study area and of this study itself; and 3) the influence of glacial dynamics on sedimentary basins characterized by the presence of one or more petroleum systems. ***Sub-section 1.2.1***, presents as well the scientific reasons for the definition of the Methane on the Move (MOM) project, which is as well the "umbrella" project of several sub-projects (including this PhD study).

Sections 1.2.2 to ***1.2.5*** present a brief description of the origin of petroleum, defines the petroleum systems approach and its elements, and the petroleum system modelling. It is necessary to understand these concepts, since the main goal of MOM is to accomplish the quantification of the methane flux in the subsurface (in petroleum provinces) and into the surface and atmosphere. Finally, but not least, ***section 1.2.6*** presents a description of a glacier system and the glaciation processes. Once a petroleum system has been understood, then it is necessary to understand as well the processes that can influence it affecting the flux of hydrocarbons and, more importantly methane. As already mentioned the study area is located in the Arctic region and therefore has been strongly affected by glaciations. In this sense, understanding these concepts (glaciers and glaciations) will allow to have an idea on the considerations that must be taken into account when evaluating the methane flux in a petroleum province and when a petroleum system modelling with glaciations is performed.

Finally, ***section 1.3*** is presented with a focused description of the Barents Sea, including: 1) the exploration history, important due to the fact that thanks to the exploration activity developed by different oil companies more interest has been established on the area; 2) the geological background or history; 3) the uplift and erosion and the glacial history of this particular area; as well as 4) the possible petroleum systems that are present.

1.2 Theoretical background

1.2.1 Methane on the move (MOM)

During the last decades the interest in understanding the methane cycle has grown considerably, mainly because of the impact that methane can have in influencing present and past global climate change. It is well known that methane is a potent greenhouse gas (more than 20 times the greenhouse potential of CO_2) that in the atmosphere is oxidized to generate CO_2, another greenhouse gas, in a period of about 10 years. Both gases are being constantly released or produced from different sources and their accumulation in the Earth's carbon cycle have been, is currently and will continue to be affecting the climate for several thousands of years (Archer, 2005; Archer and

Brovkin, 2008; Archer et al., 2009). Methane, chemically speaking, is the most reduced form of carbon and, as stated before, can be easily oxidized, representing therefore one of the very transient species in our atmosphere, whereby, its ongoing release guarantees the maintenance of its concentration (Archer, 2007).

Methane production or release can be associated to different sources: a) the reduced interior of the Earth, through volcanic gases and hydrothermal vents; b) the photosynthesis process; c) the production of biogenic methane from organic matter degradation (Archer, 2007); and d) the methane produced abiologically upon temperatures around or above 100°C that results in thermal cracking of the buried organic matter (Milkov, 2005). This last one is also named thermogenic methane.

Based on the fact that the methane fluctuation can highly impact the climate conditions and that there could be several sources for its contribution, efforts need to continue growing in order to address the contributions from the individual sources. For instance, in a sedimentary basin, where high amounts of methane (mainly thermogenic, but also biogenic) can be generated, the methane degassing process from subsurface reservoirs could be one of the mechanisms that can explain the increases in the atmospheric CO_2. Therefore, the methane leakage from a sedimentary basin over millions of years and also over geologically short periods of time may have been one of the driven forces for global climate change (Kroeger et al., 2011; Berbesi et al., 2014).

At the German Research Centre for Geosciences (GFZ–Potsdam) the Methane on the Move (MOM) project was created with the aim of improving the understanding of the processes involved in the methane origin and remobilization cycle and its impact on paleo– and present–global climate change through an integrated basin and earth systems modeling approach. In order to develop this kind of approach it is also necessary to understand other important concepts such as the petroleum origin and occurrence and also the definition of a petroleum system.

1.2.2 Petroleum origin and occurrence

The term ***organic matter*** or ***organic material*** refers to the organic constituents derived directly or indirectly from living organisms. This organic matter is synthesized by living organisms, and afterwards upon death can be deposited and preserved together with the sediments in a sedimentary basin (Durand and Espitalié, 1976; Dow, 1977; Durand, 1980; Tissot and Welte, 1984). The geological evolution of a sedimentary basin implies the process of increasing burial and sedimentation, which also results in an increase of temperature and pressure (Tissot et al., 1974; Hood A. and Heacock, 1975; Welte and Yukler, 1981; Dickinson, 1993). This will also promote the maturation of the organic matter that has been deposited and preserved and with it the generation of ***petroleum***, a term used for crude oil and natural gas together (Tissot et al., 1974; Hood A. and Heacock, 1975; Gluyas and Swarbrick, 2004; McCarthy et al., 2011).

The thermal maturation process can be divided into three stages:

- First of all the sediment is subjected to ***diagenesis*** (Figure 1.1), which is the process that includes all the natural changes that the sediments experience (consolidation) from the time they are deposited in the basin until just before the beginning of the thermal alteration processes (Larsen and Chilingar, 1967; Tissot and Welte, 1984; Mackenzie, 2005; Vandenbroucke and Largeau, 2007; McCarthy et al., 2011). When talking about a source rock this first stage of diagenesis refers to the initial alteration of the organic matter, which generally takes place at temperatures up to roughly 60–80°C. In this stage there can be an influence of oxidation and other chemical processes that cause the breakdown of the organic matter. If the processes occur in an anoxic environment, transformation due to microbial activity may result in the organic material being converted into dry “biogenic gas” (Tissot et al., 1974; Rice and Claypool, 1981; Tissot and Welte, 1984; Behar and Vandenbroucke, 1987; Vandenbroucke and Largeau, 2007; McCarthy et al., 2011). With the increase in temperature the organic matter is further being re–structured and gradually converted into kerogen and small amounts of bitumen (Tissot, 1969; Tissot and Welte, 1984;

Behar and Vandenbroucke, 1987; Horsfield, 1997; Vandenbroucke and Largeau, 2007; McCarthy et al., 2011).

- The second stage corresponds to the ***catagenesis*** (Figure 1.1), in which the source rock experiences maturation due to the increase of heat (temperature). At this stage is when petroleum starts to be generated in a temperature range between 70 and 150°C that promotes the breaking down of chemical bonds in the kerogen. Through this process both oil and gas are produced by primary cracking reactions depending on the kerogen type (see below). Further increase of temperature and pressure bring the source rock to the end of the "oil window" and the beginning of the "gas window". At temperatures generally between 150 and over 200°C secondary cracking of the already generated products results in the formation of gas (methane, ethane, propane, butane and pentane) and condensate (Tissot and Welte, 1984; Behar and Vandenbroucke, 1987; Pepper and Corvi, 1995a; Hunt, 1996; Schenk et al., 1997a; Vandenbroucke and Largeau, 2007; McCarthy et al., 2011).

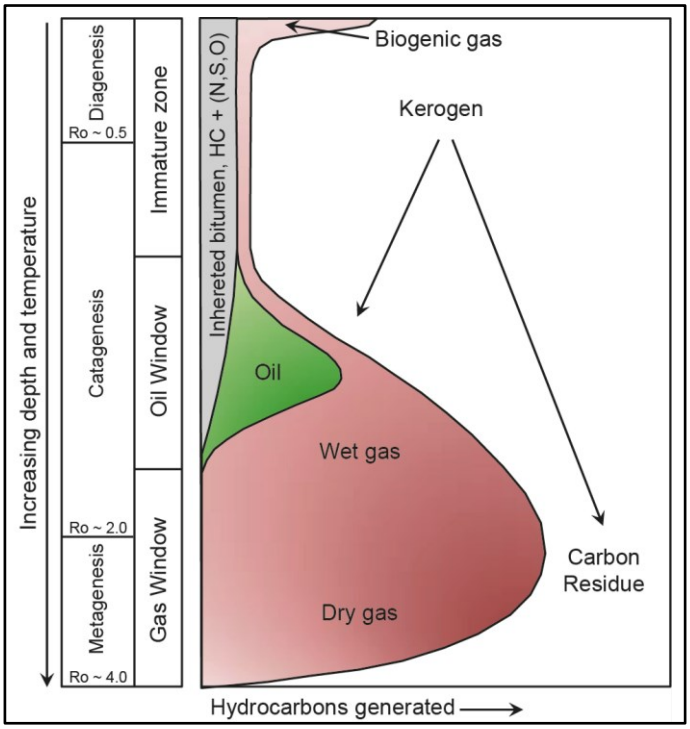

Figure 1.1 General evolution scheme of organic matter maturation (Modified from Tissot and Welte, 1984).

- The final stage of the maturation process is named ***metagenesis*** (Figure 1.1), in which the kerogen is converted into some methane and a carbon residue at temperatures exceeding 250°C (Tissot and Welte, 1984; Behar and Vandenbroucke, 1987; Vandenbroucke and Largeau, 2007; McCarthy et al., 2011).

The ***kerogen*** produced during the first stage of diagenesis is defined by Forsman and Hunt (1958), Durand (1980), Tissot and Welte (1984), Hunt (1996), Vandenbroucke and Largeau (2007) as the organic constituent of the sedimentary rocks that is neither soluble in aqueous alkaline solvents nor in common organic solvents. The second product of diagenesis, the ***bitumen***, corresponds to the fraction that can be extracted with organic solvents (Tissot and Welte, 1984).

The kerogen can be classified in four different types based on the provenance, as indicated by the macerals type, and also based in the content of hydrogen, carbon and oxygen (Tissot et al., 1974; Tissot and Welte, 1984).

- ***Kerogen type I*** – deposited predominantly in lacustrine depositional environments (some cases marine). It comprises lipid material, particularly aliphatic chains, indicating that this kerogen is derived mainly from algal material and associated forms and from other organic matter that has been extensively reworked by bacteria and microorganisms. It is rich in hydrogen and low in oxygen (H/C ca. 1.5 or more; O/C < 0.1) and generally seen as an oil prone kerogen (Durand, 1980; Tissot and Welte, 1984; Selley, 1985; Behar and Vandenbroucke, 1987; Killops and Killops, 1993; Vandenbroucke and Largeau, 2007; McCarthy et al., 2011).

- ***Kerogen type II*** – This type of kerogen is being formed in moderately deep marine environments with good reducing conditions. It is mainly derived from a mixture of plankton (phytoplankton and zooplankton) and microorganisms. It is rich in hydrogen and relatively low in oxygen and carbon (relatively high H/C and low in O/C) and usually also an oil prone kerogen, with potential to generate

gas at high maturities (Durand, 1980; Tissot and Welte, 1984; Selley, 1985; Behar and Vandenbroucke, 1987; Killops and Killops, 1993; Vandenbroucke and Largeau, 2007). A ***kerogen type II–S*** can also be observed, mainly in depositional environments that promote the incorporation of sulfur compounds (Tissot and Welte, 1984; Orr, 1986; Killops and Killops, 1993; Vandenbroucke and Largeau, 2007; McCarthy et al., 2011).

- ***Kerogen type III*** – It is a kerogen derived mainly from terrigenous (continental) plants debris that are deposited in shallow to deep marine (continental margins) or non–marine environments. It is a kerogen with low hydrogen and high oxygen content (H/C < 0.1 and O/C as high as 0.2 or 0.3) and corresponds mainly to a gas prone kerogen (Durand, 1980; Tissot and Welte, 1984; Selley, 1985; Behar and Vandenbroucke, 1987; Killops and Killops, 1993; Vandenbroucke and Largeau, 2007; McCarthy et al., 2011).

- ***Kerogen type IV*** – It is derived from residual organic matter that has been reworked. This type of kerogen has a very high carbon and oxygen content and low hydrogen content. It can be considered a dead carbon without any kind of potential for generating oil or gas (Tissot and Welte, 1984; Killops and Killops, 1993; McCarthy et al., 2011).

The process of organic matter transformation upon temperature increase, from the kerogen to petroleum (oil and gas), as previously explained, takes place in a series of parallel and consecutive reactions, which are recognized to be quasi–irreversible and controlled by chemical kinetics (Tissot, 1969). Nowadays these reactions can be described using kinetic laws, which establish a mathematical link that allows the extrapolation of measurements made at laboratory conditions to natural heating conditions (Dieckmann et al., 1998). Current compositional kinetic models are used to predict the composition of natural petroleum generated in source rocks. Initially, kinetic models could predict bulk petroleum generation that reflects the principal structural features of the different kerogens (Ungerer and Pelet, 1987; Schenk et al., 1997b). However, complete compositional kinetic models have become available that allow

describing the compositional evolution of generated fluids by using two or more petroleum compounds (Espitalié et al., 1988; Pepper and Corvi, 1995a, b; Pepper and Dodd, 1995; Sweeney et al., 1995; Dieckmann et al., 1998). Compositional kinetics have been used in this study for petroleum generation in the basin modelling, details will be described later on in section 2.1.2.

1.2.3 Petroleum system

A petroleum system (Figure 1.2) is defined as a natural system that encompasses an active source rock and the oil and gas derived from it as established by geochemical correlation (Dow, 1974; Magoon, 1987; Perrodon, 1992; Magoon and Dow, 1994; Magoon and Beaumont, 2000; Allen and Allen, 2005; Al-Hajeri et al., 2009). The concept also includes all other geologic elements and processes which are needed for the accumulation of the oil and gas. These elements are a reservoir, a seal and an overburden rock; the last one is necessary in the system since it facilitates thermal maturation of the source rocks and burial of the other elements. The processes include trap formation, generation, expulsion, migration, accumulation, and eventual leakage of petroleum. These elements and processes must occur in the proper order for a petroleum system to succeed (Perrodon, 1992; Magoon and Beaumont, 2000; Allen and Allen, 2005; Al-Hajeri et al., 2009).

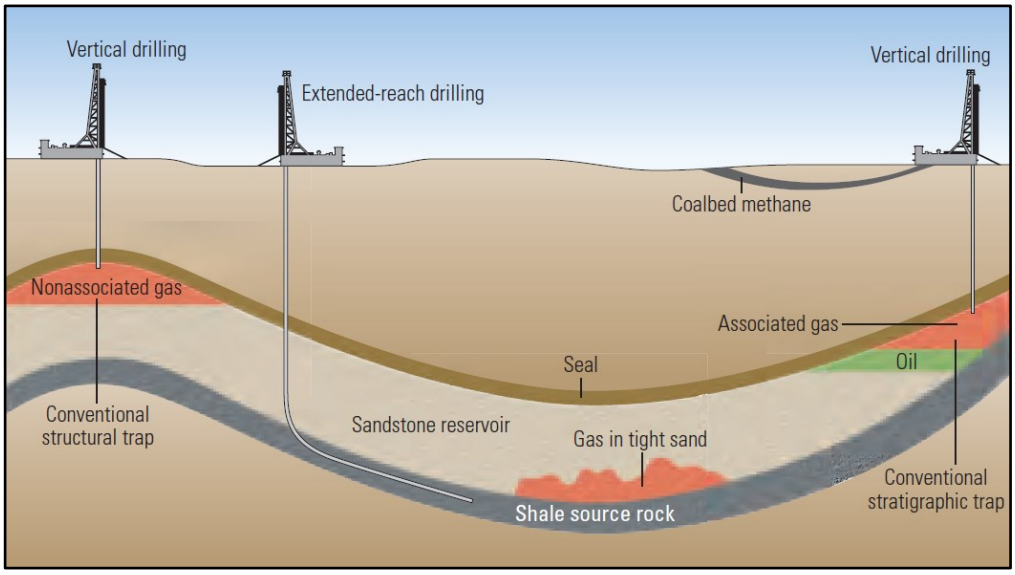

Figure 1.2 Sketch for a typical conventional petroleum system (McCarthy et al., 2011).

Magoon and Beaumont (2000) have described the petroleum as a compound that includes high concentrations of any of the following substances: a) thermal and biological hydrocarbon gas (found in conventional reservoirs as well as in gas hydrates, tight reservoirs, fractured shale and coal); b) condensates; c) crude oils; and d) natural bitumen (in siliciclastic and carbonate reservoir rocks).

1.2.4 Petroleum system elements and processes

A ***source rock*** is conventionally defined as any fine–grained rock rich in organic matter preserved by deposition in a low–oxygen environment. It is capable of generating petroleum (oil and gas) when is subjected to enough heat or temperature (Demaison and Moore, 1980; Jacobson, 1991; Doré, 1995; Gluyas and Swarbrick, 2004; McCarthy et al., 2011). The petroleum–generating potential of a source rock is directly related with its volume, organic richness and thermal maturity. The first is a function of the thickness and the areal distribution of the rock; the second is related to the amount (determined by the total organic carbon content) and type (determined by the hydrogen and oxygen content) of organic matter that is contained in the rock; and the third is associated with the exposure of the source rock to heating over the geological time. The increasing of heating occurs since the rock is buried deeper beneath a successive sequence of sediments (***overburden rock***) and in accordance with the geothermal gradient of the particular basin. Upon heating increase the organic matter suffers a thermal transformation or cracking and therefore ***generation*** of petroleum takes place (Tissot et al., 1974; Welte and Yukler, 1981; Jacobson, 1991; McCarthy et al., 2011).

The ***reservoir*** can be any rock having sufficient porosity (primary/depositional, secondary/diagenetic or fractures) to accumulate a significant amount of hydrocarbons; and also the capacity of transmitting and exchanging fluids (high permeability). The ***seal*** is represented by an impermeable rock such as shale, anhydrite or salt, which forms a barrier above and around the reservoir avoiding the fluids migration beyond it. A ***trap*** is a concept closely linked to the seal. By definition it is a configuration or geometric arrangement of rocks that allows the significant accumulation and sealing of hydrocarbons. As such, they could be ***structural traps***, which are those created by the

syn– to post–depositional deformation of strata into a geometry, usually folds and faults; and ***stratigraphic traps***, which are basically associated to areas with a variation of the stratigraphy or a change in the rock types (unconformities, pinch–outs and reefs) (Magoon, 1987; Perrodon, 1992; Biddle and Wielchowsky, 1994; Gluyas and Swarbrick, 2004; Schlumberger, 2014).

Migration is defined as the process by which the petroleum (oil and gas) moves from the low–porosity source rock where it has been generated, to a higher porosity source rock (Figure 1.3), where it will probably form a large accumulation if the right conditions or circumstances are present (England et al., 1987). Two types of migration have been defined. ***Primary migration*** is related to the initial movement of the generated petroleum from the low permeability source rock towards a rock or bed with higher permeability (usually sandstone or a fractured limestone body). The displacement involves in general a distance up to 1 km. ***Secondary migration*** corresponds to the subsequent movement of the first migrated petroleum through higher permeability strata known as carrier beds (Figure 1.3). A hydrocarbon accumulation will be formed during this migration if a suitable reservoir structure is found. This secondary migration can involve distances up to or exceeding 100 km, depending on the petroleum and rock types as well as on the volume (Welte and Yukler, 1981; England et al., 1987; England et al., 1991; Palciauskas, 1991; Gluyas and Swarbrick, 2004).

The ***accumulation*** or ***trapping*** of migrating petroleum is a process that takes place in an area where all the forces that are controlling petroleum migration converge. For this to take place the presence of a seal rock is necessary, which prevents the further vertical movement or leakage of the petroleum by capillary forces (England et al., 1987).

There are two aspects that are also important because they limited the presence or success of a petroleum system, which are the temporal and the spatial aspects. The *temporal aspects* are related to the age, the critical moment and the preservation time. The age basically refers to time itself that is required for the entire process of generation, migration and accumulation of petroleum to take place. The critical moment corresponds to the time that best depicts this process of generation, migration and

accumulation in a petroleum system. Finally the preservation time is represented by the time in which a full cycle covering generation, migration and accumulation occurs and the present–day. During this time several other processes can take place then in the reservoir and affect the original entrapped petroleum (Magoon, 1987; Magoon and Dow, 1994; Magoon and Beaumont, 2000).

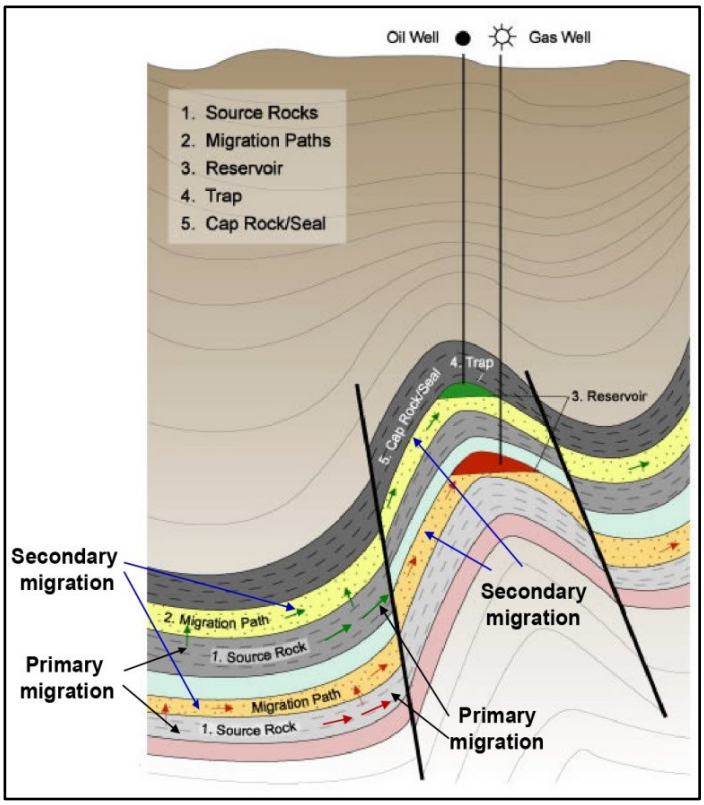

Figure 1.3 Sketch of the migration and trapping processes in a petroleum system.

The *spatial aspects* are related to the geographic and the stratigraphic extent of the petroleum system. The geographic extent is defined at the critical moment. It encompasses a line that puts together the kitchen area for the source rock and all the accumulations that were filled with hydrocarbons generated by that source rock. The stratigraphic extent refers to the span of all the lithological units which includes all the elements within the geographic extent of a petroleum system (Magoon, 1987; Magoon and Dow, 1994; Magoon and Beaumont, 2000).

Results from this work on petroleum system dynamics are presented in 3 scientific papers. Papers 1 and 3 present examples for the petroleum systems evolution in the

Southwestern Barents Sea, including basinal areas (Hammerfest, Bjørnøya and Maud Basins), structural highs (Loppa High) and platforms (Bjarmeland Platform). Detailed information in relation with the possible source rocks present in the area, as well as the generation, migration and accumulation processes are described. Paper 2 includes a geochemical correlation which allowed a much better understanding and a clear definition of the petroleum systems in the area.

1.2.5 Petroleum systems modelling

A ***petroleum system model*** corresponds to a digital data model of a petroleum system in which all the processes that are interrelated and their results can be simulated. In some or most of the cases it is a 3D representation of geological data for a specific area of interest, and it can be done for a single drainage area or for an entire basin (Hantschel et al., 2000; Hantschel and Kauerauf, 2009). On the other hand, ***basin modelling*** is defined by Hantschel and Kauerauf (2009) as a dynamic simulation of the geological processes that take place in a particular sedimentary basin over geological time. The simulation reproduces in several stages or time steps the sedimentation of the stratigraphic sequences in the basin, starting with the oldest layer until the present–day layer. At the same time, geological processes as deposition, compaction, heat flow, petroleum generation, expulsion, migration, and accumulation are calculated and updated at each time step.

The two previous concepts can be combined to produce what is named a ***basin and petroleum system modelling (BPSM)***. A BPSM is performed with the aim of reproducing the evolution of a basin through time, which is being filled with sediments that may eventually generate or contain hydrocarbons. Based on this a BPSM allows therefore the simulation of the hydrocarbon generation process, which at the same time allows to calculate the volume of hydrocarbons available for entrapment, to predict the volumes and locations of accumulations and their properties, as well as the fluid flow (Al-Hajeri et al., 2009).

Several steps have to be followed in order to construct a basin model; they are explained in detail by Al-Hajeri et al. (2009) and Hantschel and Kauerauf (2009), and summarized here:

- Creation of a depth–based structural model of the area of interest, in which a single or multiple petroleum systems in a basin or many basins are to be modeled.
- Description of the deposition chronology and the physical properties of the basin and the identification of post–depositional processes.
- Age assignment process, which relates the present–day horizons and stratigraphic layers with the geologic age of their deposition and/or erosion, in case erosion occurs.
- Identification or definition of the geological facies and their properties. The geological facies are defined as parts of layers/horizons with approximately the same sedimentation environments and properties (Hantschel and Kauerauf, 2009). In BPSM the facies are divided into the *rock facies or lithology*, in which physical properties such as permeability, porosity, thermal conductivity, heat capacity, radiogenic heat production, compressibility and capillary entry pressures are defined; and the *organic facies* such as the total organic carbon (TOC) and hydrogen index (HI), which are assigned only to source rock intervals.
- Input of calibration data. This step includes input of borehole data, as vitrinite reflectance measured in samples taken at different depths in a specific well and the temperature data also collected for the wells during the drilling campaigns. Iterative model calibration is then performed in order to adjust the model and obtain the best matching of the simulated vitrinite reflectance and temperature with the well data.
- Reconstruction of the temperature and heat flow history over geologic time and across the basin or area of interest. This step has to be done by defining the boundary conditions: paleo–bathymetry or paleo–water depth, the sediment–water interface temperatures and the paleo heat–flow.

As previously stated, this study involved the evaluation of the petroleum systems evolution through time in the Southwestern Barents Sea. Since this area has been strongly affected by glaciations during the recent past, the model had to account for the effect of these glaciations in the evolution of the petroleum system, which required a detailed understanding of glacier systems and glaciation processes, which will be briefly explained bellow.

1.2.6 Glaciers and glaciations

Glacier

A ***glacier*** by definition, and in accordance with the U.S. Geological Survey (Molnia, 2014) corresponds to a large and perennial accumulation of ice (Figure 1.4) that is continuously moving under the influence of its own weight and gravity (Hambrey and Alean, 2004; Molnia, 2014).

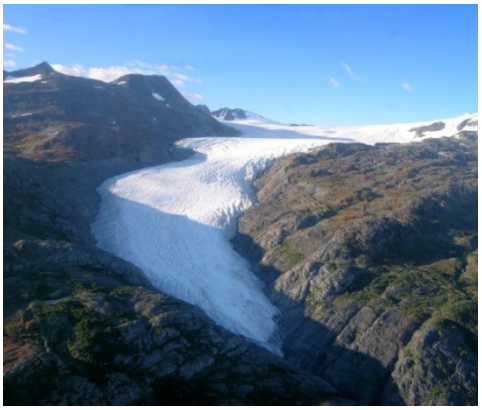

Figure 1.4 Different glacier images. The Arctic Glacier (left; image from Red Orbit - Your universe online, 2011) and the Wolverine Glacier (right; image from USGS, 2014)

Together with sea ice, lake ice, snow cover and ground ice, glaciers and ice–sheets comprise the cryosphere. There is a continuous interaction in terms of mass and energy exchange between the cryosphere and the hydrosphere, atmosphere, biosphere and lithosphere. At the same time, glaciers are very important and sensitive barometers for detection of climate changes, since they are growing and shrinking constantly based on changes of the temperature, snowfall and other factors. The glaciers have been in several cases responsible of the landscape shaping of huge areas of the Earth's surface,

scouring out rock and sediment and promoting the deposition of thick glacial debris accumulations (Benn and Evans, 2010).

Glacier Morphology

There are two ways of classifying the glaciers, the first one is related with their shape and their relationship with the surrounding and underlying topography (Hambrey and Alean, 2004; Benn and Evans, 2010); and the second one has to do with the distribution of the temperature through the glacier body (Hambrey and Alean, 2004).

Glaciers according to topography

Ice–sheets and ice caps

These glaciers submerge the landscape and have major patterns of ice flow, without any dependency on the bed undulations. A size of 50,000 km^2 has been established as the threshold between the two of them, with the ice–sheets being larger, and the ice caps smaller (Hambrey and Alean, 2004; Benn and Evans, 2010). Both ice–sheets and ice caps can discharge through valleys on land, and also directly to the sea. When ice–sheets and caps flow into the sea they form ice streams; which are zones of much faster flow with well–defined boundaries and slow–moving ice (Hambrey and Alean, 2004).

Ice shelves

Ice shelves correspond to ice slabs of a glacier that float on the sea but are still linked to the land. The thickness can range from over 2 km in the inner parts to 200 m at their end where they can actually form icebergs; this process is known as calving (Hambrey and Alean, 2004).

Glaciers according to the temperature distribution

Warm or temperate glaciers

The ice is at the melting point throughout, although a thin surface layer cools below 0°C in winter. Melt–water is abundant in summer and it continues to be discharged by the glacier even in winter in most of the cases. Since they can slide due to the melt–water at the base, they can strongly erode the terrain (Hambrey, 1994; Hambrey and Alean, 2004).

Cold glaciers

The ice is entirely below the melting point. In the upper twelve metres the glacier temperature varies depending on the season, but below this depth the temperature is close to the mean annual air temperature. At the glacier bed the melting point can be reached due to warming coming from the bedrock heat flow; therefore if the glacier is thick enough it will melt at the base resulting in sliding. The cold glaciers in the Arctic produce a lot of melt–water during the short summer time. When they are frozen to the bed then they are relatively passive, without eroding the terrain (Hambrey, 1994; Hambrey and Alean, 2004).

Polythermal glaciers

These glaciers are actually characterized for having the previous two types of glaciers at the same time. The snout and margins are frozen to the bed, but the thicker upper part might be wet at the base (Hambrey and Alean, 2004).

Glacier formation and decay

A glacier is formed when the snow is transformed into ice. This happens when the snowfall during winter time is large enough for some of the snow to last throughout the summer. This cycle is repeated for several years and then due to the pressure exerted by its own weight the snow is transformed into ice. This process of transformation is a long and complex process and depends on the temperature and the depth of the overlying snow. It can take from 50–10 years up to hundreds of years (Hambrey and Alean, 2004).

The changes of snow to ice and movement down–slope are manifested in terms of the balance between accumulation and loss or ablation (Hambrey and Alean, 2004). It is generally agreed that an ice–sheet takes much longer to grow than to decay. On any glacier or ice–sheet the ablation rates are usually three or four times the accumulation rates; therefore decay times should be represented as one–third or one–quarter of growth times. However, rapid ice–sheet decay is recorded in rising global sea–levels (Hambrey, 1994).

Moreover, the growth of ice sheets with large marine–based components was explained by the marine ice transgression hypothesis (MITH), which establishes that the development of a glacier is triggered by the extension of permanent sea–ice into inter–island channels and large marine embayments. The sea–ice then develops into fast ice. The ice cover reflects radiation out to space, thus reducing regional temperatures so that the snow line can sink to sea–level (Benn and Evans, 2010).

Glaciers and sea–level

The growth and decay of glaciers or ice sheets has a profound effect on global sea–level (Benn and Evans, 2010). Basically glaciers store water and delay its return to the ocean. In this sense, when the glaciers expand the oceans are depleted and sea level falls. However, the changes of sea–level through time are also related to other several factors, some of them related to glaciers. The two major types of sea–level changes correspond to those related to the change of the water volume in the ocean and those related with the changes of the elevation of the Earth's crust. Therefore, when considering that sea–level change associated with glaciation it is necessary to consider both, volumetric and isostatic changes. The main concepts to consider here are: glacial eustasy, glacial isostasy and hydro isostasy (Knight, 1999).

Glacial eustasy or glacioeustasy

This term refers to the removal of water from the oceans by glacier expansion and its return by glacier melting. This eustatic response to ice–volume change takes place relatively quick (Knight, 1999; Benn and Evans, 2010).

Glacial isostasy or glacioisostasy

This term is connected with the load placed by an ice–sheet on the Earth's crust, which causes the sinking down of Earth's crust into the underlying mantle, depressing the land surface relative to sea–level (Benn and Evans, 2010). The deglaciation process is associated to the process of removal of the weight of ice; thus leading to an isostatic rebound or recovery of the land (Knight, 1999).

Hydro isostasy

This is the phenomenon of depression of the basin floor into the asthenosphere below, associated to the weight that the volume of water released into the ocean basin exerts onto the crustal floor of the basin. Due to the densities of all the materials involved, the amount of crustal depression is about one–third of the depth of extra water (Knight, 1999).

Physical properties of ice

The characteristics of ice in glaciers depend on: a) properties derived from the atomic/crystalline structure; b) properties based on relationships between crystals, and c) properties derived from the effect of impurities within the ice. Many of the properties are sensitive to environmental conditions. For instance the density of ice is 0.9167g/cm^3 at 0 °C and atmospheric pressure; in the natural environment the maximum density corresponds to 0.9295 g/cm^3. The melting temperature is 0 °C considering atmospheric pressure and decreases with increasing pressure at a rate of 0.072°C per million pascals (Knight, 1999; Benn and Evans, 2010). Table 1.1 shows an overview of the ice properties.

Table 1.1 Some of the physical properties of ice (Knight, 1999).

Property	Value	Unit
Density (glacier ice)	0.84 – 0.917	g/cm^3
Density (pure ice)	0.916 – 0.93	g/cm^3
Volume coefficient of thermal expansion	1.53 x 10^{-4}	1/K
Latent heat of fusion at 0°C/–10°C/–20°C	334/285/241	kJ/kg
Latent heat of vaporization	2800	kJ/kg
Heat capacity	37.7	J/mol.K
Thermal diffusivity at 0°C	2.1 x 10^{-6}	m^2/s
Thermal conductivity at 0°C	2.51	W/m.K

The temperature of a glacier is quite important since it controls its characteristics. This temperature is controlled by heat sources at the surface, at the base and in the interior of the ice, as well as by the heat transfer through the ice. The temperature of the upper

surface of a glacier is determined mainly by local climate and meteorological conditions (elevation, latitude and continentality). Whilst the heat flux at the glacier's base is determined by the geothermal heat input, the heat generated by friction associated to basal sliding, and the heat released by freezing of water or consumed by melting of ice (Knight, 1999).

1.3 Study areas

As well as the understanding of a petroleum system, its elements and the processes that could affect its evolution; it is also important to have a good control and knowledge of the study area that has been considering for this particular PhD study. Therefore, the next sub-sections will present information regarding the exploration history of the area, which is important because it gives information on its potential as a petroleum province. At the same time it is important to know as well the geological evolution and the main processes that could have been developed, such as uplift, erosion and glaciations. The information of the possible petroleum plays established in the Southwestern Barents Sea is also valuable for the understanding of the petroleum potential.

1.3.1 Exploration history

The first licenses in the Norwegian Barents Sea were awarded back in 1979; marking the beginning of the exploration history in the area. The first two exploration wells were drilled in 1980 followed by the discovery of the Alke and Askeladd gas fields in 1981. From 1979 until 1989, 26 licenses were awarded covering a cumulative area of 12,500 km^2. As a result of the work performed in these awarded licenses, 44 exploration wells were drilled by August 1990 in which 15 finds were made with total recoverable resources of 295 billion Sm^3 of gas and 35 million Sm^3 of oil and condensate. From these findings, 11 were made in Lower–Middle Jurassic Sandstones, including all the oil and condensate, three gas findings with some oil in Upper Triassic sandstones and one oil discovery in Lower Cretaceous sandstones. With the exception of the last one, all other discoveries were made in fault bounded structural traps. By 1987, the most explored basin in the Barents Sea was the Hammerfest Basin, where 13 of the 15 discoveries are located. During 1988 and 1989 the entire South Barents Sea was opened

for exploration activities with a total area of 230,000 km^2 (Larsen et al., 1993). In 1989 the exploration activity performed in the Barents Sea area proved that the majority of the oil discoveries have been made in the east, while the biggest gas discoveries were made in the western parts (Johansen et al., 1993).

The exploration results over the last few years have been received with a certain degree of disappointment. However optimism has returned to the area based on the results from a few exploration wells drilled from 2011 to 2014 and the finding of new discoveries like: the Johan Castberg oil and gas (7220/8–1 Skrugard, 7220/7–1 Havis, 7220/7–2S, 7220/7–3S), the gas discovery in well 7220/4–1, the 7120/1–3 oil discovery, the 7225/3–1 (Norvarg) gas discovery, the 7324/8–1 oil discovery (Hoop area), among others. Therefore, this good exploration results over the past three years have brought back the interest in drilling in the Barents Sea. The Hoop area, located to the northwest of the Mercurius High (Figure 1.5), is the northernmost part of the Norwegian Continental Shelf where acreage has been awarded, and a few wells are planned to be drilled in the area during the coming next years. Approximately 390 billion Sm^3 of gas and 210 million Sm^3 of oil have been proven in the Barents Sea by the 31st of December 2012 (Norwegian Petroleum Directorate, 2013). Another important fact is that from July 2011 an effort began with the intention of opening the Barents Sea South–East for petroleum activities. The sea area cover approximately 44,000 km^2, which is bounded to the east by the Russian sector and to west by the open area of the Barents Sea South (Norwegian Petroleum Directorate, 2013).

1.3.2 General description of the study areas

The Barents Sea is a large epicontinental sea bounded by young passive continental margins to the west and north, which were developed during the Cenozoic opening of the Norwegian–Greenland Sea and Eurasia basin (Faleide et al., 1984; Dimakis et al., 1998). The Southwestern Barents Sea contains several basins, highs and platforms (Figure 1.5). Some of these basins and highs are considered as very interesting exploration areas, among them the Loppa High, the Stappen High, the Bjørnøya Basin, the Tromsø Basin, the Nordkapp Basin, and the Hammerfest Basin (Nøttvedt et al.,

1993). The Hammerfest Basin is the best known basin so far since a variety of petroleum systems and discoveries have been done after years of exploration activities, with almost all the accumulations being dominated by natural gas (Johansen et al., 1993; Larsen et al., 1993; Doré, 1995). The well explored Hammerfest Basin and the structural Loppa High represent the main areas of interest of this study, in terms of evaluation of the presence and evolution of the petroleum systems. A brief description of their formation and evolution will follow according with the description made by Gabrielsen et al. (1990) and Larsen et al. (1993).

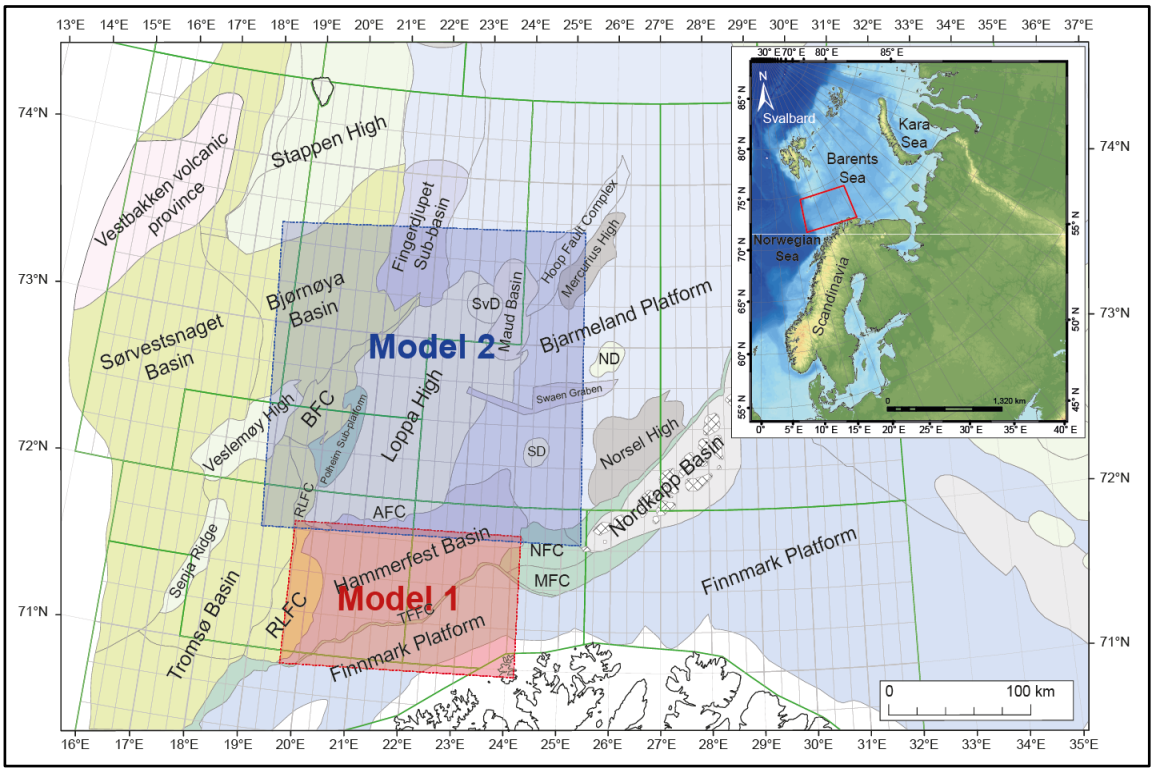

Figure 1.5 The Southwestern Barents Sea. The colored squares represent the areas for which the models were built. Red square corresponds to model 1 presented in papers 1 and 2; and blue square corresponds to model 2 presented in paper 3 (AFC: Asterias Fault Complex; BFC: Bjørnøyrenna Fault Complex; MFC: Måsøy Fault Complex; ND: Nordvarg Dome; NFC: Nyslepp Fault Complex; RLFC: Ringvassøy–Loppa Fault Complex; SD: Samson Dome; SvD: Svalis Dome; SLHFC: Southern Loppa High Fault Complex; TFFC: Troms–Finnmark Fault Complex).

Hammerfest Basin

The Hammerfest Basin is bounded by the Finnmark Platform in the south and by the Loppa High and the Bjarmeland Platform in the north. The basin is separated from the

Finnmark Platform to the south by the Troms–Finnmark Fault Complex and from the Loppa High to the north by the Asterias Fault Complex. Its western limit towards the Tromsø Basin is defined by the southern segment of the Ringvassøy–Loppa Fault Complex, whereas its eastern border has the nature of a flexure against the Bjarmeland Platform (Figure 1.5).

This basin was probably established in the Late Carboniferous. The main subsidence occurred in the Triassic and Early Cretaceous and the basinal development culminated in the Middle Cretaceous, but highly condensed upper Cretaceous and thin lower Paleogene–Neogene shales are also preserved in the basin, in spite of extensive late Paleogene–Neogene uplift. The basin internal structure is characterized by a central dome located along the basin axis and by trending faults; all of these features predominantly reflect Late Jurassic–Early Cretaceous tectonism. The structuring of the Hammerfest Basin has been dominated by extension (rifting), although it has been suggested that the deformational style indicates reactivation by strike–slip in the Late Jurassic to Early Cretaceous.

Loppa High

The Loppa High corresponds to a structural high that has been developed as a response of several phases of uplift and subsidence, which at the same time resulted in tilting and erosion. The boundaries of the high are represented by the Bjarmeland Platform to the east; the Hammerfest Basin to the south and southeast; the Bjarmeland Platform, the Maud Basin and the Fingerdjupet Sub–basin to the north; the Polheim Sub–platform and the Tromsø and Bjørnøya Basins to the west (Figure 1.5).

The Loppa High initially had rift topography during Middle Carboniferous, which was filled by Upper Paleozoic siliciclastic deposits, as well as evaporites and carbonates. During the Late Permian–Early Triassic the structure suffered a tectonic tilting and uplift; this was followed by a gradual onlap during the Early and Middle Triassic. Afterwards a rapid subsidence and the deposition of a thick succession during the Late Triassic occurred. During the Early–Middle Jurassic the high was part of a regional cratonic platform that included the Hammerfest Basin and the Bjarmeland Platform. In

most of the Cretaceous the Loppa High evolved as an island characterized by the formation of deep canyons cutting into the Triassic sequence. This was followed by subsidence and deposition of shales during the Paleogene; most of which were eroded during the uplift phase that took place in the Late Cenozoic. In general, the high as defined today is mainly the result of the Late Jurassic–Late Cretaceous and Late Cretaceous–Paleogene tectonism.

1.3.3 Geological evolution

The Barents Sea is divided into several basins and highs (Figure 1.5) that were active at different stages during the geological history of the area (Nøttvedt et al., 1993). The geological evolution is represented by the formation of these basins due to a series of extensional phases associated to rifting events, from post–Caledonian orogenic backsliding and collapse in Devonian times, to the development of a passive margin during Early Eocene (Faleide et al., 2008).

The geological history of the Barents Sea dates back to the latest Proterozoic when the opening of the Iapetus Ocean began (Berglund et al., 1986). Afterwards, the Caledonian Orogeny started, representing the earliest compressional event associated with the closure of the Iapetus Ocean and the suturing of Greenland against Norway and Spitsbergen, which occurred in the Late Cambrian (Early Paleozoic). This formed the metamorphic basement of the Barents Sea (Berglund et al., 1986; Dengo and Røssland, 1992). The Caledonian structures trend is similar to the trend of many of the extensional basins, which suggests that the Caledonian structures had a fundamental control in the development and location of the major northeast and northwest trending basin–bounding normal faults. Right after the closure of the Iapetus Ocean, in Late Silurian–Early Devonian time, erosion of the Caledonian Orogen took place, which contributed with the deposition of continental clastic sediments, named the Old Red Sandstones (Dengo and Røssland, 1992). During Late Paleozoic several basins associated to rifting episodes were formed between Norway and Greenland and in the western Barents Sea along the NE–SW Caledonian trend. It has been suggested that the main Late

Paleozoic–Early Mesozoic rift episodes took place in Middle Carboniferous, Carboniferous–Permian and Permian–Early Triassic times (Faleide et al., 2008).

The Late Devonian–Middle Carboniferous period was characterized by the initial phase of crustal extension between Greenland and Norway, which produced broad depressions and half graben structures with a deposition of continental (interbedded coarse and fine clastics and coals) and mixed continental–marine clastics, carbonates and evaporites (Figure 1.6) (Dengo and Røssland, 1992; Nøttvedt et al., 1993). The Late Carboniferous–Permian is described as a period of tectonic quiescence (Nøttvedt et al., 1993). The active crustal extension ceased and led to a transition into a sag phase with subsidence. Sedimentation changed from continental to shallow–marine siliciclastic deposition, followed by carbonate and evaporite deposition at the end of the period (Figure 1.6). Salt deposition is interpreted to have occurred in some areas like the Tromsø, Nordkapp, west Bjørnøya and Hammerfest basins (Dengo and Røssland, 1992). During the Late Permian intraplate re–alignments and incipient intracratonic rifting occurred across the Barents Shelf. At this time a relative sea level rise also took place with the deposition of mixed siliciclastics cherts and carbonates (Figure 1.6) (Nøttvedt et al., 1993).

The Early–Middle Triassic is characterized by the interplay between tectonics and eustasy. During this time large amounts of sediments were deposited along the Barents Sea, which contributed with the development of three progradational sedimentary units (Figure 1.6): the Havert, Klappmyss and Kobbe formations (Nøttvedt et al., 1993). This sediment loading triggered the reactivation of some basement–involved normal faults and the increased withdrawal of salt accompanied also by the development of new normal faults (Dengo and Røssland, 1992). On top of this sedimentary package the Snadd Formation was deposited (Figure 1.6), which has an overall upwards coarsening character due to the progradational nature from marine to continental (Nøttvedt et al., 1993).

In the Late Triassic (Carnian) a considerable change in paleogeography took place. The influence of a system of rivers with a northeast–southwest orientation can be suggested

in the central Barents Sea, based on incised valleys observed on seismic. The Fruholmen Formation was deposited during the Late Triassic (Norian), which also has an upwards coarsening character and a progradation of continental facies (shallow marine and deltaic environments; Figure 1.6). This succession is characterized by good quality reservoir sandstones compared to the underlying units. The Late Triassic period terminated with non–deposition, erosion and condensed development across the eastern and northern Barents Sea. Deposition continued to the west of the Loppa High (Nøttvedt et al., 1993).

The Late Triassic–Early Jurassic is represented by a complex interplay of tectonic subsidence and eustatic sea level changes (Berglund et al., 1986). Sedimentation (mainly deltaic) continued in Early Jurassic to the west and partly to the east, with the deposition of the Tubåen, Nordmela and the lower Stø formations (Johansen et al., 1993; Nøttvedt et al., 1993). More marine conditions were established to the northeast at the end of the Early Jurassic due to a sea level rise. Transgression conditions continued into the Middle Jurassic. The Middle Jurassic sedimentary succession is therefore associated to a relative rise in sea–level and has two progradational cycles, represented by the middle and upper Stø Formation. A regional hiatus marks the boundary to the late Middle Jurassic and on top of the unconformity shales were deposited (Nøttvedt et al., 1993). In the Late Jurassic an important tectonic phase developed, with the beginning of repeated block faulting and footwall uplift along the structural highs in the western Barents Sea (i.e. Loppa High); this occurred due to an overall sinistral shear in the region. In terms of sedimentation, the Late Jurassic can be divided into a succession of shale and marly shale corresponding to the Fuglen Formation, on top of which organic–rich shales were deposited corresponding to the Hekkingen Formation (Figure 1.6) (Nøttvedt et al., 1993).

A new crustal extension event between Greenland and Norway (NE Atlantic – Arctic) is recorded during the Late Jurassic–Early Cretaceous with a shifting in the extensional stress field vector to NW–SE. This rifting episode was responsible for the development of several deep Cretaceous basins mainly in the Southwestern Barents Sea (Harstad, Tromsø, Bjørnøya and Sørvestsnaget basins; Figure 1.5). These basins underwent a

quick subsidence and segmentation into sub–basins and highs. Most of the deformation occurred west of the Loppa High (Dengo and Røssland, 1992; Faleide et al., 2008). The Early Cretaceous is represented by faulting and tensional events, combined with relative sea level fluctuations. As a consequence several regional hiatuses and unconformities across the southern Barents Sea were defined (Berglund et al., 1986; Nøttvedt et al., 1993). At this time, the marine shales of the Knurr and Kolje formations were deposited in the basinal areas of the western Barents Sea (Figure 1.6), whereas sandy sediments were locally removed from the structural highs. A sea level fall in Barremian–Aptian was developed and followed by renewed transgression and the deposition of the Kolmule Formation during Aptian–Albian (Figure 1.6). A significant marine transgression occurred during the Late Cretaceous, with the development of the marine succession equivalent to the Kveite and Kviting formations (Nøttvedt et al., 1993).

Breakup in the NE Atlantic during Late Jurassic–Early Cretaceous was preceded by prominent rifting during Late Cretaceous–Paleogene. This rifting phase that occurred between Norway and Greenland was initiated by strike–slip movements, with local and sub–regional truncation and planation of Cretaceous strata along the Greenland – Barents plate boundary. As a consequence pull–apart basins were formed in the Southwestern Barents Sea. The final lithospheric breakup at the Norwegian margin occurred near the Paleocene–Eocene transition (at ~55–54 Ma) and culminated in a period from 3 to 6 Myr of massive magmatic activity and the onset of sea–floor spreading (Nøttvedt et al., 1993; Faleide et al., 2008). In the Late Paleocene shales of approximately uniform thickness were deposited across most of the Southwestern Barents Sea area, which are equivalent to the Torsk Formation (Figure 1.6) and indicates an overall relative sea level rise (Nøttvedt et al., 1993). The Southwestern Barents Sea margin therefore developed during the Eocene opening of the Norwegian–Greenland Sea, first by continent–continent shear and followed by continent–ocean shear (Faleide et al., 2008). Along the Senja and Hornsund Fracture Zones transform movements took place, whereas rifting and creation of new oceanic crust took place along divergent plate boundaries in the Vestbakk Volcanic Province area, between the two transform zones (Nøttvedt et al., 1993).

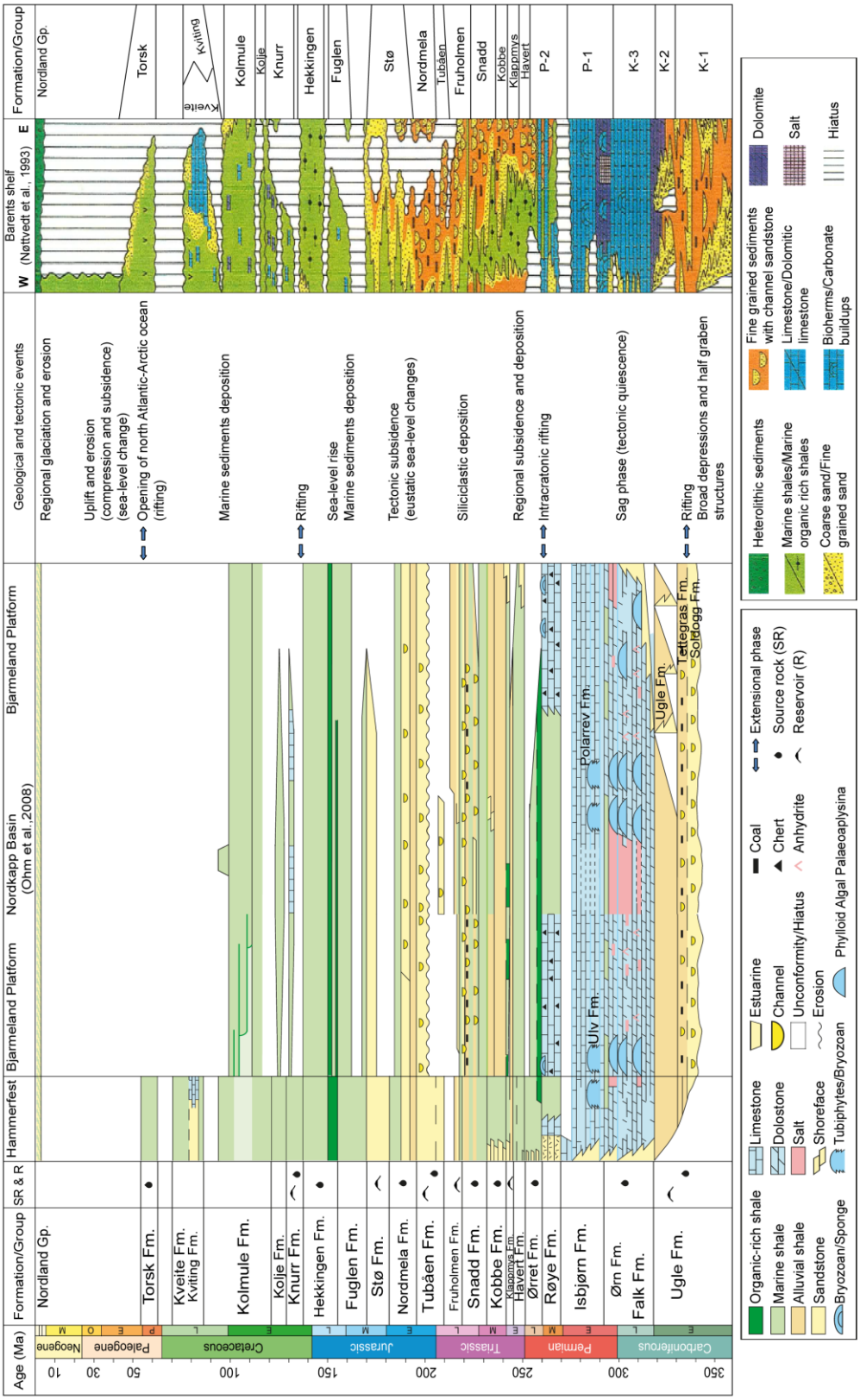

Figure 1.6 General lithostratigraphy of the Barents Sea (adapted from Nøttvedt et al., 1993; Ohm et al., 2008). The potential source rocks (SR) and reservoirs (R) that have been proposed and found in the area, as well as the general overview of the geological and tectonic events are also shown.

Deep marine conditions developed in the Southwestern Barents Sea throughout Eocene time, together with the deposition of submarine fans constituted by sandy sediments (Faleide et al., 2008). Greenland finally rifted away from the Barents plate in Late Paleogene (Early Oligocene) times, the previous sheared margin was transformed into a passive margin; the areas located to the east of the western Barents Shelf were exposed to deep erosion (Berglund et al., 1986; Nøttvedt et al., 1993).

Since about 2.50 Myr, deterioration in the climate of the northern hemisphere occurred and glaciations started to develop in a more regional extent (Vorren et al., 1991; Faleide et al., 1996). In response to the development of these glaciations in the Barents Sea, uplift and glacial erosion and the formation of large submarine fans, filled with glacial deposits in front of bathymetric troughs (western margin of the Barents Shelf) also occurred. On the other hand the uplift and glacial erosion brought as a consequence a regional tilt of the margin (Faleide et al., 2008). Finally a thin layer of sediments (Nordland Group, Figure 1.6) of Late Pliocene to Pleistocene/Holocene age covers most of the Barents Shelf; these sediments are highly compacted due to loading from ice–sheets (Berglund et al., 1986; Dalland et al., 1988).

1.3.4 Uplift and erosion

The Barents Sea has experienced multiple uplift and erosion events since Paleogene times. The major uplift and erosion of the Barents Sea can be related to two important regional events: I) the structural development linked to the rifting, break–up, and subsequent opening of the Norwegian–Greenland Sea during the Oligocene–Miocene, and II) the glacial activity during the Late Cenozoic or Pliocene–Pleistocene time (Berglund et al., 1986; Vorren et al., 1991; Nyland et al., 1992; Riis and Fjeldskaar, 1992; Knutsen et al., 1993; Richardsen et al., 1993; Reemst et al., 1994; Dimakis et al., 1998; Cavanagh et al., 2006).

Pre–Cenozoic erosions have also been reported, while deposition took place in the adjacent lows or basinal areas, like the Hammerfest and Bjørnøya Basins. Nardin and Røssland (1993) and Reemst et al. (1994) reported a couple of uplift and erosion events

from Paleozoic to Early Cenozoic times, which were tectonically controlled. The main areas subjected to uplift were the structural highs, as the Loppa, Stappen and Veslemøy Highs (Reemst et al., 1994). The first erosion event reported by Nardin and Røssland (1993) is between Middle Jurassic and Early Cretaceous, and is associated to the rifting along the western margin of the Barents Sea. It occurred mainly at the crest of the Loppa High and along the southern margin of the Finnmark Platform. Between 100 and 2300 m were removed in the Loppa High with the maximum erosion at the crest towards the western margin of the high. In the Finnmark Platform the maximum erosion is around 1000 m. The sediments originated as a response of this erosion phase are mainly preserved as clastic wedges in the rotated fault blocks located to the sides of the structural highs in the lows or basinal areas, like the Hammerfest and Bjørnøya Basins (Nardin and Røssland, 1993; Reemst et al., 1994). The second period also reported by Nardin and Røssland (1993) is between Late Cretaceous and Early Paleogene which coincides with most of the faulting and folding that occurred to the west of the Loppa High. It has a more regional extension, affecting the entire Finnmark and Bjarmeland Platforms and also the northeast part of Bjørnøya Basin and the Fingerdjupet Sub–basin. The erosion increased northeastwards across the Bjarmeland Platform, where as much as 1200 m were removed. The amount of erosion in the Finnmark Platform is mainly between 100 and 300 m.

Establishing the timing of erosion is in general very important, since this will affect the evolution/development of a petroleum system, regarding the maturation of the source rocks, and the generation, migration and accumulation of hydrocarbons. In the case of the Cenozoic erosion, according to apatite fission track analysis (AFTA) the Oligocene–Miocene uplift and erosion phase followed the maximum burial (around 30 Ma) and apparently had a greater magnitude –by about 500 m– than the Pliocene–Pleistocene phase (Nyland et al., 1992). However, there is an indication that the erosion in the Barents Sea must have been intense and rapid during the last 2.3 Myr in connection with the glaciations of the area. This is based on the observation made in the stratigraphic sequences deposited in the fans present in the western and northern margins of the Barents Sea, which reveals that approximately 2/3 of the sediments, were deposited during this period of time (Dimakis et al., 1998). On the other hand,

Cavanagh et al. (2006) proposed the Quaternary glacial erosion as the most important of the Cenozoic exhumations, since its inclusion into their 2D basin model allowed the best thermal calibration. At the same time sediment biostratigraphic datings of the wedge on the Senja Ridge indicate that a strong erosion event was due to glaciations (Nyland et al., 1992; Riis and Fjeldskaar, 1992).

In the Southwestern Barents Sea, the estimated values of the total Cenozoic erosion derived from different methods and data such as vitrinite reflectance, AFTA, sandstones diagenesis, and mass balance calculations range from 500 to 3000 m, increasing from west to east and to the north and northwest (Berglund et al., 1986; Nyland et al., 1992; Riis, 1992; Reemst et al., 1994; Ohm et al., 2008; Henriksen et al., 2011a).

A regional net erosion map was created by Henriksen et al. (2011a), using available geological and geophysical data. They established that an increase of the net erosion on structural highs may coincide with areas affected by compressional or transpressional tectonic regimes related to the opening stages of the Atlantic and Arctic Oceans. The sedimentary basins show net erosion ranging from 900 to 1400 m. The change along the central axis of the Barents Sea is probably related to a structural trend. Further to the west Henriksen et al. (2011a) suggested a zero line with no net erosion. Riis and Fjeldskaar (1992) interpreted the zero line of no erosion based on seismic. They recognized the erosions to the west based on a seismic reflection which cuts across the seismic stratification in the Late Paleocene and Early Eocene layers. The reflection shows a regional dip to the west that is in accordance with the transition from Opal A to Opal CT (microcrystalline quartz). The dipping of the reflector associated to this diagenetic change may be explained by tilting and erosion after its formation. The deepest level observed for the reflector was assumed to be the level of no erosion and the erosion in the other areas was calculated by difference in the elevation.

Nyland et al. (1992) created as well a regional uplift and erosion map using vitrinite reflectance data from all the wells in the region. Based on this data the least uplift and erosion is observed in the western part towards the Senja Ridge and the Tromsø Basin with erosion amounts between 0 and 500 m. The values increase to about 1000 and

1500 m in the Hammerfest Basin and the Loppa High. On the Finnmark Platform the erosion decreases to the south and east and the estimated amount of erosion is between 1500 and 2000 m. The magnitudes of uplift and erosion also increase towards the north and northwest with more than 2000 m towards the Stappen High and the Bjørnøya Basin. Some other methods have been also used by Nyland et al. (1992) in order to estimate the amount and time of erosion, between them: shale compaction curves, compaction estimates from drilling parameters, fission track analyses and diagenesis of clay minerals. The results from shale compaction curves, fission track analysis and diagenesis of clay minerals are in good agreement with those from vitrinite reflectance regarding the amount of erosion.

1.3.5 Glacial history

Several periods of ice–sheet growth and retreat occurred during the Late Cenozoic. Climate deterioration started in the northern hemisphere at around 2.50 Ma, which resulted in the development of glaciations (Jansen and Sjoholm, 1991; Vorren et al., 1991). Eidvin et al. (1993) observed that there is a correlation between the onset of glacigenic debris deposition in the fans located at the Barents Sea shelf and the cooling and increase in ice volumes for the period between 3.0 and 2.5 Ma. This also correlates with the information associated to the biostratigraphy and radiometric dates studies performed in the deep wells and shallow borings on the Senja Ridge and west of Bjørnøya (Eidvin et al., 1993; Mørk and Duncan, 1993; Sættem et al., 1994; Solheim et al., 1996). From the period in which the glaciations started (between 3.0 and 2.5 Ma) to approximately 1.0 Ma the ice volumes changed predominantly in 41,000 years cycles, indicating that an extensive ice–sheet in large areas was probably not developed. From ~1.0 Ma on the 100,000 years cycles were predominant, therefore a larger ice–sheet development should be expected (Kukla and Cílek, 1996; Mangerud et al., 1996; Solheim et al., 1996).

Knies et al. (2009) developed a glaciation model for the Barents Sea region in which they included three phases of glacial development: the first one corresponds to an initial growth phase between ~3.5 and 2.4 Ma, the second one was defined as a transitional

growth phase between ~2.4 and 1.0 Ma, and the third and last one was defined as a final growth phase with an increase of the glacial scale since ~1.0 Ma. In the first and second phases the ice–sheets were of limited extent with a glacial build–up limited to the land areas in Scandinavia, Novaya Zemlya and Svalbard. For the last phase, the ice–sheet development and extension was larger covering most of the Barents Sea. Knies et al. (2009), reported that during this last phase, there must have been abundant glacial ice and repeated glaciations to the shelf edge, based on the presence of large fan deposits along the western margin of the Barents Sea.

Ingólfsson and Landvik (2013) on the other hand, tried to perform an evaluation of the development of the Late Quaternary Svalbard–Barents Sea glacial history, considering terrestrial and marine observations. In general, they concluded that all the reconstructions made in the area point to the fact that the Svalbard–Barents Sea region was covered by ice–sheets that have reached the shelf edge west of Svalbard. During this time (Late Quaternary) at least four glaciation phases have been recognized by Mangerud et al. (1998). They include an extensive Svalbard–Barents Sea Saalian (marine isotope stage 6 (MIS6)) glaciation, followed by a deglaciation during the Eemian interglacial (MID5e), together with a marine to littoral sedimentation. Also three Weichselian glaciations, which have reached the continental shelf west of Svalbard, and correspond to: the Early Weichselian (around 110 kyr BP, MIS5d), the Middle Weichselian (between 70 and 50 kyr BP, MIS4) and the Late Weichselian (at around 20 kyr BP, MIS2) (Mangerud et al., 1998; Svendsen et al., 2004).

Siegert et al. (2001) constructed two glacial models for the Weichselian, which were named the maximum and minimum model. The maximum model includes four prominent phases of glaciation that become progressively larger from Early Weichselian to Late Weichselian. The first phase corresponds to the Early Weichselian, which is predicted to be around 90,000 years ago. It has a 1.75 km thick ice cap that grew over Scandinavia and a 0.75 km thick ice mass developed from Novaya Zemlya and covering most of the Barents and Kara seas. This ice–sheet decayed approximately 80,000 years ago. The next phase corresponds to the Middle Weichselian. It is represented by an ice growth over 20,000 years to a maximum glaciation 60,000 years ago, where the entire

northern and western Eurasian continental margins were covered by grounded ice. An ice thickness of 1.25 km was reached in the central Barents Sea; while the southern Barents and Kara seas were not covered by grounded ice. Deglaciation of this ice–sheet began around 56,000 years ago until 50,000 years, leaving a small ice cap over Scandinavia that existed for around 20,000 years and corresponds to the third phase. At around 30,000 years ago, the ice–sheet started to grow again to a maximum position; this one corresponds to the last phase modeled by Siegert et al. (2001) and is named Late Weichselian. During this phase the ice thickness over Scandinavia was around 2.75 km, while over the Barents Sea it was around 1.75 km. The fact of having a glaciation over the entire Barents and Kara seas, promoted the development of fast–flowing sediment–transporting ice streams within the bathymetric troughs. Late Weichselian deglaciation started at around 16,000 years ago and was completed by 10,000 years ago. The minimum model includes the same glacial phases; however, reduced ice thickness was considered and also some differences in the areas where the ice–sheet was developed.

Siegert et al. (2001) established at the same time that the peaks of the ice–rafted debris (IRD) are associated to ice–sheet fluctuations and may have occurred over the cycle of ice growth and decay. Based on this, five major phases of deglaciation are recognized during the Weichselian. The IRD events at around 15,000 and 50,000 years BP reflect the deglaciation of two very large ice–sheets.

1.3.6 Petroleum plays in the Barents Sea

A ***hydrocarbon*** or ***petroleum play*** can be defined as a group of several prospects which have the characteristic of sharing similar conditions in relation with the source rock, reservoir and trap (Johansen et al., 1993). A play has also been defined by the Norwegian Petroleum Directorate (2011) as a geographically and stratigraphically delimited area where a specific set of geological factors such as reservoir rock, trap, mature source rock and migration paths exist in order that petroleum accumulations may occur.

In relation with the source rocks, several intervals have been proven in the Barents Sea from Silurian to Cretaceous times (Johansen et al., 1993; Henriksen et al., 2011b). A Silurian to Late Devonian source rock, represented by the Domanik Formation, is more common in the eastern part of the Barents Sea towards the Timan–Pechora Basin, with an extension into the South Barents Basin and towards the west coast of Novaya Zemlya (Johansen et al., 1993; Henriksen et al., 2011b). Carboniferous (Visean) shales and coals have been proven on the Finnmark Platform and in outcrops on Svalbard (Ugle/Tettegras formations, Figure 1.6). Lower Permian evaporites (Ørn Formation) have also some potential as source rocks in the Nordkapp Basin, as well as some Lower Permian shales on Svalbard. In addition, carbonate facies have been developed in the basinal areas which can contribute to hydrocarbon generation (Johansen et al., 1993). The Late Permian (Ørret Formation; Figure 1.6) source rock has been proven in some of the wells in the Nordkapp and Maud Basins, and it is also believed that this source rock is quite well represented in the western areas, being the main contributor of gas for some of the plays (Johansen et al., 1993). The Early–Middle Triassic source rocks (Kobbe and Snadd formations) are best developed to the west in the basinal areas around the Loppa High and in the western part of the Bjarmeland Platform (Henriksen et al., 2011b). The Late Triassic shales have approximately the same distribution as the Middle Triassic source rocks (Johansen et al., 1993). The Upper Jurassic Hekkingen Formation (Figure 1.6) is the source rock with the best quality and also corresponds to the best distributed source rock. It corresponds to shales deposited in an anoxic marine environment over almost the entire area. There are some exceptions where this source rock is not present, mainly in the structural highs and areas affected by uplift and erosion (Johansen et al., 1993; Henriksen et al., 2011b). The Barremian shales (Knurr Formation; Figure 1.6) are the youngest source rocks proven in the Barents Sea, but they are mainly developed in the western areas, since here is where they have higher maturity (Johansen et al., 1993).

Ohm et al. (2008) made an overview of the source rocks in the Barents Sea. They have pointed out to the fact that the most prolific source rock corresponds to the Upper Jurassic Hekkingen Formation as stated before, since it has high values of total organic carbon (TOC), hydrogen index (HI) and hydrocarbon generative potential (S_2 from

pyrolysis Rock–Eval). They also indicated that the Middle to Lower Jurassic shales as well as the shales intervals in the Triassic, Permian and Carboniferous shown to have hydrocarbon generation potential.

Johansen et al. (1993) described in detailed the different petroleum plays present in the Barents Sea, a brief description is presented below:

Paleozoic plays

In the Paleozoic several reservoir rocks are important, which includes carbonates and clastics. Important reservoirs north of the onshore area in the Timan–Pechora basin include the Middle and Upper Devonian clastics, the Upper Devonian to Lower Carboniferous carbonates and the Lower Carboniferous (Visean) to Permian carbonates and clastics (Figure 1.6). In the offshore area of the Pechora block the main discoveries have been made in reservoirs of Carboniferous and Permian age. Towards the southwestern platform areas these reservoirs have not been tested, however they are likely to be present. The traps for this play are mainly related with low relief, fault bounded structural closures. The development of carbonate platforms in most of the Barents Sea during the Upper Carboniferous and Lower Permian give the conditions for the development of good reservoirs. Good clastics reservoirs of the same age could have been developed locally in the area, mainly to the southwest. During the Upper Permian the clastics reservoirs developed, but they are mainly concentrated in the east.

Triassic plays

The Triassic section is characterized by a thick interval and a very complex lithostratigraphy (Figure 1.6) that makes this play a quite complicated one. Some reservoirs have been found to the east in the lower part of the Triassic section. Some other gas discoveries were also made on the Nordkapp Basin margin, in the eastern Hammerfest Basin and in the Snøhvit field within the Lower, Middle and Upper Triassic levels respectively. The main trapping mechanisms correspond to fault structures, large domes and salt tectonics, together with some stratigraphical mechanisms.

Jurassic Plays

The reservoirs are mainly represented by Lower and Middle Jurassic sandstones, which are widespread in the Barents Sea (Figure 1.6). Some Lower–Upper Jurassic sandstones were also developed as reservoirs, but they are mainly concentrated in the North and South Barents Basin areas and offshore Novaya Zemlya. The seal is represented by Upper Jurassic and Lower Cretaceous shales and the trap mechanisms are mainly rotated fault blocks and domes. Some stratigraphic traps might have also been present associated with pinch–outs and onlapping.

Cretaceous Plays

The reservoirs are mainly represented by Lower Cretaceous sandstones (Figure 1.6) with stratigraphic traps, developed close to the structural highs in the western areas. These sandstones have also been developed in the eastern part of the Barents Sea. The trap mechanisms are mainly stratigraphic. In the eastern part the trap mechanisms are represented by drapes over older structural highs as well as stratigraphic traps on the slopes of the basins. The cap rock is represented by Lower Cretaceous shales (Figure 1.6).

Paleogene–Neogene Plays

These plays are developed towards the western margin of the Barents Sea. Good reservoir rocks may have been deposited in some wedges in the vicinity of the highs. However, they have not been tested so far. Several structural traps might have developed in connection with the opening of the Norwegian–Greenland Sea. Some stratigraphic traps can also be considered. The seal is mainly represented by the unconsolidated muds which could have some sealing capacities.

The Norwegian Petroleum Directorate (2011) has also defined for the Norwegian Barents Sea a group of seven petroleum system plays (Figure 1.7): Lower Carboniferous, Carboniferous to Permian, Middle to Upper Permian, Triassic, Lower to Middle Jurassic, Upper Jurassic to Lower Cretaceous and Paleocene–Supra Paleocene. A brief description of these seven plays is presented as well in Table 1.2.

Table 1.2 Main characteristics of the petroleum plays in the Southwestern Barents Sea, compilation from the Norwegian Petroleum Directorate (2011).

Name	Code	Group/Formation	Age	Area	Reservoir rock	Depositional environment	Trap	Source rock
Paleocene – Supra Paleocene	**BPC-1 (Unconfirmed)**	Sotbakken Group (Torsk Formation)	Danian-Chattian	Harstad Basin	Sandstone	Deltaic and shallow marine, submarine fan deposites	Rotated fault blocks and stratigraphic pich-out	Late Jurassic and Cetaceous shales
	BEO-1 (Unconfirmed)		Ypresian-Priabonian	Harstad Basin, Sørvestsnaget Basin and Vestbakken volcanitic province		Shallow marine to moderately deep marine		Cretaceous shale
Upper Jurassic to Lower Cretaceous	**BJU, KL-3**	Adventdalen Group (intra Hekkingen, Knurr and Kolje formations)	Kimmeridgian - Albian	Part of Troms-Finnmark Fault Complex, Polheim Sub-Platform, Ringvassøy-Loppa Fault Complex, Bjørnøyrenna Fault Complex, Veslemøy High, Bjørnøya Basin and southern part of Hornsund Fault Complex	Sandstone	Shallow to moderately deep marine	Stratigraphic pinch-out and occasionally fault dependent	Late Jurassic shale (Hekkingen Formation)
	BKU-1 (Unconfirmed)	Adventalen Group (Kolje and Kolmule formations)	Hauterivian - Albian	Harstad Basin and part of Troms-Finnmark Fault Complex				Cretaceous shale and Late Jurassic shale (Hekkingen Formation)
Lower to Middle Jurassic	**BJL, MJ-5**	Kapp Toscana Group (Tubåen, Nordmela and Stø formations)	Rhaetian-Bajocian	Hammerfest Basin	Sandstone	Fluvial, deltaic, estuarine tidal and shallow marine	Rotated fault blocks and horst structures	Upper Jurassic shale (Hekkingen Formation), with a possible contribution from Triassic shales
	BJL, MJ-6		Hettangian-Bajocian	Troms-Finnmark Fault Complex, Tromsø Basin, Veslemøy High, Bjørnøya Basin, Stappen High				Upper Jurassic shale (Hekkingen Formation), with a possible contribution from older source rocks
	BJL, MJ-7			Bjarmeland Platform and Nordkapp Basin			Rotated fault blocks and horst structures. In the Nordkapp Basin: Stratigraphic traps related to salt diapirs, rotated fault blocks may also occur	Early to Middle Triassic Steinkobbe Formation
Triassic	**BRL, RM-4**	Sassendalen Group (Havert, Klappmyss and Kobbe formations)	Induan-Anisian	Finnmark- and Bjarmeland Platform, Nordkapp Basin and Norsel High	Sandstone	Fluvial, deltaic, shallow marine, tidal and estuarine	Mainly stratigraphic, but also structural (rotated fault blocks and halokinetic)	Upper Devonian – Lower Carboniferous coal (Billefjorden Group), Upper Permian shales (Tempelfjorden Group) and Upper Triassic delta plain shales
	BRL, RM-5			Loppa High, Maud Basin, Mercurius High, Hoop Fault Complex and western part of the Bjarmeland Platform			Stratigraphic	Middle Triassic shale (Botnheia equivalent), Lower Carboniferous coal (Billefjorden Group) and Upper Permian shales (Tempelfjorden Group)
	BRU-1	Kapp Toscana Group (Snadd Formation)	Ladinian-Early Norian	Finnmark- and Bjarmeland Platform, Nordkapp Basin and Norsel High			Stratigraphic (rotated fault blocks and halokinetic)	Upper Devonian – Lower Carboniferous coal (Billefjorden Group), Upper Permian shales (Tempelfjorden Group) and Upper Triassic delta plain shales
	BRU-2			Loppa High, Maud Basin, Mercurius High, Fingerdjups Sub-basin, Veslemøy High, parts of Bjørnøya Basin, Stappen High, Bjørnøyrenna Fault Complex, Hoop Fault Complex and western part of Bjarmeland Platform				Middle Triassic shale (Botnheia equivalent), Lower Carboniferous coal (Nordkapp Formation), Upper Permian shales (Tempelfjorden Group) and Lower Permian marls (Tyrellfjellet Member equivalent)

Table 1.2 (Continue) Main characteristics of the petroleum plays in the Southwestern Barents Sea, compilation from the Norwegian Petroleum Directorate (2011).

Name	Code	Group/Formation	Age	Area	Reservoir rock	Depositional environment	Trap	Source rock
Middle to Upper Permian	BPM,PU-4 (Unconfirmed)	Bjarmeland Group (Ulv, Polarrev and Isbjørn formations) and Tempelfjorden Group (Røye Formation)	Sakmarian-Artinskian	Finnmark Platform	Limestones and dolomites	Marine, temperate water	Stratigraphic, but also a combination of stratigraphic and structural	Lower Carboniferous coal (Billefjorden Group), Upper Permian shales (Tempelfjorden Group) and Middle Triasic shales (Botnheia equivalent)
	BPM,PU-5 (Unconfirmed)			Loppa High				
	BPM,PU-7 (Unconfirmed)	Miseryfjellet Formation	Late Cisuralian-Guadalupian	Stappen High	Mixed siliciclastic and bioclastic strata, partly silisified	Marginal to shallow marine		Lower Carboniferous coal and carbonaceous shales (Billefjorden Group), Lower Permian marls (Tyrellfjellet Member equivalent), Upper Permian shales (Tempelfjorden Group)
	BPU-4 (Unconfirmed)	Tempelfjorden Group (Røye Formation)		Finnmark Platform	Silisified carbonates and sandstones	Marine, temperate water		
Carboniferous-Permian	BCU,PL-3 (Unconfirmed)	Gipsdalen Group (Falk and Ørn formations)	Late Bashkirian-Late Sakmarian	Finnmark Platform	Limestones and dolomites	Carbonate buildups in shallow marine	Stratigraphic, but a combination of stratigraphic and structural cannot be excluded	Upper Devonian-Lower Carboniferous shales, Lower Carboniferous coal (Billefjorden Group), Upper Permian shales (Tempelfjorden Group), Middle Triassic shales (Botnheia equivalent)
	BCU,PL-4 (Unconfirmed)			Loppa High and Polheim Sub-platform				Lower Carboniferous coal (Billefjorden Group) and Upper Permian shales (Tempelfjorden Group)
	BCU,PP-4 (Unconfirmed)	Gipsdalen Group (Falk and Ørn formations) and Tempelfjord Group (Røye Formation)	Late Sakmarian - Wordian	Finnmark Platform	Sandstone	Mostly marginal to shallow marine, with alluvial and fluvial inputs in the Carboniferous		Upper Devonian-Lower Carboniferous shales, Lower Carboniferous coal (Billefjorden Group), Upper Permian shales (Tempelfjorden Group)
	BCU,PP-5 (Unconfirmed)			Loppa High				Upper Devonian-Lower Carboniferous shales, Lower Carboniferous coal (Billefjorden Group), Upper Permian shales (Tempelfjorden Group) and Middle Triassic shales (Botnheia equivalent)
	BCU,PP-7 (Unconfirmed)	Gipsdalen Group (Landnørdings-vika, Kapp Kåre, Kapp Hanna and Kapp Duner Formations)	Middle Bashkirian - Late Wordian	Stappen High				Upper Devonian-Lower Carboniferous shales, (Norhamna Member, Kapp Harry Member), Lower Permian organic marls (Kapp Dunér Formation equivalent)
Lower Carboniferous	BCL-3 (Unconfirmed)	Billefjorden Group (Blærerot, Tettegras and Soldogg formations)	Tournaisian - Visean	Finnmark Platform	Sandstones and conglomerates	Fluvial and alluvial, river and floodplain deposits	Structural and stratigraphic	Upper Devonian – Lower Carboniferous coal and carbonaceous shales from the Billefjorden Group
	BCL-4 (Unconfirmed)			Loppa High, Polheim Sub-Platform and Stappen High				

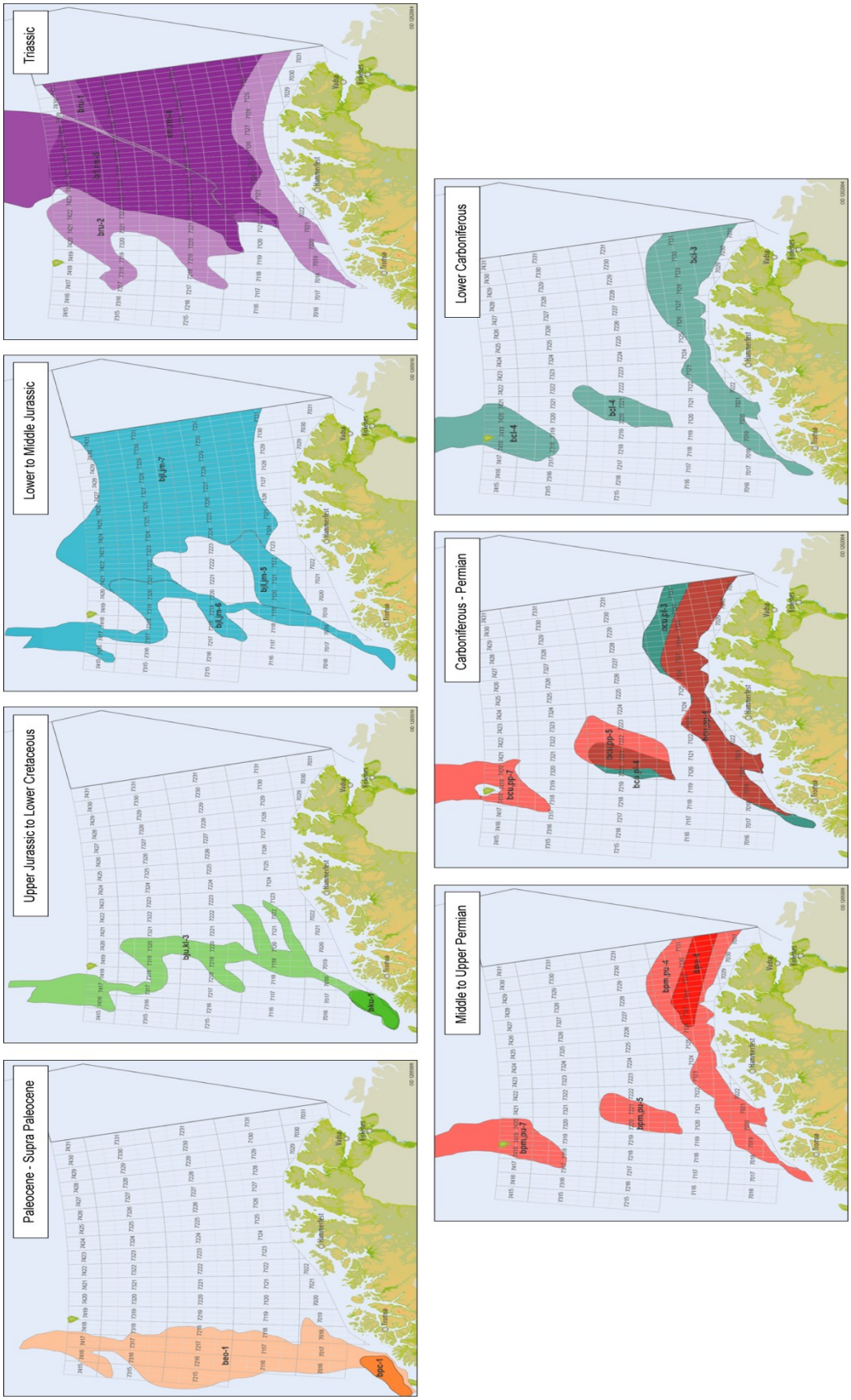

Figure 1.7 Geographical distribution of the petroleum plays in the Southwestern Barents Sea (adapted from Norwegian Petroleum Directorate, 2011).

2 Data and methods

2.1 Petroleum system model building workflow and input

In order to achieve the goals of this study, two petroleum system models were developed which have been shown and described in papers 1 and 3. The first one corresponds to the model with focus on the Hammerfest Basin and the second was a model focusing on the Loppa High, which also includes other relevant areas important for petroleum exploration (Figure 1.5).

The Schlumberger software PetroMod is a petroleum systems modelling software that integrates seismic, well and geological information in order to model the evolution of a sedimentary basin. The modelling includes the source and timing of hydrocarbon generation, migration routes, quantities, and hydrocarbon type in the subsurface or at surface conditions. The 3D petroleum system modelling of the two study areas previously mentioned was done using the PetroMod v.11 ®. The general geometry of the modeled areas and the main sequences are represented by 16 regional structural maps, which were derived from seismic interpretation and provided by Lundin Norway AS. These maps correspond to the top or base of the main stratigraphic sequences, from the Late Permian (Ørret Formation) to the current seabed (Figure 2.1). The maps were edited and limited to the specific areas of interest as shown in Figure 2.1.

The input definitions included for the building of the models correspond to:

- The age assignment of each stratigraphic unit (Table 2.1); this also includes the definition of erosion and hiatus events.
- Definition and assignment of the predominant lithologies and facies variation (vertically and horizontally). The specific lithologic properties like thermal conductivity, radiogenic heat, heat capacity, compaction behaviour and permeability are defined by default by the software (Table 2.2).
- Definition of the petroleum system elements (source, reservoir, seal and overburden rocks), the total organic carbon (TOC), the hydrogen index (HI) and the kinetic models for petroleum generation and cracking (Table 2.3).

- Definition of the boundary conditions corresponding to heat flow, paleo–water depth and sediment–water interface temperatures.
- Creation and assignment of erosion maps and definition of the glacial events (ice thickness maps and their evolution through time).

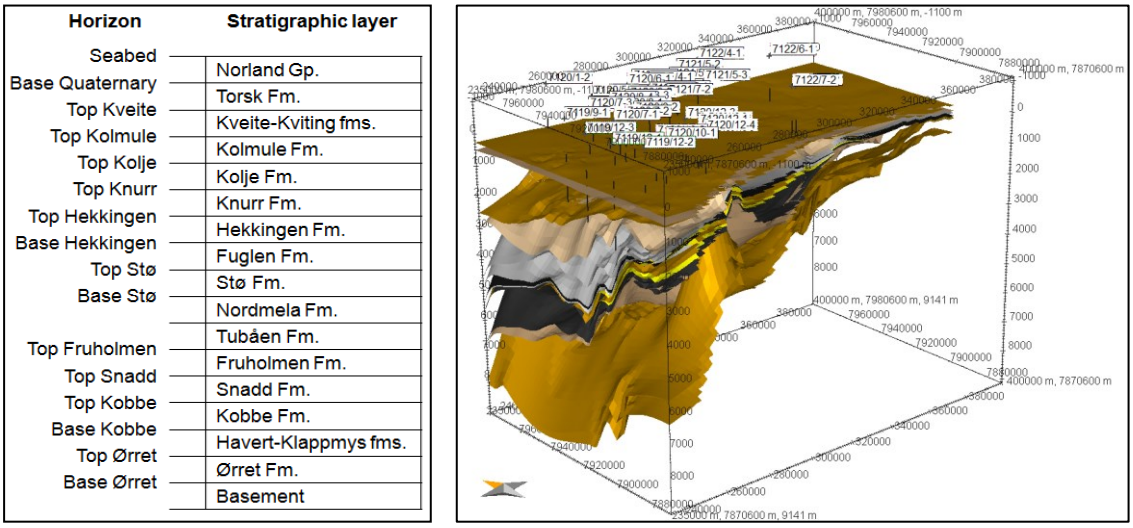

Figure 2.1 Identification of the structural maps (left) provided by Lundin Norway AS and their 3D view for the study area of model 1 (right).

Table 2.1 Age assignment of each stratigraphic unit and also of the erosion events.

Name	Deposition age from (Ma)	Deposition age to (Ma)	Erosion age from (Ma)	Erosion age to (Ma)
Quaternary	0.01	0.00		
Oligo-Miocene (manuel layer)	**40.00**	**30.00**	**30.00**	**15.00**
Plio-Pleistocene (manual layer)	**52.00**	**40.00**	**2.50**	**0.01**
Torsk	65.50	52.00		
Kveite-Kviting	96.60	65.50		
Kolmule	120.00	96.60		
Kolje	130.00	120.00		
Knurr	140.20	130.00		
Hekkingen	155.60	140.20		
Fuglen	167.70	155.60		
Stø	184.00	167.70		
Nordmela	196.50	184.00		
Tubåen	200.00	196.50		
Fruholmen	210.00	200.00		
Snadd	237.00	210.00		
Kobbe	245.00	237.00		
Havert_Klappmys	260.00	245.00		
Ørret	265.00	260.00		
Basement	266.00	265.00		

Table 2.2 Description of the lithology used for each of the layers (including the ice–sheet) and the respective properties.

Name	Lithology	Thermal conductivity (W/m/K)		Rediogenic heat			Heat capacity (kcal/kg/K)		Mechanical properties		Permeability
		at 20°C	at 100°C	U (ppm)	Th (ppm)	K (%)	at 20 °C	at 100°C	Density (kg/m^3)	Initial porosity (%)	[log(mD)]
Nordland Gp.	Siltstone (organic lean)	2.05	1.99	2.00	5.00	1.00	0.22	0.25	2720	55	0.71
Torsk Fm.	Shale (organic lean, typical)	1.70	1.74	3.70	12.00	2.70	0.21	0.24	2700	70	-1.00
Kveite-Kviting fms.	Siltstone (organic lean)	2.05	1.99	2.00	5.00	1.00	0.22	0.25	2720	55	0.71
Kolmule Fm.	Shale (organic lean, silty)	1.77	1.79	3.00	11.00	2.60	0.21	0.24	2700	67	0.50
Kolje Fm.	Shale (typical)	1.64	1.69	3.70	12.00	2.70	0.21	0.24	2700	70	-1.00
Knurr Fm.	Shale (typical)	1.64	1.69	3.70	12.00	2.70	0.21	0.24	2700	70	-1.00
Hekkingen Fm.	Shale (organic rich, 8% TOC)	1.20	1.37	10.00	11.00	2.90	0.21	0.25	2500	70	-1.00
Fuglen Fm.	Shale (organic lean, siliceous, typical)	1.90	1.88	2.00	4.50	2.00	0.21	0.24	2710	70	1.30
Stø Fm. 01	Sandstone (typical)	3.95	3.38	1.30	3.50	1.30	0.20	0.24	2720	41	4.33
Stø Fm. 02	Siltstone (organic lean)	2.05	1.99	2.00	5.00	1.00	0.22	0.25	2720	55	0.71
Nordmela Fm.	Siltstone (organic lean)	2.05	1.99	2.00	5.00	1.00	0.22	0.25	2720	55	0.71
Tubåen Fm.	Sandstone (clay poor)	5.95	4.85	0.70	2.30	0.60	0.20	0.23	2700	42	4.84
Fruholmen Fm.	Siltstone (organic rich, 2-3% TOC)	2.00	1.96	2.50	6.50	2.00	0.22	0.26	2700	55	0.71
Snadd Fm.	Siltstone (organic rich, 2-3% TOC)	2.00	1.96	2.50	6.50	2.00	0.22	0.26	2700	55	0.71
Kobbe Fm.	Siltstone (organic rich, 2-3% TOC)	2.00	1.96	2.50	6.50	2.00	0.22	0.26	2700	55	0.71
Havert-Klappmys fms.	Shale (organic lean, silty)	1.77	1.79	3.00	11.00	2.60	0.21	0.24	2700	67	0.50
Ørret Fm.	Siltstone (organic lean)	2.05	1.99	2.00	5.00	1.00	0.22	0.25	2720	55	0.71
Basement	Basement	2.72	2.35	0.00	0.00	0.00	0.19	0.22	2750	5	-
Ice	Ice-sheet	2.22 (***0 °C***)	2.39 (***-20 °C***)	0.00	0.00	0.00	0.49 (***0 °C***)	0.46 (***-20 °C***)	917	1	0.00

Table 2.3 Petroleum system elements definition and source rock properties.

Name	Petroleum system element	TOC (%)	HI (mgHC/gTOC)	Kinetic model
Nordland Gp.	Overburden rock			
Torsk Fm.	Overburden rock			
Kveite-Kviting fms.	Overburden rock			
Kolmule Fm.	Overburden rock			
Kolje Fm.	Overburden rock			
Knurr Fm.	Overburden rock			
Hekkingen Fm.	Source rock	10	300	14-Components with secondary cracking
Fuglen Fm.	Seal rock			
Stø Fm. 01	Reservoir rock			
Stø Fm. 02	Overburden rock			
Nordmela Fm.	Overburden rock			
Tubåen Fm.	Reservoir rock			
Fruholmen Fm.	Overburden rock			
Snadd Fm.	Source rock	2	150	14-Components with secondary cracking
Kobbe Fm.	Source rock	3	200	14-Components with secondary cracking
Havert-Klappmys fms.	Underburden rock			
Ørret Fm.	Underburden rock			

Additionally, 48 wells (33 for model 1 and 15 for model 2) were included. The vitrinite reflectance (VR) measurements and temperature (T) data from these wells were collected and also considered as part of the input in order to achieve the model calibration. The quality of the data was checked using linear regressions (R^2), which are shown in Figure 2.2.

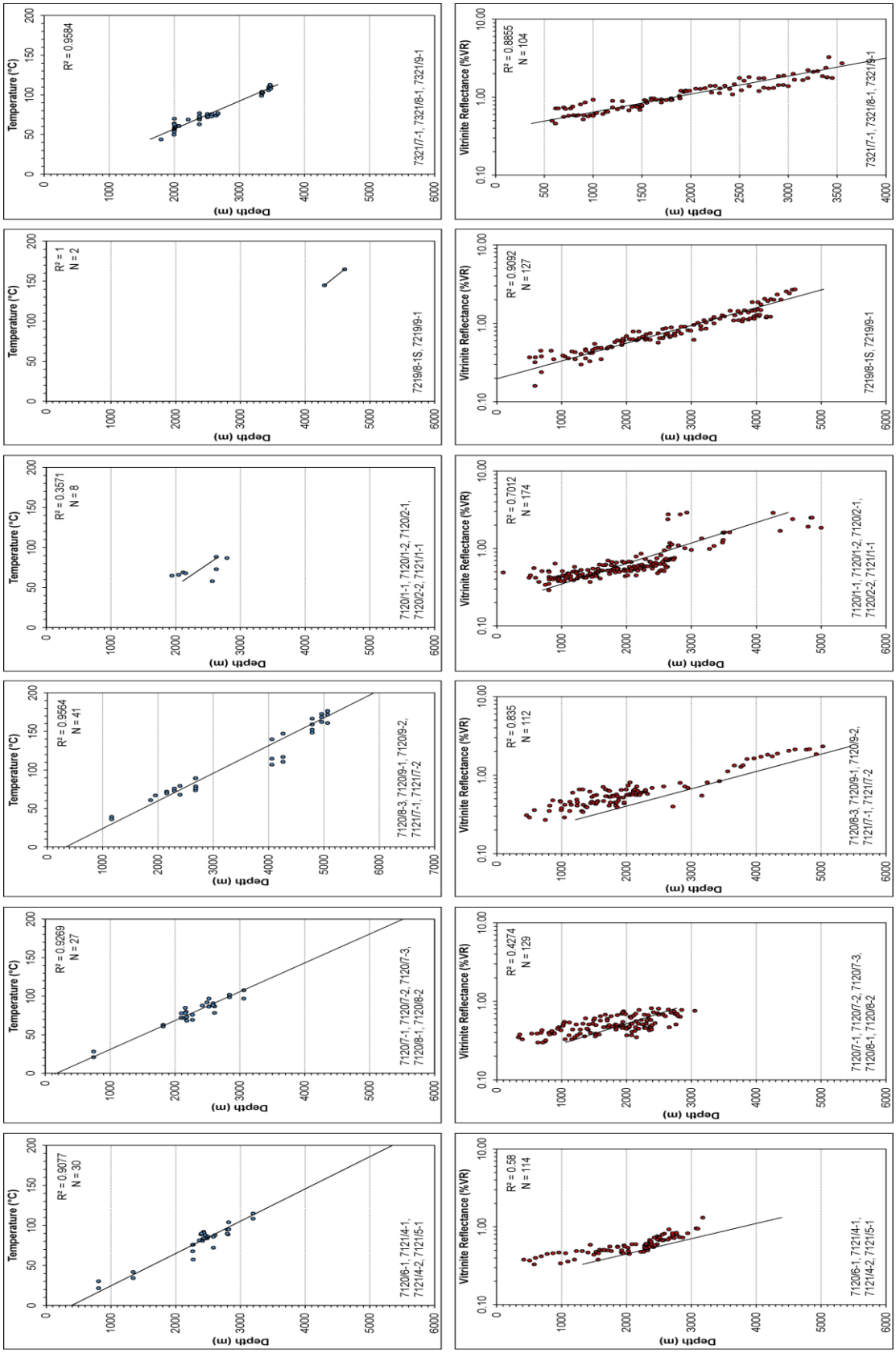

Figure 2.2 Quality control of the temperature data and vitrinite reflectance measurements for several groups of wells in the two modelled areas; based in the linear regressions.

In the following sections more details on the individual input variables used for the building of the two models are presented.

2.1.1 Lithology and petroleum system elements definition

The chronostratigraphy was established based on the International Geologic Time Scale (Gradstein et al., 2005; Ogg et al., 2008; International Commision on Stratigraphy, 2010) and the lithology assignment for each unit (Table 2.2) was done after the revision of the information/description of each stratigraphic unit considered in the models, which is available on both well data (Norwegian Petroleum Directorate, 2009) and published work (Gabrielsen et al., 1990; Ohm et al., 2008). No lateral or vertical facies changes were taken into account for the different stratigraphic units, except for the main reservoir the Stø Formation, where a lateral facies variation was introduced in order to have a better approximation of the reservoir facies distribution (i.e. the effective porous carrier beds as compared to non–carrier silty and shaly intervals of the same formation), the drainage areas and the migration pathways.

Regarding the petroleum systems it was considered, for both models, the Upper Jurassic Hekkingen Formation and the Triassic Snadd and Kobbe formations as the main source rocks (Table 2.3). Older source rocks were not considered since the maps deeper than the Ørret Formation, which only represent the upper part of the Permian, were not available for this study. In order to develop this first 3D modelling approach of the area it was necessary to establish some assumptions, which are: 1) homogeneous facies distribution within the individual source rock layers. 2) The whole layer (total thickness) is considered as a source rock interval. In this sense, it is important to mention that the Hekkingen Formation source rock has an average thickness of approximately 60 m in the western and northern part of the basin where the kitchen area is located; while the Triassic Snadd and Kobbe formations have average thicknesses around 800 and 400 m, respectively. However, even though these thicknesses appear large, it must be considered that the source rock quality and potentials are low. 3) The TOC and HI values (Table 2.3) were constant in every given source rock layer and

correspond to the average of the values reported in previous studies (Berglund et al., 1986; Linjordet and Grung-Olsen, 1992; Ohm et al., 2008).

In terms of the reservoirs, it is well known that the largest proportion of the hydrocarbons proven to date in most of the Southwestern Barents Sea is contained in the Jurassic strata. The major discoveries (about 85%) are in the Lower–Middle Jurassic sandstones of the Stø Formation (Doré, 1995). In addition, the Tubåen Formation has also some reservoir potential as reported by Berglund et al. (1986). Therefore, these were the two reservoir units considered. The seal rocks are mainly represented by two shale formations: the Fuglen and the Hekkingen formations.

2.1.2 Kinetic models

Hydrocarbon generation was simulated using a database of phase–predictive compositional kinetics (di Primio and Horsfield, 2006), consisting of 14 components and including secondary cracking (Figure 2.3). This type of compositional kinetic model is termed "**PhaseKinetics**". The particular compositional kinetics used in this study for both models was measured on samples of the main source rocks of the Barents Sea. The kinetic dataset was provided by GeoS4 GmbH–Germany. The PhaseKinetics approach links the source rock organic facies to the petroleum type it generates; this is done using a combination of open– and closed–system pyrolysis techniques. Bulk kinetic and compositional information is acquired first, then gas compositions are tuned based on a GOR–gas wetness correlation from natural petroleum fluids, and finally the corrected compositions are integrated into a 14–component compositional kinetic model (C_1, C_2, C_3, *i*–C_4, *n*–C_4, *i*–C_5, *n*–C_5, C_6, C_7–C_{15}, C_{16}–C_{25}, C_{26}–C_{35}, C_{36}–C_{45}, C_{46}–C_{55} and C_{55+}, the carbon chain length ranges are named pseudo–compounds, e.g. C_7–C_{15} is also called Pseudo C_{10}), which allows the prediction of the different petroleum properties. Moreover, the heavier components or those with long carbon chains, which are grouped from Pseudo C_{10} to Pseudo C_{60+}, can be subjected to secondary cracking (depending on the temperature regime that is modelled), with the assumption that the only compound generated is methane. The assumption that methane is the main product generated by secondary cracking is supported by natural data as reported by di Primio et al. (2011).

On the other hand, the kinetics of this oil–to–gas cracking reaction is based on those of (Pepper and Corvi, 1995a, b). It is important to note that the calculation of petroleum phase behaviour under the subsurface conditions, after petroleum migration and entrapment, is possible using these methods in combination with the basin modelling techniques.

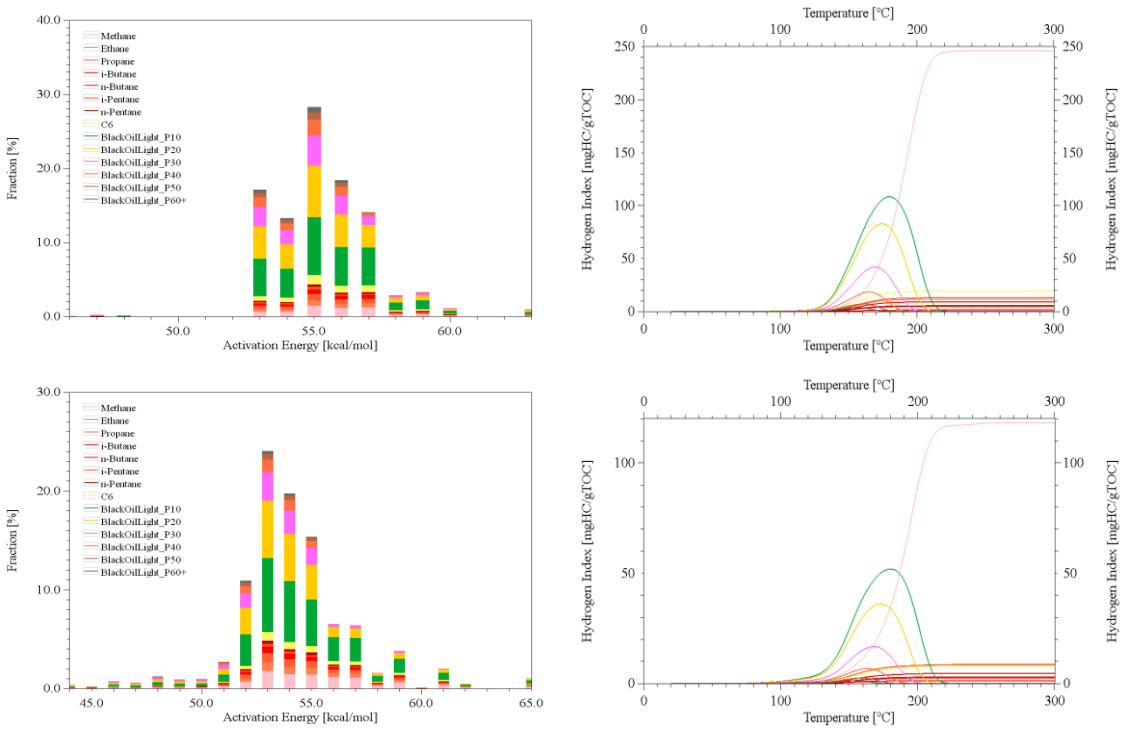

Figure 2.3 Activation energy (left) and generation curves (right) of the PhaseKinetics models used for the Upper Jurassic Hekkingen Formation (top) and the Triassic Snadd and Kobbe formations (bottom). Note that secondary cracking is also considered after approximately 150 °C (generation curves).

2.1.3 Definition of the boundary conditions

Heat flow

One of the key elements when performing a 3D petroleum system modelling is the reconstruction of the thermal history and for this to be considered is necessary to define the basal heat flow evolution. According to Skogseid et al. (2000) and Reemst et al. (1994), the Barents Sea has been influenced by four phases of lithospheric stretching: Devonian–Carboniferous (375–325 Ma), Triassic (245–241 Ma), Jurassic–Cretaceous (157–97 Ma), and Paleocene–Early Eocene (60–50 Ma). With the exception of the

Triassic (corresponding to a broad regional subsidence), these phases are associated to rifting events where heat flow is expected to have been higher as compared to the present–day value. The stretching factors (β) for these four phases are between 1.4 and 1.6 (Reemst et al., 1994), which correspond to heat flow peaks between approximately 60 and 80 mW/m^2 (Hantschel and Kauerauf, 2009). Therefore, considering the premise of a heat flow maxima or an increase in the total magnitude during rifting, followed by decay to a background value, a variable heat flow model from Paleozoic to Cenozoic was developed in this study (Figure 2.4), which at the same time provides the basis for the thermal history calibration. Specifically, the heat flow was assigned taking into account three elevated heat flow events, associated with the regional subsidence that took place in the Barents Sea (250 Ma), the rifting phases (140 and 65 Ma), and a fourth heat flow increase (around 25 Ma) related to neo–tectonics and compressional deformation (Fjeldskaar et al., 2000). This last high value was considered in connection with the local subsidence of the area following the same interpretation made by Reemst et al. (1994), in which they established a lithospheric stretching event associated to the regional Triassic subsidence, as previously mentioned. Mareschal (1987) also considered that there is a heat flow peak associated to high subsidence rates in intra–continental basins and passive margins.

The background heat flow value previously mentioned corresponds to the present–day heat flow reported in the literature for the Barents Sea. Published heat flow maps (Sundvor and Eldholm, 1992; Sundvor et al., 2000) reveal that the average landward value on the marginal escarpments is 57 mW/m^2. Shallow drill hole measurements yield values from 54 to 74 mW/m^2 (Sundvor and Eldholm, 1992; Sundvor et al., 2000). Cavanagh et al. (2006) indicated, based on their maturity model, that values between 60–65 mW/m^2 are required at maximum burial in their modeled area in the Hammerfest Basin in order to match vitrinite reflectance data.

Heat flow maps were created for each of the modelled areas with specific values between 53 and 92 mW/m^2 (Figure 2.4) and assigned to different time steps in order to reproduce the heat flow history shown in the trend in Figure 2.4. The heat flow patterns

shown in the maps for the two modelled areas correspond to the best heat flow distribution, since a good calibration was achieved using them.

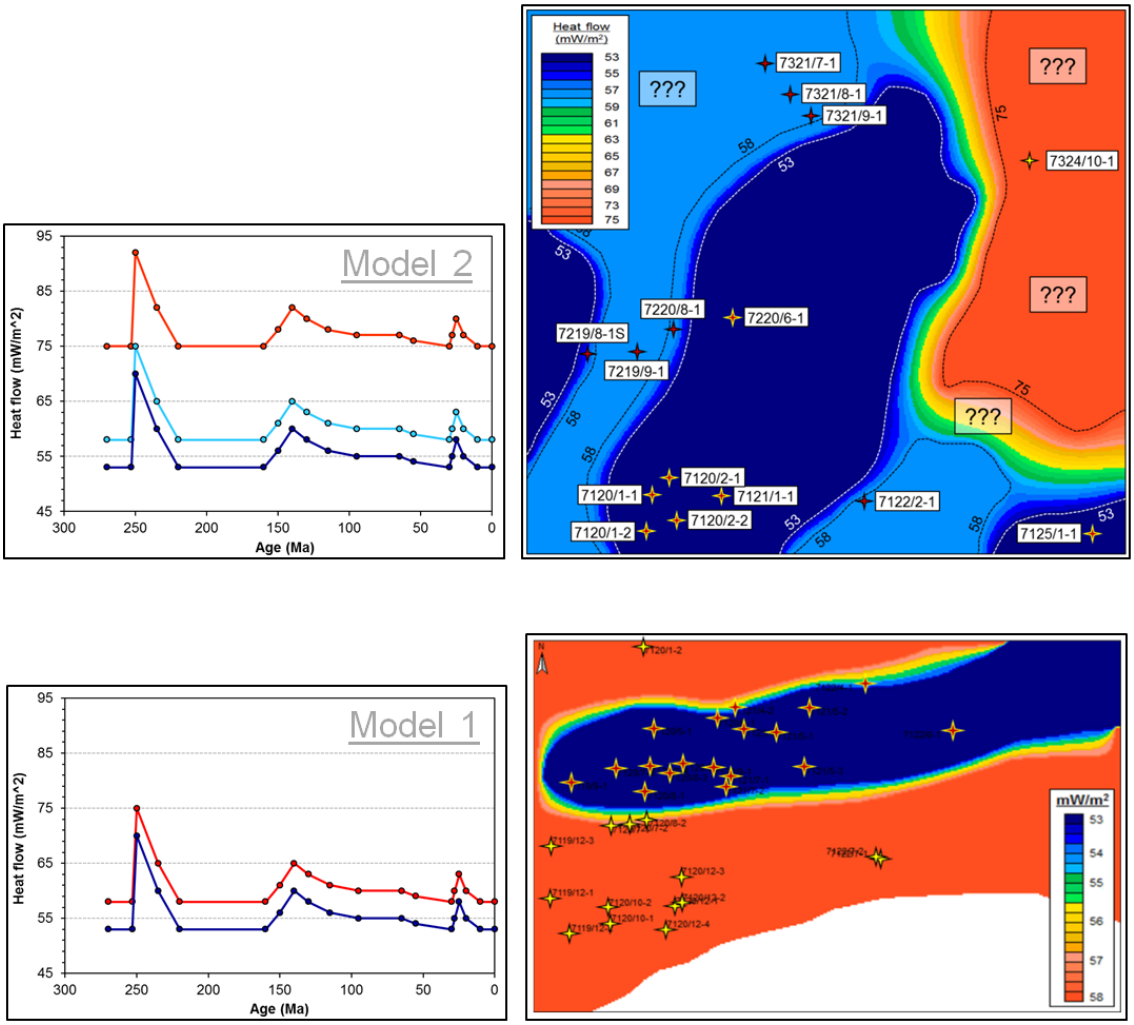

Figure 2.4 Heat flow history trends (left) and maps (right) used for model 1 (bottom) and model 2 (top). The dots shown in the trends correspond to the time for which a heat flow map was created with that specific value.

A sensitivity analysis was performed for this study, considering three heat flow history scenarios: minimum, medium and maximum. For the minimum and maximum scenarios the values of the medium trend were increased and decreased by 8 mW/m^2 (model 1) and 10 mW/m^2 (model 2).

Sediment–water interface temperature (SWIT)

The upper–boundary condition of heat transfer in sedimentary basins is given by the temperatures either at the sub–aerial surface or at the sediment–water interface, and is affected by the water depth, the paleo–geographic position and oceanic currents (Yalçın et al., 1997). For this work, two trends were created and used with the boundary between them being associated to the onset of the glaciations. The pre–glacial (from Late Paleozoic to Pleistocene) SWIT values are between 25 and 10°C (Figure 2.5), which were assigned based on the time–latitude diagram of (Wygrala, 1989).

The upper–boundary thermal condition during the Pleistocene glacial–interglacial periods is represented by the temperature trend shown in Figure 2.5. The SWIT for the interglacial periods was assumed to be around 3°C, since temperatures around this magnitude have been proposed for these stages (Siegert et al., 2001; Archer et al., 2004). On the other hand, the upper–thermal boundary for the glacial periods corresponds to the temperature at the interface between the sub–aerial ice–sheet and the atmosphere. Mean annual surface temperatures from numerical ice–sheet modeling range between –16 and –35 °C for ice thickness between 750 and 1000 m (Siegert and Marsiat, 2001). In this work, values of –15 °C were considered for an ice thickness around 500 m and –45 °C for ice thickness of ~1750 m (Figure 2.5). By using these values temperatures between 0 and –1 °C were then obtained at the interface ice–sediment. These temperatures at the ice–base are calculated by the software based on the ice thickness and its thermal properties as well as on the heat flow. The present–day SWIT was assumed to be 6 °C; this is based on benthic foraminiferal composite oxygen isotope records (Archer et al., 2004; Mienert et al., 2005) and the annual temperature for the Southwestern part of the Barents Sea (Loeng, 1991; Henrich and Baumann, 1994; National Oceanographic Data Center, 2011).

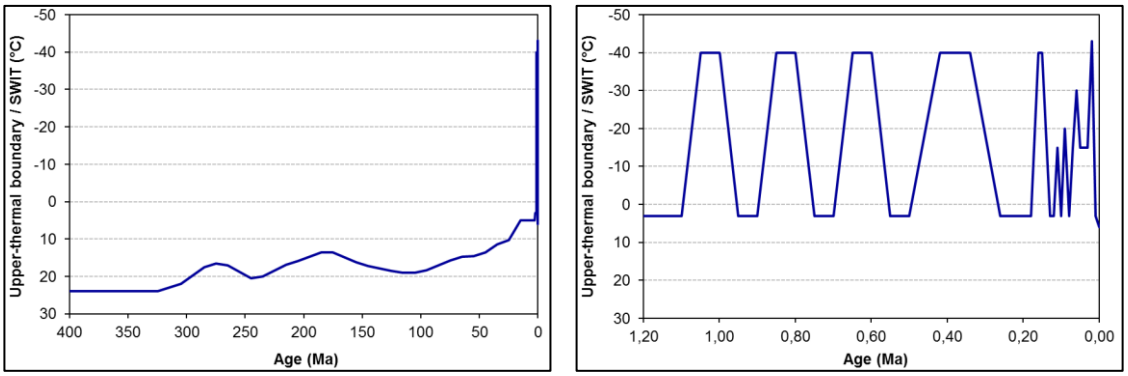

Figure 2.5 Definition of the sediment–water interface temperature (SWIT) trend, based on the time–latitude correlation of surface temperatures of Wygrala (1989) for the period before glaciation (left). Upper–boundary thermal and/or SWIT for the glacial–interglacial periods (right)

Uplift and erosional events

In section 1.3.4 a detailed explanation of the uplift and erosion events that took place in the Barents Sea was already presented. In this section the focus is on how these erosion events were implemented in the two models built for this work. The total Cenozoic erosion was divided into the two erosional events previously described, which are: The Oligocene–Miocene erosion phase associated to tectonic uplift and considered to have happened in both models between 30 and 15 Ma; and the Pliocene–Pleistocene phase associated to the glaciations (between 2.50 and 0.01 Ma). The erosion maps published in Nyland et al. (1992); Riis (1992); Riis and Fjeldskaar (1992); Dimakis et al. (1998); Ohm et al. (2008); Henriksen et al. (2011a) show only the total eroded thickness during the Cenozoic. In this study the total erosion was subdivided into the two episodes of interest mentioned above. Since model 1, corresponding to the Hammerfest Basin (paper 1), was the first approximation that has been done so far with regard to the fact of splitting and evaluating the erosional events separately, a similar erosional pattern for the two phases was considered (Figure 2.6). However, even though the pattern is the same, the amounts have a 2:1 magnitude relationship, with the largest erosion being associated to the Oligocene–Miocene phase.

For the second model (paper 3), a third erosional event was considered during Jurassic–Cretaceous time. This event played an important role in the definition of the Loppa High, which corresponds to the main area modelled. The erosion magnitudes and the erosional pattern for this phase (Figure 2.7) are based on the map reported by Nardin

and Røssland (1993). They established that the deepest erosion occurred at the crest of the Loppa High, along the southern margin of the Finnmark Platform and in the Stappen High.

For the two Cenozoic erosion phases a greater effort was applied in order to have a better constraint on the erosional patterns and the erosion magnitudes with respect to model 1, for which new considerations were made. As a first approximation for the subdivision, an erosion map was created for the Oligocene–Miocene phase (Figure 2.7) based also on another map reported by Nardin and Røssland (1993), since they only considered this Cenozoic erosion phase. They established as well that this erosion was accompanied by the deposition of westward prograding clastic wedges towards the depocenters located in the Tromsø, Sørvestsnaget, Bjørnøya and Hammerfest basins. For that reason they assumed that erosion magnitudes decrease to the west and established a limit of zero erosion towards this area in the west. For the Pliocene–Pleistocene glacial erosion phase another map was created as well (Figure 2.7), with an erosional pattern similar to the regional one reported by Henriksen et al. (2011a). Considering that glaciations occurred around almost the entire Southwestern Barents Sea, it was assumed that the glacial erosion took place in the entire modeled area and kept in mind the trends reported in the literature regarding erosion increasing from west to east and to the north–northeast. Finally, a 2:1 magnitude relationship was maintained between the Oligocene–Miocene and Pliocene–Pleistocene erosion as in the Hammerfest Basin model (paper 1).

A sensitivity evaluation of the Cenozoic erosion with respect to the magnitudes was performed through maximum, medium and minimum erosion scenarios as shown in Figure 2.6 and Figure 2.7.

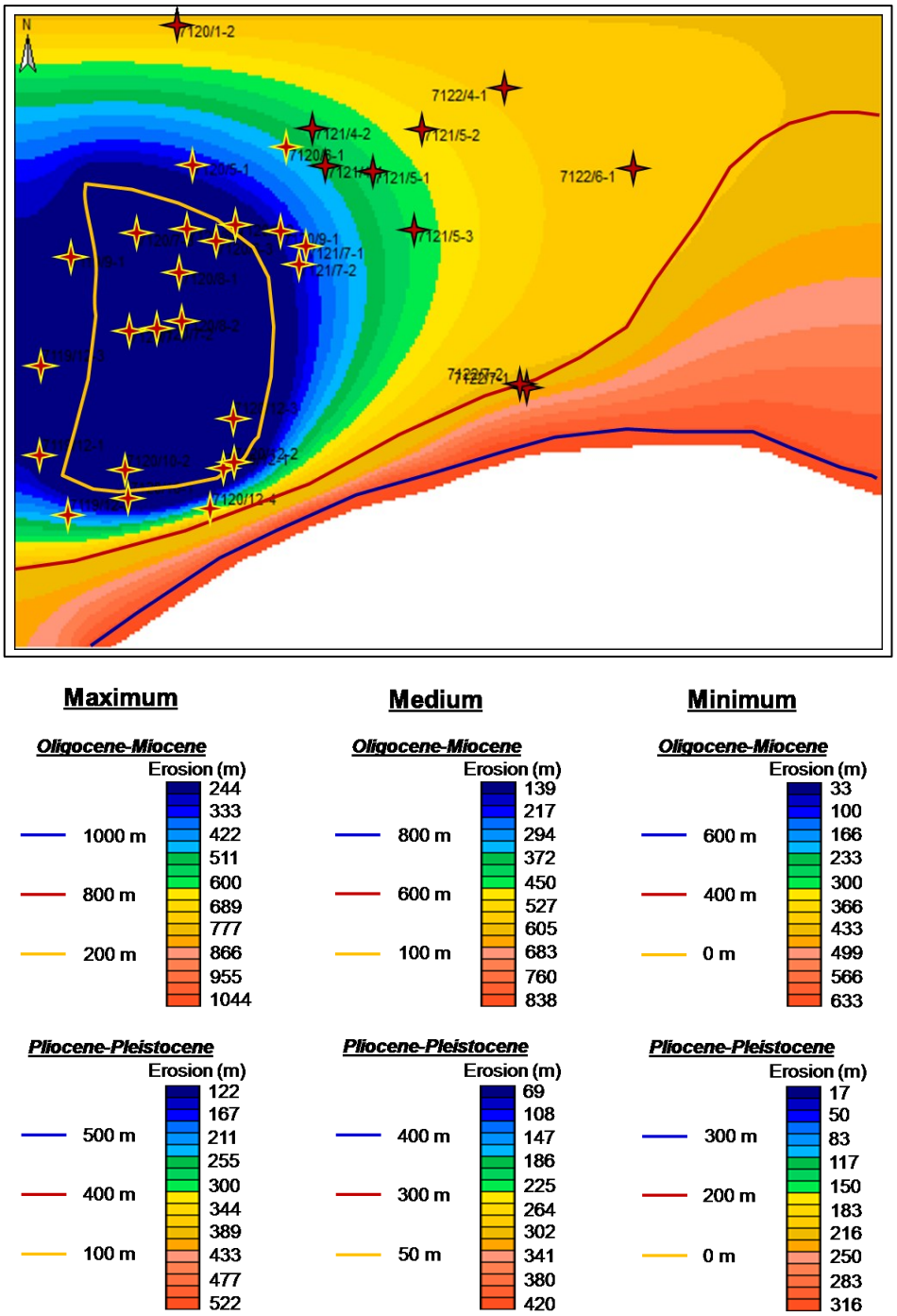

Figure 2.6 Erosion map (top) created for the two erosion events considered in model 1. The same erosion trend was used for both events, but with different magnitudes (2:3 relationship; explanation in text). The magnitudes for the three erosion scenarios (maximum, medium and minimum) considered in the sensitivity analysis are also shown (bottom). The iso–erosion lines in the maps were used for the creation of the map by interpolation.

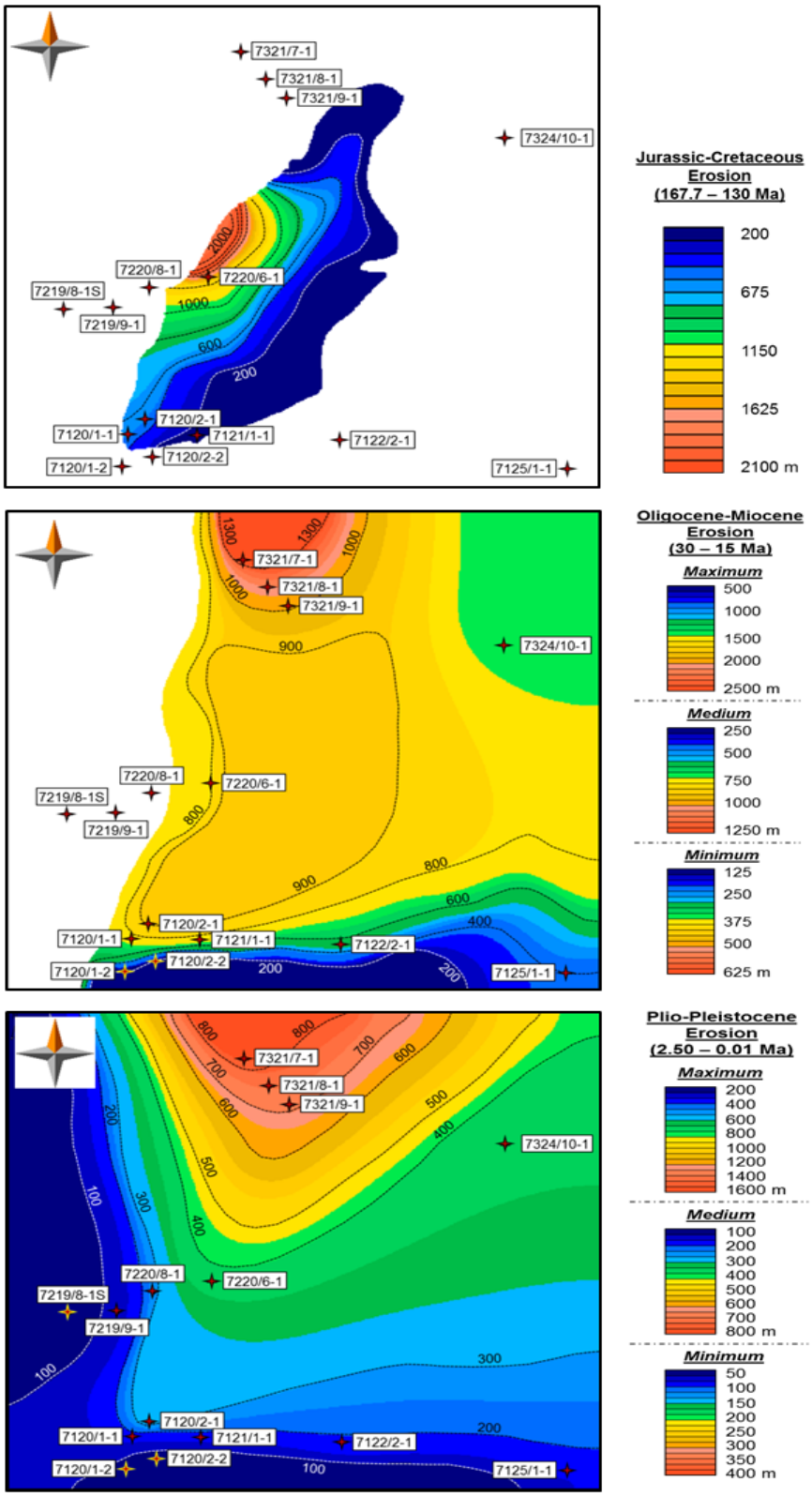

Figure 2.7 Erosion maps created for the three erosion phases considered in model 2. The magnitudes for the three erosion scenarios (maximum, medium and minimum) considered in the sensitivity analysis are also shown. The iso–erosion lines are shown which were used for the creation of the map by interpolation.

Ice–sheet modelling during glaciations and deglaciations

As for the erosion, a detailed description of the glaciers and the glaciations that were developed in the Barents Sea is presented in section 1.3.5. For this study the ice–sheet evolution was considered and modeled for the period between 1.10 and 0.01 Ma. The glacial–interglacial periods between 1.10 and 0.12 Ma were defined following the oxygen–isotope stages, and considering a subdivision into five ice megacycles (MC5 to MC1, Figure 2.8) as described by Kukla and Cílek (1996), with an acceptable ice periodicity based on the Milankovitch theory. That is, considering that the Earth's climate system has a dominant 100,000 year cycle (Broecker and Denton, 1990; Henrich and Baumann, 1994) an ice megacycle length of roughly 100,000 years was assumed. For each megacycle four phases of equal time length were defined, they correspond to: a phase of ice growth, a phase of ice stability, a phase of ice retreat and an ice–free phase or interglacial period. Therefore, with these previous assumptions two important parameters necessary to model glaciation processes can be defined, which are the duration of the glaciation and the extent of the ice cover. A third important parameter is the ice thickness for which there are no real constraints for the period prior to 0.12 million years. Hence, three scenarios of ice thickness were evaluated to address the sensitivity of the system to this parameter. These ice thicknesses correspond to 1000, 1250 and 1500 m, the last one being in the same magnitude as the value reported for the last glacial maximum (Siegert et al., 2001; Svendsen et al., 2004).

For the Weichselian glaciation, which corresponds to the period between 0.12 and 0.01 Ma, the duration, extent and ice thickness of each glacial cycle have been well defined in several studies (Elverhøi et al., 1993; Siegert et al., 1999; Svendsen et al., 1999; Siegert et al., 2001; Siegert and Marsiat, 2001; Clark and Mix, 2002). In this work the reported values were used as input for the model building and four glaciation–phases with an increasing–intensity (Figure 2.8), from Early to Late Weichselian, as proposed by Siegert et al. (2001), were implemented. The modelled ice–sheet was defined as a zero–porosity and effectively incompressible and impermeable lithology; with the density of frozen water (the physical properties used are shown in Table 2.2).

Ice–sheet topography variations were not considered in the model, because regional ice thickness maps report minor thickness variability over the study area, at least for the Weichselian period (Siegert et al., 1999; Siegert et al., 2001; Siegert and Marsiat, 2001).

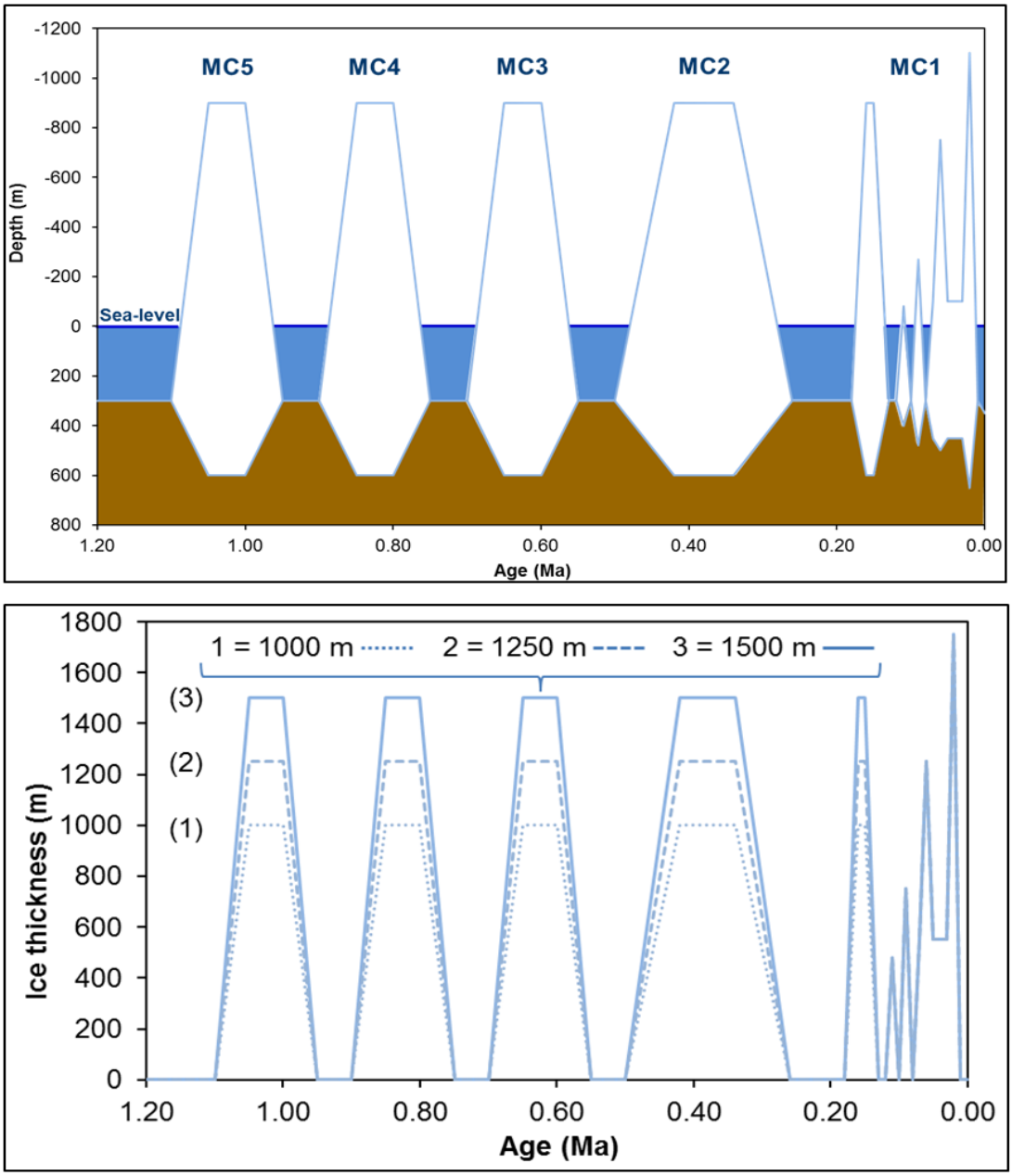

Figure 2.8 Definition of the ice–sheet evolution. *Top:* Glaciation history through five ice megacycles including isostatic response. The MC1 also includes the Weichselian period. *Bottom:* Ice thickness specification. Three ice–sheet thicknesses were considered in order to evaluate the sensitivity of the model output. For the Weichselian period (between 0.12 and 0.01 Ma) no thickness variation was considered since this period has been well constrained and several models give an estimate of the thickness.

2.2 Geochemical data

The geochemical interpretation was performed using a dataset that was kindly provided by Applied Petroleum Technology (APT) AS, Norway. APT is a well–known service company which follows the NIGOGA (Weiss et al., 2000) analytical standards. The available analytical dataset consisted of gas isotopes, gas and light hydrocarbon compositions, and biomarkers (steranes m/z 217 and 218; terpanes m/z 191; mono–aromatics steroids m/z 253; and tri–aromatic steroids m/z 231) from a total of 53 fluid samples representing the petroleum present in the main oil and gas accumulations of the Hammerfest Basin. Detailed information regarding the sample types, the fields, and their stratigraphic level are described in Table 2.4. Exact well data for these samples cannot be given due to proprietary issues.

Table 2.4 Description of the samples provided by Applied Petroleum Technology AS (Nr.: Number of samples; SLHFC: Southern Loppa High Fault Complex; HS: Headspace; Fm.: Formation; fms.: formations)

Sample type	Nr. of samples	Field/Discovery	Stratigraphic level
Oil	4	Snøhvit	Stø Fm.
	1	Albatross	Stø Fm.
	8	Goliat	Tubåen, Snadd and Kobbe fms.
	1	Tornerose	Stø Fm.
	3	7120/1-2 (SLHFC)	Hekkingen and Knurr fms.
Oil/Condensate	2	Askeladd	Stø Fm.
Condensate	3	Snøhvit	Stø and Tubåen fms.
	1	Albatross	Stø Fm.
	4	Askeladd	Stø Fm.
	1	Tornerose	Snadd Fm.
Oil/Gas	3	Tornerose	Snadd Fm.
Gas	4	Snøhvit	Stø Fm.
	13	Tornerose	Stø and Snadd fms.
HS Gas	5	Snøhvit	Stø and Tubåen fms.

3 Synthesis of the main results

In the following sections a compilation of the main results that were obtained during the development of this PhD study will be presented. Special focus will be placed on the understanding of the petroleum systems evolution (generation and expulsion of hydrocarbons, migration and accumulation), but additional important results will be also shown, since they are as well determinant for the achievement of the goals initially proposed with this study and also for a better understanding of the petroleum exploration in the Southwestern Barents Sea.

3.1 Hammerfest Basin (papers 1 and 2)

This section includes all the results from the first 3D basin modelling study, which was done considering the very well explored Hammerfest Basin as the area of interest. These results were published in the first two scientific papers (papers 1 and 2). The first one is focused in the description of the basin model building, the construction of the main petroleum systems evolution, the estimation of the petroleum volumetric (amounts of hydrocarbons generated, expelled, accumulated and leaked) as well as the evaluation of the glacial influence on the petroleum systems. The second paper shows a more detailed evaluation of the petroleum system itself involving an interpretation of the general geochemistry data obtained in the area from exploration wells and a correlation with the basin modelling results.

3.1.1 Model calibration and sensitivity analysis (paper 1)

3.1.1.1 Calibration

The thermal data available for model calibration consisted of temperature and vitrinite reflectance values from petroleum exploration wells. In Figure 2.2 a summary of this data and its quality was presented; there it was observed in general that good and abundant data is available for the model calibration. The vitrinite reflectance data was more challenging since higher variability was observed and therefore the possibility to

achieve a very good calibration is more difficult. Several models were built and used to carry out the sensitivity analyses for heat flow and erosion, as described in the previous sections.

The comparison of the results from all the models show that in general the scenario that allows the best calibration to the temperature data corresponds to a medium heat flow scenario (Figure 3.1 and Figure 3.2); which is the one with a background heat flow between 53 and 58 mW/m^2 (Figure 2.4). No major changes are observed in the temperature regime or trend when evaluating or considering different erosion scenarios, as is observed in Figure 3.2. Regarding calibration to the vitrinite reflectance data, it is important to first mention that the results obtained and presented in Figure 3.3 and Figure 3.4 show the particular variation observed very often while performing a vitrinite reflectance calibration. That is, when a variation in the heat flow scenario is performed a rotation of the vitrinite reflectance trend is observed (Figure 3.3); while when a variation on the erosion scenario is performed then a translation of the trend is characteristic (Figure 3.4). Regarding calibration with vitrinite reflectance, the results also suggest that in general the heat flow scenario that better calibrates the model corresponds to the medium heat flow. On the other hand, it can be clearly observed that the vitrinite reflectance data is more sensitive to the changes in the erosion scenarios. The best calibration for most of the data was achieved with the maximum erosion scenario (Figure 3.3 and Figure 3.4). As previously mentioned the vitrinite reflectance data is, in part, very scattered, which makes the calibration quite difficult. A variation of the magnitudes relationship between the Oligocene–Miocene (O–M) and Pliocene–Pleistocene (P–P) erosion phases was also considered from 2:1 (O–M > P–P) to 1:2 (O–M < P–P). The erosional pattern and the erosion magnitudes were maintained as shown in Figure 2.6. The results of this variation did not show a major difference between both scenarios, confirming that the timing when the largest erosion took place does not have an impact on the vitrinite reflectance.

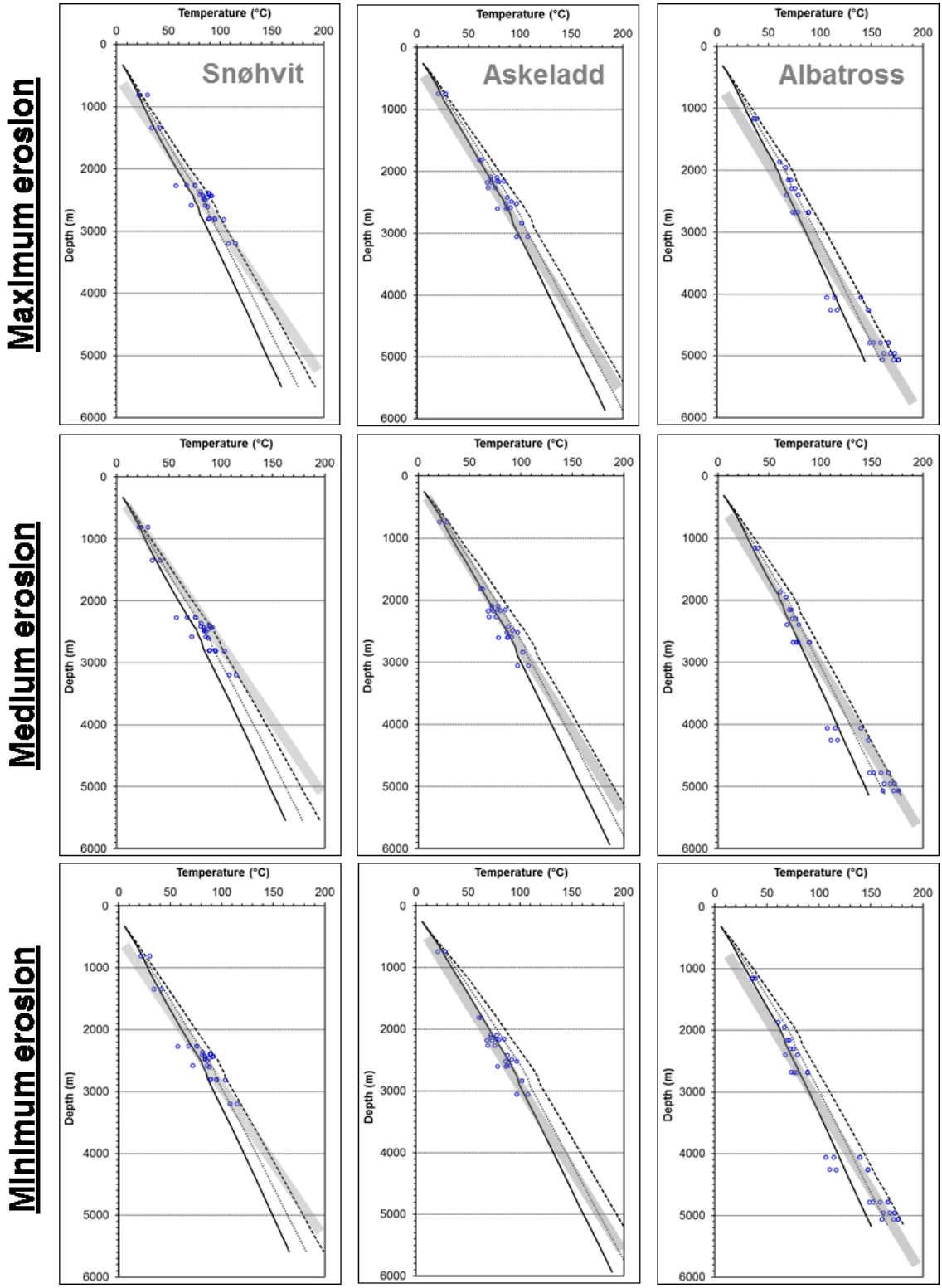

Figure 3.1 Temperature calibration results for wells around three of the main fields in the Hammerfest Basin; Snøhvit (left), Askeladd (middle) and Albatross (right). The comparison of the three erosion scenarios is displayed vertically while the comparison of the three heat flow scenarios is inside each plot: continuous line represents minimum heat flow; dotted line represents medium heat flow and segmented line represents maximum heat flow. The gray lines correspond to the best calibration zone.

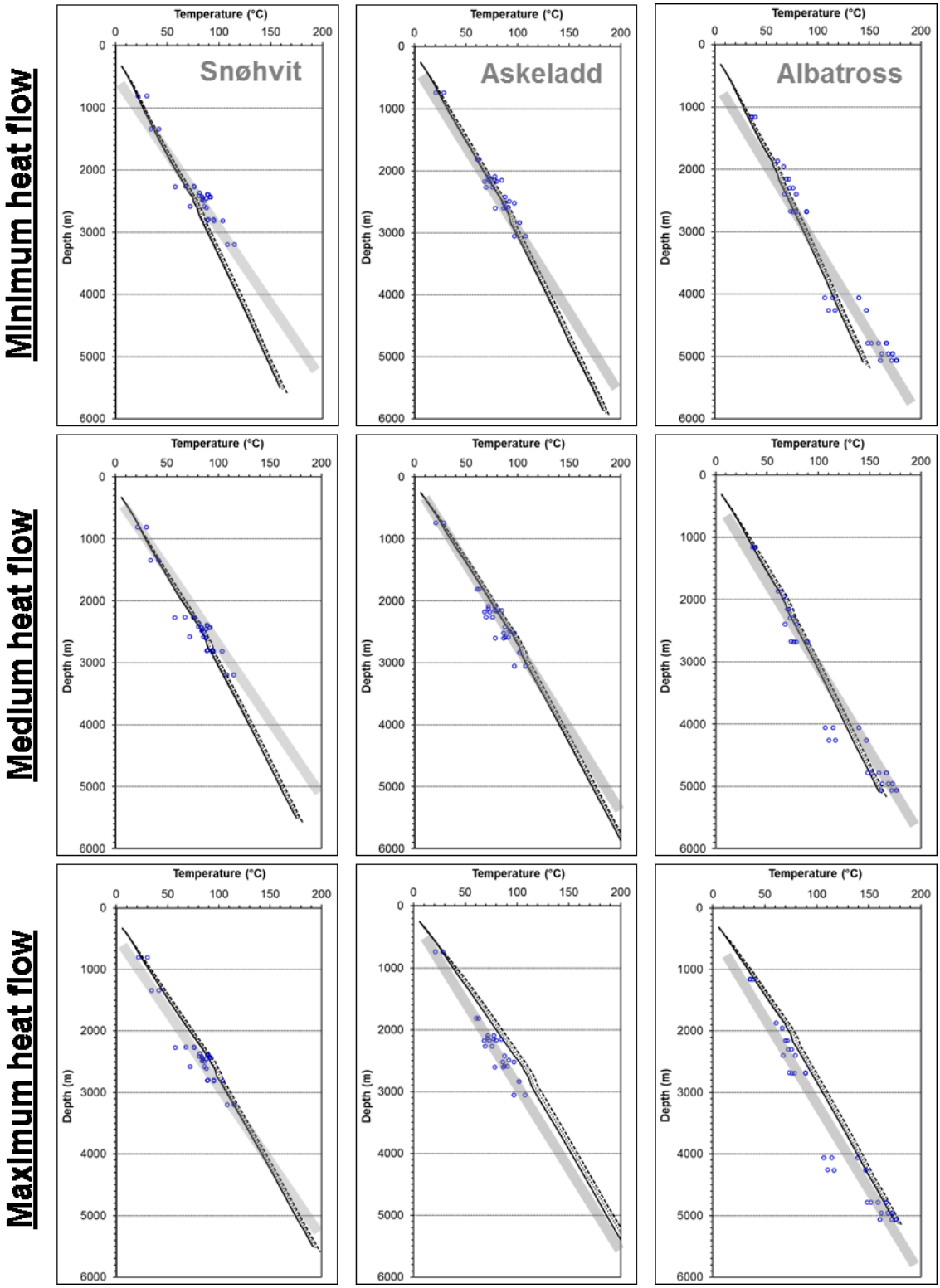

Figure 3.2 Temperature calibration results for wells around three of the main fields in the Hammerfest Basin; Snøhvit (left), Askeladd (middle) and Albatross (right). The comparison of the three heat flow scenarios is displayed vertically while the comparison of the three erosion scenarios is inside each plot: continuous line represents maximum erosion; dotted line represents medium erosion and segmented line represents minimum erosion. The gray lines correspond to the best calibration zone.

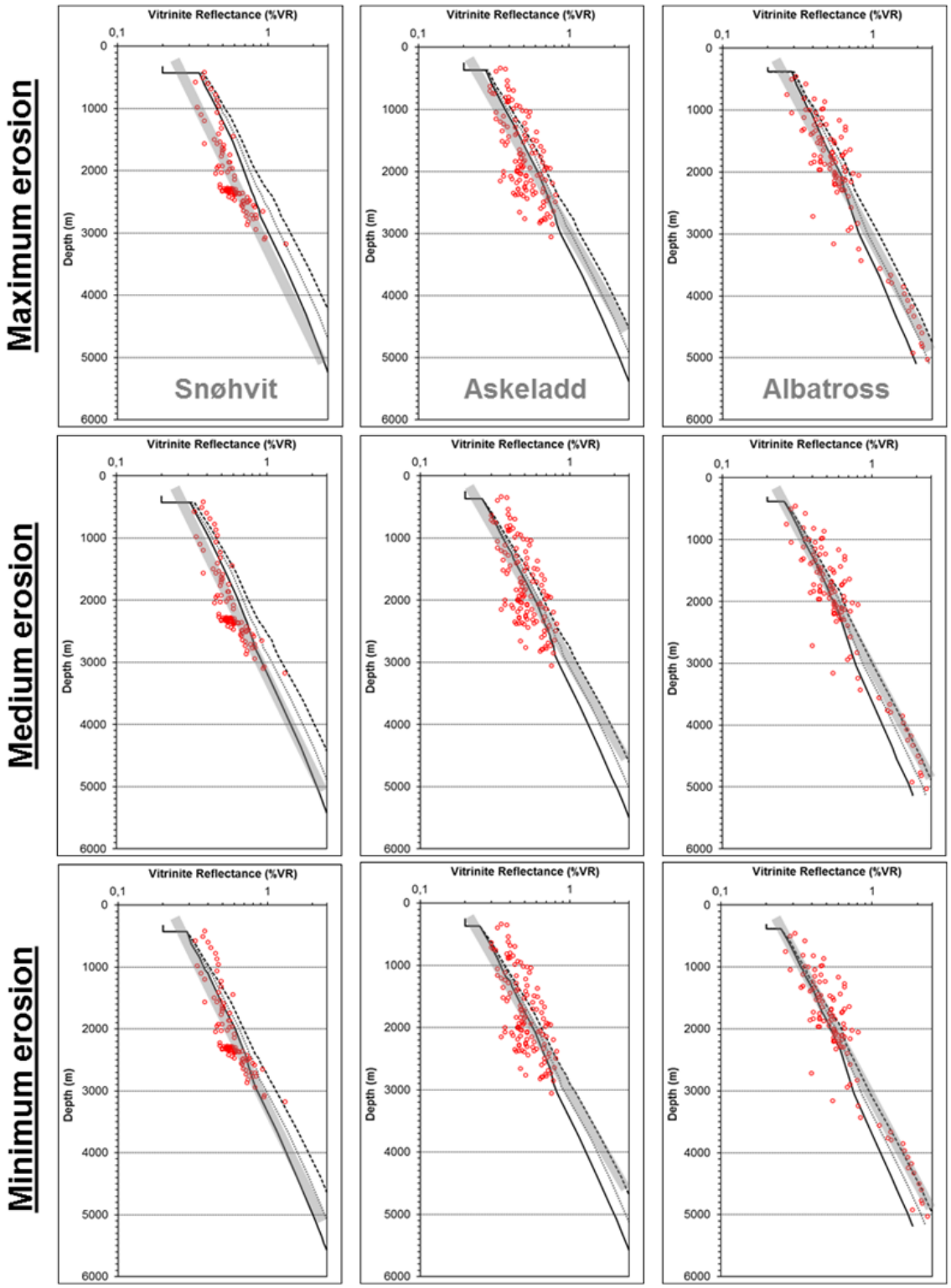

Figure 3.3 Vitrinite reflectance calibration results for wells around three of the main fields in the Hammerfest Basin; Snøhvit (left), Askeladd (middle) and Albatross (right). The comparison of the three erosion scenarios is displayed vertically while the comparison of the three heat flow scenarios is inside each plot: continuous line represents minimum heat flow; dotted line represents medium heat flow and segmented line represents maximum heat flow. The gray lines correspond to the best calibration zone.

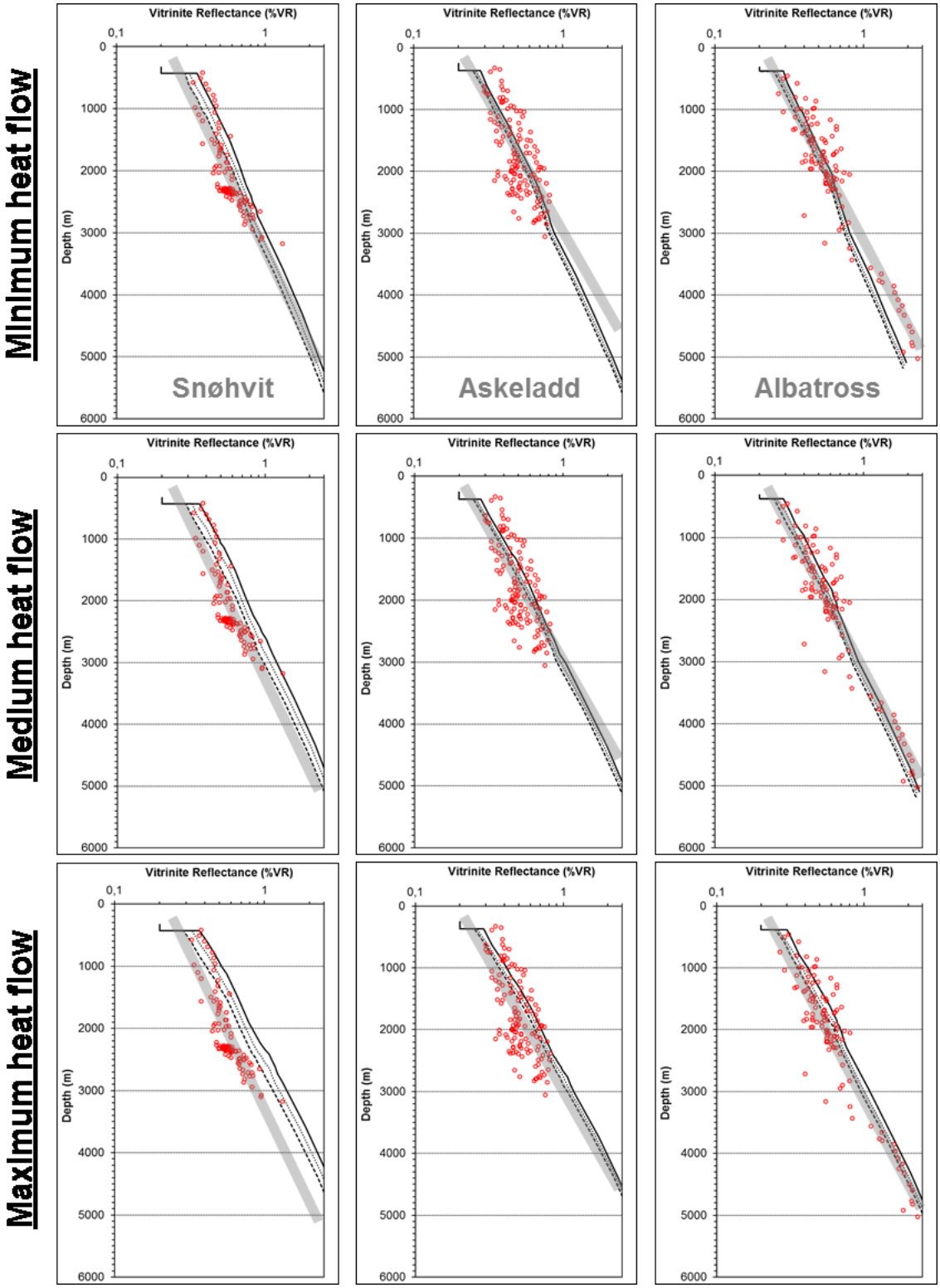

Figure 3.4 Vitrinite reflectance calibration results for wells around three of the main fields in the Hammerfest Basin; Snøhvit (left), Askeladd (middle) and Albatross (right). The comparison of the three heat flow scenarios is displayed vertically while the comparison of the three erosion scenarios is inside each plot: continuous line represents maximum erosion; dotted line represents medium erosion and segmented line represents minimum erosion. The gray lines correspond to the best calibration zone.

3.1.1.2 Sensitivity analyses

The sensitivity analysis performed in this study corresponds to the evaluation of the model output variability in terms of the oil and gas mass variations with respect to the different erosion, heat flow and ice–sheet scenarios used and previously described. Due to the fact that the kinetics implemented in this model consist of 14–components, all the masses reported for oil correspond to the sum of the liquid hydrocarbons, that is hexane (C_6), C_7–C_{15}, C_{16}–C_{25}, C_{26}–C_{35}, C_{36}–C_{45}, C_{46}–C_{55} and C_{55+}; and the masses for gas correspond to the sum of the gaseous hydrocarbons, which are methane, ethane, propane, *i*–butane, *n*–butane, *i*–pentane and *n*–pentane. In general, the model results with respect to the masses of oil and gas generated are more sensitive first to the heat flow variation and second to the erosion scenarios. No changes in the masses generated are caused by changes in the ice thickness of the ice–sheets.

If the same erosion scenario is considered (maximum erosion in this case), and a sensitivity evaluation of the heat flow is performed, it can be concluded that the masses of oil and gas generated vary in average as follows: 74 ± 3 Gt for the total amount of oil and 65 ± 22 Gt for the gaseous hydrocarbons (Table 3.1). The major influence of this parameter is observed for the gaseous hydrocarbons. The variations in relation with the expelled masses are more or less in the same order of magnitude, being: 28 ± 14 Gt for the total oil expelled, and 33 ± 19 Gt for the total amount of gas expelled (Table 3.1). If the possible effect on the masses accumulated in the reservoirs are considered, it is then observed that the variation is not significant.

The same exercise was done for the different erosion scenarios and considering in this case the same heat flow (medium heat flow). Here it was observed that the variability of the generated oil and gas masses is less sensitive, corresponding to: 72 ± 4 Gt for oil and 58 ± 7 Gt for the gaseous hydrocarbons (Table 3.2). The variation in the oil and gas expelled is more or less in the same magnitude (25 ± 5 Gt of oil and 26 ± 6 Gt of gas). The results with respect to the masses accumulated in the reservoirs are more accurate and show a smaller deviation.

Table 3.1 Comparison of the masses generated, expelled and accumulated in the reservoir with respect to the different heat flow scenarios. The values shown in brackets correspond to the detailed masses of each source rock, i.e. Kobbe + Snadd + Hekkingen formations. The value outside is then the sum of these three masses (Heat flow 1=minimum; heat flow 2=medium; heat flow 3=maximum; Gt = Gigatonnes, SD = Standard deviation).

Masses generated (Gt)		
	Oil generated	Gas generated
Heat flow 1	(33 + 31 + 7) 71	(25 + 16 + 2) 43
Heat flow 2	(28 + 37 + 12) 77	(36 + 26 + 4) 66
Heat flow 3	(23 + 35 + 8) 75	(43 + 35 + 8) 86
Mean	**74**	**65**
SD	**3**	**22**
Masses expelled (Gt)		
	Oil expelled	Gas expelled
Heat flow 1	(7.2 + 6.8 + 0.5) 14.5	(9.8 + 4.0 + 0.3) 14.0
Heat flow 2	(14 + 14 + 2) 30	(20 + 11 + 1) 32
Heat flow 3	(17 + 21 + 3) 41	(30 + 19 + 3) 52
Mean	**28**	**33**
SD	**14**	**19**
Masses accumulated in reservoir (Gt)		
	Oil accum. in Stø Fm.	Gas accum. in Stø Fm.
Heat flow 1	0,27	0,32
Heat flow 2	0,30	0,30
Heat flow 3	0,30	0,28
Mean	**0,29**	**0,30**
SD	**0,02**	**0,02**

Based on the previous results it can be noticed that the masses of generated hydrocarbons are more sensitive to heat flow variations than to the variations in erosion magnitudes, and this is basically due to the fact that the heat flow is a parameter that directly influences the thermal history of the basin, and thus the temperature and thermal maturation of the source rocks. Moreover, another sensitivity evaluation that was considered when performing the changes in the erosion scenarios is the gas losses from the reservoirs (Table 3.2); this is of importance since later in this study details regarding the dynamics of the petroleum systems in relation with the uplift and erosion will be presented. The sensitivity evaluation with respect to the ice thickness scenarios did not show a high influence on the amount of oil and gas generated. This is quite obvious, since the glaciation process took place towards the end of the geological history of the basin after maximum burial. In this case the variability is more related to the amount of oil and gas accumulated in the Stø Formation and also to the amount of gas lost from it and leaked to the surface (Table 3.3).

Table 3.2 Comparison of the masses generated, expelled, accumulated and leaked from the reservoir with respect to the different erosion scenarios (a=maximum erosion; b=medium erosion; c=minimum erosion; Gt=Gigatonnes; SD=Standard deviation).

Masses generated (Gt)		
	Oil generated	Gas generated
Erosion a	77	66
Erosion b	72	58
Erosion c	68	51
Mean	**72**	**58**
SD	**4**	**7**
Masses expelled (Gt)		
	Oil expelled	Gas expelled
Erosion a	30	32
Erosion b	24	25
Erosion c	20	21
Mean	**25**	**26**
SD	**5**	**6**
Masses accumulated in reservoir (Gt)		
	Oil accum. in Stø Fm.	Gas accum. in Stø Fm.
Erosion a	0,30	0,30
Erosion b	0,34	0,28
Erosion c	0,43	0,29
Mean	**0,36**	**0,29**
SD	**0,07**	**0,01**
Masses leaked from the reservoir (Gt)		
	Gas lost from Stø Fm.	Gas outflow (model top)
Erosion a	0,24	0,3
Erosion b	0,21	0,3
Erosion c	0,07	0,1
Mean	**0,17**	**0,2**
SD	**0,09**	**0,1**

Table 3.3 Comparison of the masses accumulated in reservoir and lost/leaked from it with respect to the different ice thickness scenarios (Gt=Gigatonnes; SD=Standard deviation).

Masses accumulated in reservoir (Gt)		
	Oil accum. in Stø Fm.	Gas accum. in Stø Fm.
Ice 1 (1000 m)	0,301	0,299
Ice 2 (1250 m)	0,300	0,303
Ice 3 (1500 m)	0,298	0,302
Mean	**0,299**	**0,301**
SD	**0,001**	**0,002**
Masses leaked from the reservoir (Gt)		
	Gas lost from Stø Fm.	Gas outflow (model top)
Ice 1 (1000 m)	0,250	0,300
Ice 2 (1250 m)	0,245	0,288
Ice 3 (1500 m)	0,244	0,289
Mean	**0,247**	**0,292**
SD	**0,003**	**0,007**

The following sections, which present more detailed results, are based on the model with the maximum erosion and with the medium heat flow, since the most consistent regional calibration was achieved with those two scenarios.

3.1.2 Petroleum generation, migration, accumulation and leakage

3.1.2.1 Source rock maturity, petroleum generation, expulsion and migration (Paper 1)

The predicted present–day transformation ratio (TR, Figure 3.5), defined as the ratio which reflects the fraction of petroleum (oil + gas) potential of the kerogen realized (Tissot and Welte, 1984), indicates that the Hekkingen Formation has reached oil window and even higher maturity, in the western and northwestern margin of the modelled area. This is as well observed by the maturity results from a pseudo–well taken in the kitchen area (Figure 3.5 and Figure 3.6), where present–day values of almost 60% TR and ~1.0 %VR have been obtained. In the central, southern and eastern parts of the basin this Upper Jurassic source rock is predicted to be thermally immature (Figure 3.5), supporting earlier interpretations (Doré, 1995; Ohm et al., 2008). The potential Triassic source rocks (Snadd and Kobbe formations) have reached complete transformation in almost the entire basin, with the Kobbe Formation being the one with the highest maturity (Figure 3.5). This therefore indicates that a great proportion of the gaseous hydrocarbon accumulations present in the Hammerfest Basin may have been sourced from these Triassic Snadd and Kobbe formations. In addition, secondary cracking of oil to gas is expected to start at temperatures of 170 °C or more, according to the kinetic models used in this study and also according to Dieckmann et al. (1998). The three source rocks considered in this model have exceeded this temperature in the western and northwestern margins by the time when hydrocarbons started to accumulate in the reservoir (Paleocene). This supports as well the presence of significant sources for thermogenic gas in the basin.

The modeled burial and maturation history of each source rock from the pseudo–well (Figure 3.5) are shown in Figure 3.6. Considering that the onset of the oil window maturity is at Ro ≈ 0.50% (Tissot and Welte, 1984), generation of oil in the upper part of the Kobbe Formation would have started in the Late Triassic (~215 Ma), in the upper part of Snadd Formation during Early Cretaceous (~125 Ma) and in the upper part of the Hekkingen Formation in Late Cretaceous (~95 Ma) time.

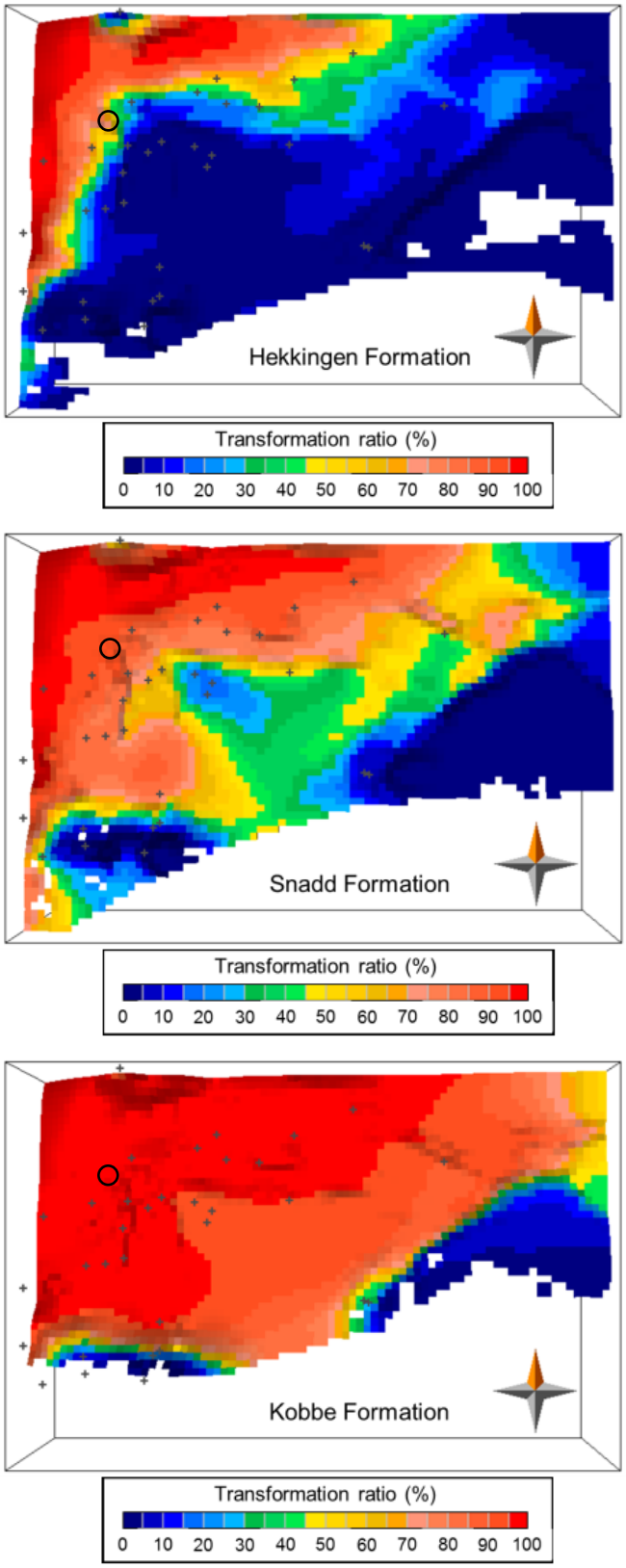

Figure 3.5 Modeled present–day transformation ratio at the top of each source rock: the Upper Jurassic Hekkingen Formation and the Triassic Snadd and Kobbe formations. The circle corresponds to the pseudo–well taken in order to have an extraction with the information presented in Figure 3.6.

Generation in the lower part of each source rock began at an earlier stage; this is most important for the Triassic Snadd and Kobbe formations which are thicker. As observed in Figure 3.6 the basin reached its maximum burial at 30 Ma, followed by the uplift and erosion events, which mark the end of hydrocarbon generation due to cooling of the source rocks, this can be visualized in the transformation ratio trends presented also in Figure 3.6.

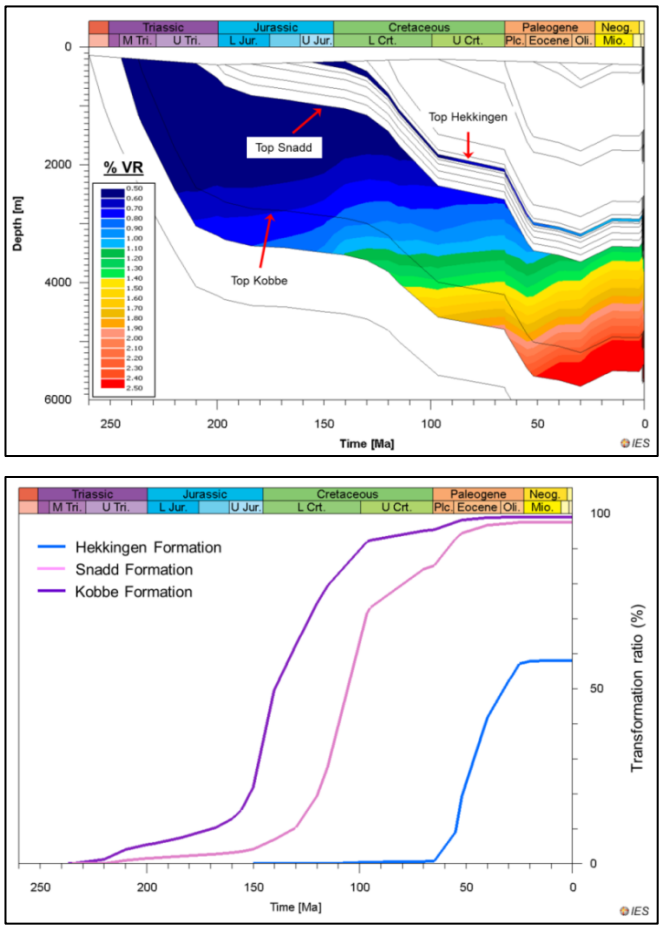

Figure 3.6 Burial history of the three main source rocks (top): Hekkingen, Snadd and Kobbe formations. The vitrinite reflectance is shown as an overly. Maturity evolution of each source rock based on the transformation ratios (Bottom). Both plots were taken from a pseudo–well northwest of the modeled area. Please look at Figure 3.5 for reference of the well location.

The 3D basin model of the Hammerfest Basin allowed a first order mass/volume estimation of the oil and gas generated through geological time in the basin as it considers the main Triassic and Jurassic source rocks volumetrically. The predicted total amount of oil corresponds to approximately 76 Gt and the predicted total amount of gas

is around 66 Gt (Figure 3.7). The detailed amounts of oil and gas generated by each source rock can be seen in Figure 3.7. There are two important things that can be noticed: the first one is the end of hydrocarbon generation at 30 Ma, which is related with the maximum burial and following inversion, as mentioned previously. The second is related to the tendency obtained for the oil mass generation in the Kobbe Formation. Between 90 and 100 Ma the cumulative oil mass starts to decrease; this is basically in response to the beginning of secondary cracking as stated above. The densities of oil and gas as separate phases at subsurface conditions are calculated in PetroMod based on the compositional predictions of the kinetic models and the respective physical properties. The approximate equivalent volumes of the total masses previously mentioned were then calculated based on the in–situ density of the individual phases. They correspond to ~140 billion m^3 of oil and ~300 billion m^3 of gas.

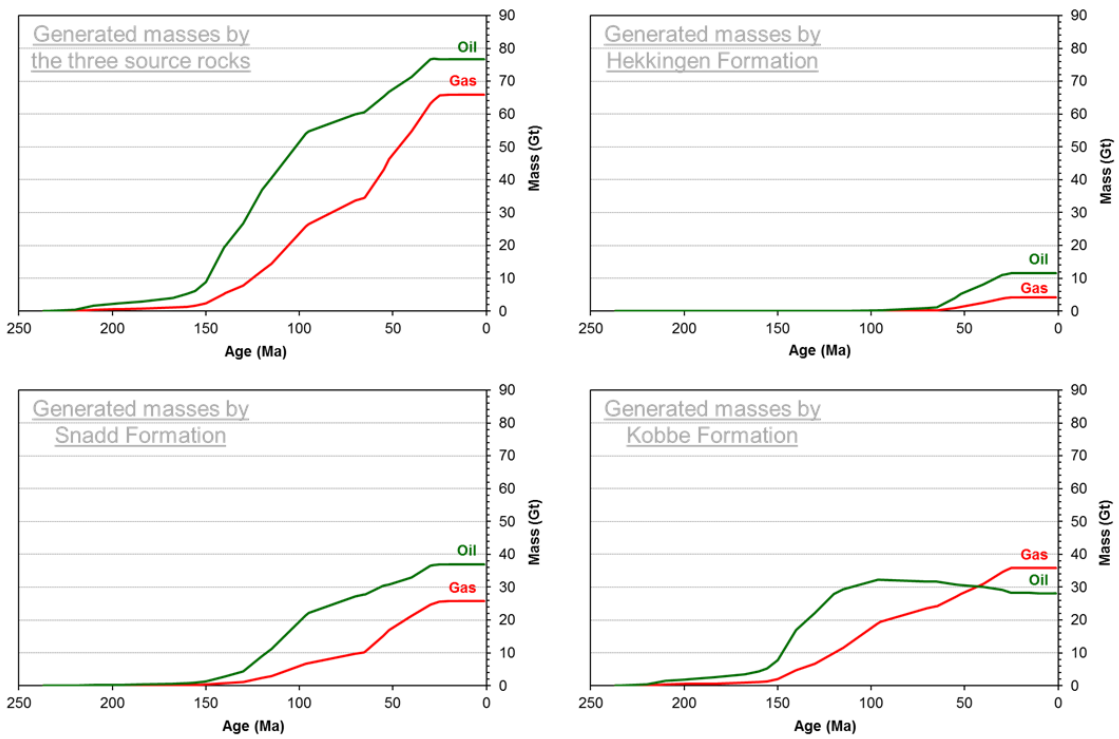

Figure 3.7 Total cumulative mass (in Gigatonnes) of oil and gas generated by the three source rocks considered in this model together (top left), and separately (top right and bottom).

Petroleum expulsion is considered in the modelling software used as a function of the critical oil (S_{oc}) and critical gas saturations (S_{gc}) once the adsorptive capacity of the kerogen is exceeded. The petroleum saturation is defined as the fraction of pore space

which is used for flow (England et al., 1987); therefore the critical oil and gas saturations represent the threshold values that distinguish between initial saturations, which must be overcome to allow flow, and residual saturations, which are immobile. Thus once the values are overcome expulsion from the source rock begins. Critical gas saturations are usually assumed to be negligible, which allows then all gas to be mobile (Hantschel and Kauerauf, 2009). In the application of PhaseKinetic models of petroleum generation, as done for this work, it is considered that under the subsurface pressure and temperature conditions the fluids generated are monophasic (di Primio et al., 1998). Accordingly an adsorption model is used which does not differentiate between oil and gas phases, for this reason the critical saturation thresholds apply to a single phase, accordingly it was ensured for this model that the oil and gas saturation thresholds have the same value in the source rock lithology (5% for shale and 0.1% for siltstones). According to Hantschel and Kauerauf (2009) critical oil saturations in shales range from 0.5 to 50% and in sandstones from 0.1 to 10% (PetroMod uses the same S_{oc} of sandstones for siltstones).

The predicted timing for initial petroleum expulsion (Appendix I – Figure I.3) from the Triassic Kobbe Formation, which corresponds to the oldest source rock, is around 120 Ma; implying that migration took place in the Hammerfest Basin since Early Cretaceous time. Expulsion from the Snadd Formation began during Middle Cretaceous (around 100 Ma) and expulsion from the Hekkingen Formation started more recently during Paleogene time or around 50 Ma. The estimated total amount of oil and gas expelled correspond to approximately 30 and 32 Gt, respectively. Based on the generated and expelled masses the expulsion efficiency, defined as the percentage of expelled petroleum in relation to total generated bitumen of a particular source rock unit, was calculated. In this model, the expulsion efficiencies were determined for the total petroleum and for the separate oil and gas phases. The different compounds taken into account for the oil and gas phases were previously specified in the sensitivity analysis section (3.1.1). Therefore, the expulsion efficiencies for the oil phase correspond to approximately 17% in the Hekkingen Formation, 38% in Snadd Formation and 50% in Kobbe Formation. The gas phase expulsion efficiencies are 25%, 42% and 55% for the Hekkingen, Snadd and Kobbe formations, respectively.

Hydrocarbon migration was simulated using the hybrid method, chosen from a variety of petroleum migration algorithms. This method is based on a domain decomposition that solves Darcy flow equations in areas of low permeabilities and applies a flowpath analysis in highly permeable areas (Hantschel et al., 2000; Hantschel and Kauerauf, 2009; Schlumberger, 2009).

3.1.2.2 Petroleum accumulation in the main reservoir, the Stø Formation (Papers 1 and 2)

As stated in section 2.1.1 the majority of the petroleum resources that have been found in the Barents Sea are contained in the Stø Formation. Therefore, here the focus will be mainly placed in this stratigraphic unit. For this Hammerfest Basin model it has been predicted that the Stø reservoir started to be filled with petroleum from approximately 80 Ma onward (Figure 3.8). The main sealing units correspond to the Fuglen and Hekkingen formations, which were already deposited and to a large degree consolidated at the age of 55 Ma, when the main charge pulse to the reservoir took place (Figure 3.8). This can be corroborated by the porosity values of both formations, which are below 15% (~11.6 % for the Fuglen Formation and 7.5% for the Hekkingen Formation, Figure 3.8). Simultaneously, the predicted permeability during that period is in the order of 10^{-6}–10^{-7} mD (Figure 3.8), which correspond to values reported by Linjordet and Grung-Olsen (1992). Such permeabilities suggest that effective sealing and the trapping of oil and gas was possible at this time. This notion is supported as well by the predicted reservoir petroleum saturation values, which start to increase at this time.

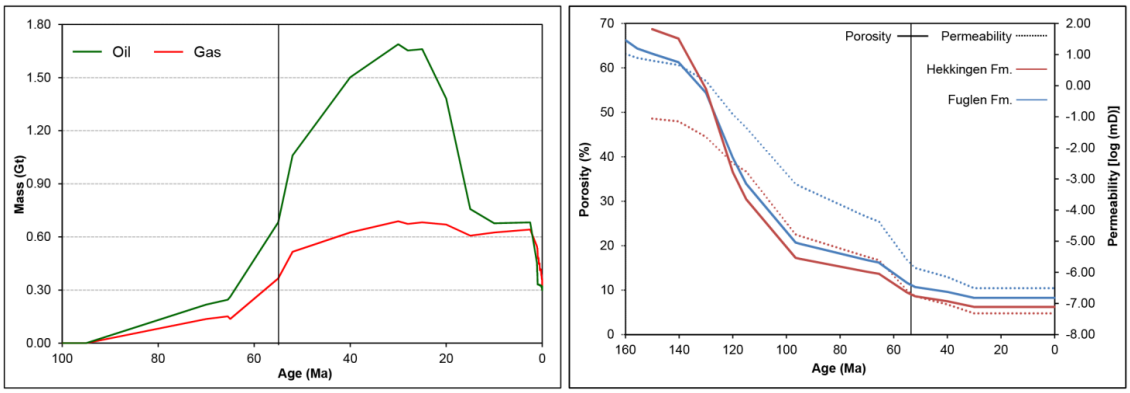

Figure 3.8 Accumulation history for oil and gas in the main reservoir, the Stø Formation (left). Porosity and permeability history for both seal rocks, corresponding to Fuglen and Hekkingen formations.

Moreover, the Hammerfest Basin model predicts that at present–day the amount of gas accumulated in the Stø Formation slightly exceeds the amount of oil (Figure 3.8), i.e. 0.302 Gt of gas and 0.298 Gt of oil. On the other hand, the modeling results reproduced quite well the natural petroleum accumulations and phases (Figure 3.9) of the main fields that are known at present–day in the basin, such as Snøhvit, Snøhvit–Askeladd, Snøhvit–Albatross and Goliat (Norwegian Petroleum Directorate, 2010b, a). In this study the first three fields were reproduced mainly as gas fields, with Snøhvit and Snøhvit–Albatross having oil legs. The Snøhvit–Askeladd field was reproduced as a pure gas accumulation. The modeled gas to oil ratios (GORs) for the oil legs are between 215 and 280 Sm^3/Sm^3 (standard cubic meters, Figure 3.9), and the reported natural GORs are also in the same range (Norwegian Petroleum Directorate, 2009). Likewise, the modeled GORs for the gaseous phases range between 8500 and 22300 Sm^3/Sm^3, and natural fluid measured GORs are between 7400 and 27000 Sm^3/Sm^3, indicating once again a good match. The Goliat field located to the southeast of the modelled area was predicted as an accumulation dominated by oil, which is in agreement with the information reported by the NPD (Norwegian Petroleum Directorate, 2009, 2010a). Modelled GOR values for this field are around 200 Sm^3/Sm^3, while the reported GOR for the fluids is around 59 Sm^3/Sm^3. The difference might be mainly related with the fact that the oils present in this field have been reported to be slightly biodegraded (Norwegian Petroleum Directorate, 2009), which would result in the reduction of liquid GOR as established by Larter and di Primio (2005). Another possible explanation for this low GOR in Goliat would be the loss of gaseous and light hydrocarbons on the migration pathways during long distance migration of petroleum from the active kitchen to the field (Karlsen and Skeie, 2006).

It is important to mention that as reported in the Norwegian Petroleum Directorate, the HCs found in the Snøhvit, Albatross and Askeladd fields are mainly stored in the Stø Formation. In the Goliat field they are hosted in the Triassic Tubåen, Fruholmen, Snadd and Kobbe formations, and in the Tornerose discovery in the Snadd and also in the Stø Formation. In this model the petroleum accumulations have been reproduced mainly in the Stø Formation unit due to the lack of detailed maps for all relevant sedimentary units. However, the model also correctly reproduced the petroleum phases and

properties in the modelled reservoirs. It is worth noting that the predicted petroleum accumulations (with the exception of Goliat) at the onset of the glaciation period (1.10 Ma) are larger than those predicted at present–day (Figure 3.9). This suggests that the glacial processes have affected the initial accumulations in the 3D model. These model predictions are in agreement with the natural situation, as most of the accumulations discovered in the Hammerfest Basin are underfilled traps with residual oil saturation below the oil water contacts, indicating a previously larger degree of filling (Ohm et al., 2008).

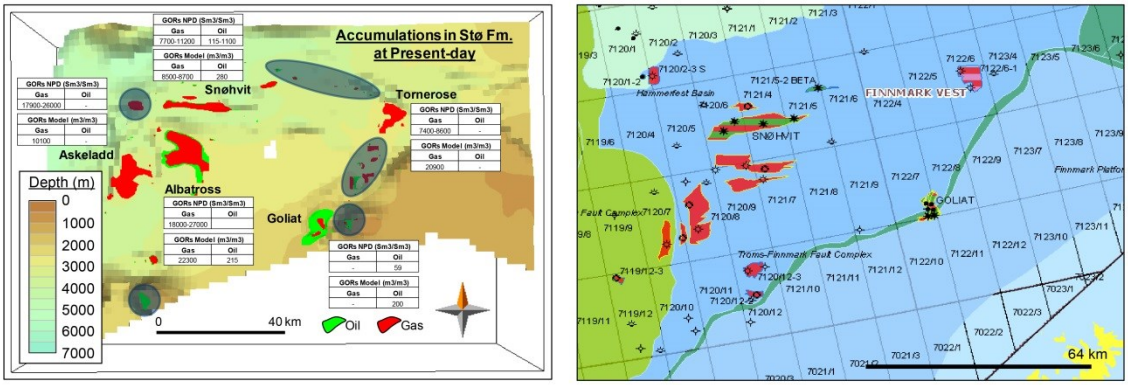

Present-day

Snøhvit, Albatross and Askeladd

NPD		Model		Model with recovery	
Original rec. Oil eq. (mill. Sm3)	Original rec. Gas (bill. Sm3)	Oil (mill. m3)	Gas (bill. m3)	Oil ~50% (mill. m3)	Gas ~70% (bill. m3)
211.13	172.80	302.89	310.84	*~151.45*	*~217.60*

Goliat

NPD		Model		Model with recovery	
Original rec. Oil eq. (mill. Sm3)	Original rec. Gas (bill. Sm3)	Oil (mill. m3)	Gas (bill. m3)	Oil ~50% (mill. m3)	Gas ~70% (bill. m3)
38.47	7.30	7.96	1.36	*~3.98*	*~0.95*

Tornerose discovery

NPD		Model		Model with recovery	
Original rec. Oil eq. (mill. Sm3)	Original rec. Gas (bill. Sm3)	Oil (mill. m3)	Gas (bill. m3)	Oil ~50% (mill. m3)	Gas ~70% (bill. m3)
0.00	3.69	0.84	17.45	*~0.42*	*~12.21*

Pre-glaciation (1.10 Ma)

Snøhvit, Albatross and Askeladd

Model	
Oil (mill. m3)	Gas (bill. m3)
457.04	595.53

Goliat

Model	
Oil (mill. m3)	Gas (bill. m3)
5.91	1.19

Tornerose discovery

Model	
Oil (mill. m3)	Gas (bill. m3)
1.55	22.40

Figure 3.9 *Top left:* Predicted hydrocarbon accumulations (Snøhvit, Albatross, Askeladd and Goliat fields and Tornerose Discovery) in the Stø Formation at present–day (top left). Minor untested accumulations predicted with this model in the area are also shown (blue circles and ellipses). The inlets in the figure list the gas–oil ratios reported in the Norwegian Petroleum Directorate (2012) and calculated in the model for each field and discovery. *Top right:* Map view of the Hammerfest Basin and the fields on it as reported by the Norwegian Petroleum Directorate. *Bottom:* Comparison of the original recoverable oil and gas volumes reported in the Norwegian Petroleum Directorate (2012) with the volumes calculated in the model. The volumes of oil and gas predicted for the time before glaciations (1.10 Ma) are also shown (bottom right).

The possible provenance of the hydrocarbons in a modelled accumulation was evaluated in this study by performing an analysis of the hydrocarbon migration pathways and the drainage areas calculated by the 3D model (Figure 3.10). The results suggest then that the Askeladd and Snøhvit fields were filled with petroleum sourced from the western and northern margins, respectively; while the Albatross field was sourced from both areas. In the case of the Goliat field and the Tornerose discovery, the drainage areas and migration pathways obtained suggest that hydrocarbons have probably been sourced mainly from the northern margin of the basin and that long distance migration might have occurred.

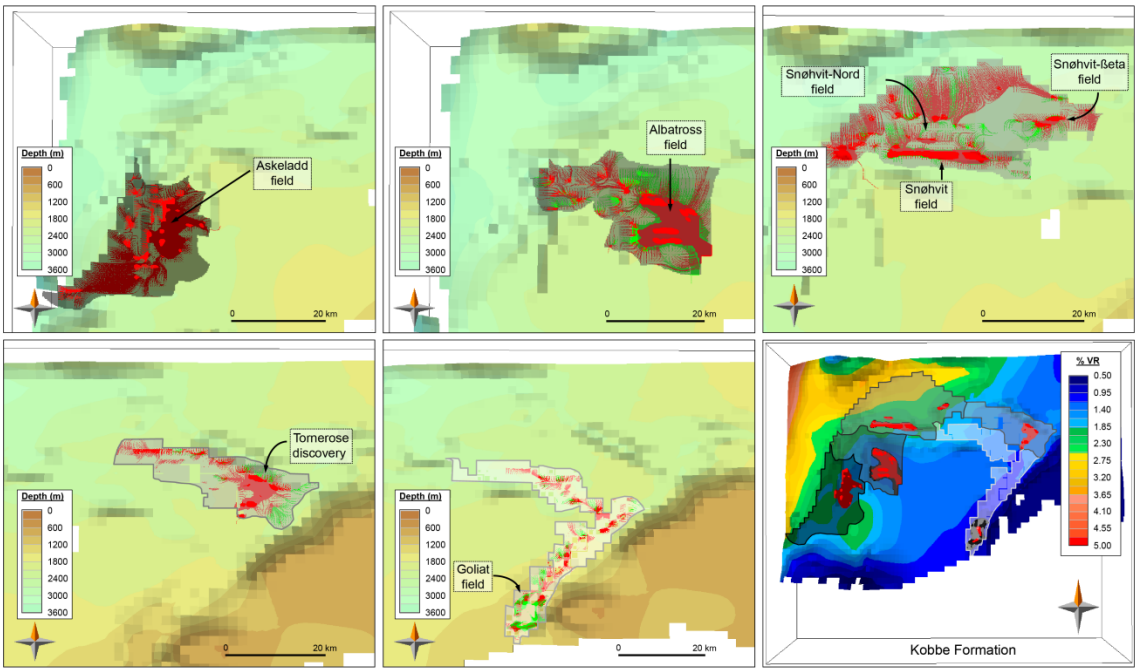

Figure 3.10 Migration pathways and drainage areas for the Askeladd, Albatross, Snøhvit, Goliat fields and the Tornerose discovery. The background shows the depth map of the Stø Formation. The maturity map at present–day of the Kobbe Formation with the five drainage areas is shown for reference (bottom right).

An analysis of the volumetric and the proportion of oil (liquid) and gas (vapor) contributions to each field and discovery from the three source rocks as predicted by the basin model was also performed (Table 3.4). This was done using a source rock tracking that consists in a tagging of the generated components with information

regarding which source rock generated them. Based on this information it is also possible to estimate the origin of the hydrocarbons present in reservoir.

Table 3.4 Contribution from each source rock to the main accumulations present in the Hammerfest Basin (mass %) based on results from the 3D basin model.

Age	Source rock	Snøhvit		Albatross		Askeladd	Goliat		Tornerose
		Vapor	Liquid	Vapor	Liquid	Vapor	Vapor	Liquid	Vapor
Jurassic	Hekkingen Fm.	43	**69**	25	28	18	24	18	30
Triassic	Snadd Fm.	**29**	22	**44**	**49**	**49**	**45**	**52**	**26**
Triassic	Kobbe Fm.	**28**	9	**31**	**23**	**33**	**31**	**30**	**44**

Final inferences can therefore be done with a combination of the maturity results previously summarized and also shown in Figure 3.5 with the drainage areas, pathways and volumetric analysis: 1) the gas contribution in the petroleum system of the Hammerfest Basin was mainly from the Triassic Snadd and Kobbe formations (Table 3.4), with generation occurring in the western, northwestern and northern areas, where the highest maturity levels (gas window) were reached by these source rocks. 2) The oil contribution was a bit more complicated and some differences were observed in comparison with the gas contribution. For the Snøhvit field the main contributor was the Jurassic Hekkingen Formation, which coincides with the information of the kitchen area for this source rock (northwest and northern margin) from modelling and also with the fact of drainage areas and migration pathways connected with it. For the Albatross and Goliat fields the modelling predicts (Table 3.4) that the main oil contribution was from the Triassic source rocks (mainly the Snadd Formation). In the case of the Albatross field the drainage areas suggest a sourcing from the west and north, where the Snadd Formation is still not overmature or with maturities reflecting the last stage of the oil window maturity (Figure 3.5 and Figure 3.10). The drainage areas associated to the Goliat field suggest, as previously mentioned, a contribution from the north (Figure 3.10), where the Snadd Formation is also at the last stage of the oil window. As stated in paper 1 (Rodrigues Duran et al., 2013) a portion of the petroleum in the Goliat field might stem as a result of spilling from the Snøhvit field in the northern margin, indicating the possibility of long distance migration contributing to the charge. On the other hand, this field could also have had a local contribution from the Kobbe Formation, whereby vertical migration is suggested since maturity levels within the oil

window were reached by this source rock in the area. The hydrocarbon migration vectors observed in the model indicate that in the Goliat area, petroleum could have migrated vertically from this Triassic source rock and into the reservoir unit.

3.1.2.3 Petroleum losses from the modelled reservoirs and leakage to the surface (Paper 1)

The modelling results show that the main loss of oil occurred after the Oligocene (Figure 3.8), which coincides with the tectonic uplift and erosion of the basin. Due to this process, changes in the reservoir conditions (pressure and temperature) have occurred and therefore an expansion of the gaseous hydrocarbons phase took place, bringing as a consequence the spilling of oil out of the structures. Therefore, the original oil might have re–migrated to other traps far from the initial ones. In paper 1 (Rodrigues Duran et al., 2013) it was established as well that the main filling of the Goliat field in the southeastern margin of the basin occurred as well after 30 Ma, indicating that a portion of the petroleum in this field was probably sourced from the north after spilling out of the structure, and corroborating at the same time the possible long–distance migration.

The main loss of gaseous hydrocarbons occurred during the Pleistocene time (Figure 3.8), being associated to the development of glaciations in the Barents Sea. Due to this and considering the importance that this fact could have in the possible leakage of gaseous hydrocarbons to the surface and in the context of our study goals, some other details were also considered and evaluated. One of them is the predicted reservoir behavior in response to the periodic loading and unloading of the basin during glacial and interglacial cycles which occurred in combination with glacial erosion. Based on the modelling results, it has been observed that transient effects in the pore and hydrostatic pressure distributions occurred (Figure 3.11), with a slight increase in pore pressure above the hydrostatic pressure gradient during maximum ice loading and glacial retreat, which generates as a consequence overpressure in the system (Figure 3.11). Variations of pore pressure are between ~3 and 6 MPa. Such pressure oscillations have certainly affected the petroleum accumulated in the reservoir, especially the highly compressible gas phase. It must be kept in mind that the results from our model are

general approximations of all the processes involved (e.g. the gas phase compression and expansion) because modelling all the complexities associated is in most cases not possible. Nonetheless, the main physical processes such as compaction, pressure evolution and gas compressibility (e.g. calculation based on the gas composition using the Peng–Robinson equation of state) are correctly treated.

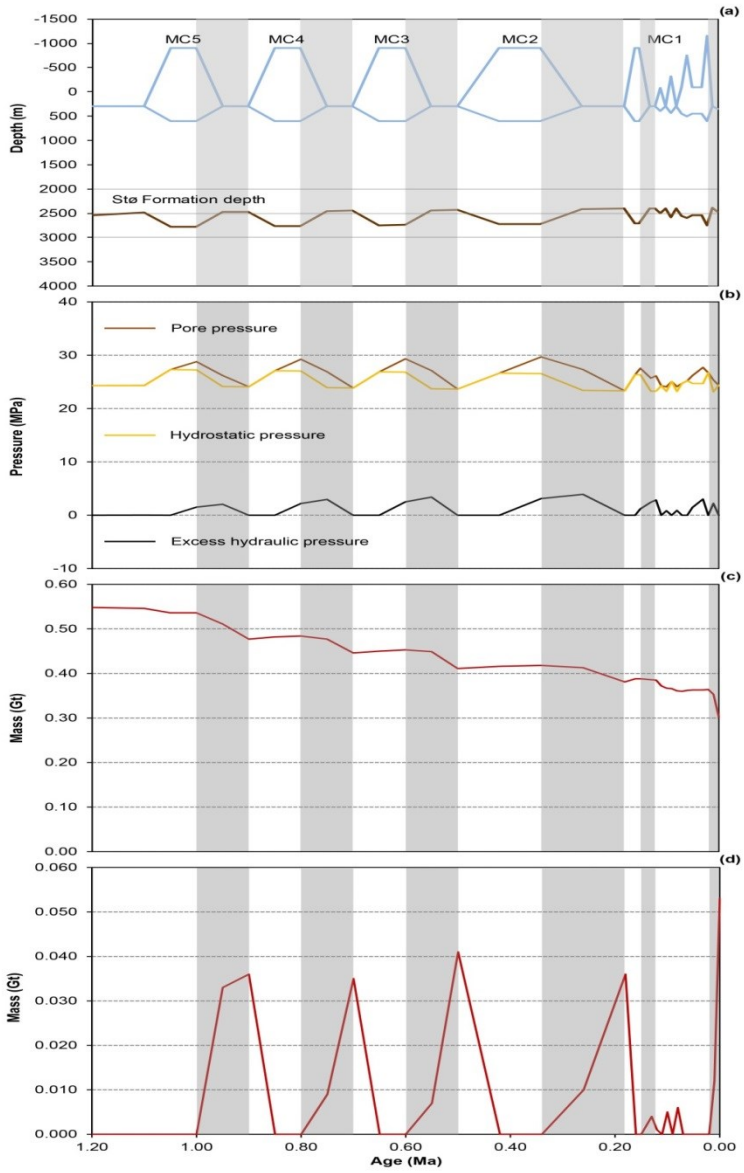

Figure 3.11 Correlation of modeled glacial history, predicted reservoir pressure conditions and gas masses trapped and leaked. a) Glacial history together with the depth variation of the Stø Formation reservoir. b) Oscillating reservoir (Stø Formation) pressure conditions (pore, hydrostatic and excess hydraulic pressures). c) Calculated gas mass in the Stø Formation during the last 1.2 Ma. Note that the main events of gas decrease occur in the transition from maximum glaciation to the interglacial period. d) Gas loss expressed as outflow at model top.

The accumulation history of the gaseous hydrocarbons in the Stø Formation at each stage during the glacial–interglacial periods (between 1.10 and 0.01 Ma) is shown in Figure 3.11. Here it is easily visualized that a large and continuous loss of gas took place, with the main loss pulses associated to the glacial retreat stages. The specific amounts of gas lost after each megacycle, which were obtained from the modeling efforts are as follows: 0.070 Gt (MC5), 0.031 Gt (MC4), 0.036 Gt (MC3), 0.030 Gt (MC2), and 0.080 Gt (MC1). This gives an estimation of the total amount of gas loss of around 0.247 Gt.

Since it is of interest for this study to evaluate the possibility of thermogenic gas leakage to the surface during the glacial–interglacial periods, part of the output from the basin modelling study was that related to the gaseous hydrocarbon losses reported as outflow at the top of the model (Figure 3.11). This information corroborated that the peaks of gas outflow are synchronous with the leakage or gas lost from the reservoir. Therefore, it is proposed that ascending gas leaked from the reservoir feeds the surface of the model. Also the calculated gas migration vectors during the same glacial–interglacial periods (Figure 3.12) demonstrate that the gas moves buoyantly towards the surface in the model.

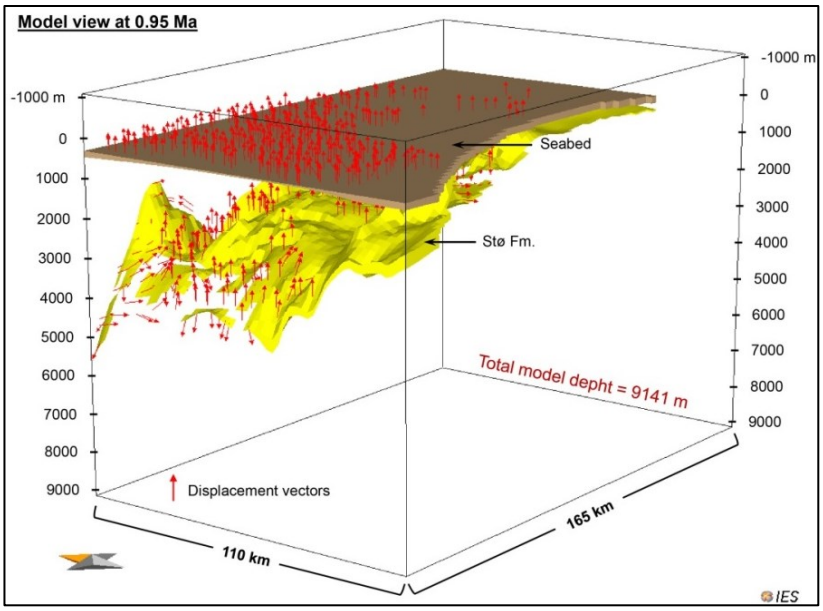

Figure 3.12 3D view at 0.95 Ma (end of the 1st glaciation) showing the Stø Formation, the shallowest layer at that time (brown layer) and the displacement vectors of hydrocarbons (red arrows); which indicate the migration of hydrocarbons from the deep reservoir unit to the shallowest layer.

3.1.3 Main discussion from basin modelling (focus in gas leakage)

This discussion is also part of the first paper, already published (Rodrigues Duran et al., 2013). The pore pressure and overpressure conditions in the subsurface were successfully simulated during the glacial–interglacial cycles in this study as previously presented. The overpressure in sedimentary basins can be generated by a variety of mechanisms as reported in several works (Mann and Mackenzie, 1990; Clayton and Hay, 1994; Osborne and Swarbrick, 1997). The dominant mechanism is related to compaction disequilibrium, in which an increase in the compressive stress results in a decrease of the sediments porosity and permeability. Therefore, an increase of the pore pressure above the hydrostatic level takes place due to the low capability of the fluids to escape from the pores, which is controlled by the decrease of permeability. This is in accordance with the results from this study, in which it has been observed that overpressure is generated in connection with the rapid burial accompanied by vertical compression due to the loading caused by the ice–sheet.

On the other hand, oscillations of the hydrostatic pressure gradient have also been observed during the glacial–interglacial cycles. Based on this situation modeled, it can be assumed that the glacier covering the Hammerfest Basin was a warm glacier, which is a glacier at the pressure melting point throughout. The large scale erosion that took place in the area also corroborates this assumption, as warm glaciers generate much more erosion than cold glaciers. However, the effects of melt water column beneath the glacier cannot be considered in the modeling software used. The specific modelling of the Northwestern Europe ice–sheet/groundwater establishes that many polar glaciers melt basally (Boulton et al., 1993; van Weert et al., 1997). In a glacially influenced sedimentary basin the meltwater underneath an ice–sheet can be discharged due to groundwater flow through the subsurface (Boulton et al., 1995). This can happen in several pulses if several glacial cycles take place. In the case of high meltwater production, the groundwater pressure may become very high, in some cases even as high as the overburden pressure (van Weert et al., 1997). Therefore, this groundwater flow can be considered a vital process in controlling subsurface pressures. For this study it can be then pointed out that the loading and unloading associated to the growth and retreat of an ice–sheet certainly affected the hydrostatic pressure and the sediment

compaction, which in turn influenced the pressure regime in the reservoir, the fluid flow direction and the sealing capacity of cap rocks.

The leakage of gas from the Stø Formation reservoir (0.247 Gt) that was observed in this modelling work is mainly the result of seal capillary failure. The capillary failure of the seal, also referred as the maximum column height that a cap rock can hold, takes place when the upward directed buoyancy pressure generated by the lower density of petroleum (especially gas), plus any excess overpressure in the reservoir, exceeds the capillary resistance pressure of the seal (Clayton and Hay, 1994; Hantschel and Kauerauf, 2009). Capillary failure is the normal mode of failure under hydrostatic or moderately overpressured conditions. In the modelling software, the increase of the pore and/or hydrostatic pressures (between 3 and 6 MPa) during glacial loading invariably leads to the compression of the gas phase, reducing the total petroleum column height, increasing the fluid density and thus inhibiting capillary failure of the seal. At the transition from glacial to interglacial periods the retreat of the ice–sheet occurs accompanied by erosion; therefore during this time, and also during the interglacials, unloading of the basin take place, which causes the expansion of the gas column to a volume larger than the initial, resulting in a larger hydrocarbon column height, the capillary failure of the cap rock and hydrocarbon leakage from the reservoir. The gas leakage is determined by the physical process occurring in the basin during its geological evolution. All of the processes discussed above (gas compressibility, PVT effects, spilling, remigration, capillary flow and leakage) were taken into account by the modelling software. However, one parameter not included in this model corresponds to the structural geology of the area, which can play an important role on the leakage of hydrocarbons since structural patterns like faults can act as migration pathways. An abundance of faults and associated indications of gas leakage have been described for the Snøhvit field (Ostanin et al., 2012; Ostanin et al., 2013). Other mechanisms can also play a role and determine the petroleum leakage from the reservoir through the seal, such as hydraulic leakage and diffusive/molecular transport (Krooss and Leythaeuser, 1996; Corcoran and Doré, 2002; Karlsen and Skeie, 2006).

Accordingly, the estimates on leakage for this study must be seen as one possible scenario of petroleum leakage in the Hammerfest Basin. However, the fact that volumetric proportions of oil versus gas hosted in the individual fields of the study area, their respective GORs, and the fact that underfilled structures are reproduced indicates that the leakage estimates calculated may be realistic.

3.1.4 Geochemical – basin modelling correlation (paper 2)

In the next sections a correlation of the basin modelling results with the interpretation from geochemical fluid data will be summarized. This will be done through an overview of the data available and the information this data can give in relation to the understanding of the petroleum systems in the Hammerfest Basin. This geochemistry data will be presented according to the different fluid fractions, which are: gas phase (C_1–C_5), light hydrocarbons (C_6–C_{10}) and the oil phase (C_{10+}).

3.1.4.1 Gas phase (C_1–C_5)

The analysis of gas isotopes and gas composition can be used in order to differentiate sources of gas, alteration mechanisms and maturity. In order to follow these investigations a few well–known interpretation schemes were used in this study (Bernard et al., 1978; Tissot and Welte, 1984; Berner and Faber, 1988; Whiticar, 1994; Aali et al., 2006).

The first two interpretations considered are more or less the same and allow identifying the origin of the gas and the possible influence of alteration mechanisms. They correspond to the correlation of $\delta^{13}C$ of methane versus gas dryness (Figure 3.13), defined as the proportion of methane in relation to ethane and propane or C_1/C_2+C_3 (Bernard et al., 1978); and the correlation of $\delta^{13}C$ of methane versus the wetness percentage (Figure 3.13), defined as the proportion of C_2–C_4 hydrocarbons in the total C_1–C_4 gas mixture (Tissot and Welte, 1984). Both plots show that all the gaseous fluids accumulated in the Hammerfest Basin have a dominantly thermogenic origin. Some of the samples from the Goliat field, which are fluids taken from the Tubåen and Snadd formations, plot in an area with a tendency towards the mixed microbial–thermogenic

gas, this indicates that some generation of biogenic methane due to microbial activity occurred; a process well known during biodegradation and also reported for the Goliat field by Ohm et al. (2008) and the Norwegian Petroleum Directorate (2010a).

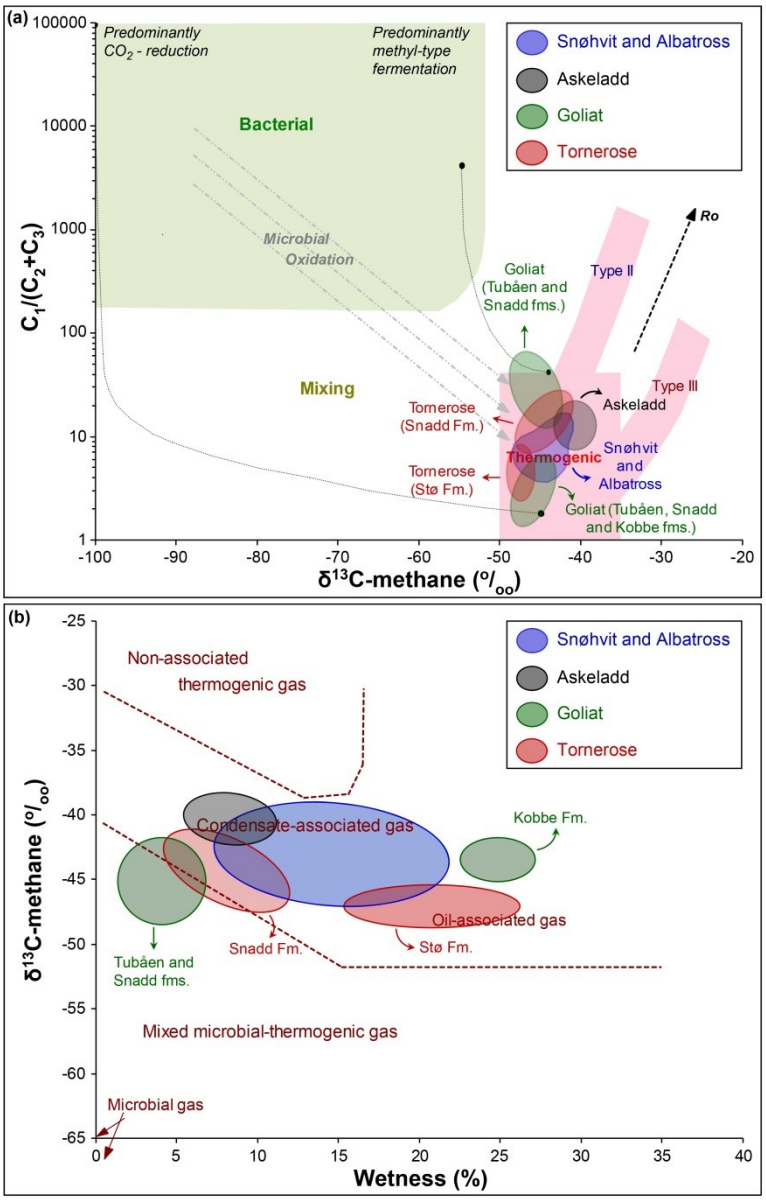

Figure 3.13 a) Correlation of gas–dryness ($C_1/(C_2 + C_3)$) with the methane isotopic composition. b) Correlation of wetness percentage with the methane isotopic composition. Description of gas–dryness and wetness percentage can be found in the text (section 3.1.4). The data for the Goliat field and the Tornerose discovery is shown in two separate areas corresponding to the stratigraphic levels where the fluids were encountered, which are: the Tubåen, Snadd and Kobbe formations for the Goliat field, and the Stø and Snadd formations for the Tornerose discovery. The interpretation overlays stem from pIGI software and this correspond to an IGI's syntheses of the references given in the software.

Alternatively, it can also be established that all the samples are associated gases (Figure 3.13). The samples from the Askeladd field, as well as some samples from Snøhvit, Albatross and Goliat (Tubåen and Snadd formations) fields and the Tornerose discovery (in the Snadd Formation) are mainly condensate–associated gases, while other samples from the same fields and the Tornerose discovery are oil–associated gases. The basin modelling results do not give enough information such that it can be used to make a correlation with the previous interpretation regarding oil– or condensate–associated gas origin. However, based on the predicted petroleum phases for each field in the model, it can be assumed that in the case of Snøhvit, Albatross and Goliat fields where oil and gas columns have been predicted, a dominant oil–associated gas should be expected. The Askeladd field and the Tornerose discovery, on the other side, were reproduced as pure gas fields, indicating that higher maturity fluids should dominate the system and therefore a condensate–associated gas should be expected.

The second interpretation performed allows characterizing the maturity of the gas samples. This interpretation can be done by using the gas isotopic correlations of ethane vs. propane and methane vs. ethane (Figure 3.14). The isotopically lightest sample and also the one presenting the lowest maturity (~0.70% VR), is found in the Tornerose discovery within the Stø Formation reservoir. This correlates quite well with the model results since approximately same maturity levels have been reached by the Snadd and Hekkingen formations in the area (Figure 3.5). Samples from Snøhvit and Albatross fields, as well as some samples from the Goliat field and the Tornerose discovery show a maturity level between 0.85 and 1.30% VR (early mature or oil window to gas mature). The samples from the Askeladd field show the highest maturity level (between 1.30 and 1.80% VR). These observations are correlated as well with the modelling results, as the highest maturity levels from both the Kobbe and Snadd formations were reached in the western areas from where the Askeladd field has been filled (Figure 3.5 and Figure 3.10).

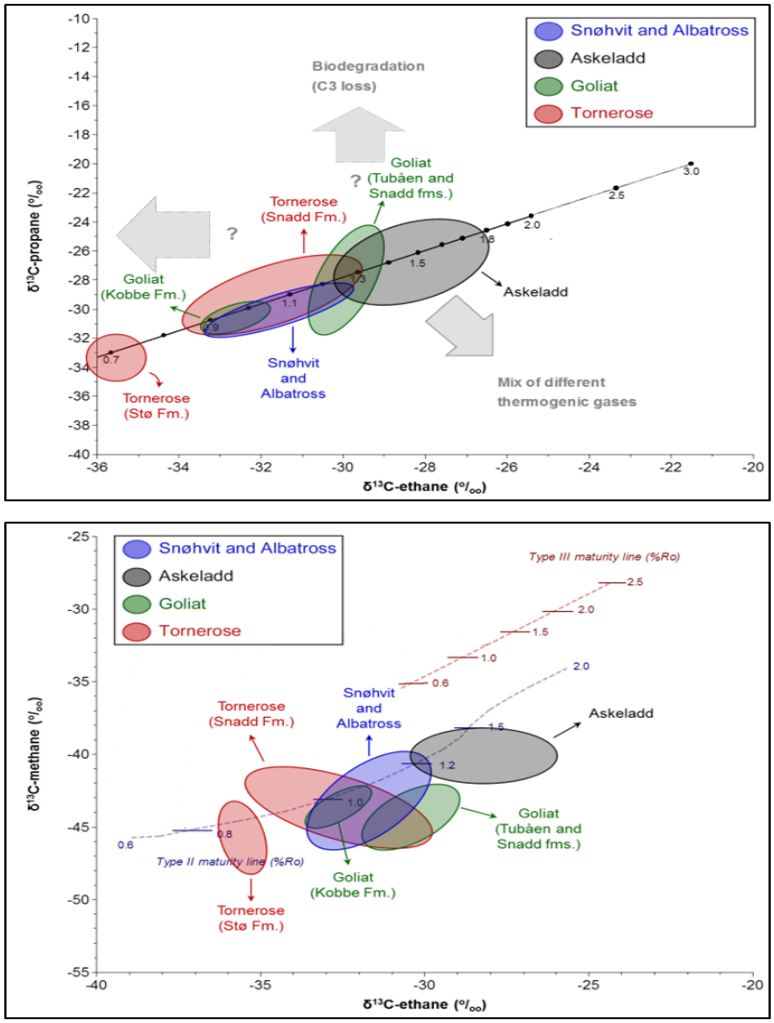

Figure 3.14 Maturity interpretation using gas isotopic composition. The interpretation overlays of this figure stem as well from pIGI software.

3.1.4.2 Light hydrocarbons fraction (C_6–C_{10})

The compositional data of the light hydrocarbons was used in order to correlate the samples from the different fields and also to evaluate the influence of secondary processes, such as biodegradation, water washing and evaporative fractionation. To achieve this, two main interpretations of the data were made based on the parameters established by Halpern (1995) and Thompson (1983) and by using star diagrams. For the Halpern parameters two diagrams were plotted (Figure 3.15), corresponding to the C_7 oil–correlation and C_7 oil–transformation star diagrams (Halpern, 1995). The C_7 oil–correlation diagram shows a similar pattern for all the samples, this can therefore indicate that these fluids probably belong to the same oil family and/or that they share the same source. Moreover, in the C_7 oil–transformation diagram differences are

observed mainly with respect to the fluid samples from the Goliat field. The ratios in this plot, with the exception of the Tr_1 and Tr_6, are especially sensitive to biodegradation. In this sense the variability observed among these samples can be attributed to biodegradation as also described by Ohm et al. (2008). The Tr_1 and Tr_6 ratios are more useful to indicate the loss of water–soluble aromatic compounds due to water washing or due to long–distance migration. These two ratios (Tr_1 and Tr_6) are plotting differently for the light hydrocarbons from Goliat and Tornerose with respect to the other fields. Thus, this can corroborate the influence of long–distance migration of the light hydrocarbons present in these two areas, as already suggested by the basin modelling results.

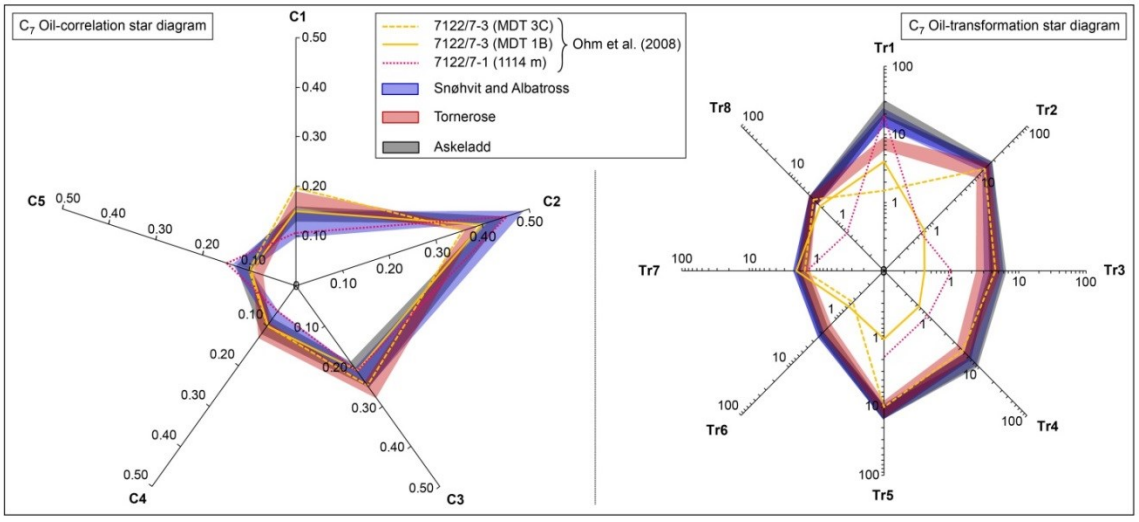

Figure 3.15 Light hydrocarbons (C_7) oil–correlation and oil–transformation star diagrams (Halpern, 1995). The results for the Goliat field (yellow and pink lines) were taken from the work of Ohm et al. (2008).

A star diagram considering the Thompson (1983) parameters has also been generated for each field (Figure 3.16). These parameters are quite similar for the light hydrocarbons in the Snøhvit, Albatross and Askeladd fields and the Tornerose discovery. The light hydrocarbons from the shallower reservoirs in the Goliat field (Tubåen and Snadd formations) show a clear signature of biodegradation (Figure 3.16). The deepest samples in the Goliat field (Kobbe Formation) are similar to the samples in the other fields; however there is a slight variation that can be used to suggest the

possibility of a different source or, additionally, to indicate a modest water washing and therefore corroborate once again the long–distance migration.

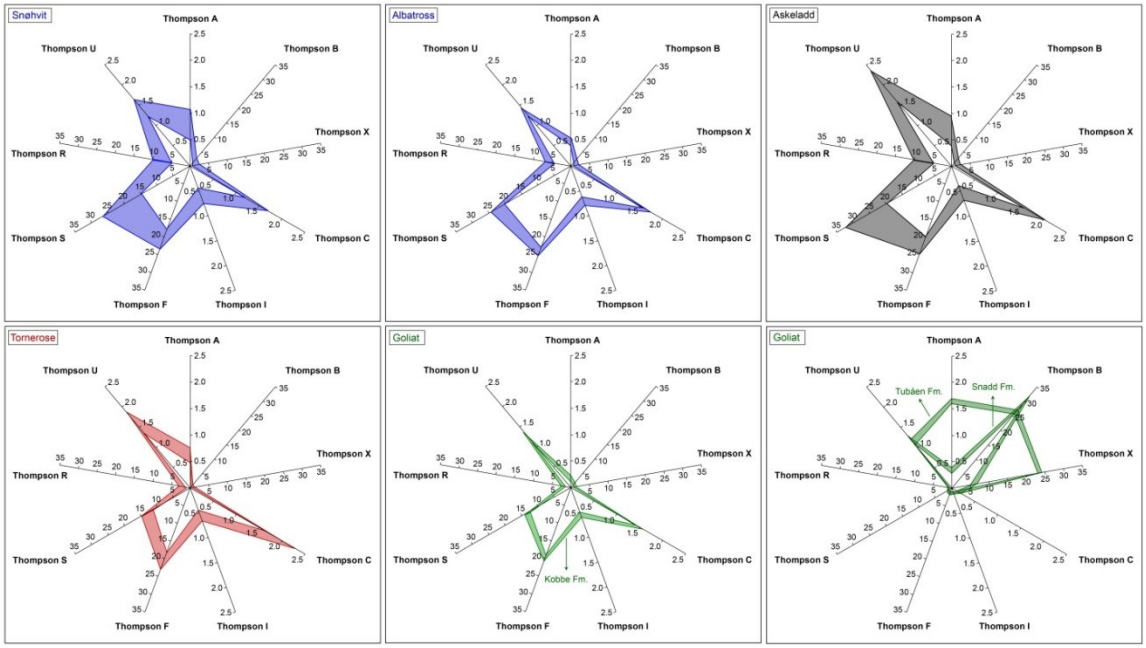

Figure 3.16 Light hydrocarbons star diagrams using the Thompson (1983) parameters. The different parameters correspond to: A=Benzene/*n*–hexane; B=Toluene/*n*–heptane; X=(*m*–xylene + *p*–xylene)/*n*–octane; C=(*n*–hexane + *n*–heptane)/(cyclohexane + methyl-cyclohexane); I=(2– + 3–methyl-hexane)/(1*cis*3 + 1*trans*3 + 1*trans*2–dimethyl-cyclopentanes); S=*n*–hexane/2,2–dimethyl-butane; F=*n*–heptane/methyl-cyclohexane; R=*n*–heptane/2–methyl-hexane; U=cyclohexane/methyl-cyclohexane.

Finally an interpretation was also done using the cross plot of the Thompson heptane and *iso*–heptane indices (Thompson, 1983), which allows the assessment of source, maturity and alteration effects (Figure 3.17). The samples from the Snøhvit, Albatross and Askeladd fields plot close together in the mature zone of the diagram and close to the type II kerogen curve (or aliphatic curve) based on the Thompson (1983) interpretation. The trend observed from Snøhvit to Albatross can tentatively correspond to a maturity trend (also supported by the gas isotopes, Figure 3.14). The fluid data from the Askeladd field extends to the areas with higher maturity and with a slight shift towards the type III kerogen trend line. The samples from the Tornerose discovery plot close to the type III kerogen curve (or aromatic curve); this can be an indication of likelihood for a different source contribution here with respect to the western fields in the Hammerfest Basin. The samples from the Goliat field have low heptane and *iso*–

heptane ratios, and therefore plot in the biodegradation zone, corroborating previous results and information from well reports (Ohm et al., 2008; Norwegian Petroleum Directorate, 2010a).

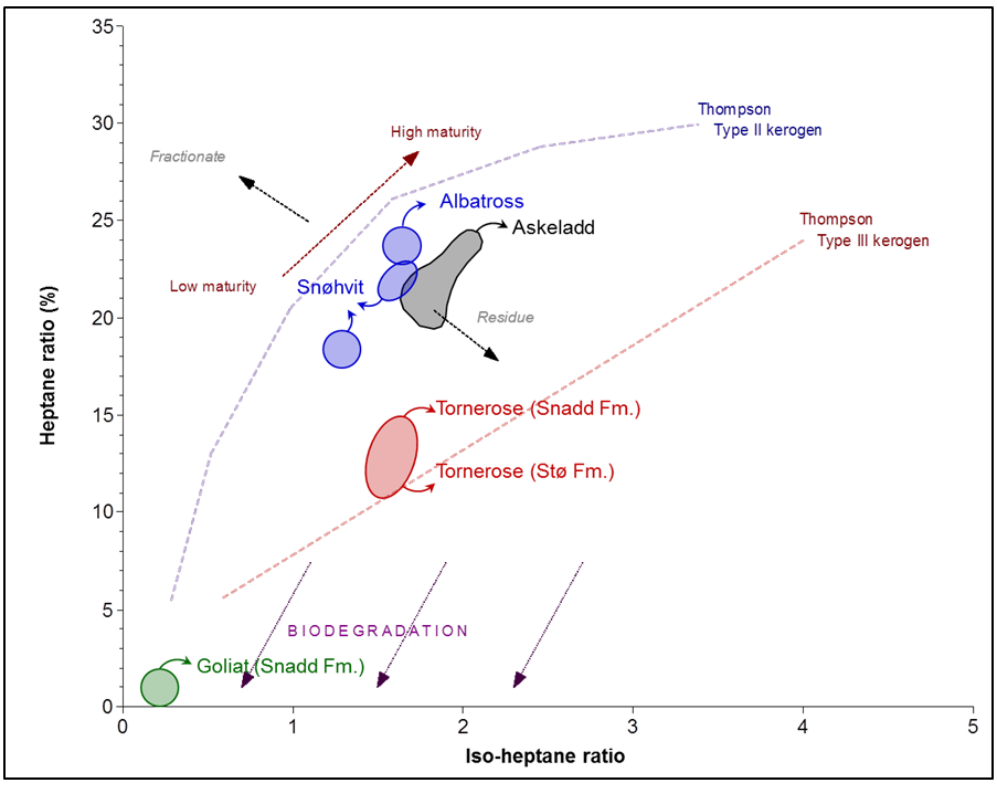

Figure 3.17 Correlation of the heptane and *iso*–heptane ratios according to Thompson (1983).

3.1.4.3 Oil phase (C_{10+}) – Paleo–environment interpretation

The correlation of pristane/*n*–C_{17} versus phytane/*n*–C_{18} (Figure 3.18) indicates that all the oil samples in the Hammerfest Basin fields are in the early mature stage and should have been predominantly derived from a similar type of organic matter, which according with the interpretation from Figure 3.18 corresponds to mixed sources, that is a mixing of marine and terrigenous organic matter input. The Askeladd field oil samples are slightly shifted towards a more oxic depositional environment indicative of a more terrigenous organic matter deposition. This supports as well the trend observed in the light hydrocarbon analysis previously presented (Figure 3.17).

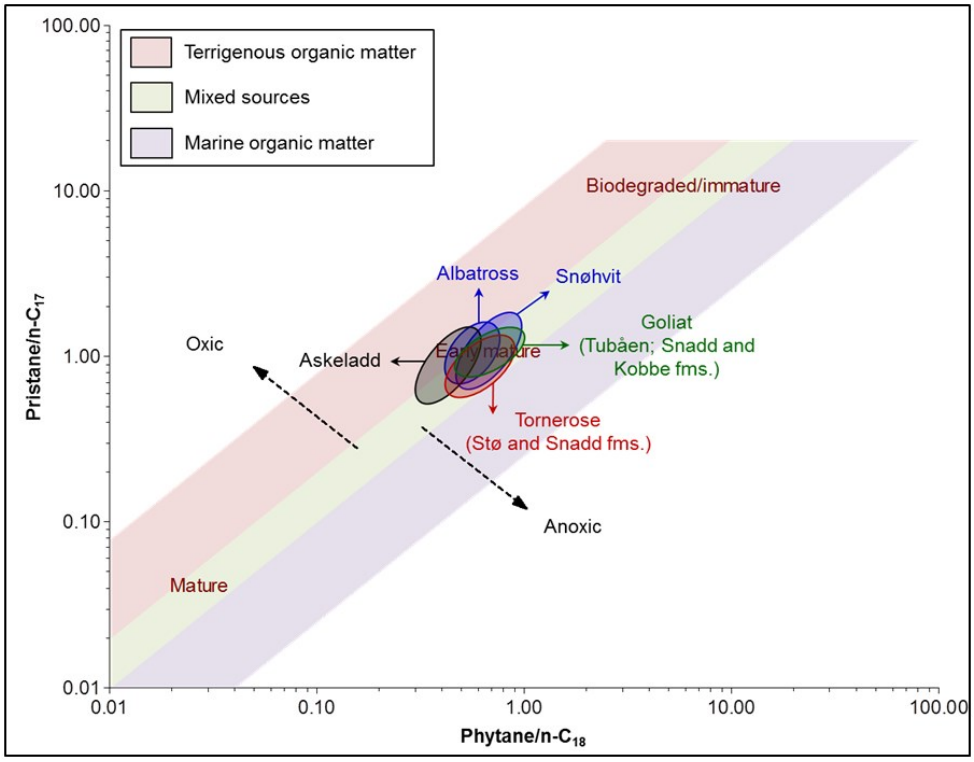

Figure 3.18 Paleo–environment interpretation using the correlation of pristane/*n*–C_{17} versus phytane/*n*–C_{18}

On the other hand, the steranes and aromatic data (Figure 3.19) was also used to target the depositional environment of the source rocks that generated the oils accumulated in the area. Mainly a depositional marine environment for the source rocks that have generated the oils in the Snøhvit, Albatross and Askeladd fields and in the Tornerose discovery (Stø Formation) can be suggested. A more transitional environment (shallow marine to coastal) is observed based on the steranes distribution for the source rocks that generated the oils in the Goliat field and also the oil in the Snadd Formation in the Tornerose discovery (Figure 3.19). This could also be due to the fact of some biodegradation influence, which produces a selective depletion in the C_{27} steranes (Peters et al., 2005). However, the level of biodegradation necessary to affect the steranes has not been reported for any of the fields in the Hammerfest Basin. The variability in the steranes distribution most likely reflects the sourcing from the same general type of source rock but with some possible organic facies variation. The aromatic data together with the isoprenoids (Figure 3.19) also show that the depositional environment of the source rocks might correspond to a marine environment, with minor facies variability in the sample set.

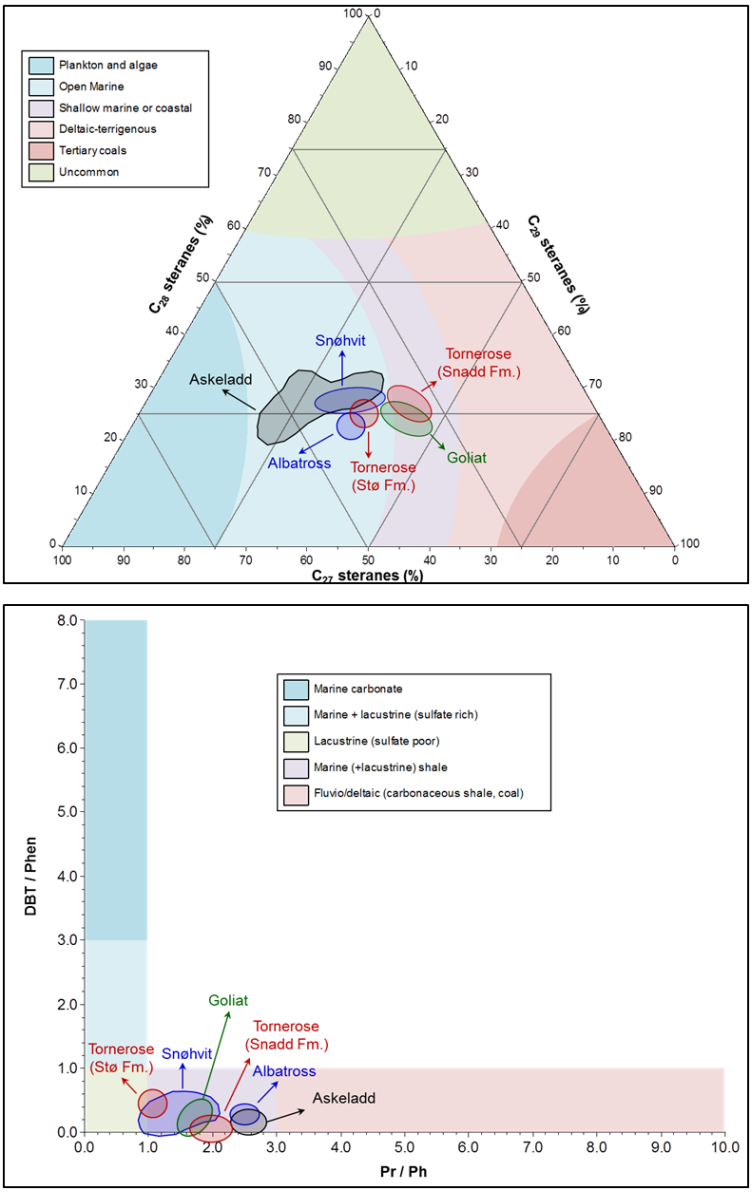

Figure 3.19 Paleo–environment interpretation using the C_{27}, C_{28}, C_{29} steranes percentage (top) and the correlation of the dibenzothiophene/phenantrane ratio versus pristine/phytane ratio (bottom).

3.1.4.4 Oil phase (C_{10+}) – Maturity–related biomarkers

For the maturity interpretation of the oil phase seven parameters or ratios were selected based on the steranes and terpanes biomarkers and on the aromatic steroids (Figure 3.20). The oils from the Snøhvit, Albatross and Askeladd fields have two trends, which may reflect two different oil families with different maturity levels or maybe contribution from two different source rocks. For the Goliat field and the Tornerose discovery there are also two trends which at the same time differ from the two previous trends observed in the Snøhvit, Albatross and Askeladd fields.

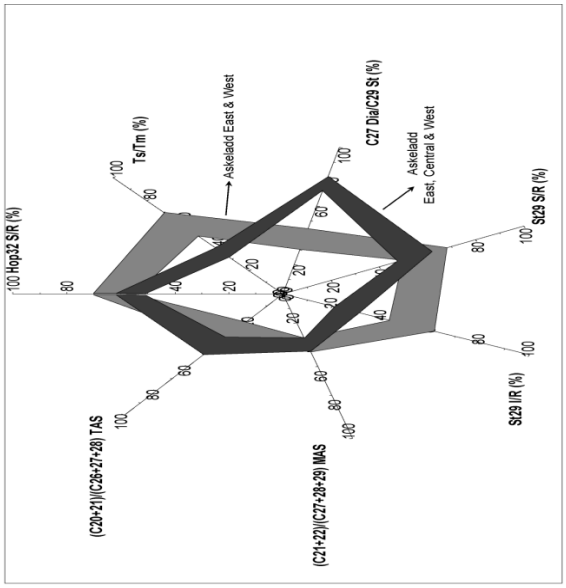
100 Hop32 S/R (%)
Ts/Tm (%)
C27 Dia/C29 St (%)
St29 S/R (%)
St29 I/R (%)
(C21+22)/(C27+28+29) MAS
(C20+21)/(C26+27+28) TAS
Askeladd East & West
Askeladd
East, Central & West

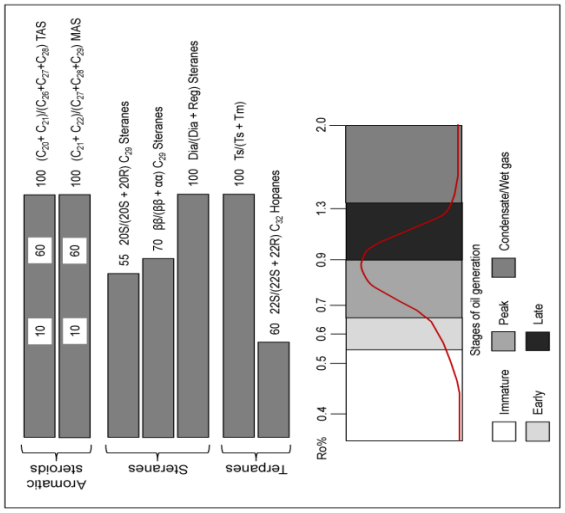
Aromatic
steroids
Steranes
Terpanes
100 (C20+ C21)/(C26+C27+C28) TAS
100 (C21+ C22)/(C27+C28+C29) MAS
55 20S/(20S + 20R) C29 Steranes
70 ββ/(ββ + αα) C29 Steranes
100 Dia/(Dia + Reg) Steranes
100 Ts/(Ts + Tm)
60 22S/(22S + 22R) C32 Hopanes
Ro%
Stages of oil generation
Immature
Peak
Condensate/Wet gas
Early
Late

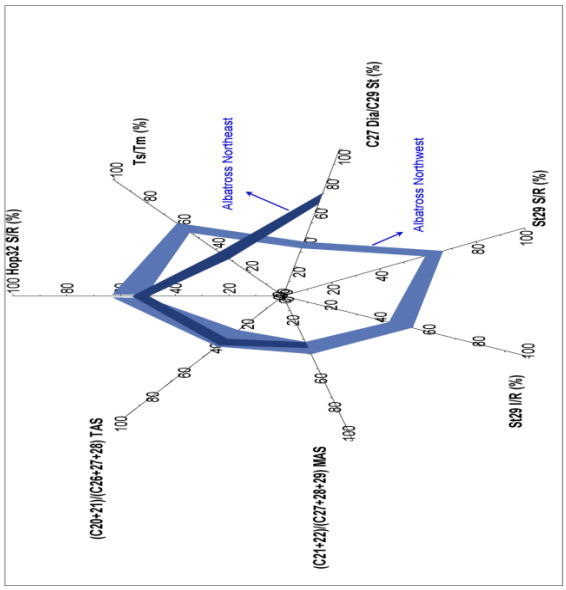
100 Hop32 S/R (%)
Ts/Tm (%)
C27 Dia/C29 St (%)
St29 S/R (%)
St29 I/R (%)
(C21+22)/(C27+28+29) MAS
(C20+21)/(C26+27+28) TAS
Albatross Northeast
Albatross Northwest

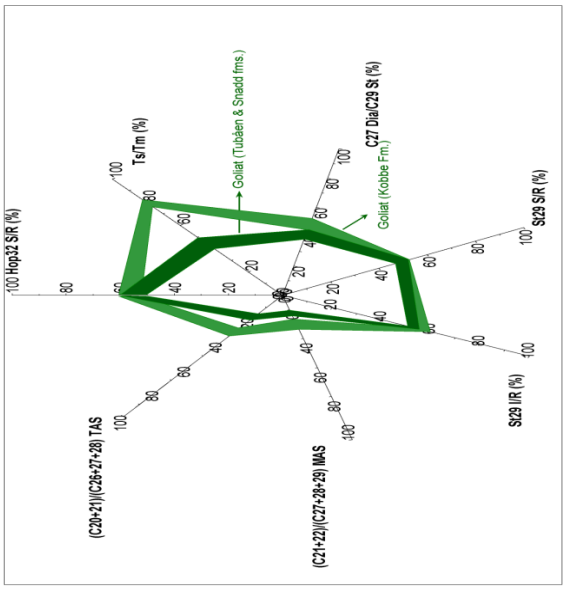
100 Hop32 S/R (%)
Ts/Tm (%)
C27 Dia/C29 St (%)
St29 S/R (%)
St29 I/R (%)
(C21+22)/(C27+28+29) MAS
(C20+21)/(C26+27+28) TAS
Goliat (Tubåen & Snadd fms.)
Goliat (Kobbe Fm.)

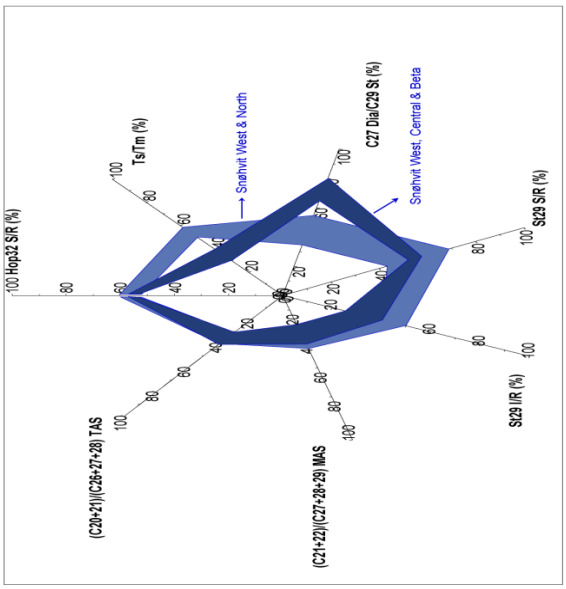
100 Hop32 S/R (%)
Ts/Tm (%)
C27 Dia/C29 St (%)
St29 S/R (%)
St29 I/R (%)
(C21+22)/(C27+28+29) MAS
(C20+21)/(C26+27+28) TAS
Snøhvit West & North
Snøhvit West, Central & Beta

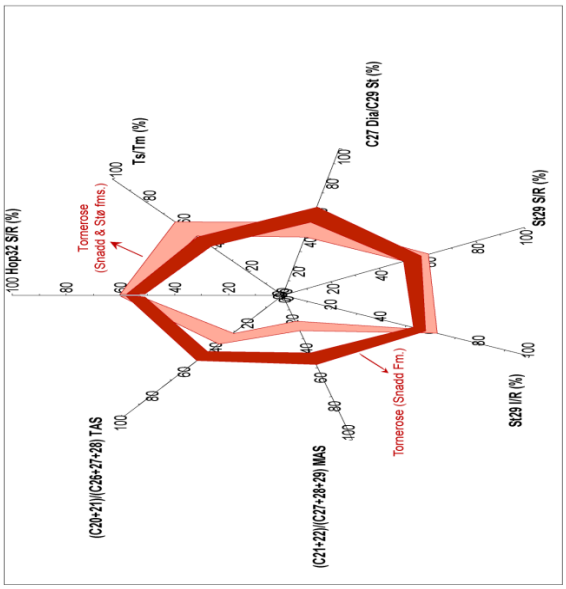
100 Hop32 S/R (%)
Ts/Tm (%)
C27 Dia/C29 St (%)
St29 S/R (%)
St29 I/R (%)
(C21+22)/(C27+28+29) MAS
(C20+21)/(C26+27+28) TAS
Tomerose
(Snadd & Stø fms.)
Tomerose (Snadd Fm.)

Figure 3.20 Maturity interpretation based on six biomarkers and aromatics, which are: (1) C_{32} 22S homohopane relative to C_{32} 22R homohopane ratio; (2) 18α 22,29,30 Trisnorhopane (Ts) relative to 17α 22,29,30 Trisnorhopane (Tm); (3) C_{27} diasteranes [13β, 17α (20S, 20R) diacholestanes and 13α, 17β (20S, 20R) diacholestanes] relative to C_{29} steranes [5α, 14α, 17α (20S, 20R) regular steranes and 5α, 14β, 17β (20S, 20R) isosteranes] ratio; (4) Isomerization index for C_{29} regular steranes (5α, 14α, 17α 20S regular steranes and 5α, 14α, 17α 20R regular steranes); (5) Racemization index for C_{29} steranes or ββ/(ββ+αα) ratio [5α, 14β, 17β (20S, 20R) C_{29} isosteranes relative to 5α, 14α, 17α (20S, 20R) C_{29} regular steranes], (6) mono–aromatic steroids ratio; and (7) tri–aromatic steroids ratio. *Bottom right:* Approximate ranges of biomarker maturity ratios against vitrinite reflectance (Peters et al., 2005). Here the terms west, east, northwest, northeast, central, Beta and North for the Albatross, Askeladd and Snøhvit fields are used. This nomenclature is based on the location of the samples as observed in the fields at the Norwegian Petroleum Directorate website (FactMaps).

The 22S/ (22S+22R) C_{32} homohopane as well as the 20S/ (20S+20R) C_{29} sterane ratios show full isomerization in all cases (Figure 3.20); therefore they are not any more useful for maturity interpretations. The main differences are related to the Ts/ (Ts + Tm), the diasteranes/steranes, and the C_{29} *iso*/regular steranes ratios, the three of them are not only maturity sensitive; they are also sensitive to facies variations. The Ts/ (Ts + Tm) is most reliable as a maturity indicator when evaluating oils from a common source of consistent organic facies (Peters et al., 2005). The maturity results observed with the ratios used allow separating the oil samples in two groups. One group shows that the samples with a higher Ts/ (Ts + Tm) and C_{29} *iso*/regular steranes ratios are associated to a lower diasterane/sterane ratios. This group has samples from Snøhvit West and Nord, Albatross NW, Askeladd East and West, and Tornerose in the Snadd and Stø formations. The second group shows that the samples are plotted the other way around, that is elevated diasteranes/steranes ratios associated to lower Ts/ (Ts+Tm) and C_{29} *iso*/regular steranes ratios values. In this group were found samples from Snøhvit West, Central and Beta, Albatross NE, Askeladd East, central and West, and Tornerose in the Snadd Formation. Tentatively, these groups of fluids could be attributed to be products of different source rocks that reached different maturity levels. A clear representation of the samples distribution for the first two ratios is shown in Figure 3.21.

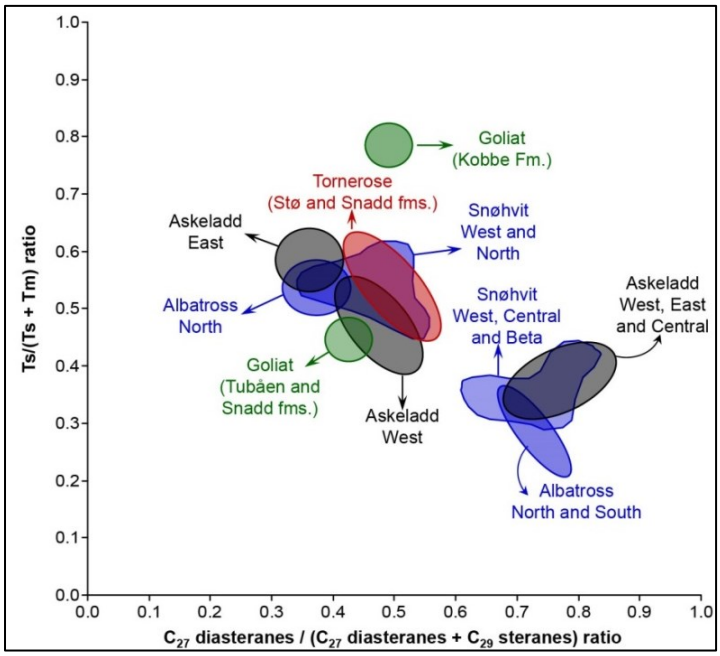

Figure 3.21 Correlation of the Ts/ (Ts + Tm) and diasteranes/steranes ratios.

According to this cross plot, samples from Goliat in the Kobbe Formation are separated from the rest indicating a likely contribution from a different source rock. For this particular case it could tentatively be postulated that the hydrocarbons were sourced from the same sequence in which they were found, that is the Kobbe Formation; since this corresponds to one of the potential source rocks for the area also considered in the basin modelling and predicted to have reached oil window maturity levels in the Southwestern margin around the Goliat field (Figure 3.5). On the other hand, the variability among the other two groups that occurs within the individual fields could certainly indicate facies differences, sourcing from different rocks, mixing of hydrocarbons in the reservoirs and/or different maturity levels.

The mono– and tri–aromatic steroids together with the C_{29} *iso*/regular steranes ratios are, in this case, the only maturity indicators that can be used as well for the late oil window maturity, with at least the first two not being dependent on facies variation. They suggest maturity levels between 0.7 and 0.8% VR for almost all the fields with the exception of Goliat. In the Goliat field these ratios suggest lower maturity levels, i.e. VR between 0.6 and 0.7%. The maturity interpretation from vitrinite reflectance is

based on the extrapolation of the ratio percentage to the percentage of vitrinite reflectance (Peters et al., 2005).

3.1.4.5 Oil phase (C_{10+}) – Age–related biomarkers

The extended tricyclic terpane ratio or ETR (Holba et al., 2001) and the C_{28}/C_{29} steranes ratio (Grantham and Wakefield, 1988) were used as age diagnostic biomarkers to address contributions from Jurassic and Triassic source rocks. This is based on the assumption that most of the petroleum found in the Hammerfest Basin has been predominantly sourced by the Upper Jurassic Hekkingen Formation and the Triassic Snadd and Kobbe formations. The ETR ((C_{28} + C_{29}) / (C_{28} + C_{29} + Ts)) defined by Holba et al. (2001) can be used to differentiate crude oils (within the oil window) that were generated from Triassic, Lower Jurassic, and Middle–Upper Jurassic source rocks. The study made by Holba et al. (2001) was done using a worldwide crude oil sample dataset, which shows that the Triassic oil samples have ETRs ≥ 2.0; Early Jurassic oil samples have ETRs ≤ 2.0; and Middle or Late Jurassic oil samples have ETRs in most of the cases < 1.2. In the dataset used in this study it was observed that all the values for this ratio in the Hammerfest Basin are below 1.2 (Figure 3.22).

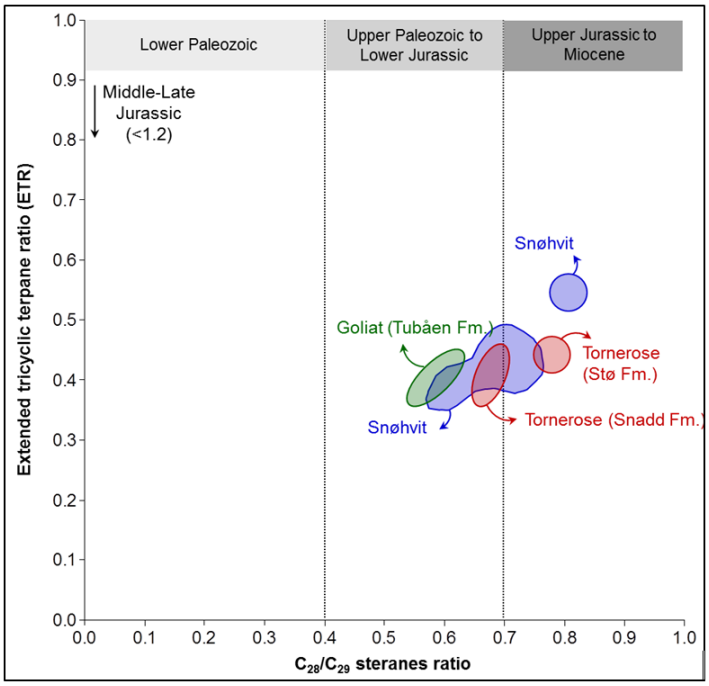

Figure 3.22 Correlation of two age–related biomarker ratios, the extended tricyclic terpane ratio (ETR) and the C_{28}/C_{29} steranes ratio.

The C_{28}/C_{29} steranes ratio is also an age–related parameter, but it has been mainly used for oils lacking terrigenous input. Grantham and Wakefield (1988), evaluated the variations in the sterane carbon number distribution (from C_{27} to C_{29}) of crude oils that were derived from marine source rocks, in correlation with the time at which the source rocks were deposited. They observed that the relative proportions of C_{27} steranes show no particular trends through geological time. However, the C_{28} steranes show a clear trend of increasing percentages through time and the C_{29} steranes show a broad trend of decreasing percentages through geological time. Then, Grantham and Wakefield (1988) combined the percentages of C_{28} and C_{29} steranes as a ratio and plotted this ratio against the geological age of the source rocks. Their results show that the ratio is <0.5 for Lower Paleozoic and older oils, values between 0.4 and 0.7 are observed for oils from Upper Paleozoic to Lower Jurassic and for Upper Jurassic to Miocene oils the values are greater than ~0.7. For this study, the oil samples from the Snøhvit and Goliat fields and the Tornerose discovery plot in an interval from 0.5 to 0.9, indicating a highly variable source age extending from Triassic to Upper Jurassic. This means that a clear source differentiation based only on age related biomarkers is quite difficult or not possible. However, the general trend in which the samples plot indicates that some of the Snøhvit and Tornerose oils are likely sourced from the Upper Jurassic Hekkingen Formation, while most other fluids show a tendency for contributions from older, probably Triassic, source rocks. Data for Askeladd and Albatross was unfortunately not available.

3.1.5 Main discussion geochemistry and basin modelling correlation

Based on the results previously presented, not just from the geochemical interpretation but also from the basin modelling side, it is possible to say that a conclusive interpretation regarding the petroleum sources in the Hammerfest Basin is very difficult. The reasons can be related to the fact that this is an area characterized by multiple source rocks and reservoirs, by single and/or two phase accumulations, by a complex geologic history, as well as by a variable analytical coverage of the available samples. Especially the comparison of interpretations based on analysis of different compound ranges, e.g. gas phase, light hydrocarbons and oil phase, proved challenging.

It is quite important to emphasized that the comparison of geochemical interpretations in relation with source rocks contributing to individual reservoirs, versus results derived from the numerical simulation of a basin evolution (which includes source rock maturation, petroleum generation, migration, accumulation and leakage), requires consideration of the scales for which analytical or modelling results apply. The geochemical analysis gives on one side information on particular samples which are representative for an individual carrier in a reservoir. The basin modelling of petroleum charge of the same reservoir provides, on the other side, results at the resolution of the entire field. Nevertheless, both data types can be integrated and used as a comparison method in order to improve the understanding of the petroleum system in an area, the Hammerfest Basin in this case study.

The basin modelling and geochemical data indicate that the hydrocarbons present in the main accumulations of the Hammerfest Basin represent a mixture of hydrocarbons that have been sourced from both Triassic and Jurassic source rocks. This general conclusion is in accordance with results reported by Ohm et al. (2008). They have observed the presence of isotopically heavy values of oil fractions (isotopically heavier than 29 ‰) in most of the Hammerfest Basin oils and indicated that this could be in response of the mixing of Hekkingen–derived oils with pre–Jurassic oils (Triassic and even Paleozoic oils). A mixing of hydrocarbons after they have reached the reservoir structure is possible considering the complex geologic history of the basin, especially during the Cenozoic.

Gaseous hydrocarbons present in the Askeladd field were probably charged from the Triassic Snadd and Kobbe formations. This is based on the fact that gas isotopes suggest for this field the highest maturity levels of 1.3–1.5% VR (Figure 3.14) and model results show that the drainage areas for this field are linked to the western margin of the basin where high maturity levels were reached by the respective source rocks (Figure 3.5 and Figure 3.10). Mass balances from the basin modelling (Table 3.4) also suggest that the main contribution was from the Triassic source rocks, mainly the Snadd Formation. Sourcing from these two formations can also be supported by the maturity–related biomarkers (Figure 3.20), which show the presence of hydrocarbons with two maturity

tendencies. However, it should be kept in mind that the ratios which indicate the highest maturity are the diasteranes/steranes and the Ts/ (Ts + Tm), and as already mentioned, these ratios are not 100% indicators of maturity. On the other hand, as observed in Figure 3.7 the Kobbe and Snadd formations have generated oil during early maturation. This oil is predicted to have been expelled and accumulated in the Askeladd, Albatross and Snøhvit fields during Late Cretaceous time. Later on, during Early Paleocene, with the increasing of maturity, gas was generated and expelled, then started to be accumulated as well in the reservoirs, resulting in the displacement of oil out of the structures.

The Snøhvit and Albatross fields show lower maturity levels (between 0.85 and 1.30% VR) based on the gas isotopic compositions (Figure 3.14), indicating that these fields have probably been mainly sourced from the Jurassic Hekkingen Formation, as this maturity stage is observed for this source rock in the northern margin (Figure 3.5); whereas the Kobbe and Snadd formations are overmature. The gas isotopic compositions also suggest that these two fields contain condensate– and oil–associated gas. This is in accordance with the well data (Norwegian Petroleum Directorate, 2009) and with the results from 3D modelling (Rodrigues Duran et al., 2013), where especially the Snøhvit field is characterized as a gas accumulation with an oil leg. Biomarker parameters (Figure 3.20) also suggest the same maturity tendencies. The possible contribution from both sources (Triassic and Jurassic source rocks) is suggested by the source rock tracking performed in this study and reported in Table 3.4.

In the case of the Goliat field and the Tornerose discovery maturity levels between 0.70 and 1.30% VR have been inferred according to the gas isotopic composition (Figure 3.14). Looking at the basin scale source rock maturities from the 3D model (Figure 3.5) generation from a local source and subsequent vertical migration can only be suggested to have occurred from the Triassic Kobbe and Snadd formations, because they have reached oil window maturity levels in the areas where the accumulations are located. This can be correlated with the fact that accumulations in the Goliat field are found within Triassic intervals (Norwegian Petroleum Directorate, 2010a). However, charging from the northern margin is suggested according to the modelled flow–paths and

drainage areas (Figure 3.10). In this case, modelling suggests the possibility of long–distance migration from the north and thus a possible contribution from the Jurassic Hekkingen Formation.

The maturity–related biomarkers (Figure 3.20) indicate two trends for both the Goliat field and the Tornerose discovery. In the case of Goliat field the two different groups observed could be attributed to the fact that the shallower oil has experienced some biodegradation, as discussed earlier, and not due to the presence of two different petroleum families coming from two different sources with different maturities. However, the two possibilities should not be excluded, i.e. less mature petroleum sourced from Hekkingen Formation and migrating long distances or petroleum sourced from the higher mature Triassic sequences, mainly the Kobbe Formation, which could also have contributed to the gaseous hydrocarbons found in the field as stated in paper 1 (Rodrigues Duran et al., 2013). This dual contribution is visible from the modelling results (Table 3.4), which indicate that the liquid phase in the Goliat field has been sourced in equal proportions from both sequences, Jurassic and Triassic. In addition, Ohm et al. (2008) also performed a detail analysis of the oils in the Goliat field, and suggested that these oils represent a mixing of Triassic and Jurassic oils based on the *n*–alkane profiles and the isotopic values of the saturated oil fraction.

Two maturity levels are also observed for the hydrocarbons in the Tornerose discovery, one between 0.85 and 1.30% VR (according to the gas–isotopic composition, Figure 3.14) and the second between 0.70 and 0.80% VR (gas isotopes and maturity–related biomarkers, Figure 3.14 and Figure 3.20). The flow–paths and drainage area analysis from the model results indicate that hydrocarbons present in this discovery have been sourced from the northern margin (Figure 3.10). Therefore, petroleum could have been sourced from the Jurassic Hekkingen Formation or even from the Triassic Snadd Formation, which reached same maturity levels in the northern margin. Modelling results correctly suggest that the accumulation consist mainly of gas (Rodrigues Duran et al., 2013) with a main contribution from the Triassic Kobbe and Snadd formations as inferred from the source rock tracking (Table 3.4).

As previously stated, the age–related biomarkers did not show a clear tendency with respect to the origin of the hydrocarbons. The C_{28}/C_{29} steranes ratio suggests that the hydrocarbons present in the fields and discoveries (Figure 3.22) are sourced from both the Triassic and Jurassic source rocks. For the particular case of the Snøhvit field and the Tornerose discovery two groups are observed, one suggesting an Upper Jurassic origin (Hekkingen Formation source rock), and the second one suggesting a Lower Jurassic or Triassic origin (maybe Snadd and Kobbe formations source rocks). A Jurassic origin is suggested from the ETR, which indicated that all the oil samples should have been sourced from a Jurassic source rock (values < 1.2) according to Holba et al. (2001). However, Ohm et al. (2008) found values of ETR from two Triassic source rock extracts from the well 7120/2–1 (southern part of the Loppa High) to be around zero and they argued that the low ETR is a result of low maturity. Therefore, this indicates that low ETR values do not always support a Jurassic origin. On the other hand, Ohm et al. (2008) also compared the *n*–alkane distribution of the Snadd and Kobbe formations oils from Goliat with Triassic oils from the Sverdrup Basin and Alaska, and observed a very good match, suggesting that Goliat oils could have a Triassic origin, even though the show low ETR.

3.2 Loppa High model (paper 3 – ready for submission)

In this final section are included the results from the second 3D basin model built, in which the main area of interest corresponds to the Loppa High. However, part of the young sedimentary basins to the west and the platform area to the east were also modeled. The main idea was to investigate the evolution of the same petroleum systems considered in the Hammerfest Basin model.

3.2.1 Model calibration

As for the first model in the Hammerfest Basin, calibration was performed using vitrinite reflectance and temperature data from 15 wells. The calibration results are presented in Figure 3.23 to Figure 3.26. For this model the sensitivity evaluation was also done with the minimum, medium and maximum scenarios for both, the erosion and heat flow.

Once again it is observed that the vitrinite reflectance is more sensitive to variations in the erosion scenarios than the temperature; this means that no significant changes in temperature trend were observed when a variation of the erosion was performed. The erosion scenario that provides the best calibration against vitrinite reflectance corresponds in general to the medium erosion case (Figure 3.23 and Figure 3.24); with erosion magnitudes between 200 and 1300 m for the Oligocene–Miocene event and between 100 and 800 m for the Pliocene–Pleistocene event (Figure 2.7). The vitrinite reflectance data is for some of the wells quite variable (high dispersion in the data) and therefore a clear trend is not easy to identify. On the other hand, there are also some cases in which the erosion magnitudes for the three scenarios are not that large and therefore any of the three scenarios can matches the data (e.g. wells 7219/8–1S and 7219/9–1, Figure 3.24). In the case of wells 7120/1–1, 7120/1–2, 7120/2–1, 7120/2–2, 7121/1–1 and 7220/6–1, it is quite difficult to distinguish between the minimum and medium erosion cases. However, as mentioned previously, calibration is achieved in most of the cases by the medium scenario.

Moreover, the heat flow scenario that provides the best calibration against both, temperature and vitrinite reflectance data, corresponds to the medium scenario (Figure 3.25 and Figure 3.26). That is the one represented by a background heat flow in the area with values of 53, 58 and 75 mW/m^2 (Figure 2.4). The temperature data for wells 7120/1–1, 7120/1–2, 7120/2–1, 7120/2–2 and 7121/1–1 (Figure 3.26) is quite scattered and not robust, therefore this also make difficult to establish a particular trend regarding the heat flow against temperature for this specific area.

The following sections will present in detail the results from the basin modelling and this will be done for the best calibrated model which corresponds to the one with the medium scenarios.

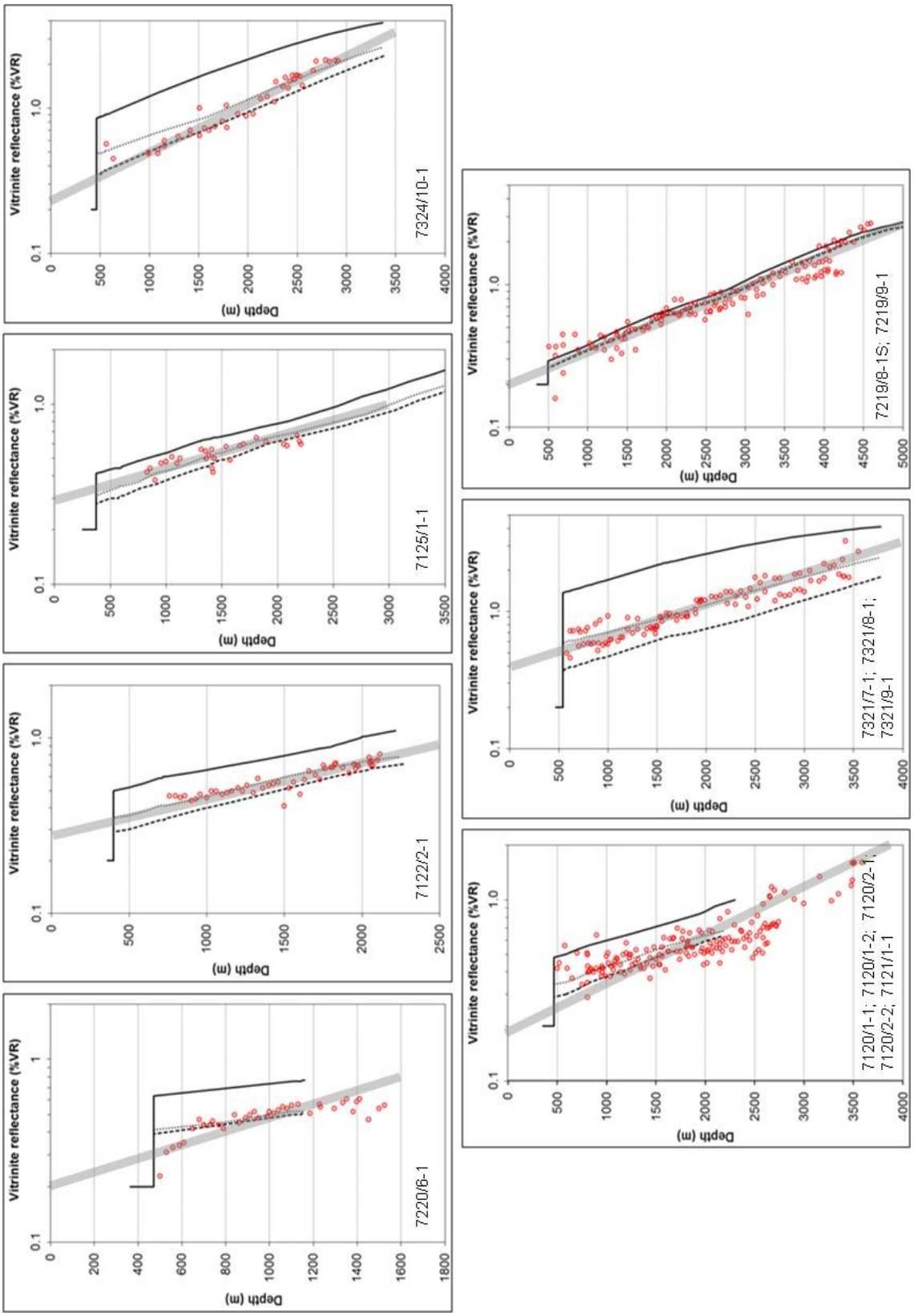

Figure 3.23 Vitrinite reflectance calibration with comparison of the three erosion scenarios. Continuous line represents maximum erosion, dotted line represents medium erosion and segmented line represents minimum erosion. The gray lines correspond to the best calibration zone.

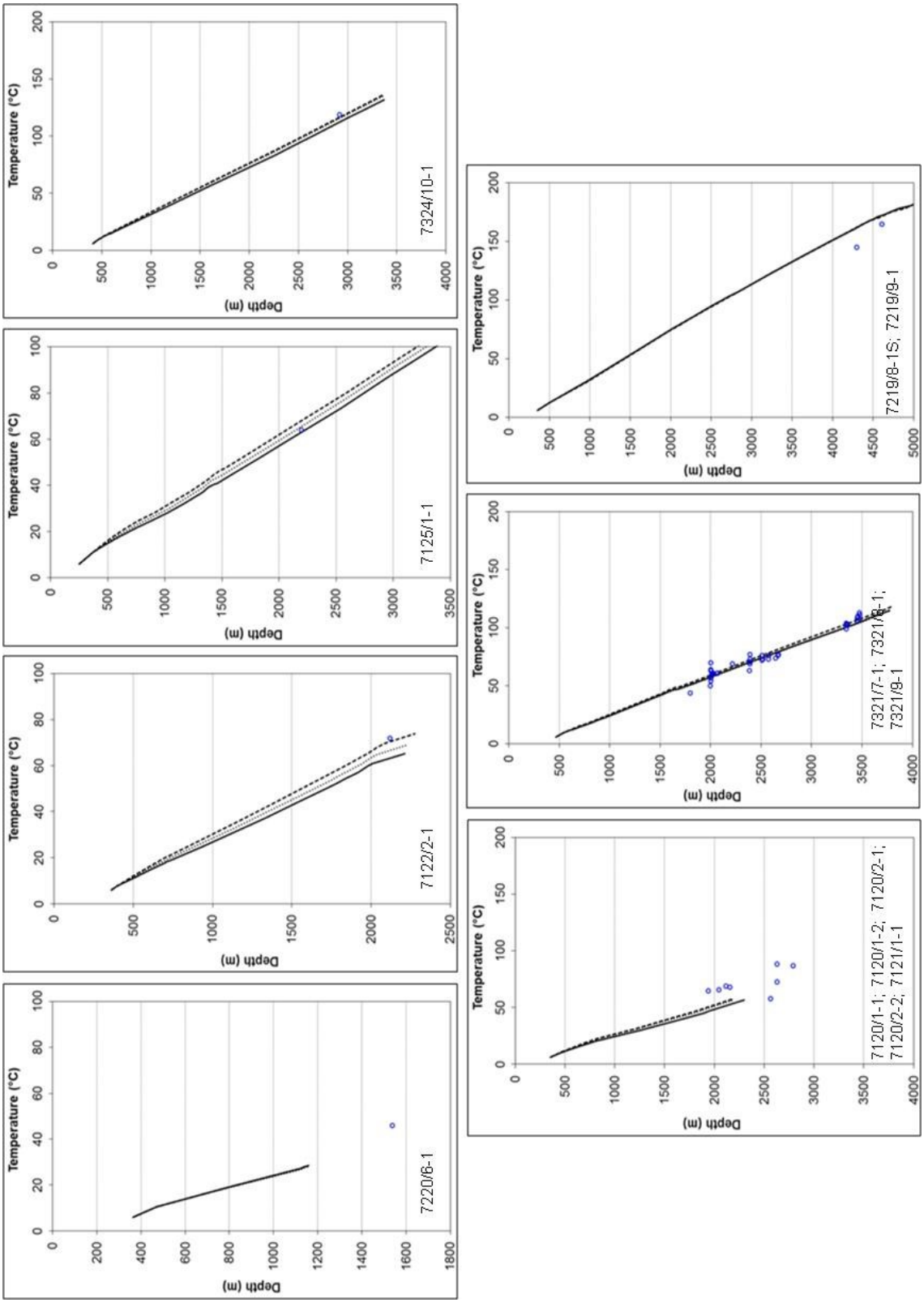

Figure 3.24 Temperature calibration with comparison of the three erosion scenarios. Continuous line represents maximum erosion, dotted line represents medium erosion and segmented line represents minimum erosion.

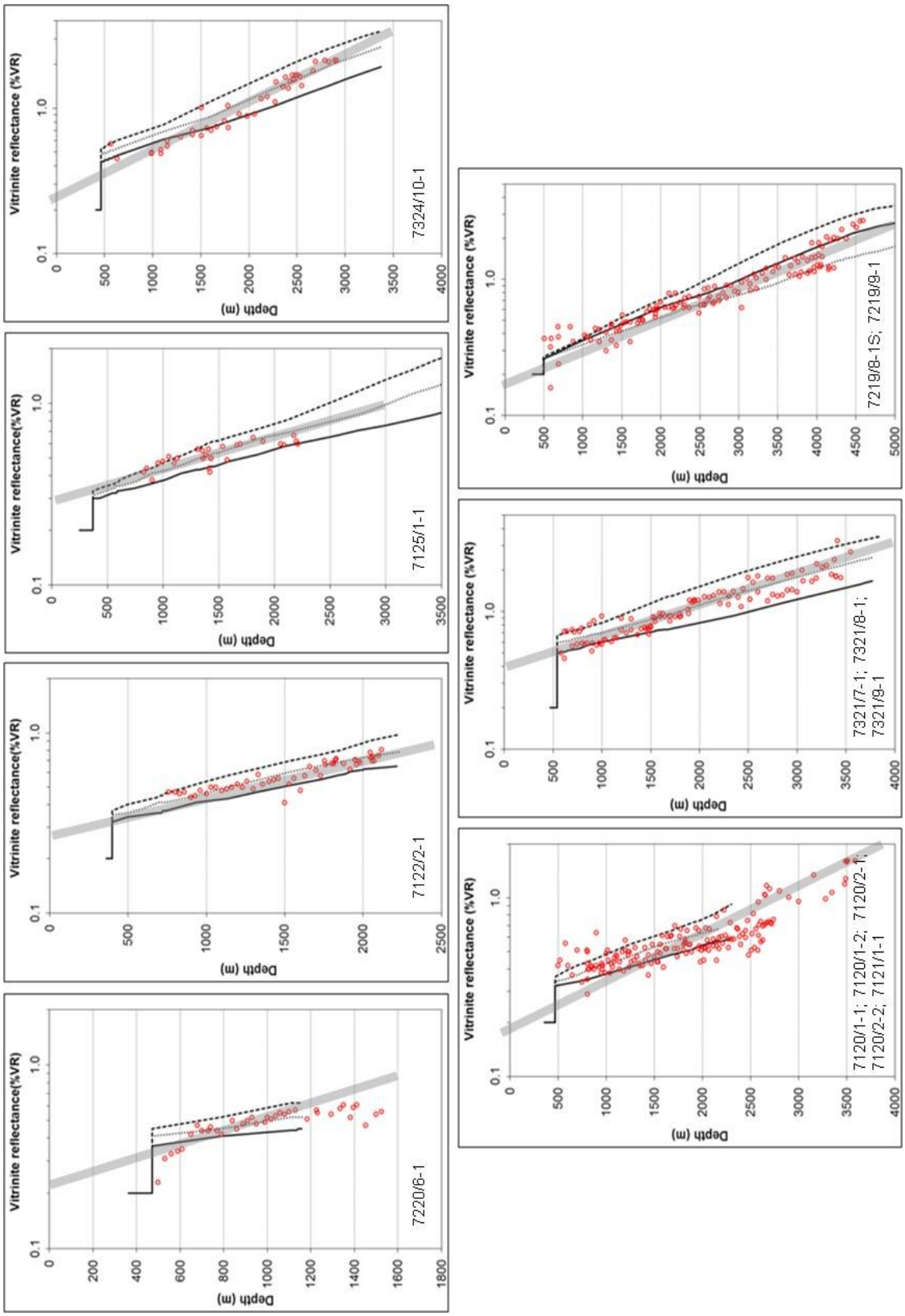

Figure 3.25 Vitrinite reflectance calibration with comparison of the three heat flow scenarios. Continuous line represents minimum heat flow, dotted line represents medium heat flow and segmented line represents maximum heat flow. The gray lines correspond to the best calibration zone.

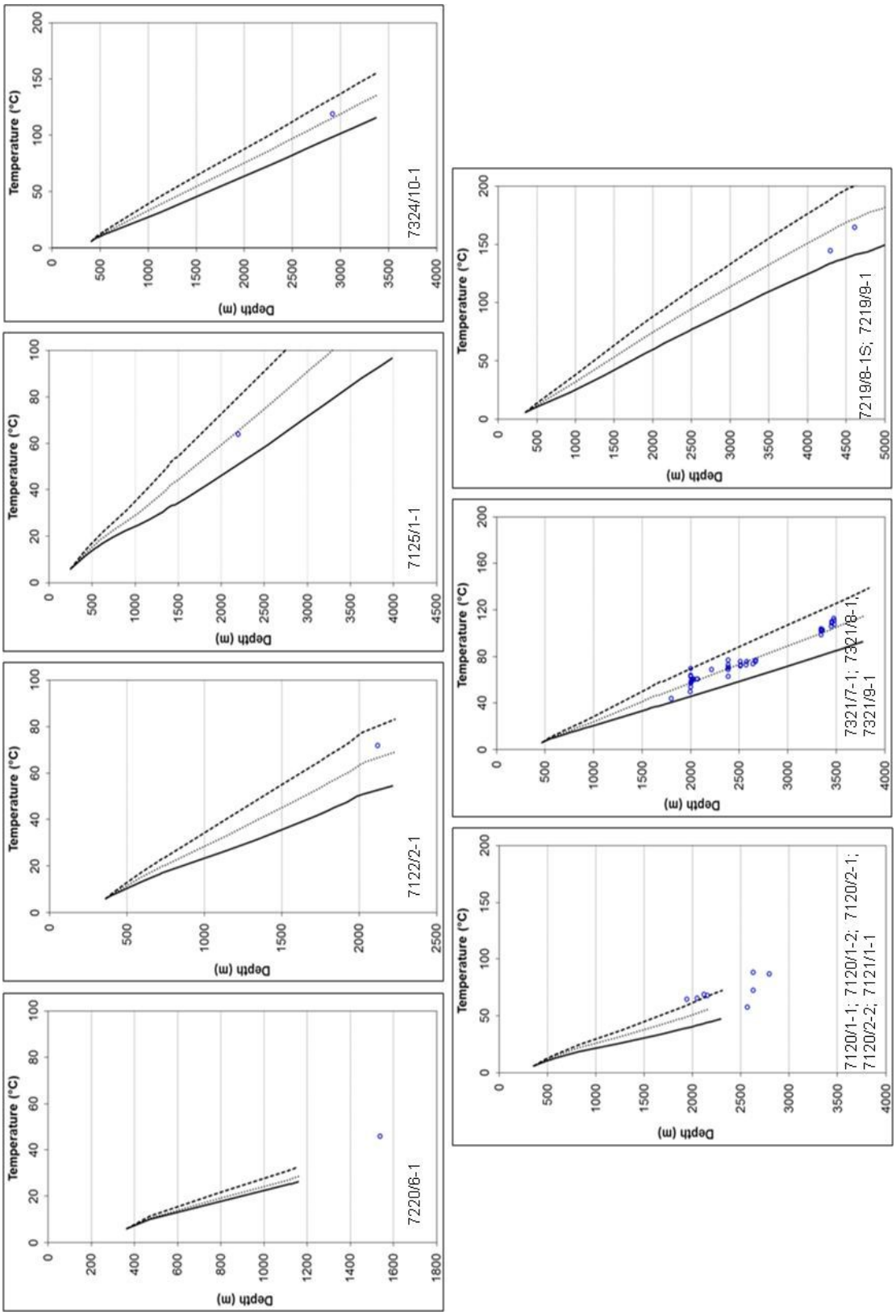

Figure 3.26 Temperature calibration with comparison of the three heat flow scenarios. Continuous line represents minimum heat flow, dotted line represents medium heat flow and segmented line represents maximum heat flow.

3.2.2 Petroleum generation, migration and accumulation

3.2.2.1 Source rock maturity and timing of generation (Paper 3)

The modeling results indicate that the three source rocks considered for the petroleum systems of this model, which also correspond to the Upper Jurassic Hekkingen Formation and the Triassic Snadd and Kobbe formations, have reached very high maturity or overmature levels in the deep Tromsø and Bjørnøya basins located to the west of the modeled area, with vitrinite reflectance values over 4% and 100% transformation ratio (Figure 3.27). The Triassic Kobbe Formation shows as well elevated maturity levels in some areas in the eastern part of the model, mainly in the Bjarmeland platform, in the Maud Basin and in the northern part of the Hammerfest Basin, with vitrinite reflectance between 1 and 2.5% and transformation ratio between 70 and 100% (Figure 3.27). The Snadd and Hekkingen formations also show relatively high maturity levels (between 1.4 and 1.6% vitrinite reflectance and 80–90% transformation ratio) in the deepest part of the Maud Basin to the northeast (Figure 3.27).

Due to the fact of having several areas with interesting maturity results which could be important since that will determine the generation of hydrocarbons and their migration to reservoirs, a follow up of the maturity evolution was also perform as part of this investigation. This was done for five specific areas (identified in Figure 3.27) and using the modeled transformation ratios (Figure 3.28). The area close to well 7120/1–3 ("A" in Figure 3.27, southwest of the modelled area), where a recently discovery has been made, shows generally very low maturity with transformation ratios less than 5% for both the Snadd and Kobbe formations (Figure 3.28); the Hekkingen Formation is not present at this location. Moving northwest of this point, into the Ringvassøy–Loppa Fault complex and the Bjørnøya Basin ("B" and "C" in Figure 3.27), a clear increase of maturity is observed (Figure 3.28). The Triassic source rocks have reached almost 100% transformation ratio in the first location with the onset of generation occurring between 140 and 160 Ma; while the Jurassic Hekkingen Formation still has potential for generation since it has reached approximately 30% transformation ratio. The beginning of generation for this source rock has occurred at approximately 60–50 Ma. In the Bjørnøya Basin the three source rocks have reached full transformation with the onset

of generation taking place at around 210 Ma for the Kobbe Formation, around 170 Ma for the Snadd Formation and around 130 Ma for the Hekkingen Formation (Figure 3.28). In the northeast area, around the Maud Basin margin, a different maturity evolution is observed.

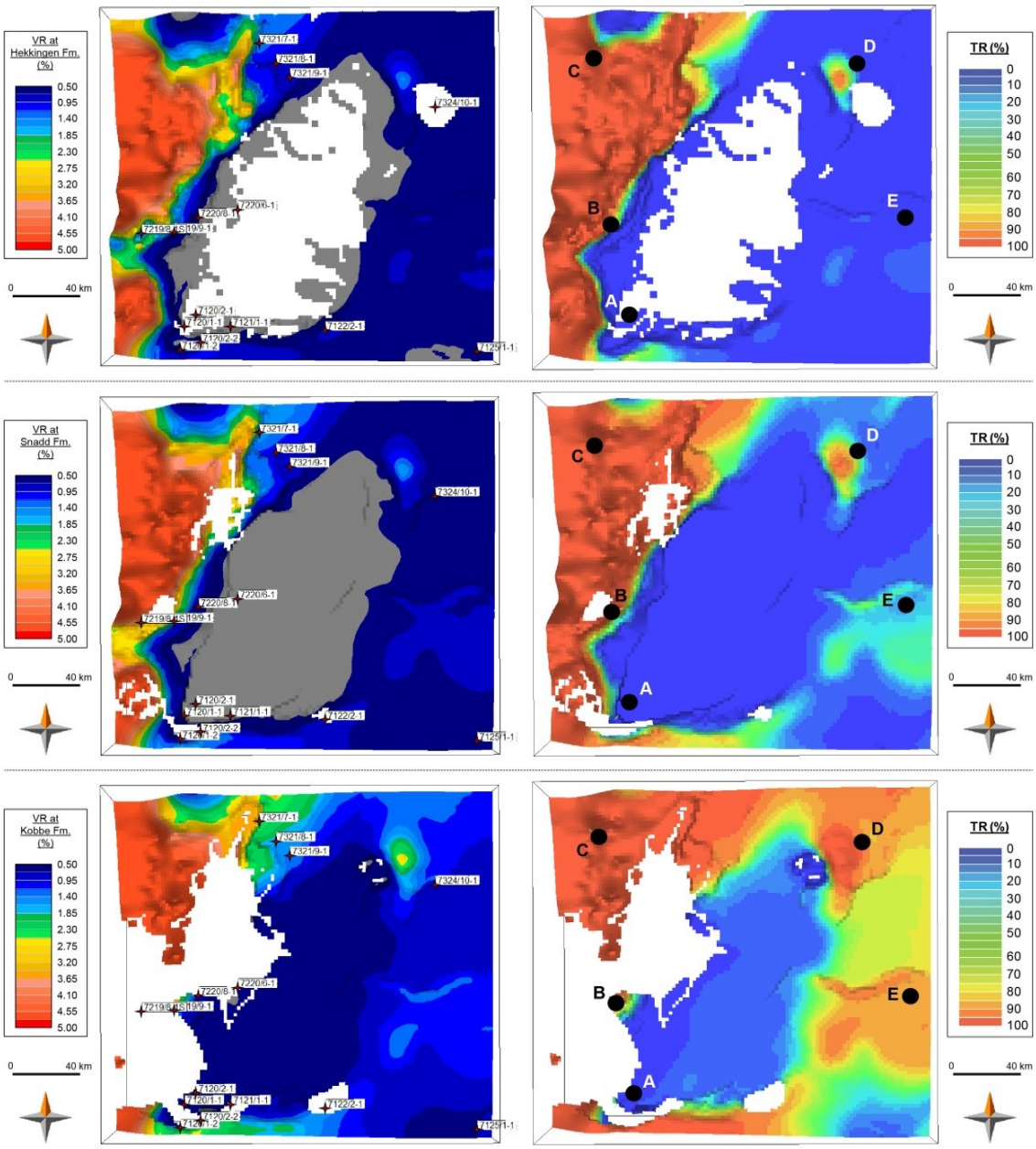

Figure 3.27 Maturity at present–day of the Hekkingen (top), Snadd (middle) and Kobbe (bottom) formations based on vitrinite reflectance (VR, left) and transformation ratio (TR, right). The lower boundary is 0.5% VR, meaning that areas in gray have maturity levels below this value. The black dots observed in the maps to the right correspond to the areas where an extraction has been done in order to obtain the maturity evolution shown in Figure 3.28.

The deepest Kobbe Formation source rock has reached high maturity at present–day, with transformation ratios higher than 90% and the onset of generation at approximately 230 Ma, with continues increase of the maturity through time (Figure 3.28). The Snadd Formation started to generate very late in comparison with the Kobbe Formation, at around 100–110 Ma with the main generation pulse between 40 and 30 Ma. The present–day transformation ratio for this source rock stills below 30%. The Hekkingen Formation is the least mature source rock with a present–day transformation ratio <5%.

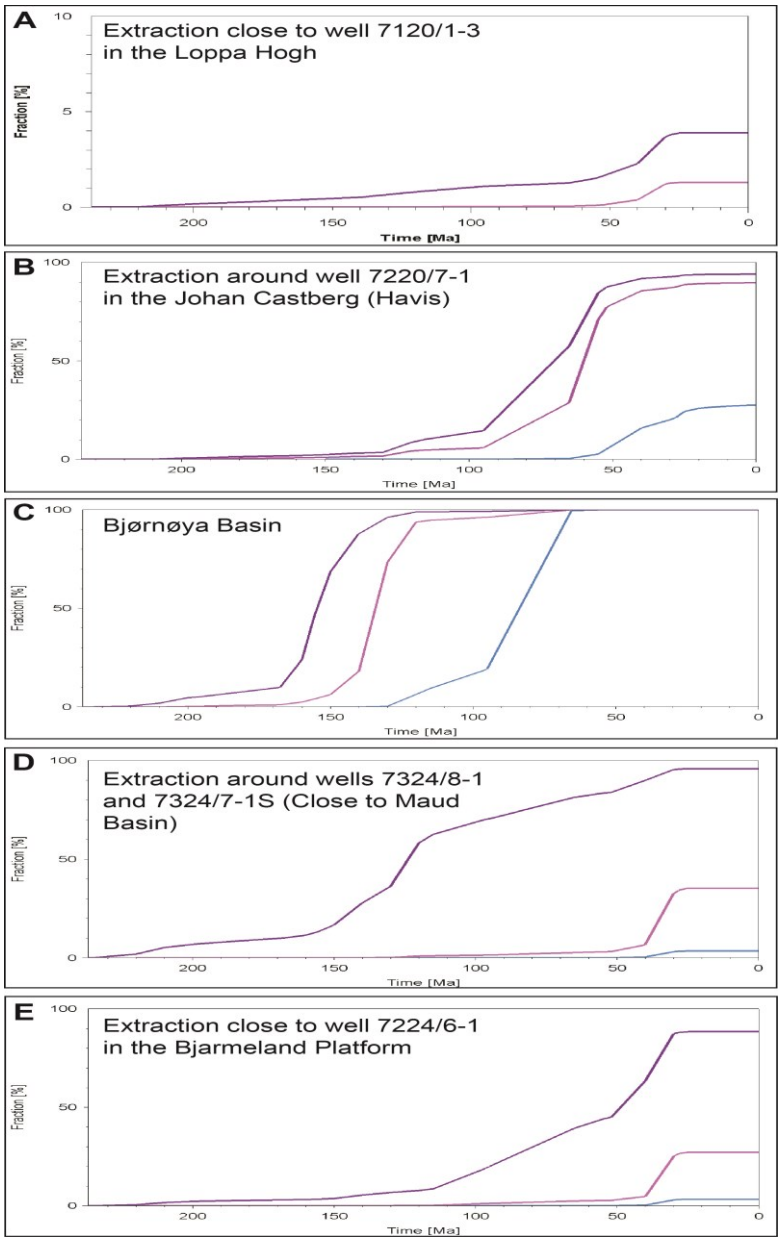

Figure 3.28 Maturity evolution based on transformation ratios for the five areas marked with black dots (A – E) in Figure 3.27.

It is important to mention that this maturity corresponds to the margins or shallower parts of the Maud Basin, in the deepest parts of the basin, the three source rocks have reached very high maturity levels (late oil–gas window maturity, Figure 3.27). In the last area corresponding to the Bjarmeland Platform a similar trend as that described for the Maud Basin is observed for the Snadd and Hekkingen formations (Figure 3.28). For the case of Kobbe Formation even though generation from this source rock started at approximately the same age as in the Maud Basin, the main pulse of generation is predicted to have occurred later (Figure 3.28). It is clear, based on the results presented in Figure 3.28 that petroleum generation has stopped at around 30 Ma in the areas where uplift and erosion took place; however some areas to the west are still generating or having potential for generating since they were not highly affected by erosion.

An emphasis can be done on the fact that in the western part of the Barents Sea, Aptian–Albian shales corresponding to the Kolmule Formation have been proven as the youngest source rocks. The shales have a good light oil and gas generating potential, but are mature mainly in the westernmost parts of Barents Sea (Johansen et al., 1993). As previously described the Paleocene–Supra Paleocene plays are mainly restricted to the western margin; however they are still speculative due to the lack of information (Johansen et al., 1993; Norwegian Petroleum Directorate, 2011). Even though the Cretaceous Kolmule Formation has not been considered as a source rock in this study, a couple of 1D extractions were taken in the western part of the modeled area in order to see the maturity evolution and the present–day maturity level of this potential source rock (Figure 3.29).

The present–day vitrinite reflectance map of the Kolmule Formation shows that maturity levels of up to 4%VR have been reached in the deepest parts of the Bjørnøya Basin (Figure 3.29). On the other hand, vitrinite reflectance values as high as 2.5% are observed in the Southwestern part of the modeled area where the Tromsø Basin and the Ringvassøy–Loppa Fault Complex are located. The maturity profiles for these two areas show that the Kolmule Formation started to reach oil window maturities between 90 and 100 Ma. However, these maturities correspond to the deepest parts of both areas, but in the rims of the basinal areas or at shallower depths, this source rock has low maturities.

Moreover, it should be noticed that this area is characterized by continuous burial without the influence of Cenozoic erosion; indicating that this stratigraphic interval must still being a potential source rock with generation hydrocarbons taking place at present–day.

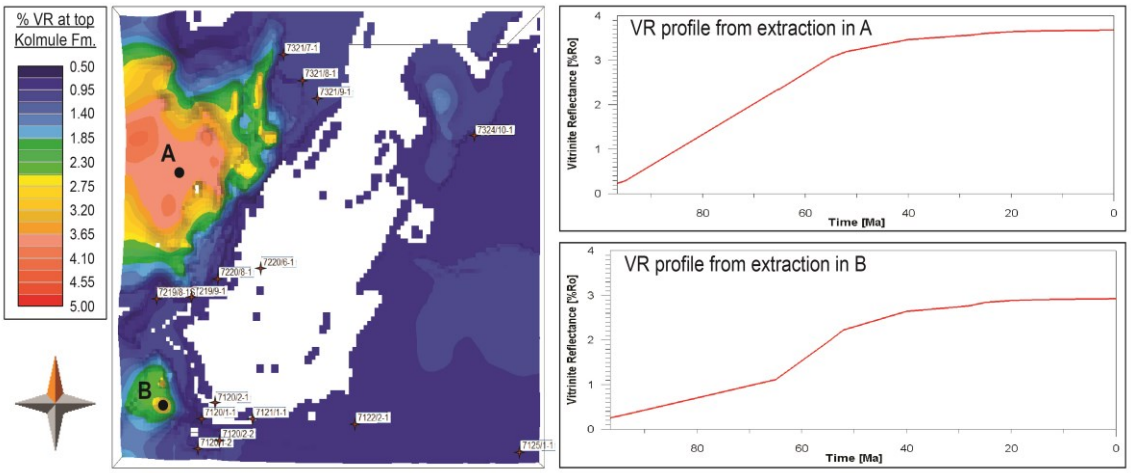

Figure 3.29 Evaluation of the Kolmule Formation maturity. Present–day vitrinite reflectance map (left) and vitrinite reflectance evolution through time for the two locations shown in the map

3.2.2.2 Expulsion, migration and accumulation of hydrocarbons (Paper 3)

The onset of petroleum expulsion from the three source rocks was also evaluated with the model output (Figure 3.30). A general pattern is observed for all source rocks, which indicates that an older expulsion occurred in the west where the deep Bjørnøya and Tromsø basins are located, becoming younger towards the eastern basin flanks. The deepest Kobbe Formation source rock expels first, almost synchronously with the Snadd Formation, whereas the Hekkingen Formation follows the expulsion process with a delay of approximately 50 Myr (Figure 3.30). In the eastern part of the modelled area, a more recent expulsion has been observed for the Kobbe Formation in both, the Bjarmeland Platform and the Maud Basin. The Snadd and Hekkingen formations, on the other hand, just show a recent expulsion in the Maud Basin.

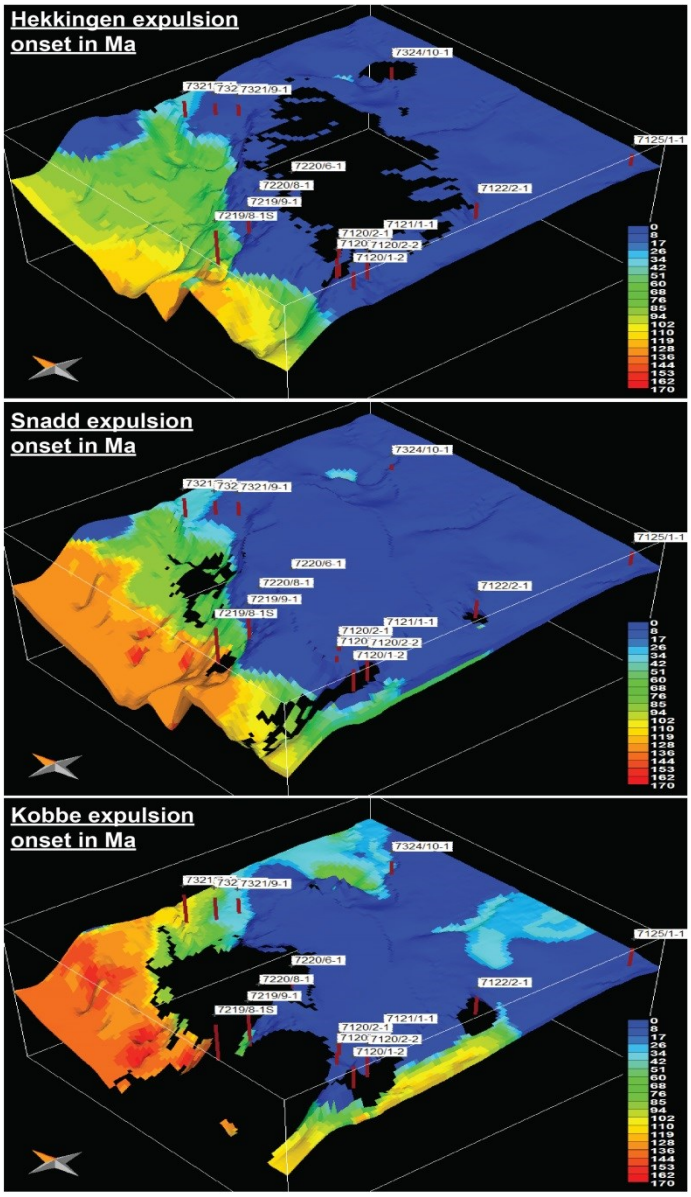

Figure 3.30 3D view of the three source rocks using the expulsion onset as an overly.

With respect to the migration process, an evaluation of the present–day migration pathways in the Stø and Tubåen reservoirs was done (Figure 3.31). They show a migration mainly from the deepest part of the basinal areas (Bjørnøya, Tromsø and Maud basins and Fingerdjupet Sub–basin) up to the margins of the basins and the highs (Loppa and Stappen highs and the Bjarmeland Platform). Gas migration pathways in the Stø Formation extend to the deepest part of these basinal areas where the kitchen with the highest maturity (overmature/gas generative stage) is located (Figure 3.31). It is also observed that they cover a larger area than the gas migration pathways in the Tubåen

Formation, which extend to shallower areas where the source rocks also still have a high maturity. The oil migration pathways are mainly observed in the shallower parts as expected, since lower maturity levels have been reached towards the highs boundaries or the basin margins (Figure 3.27 and Figure 3.31).

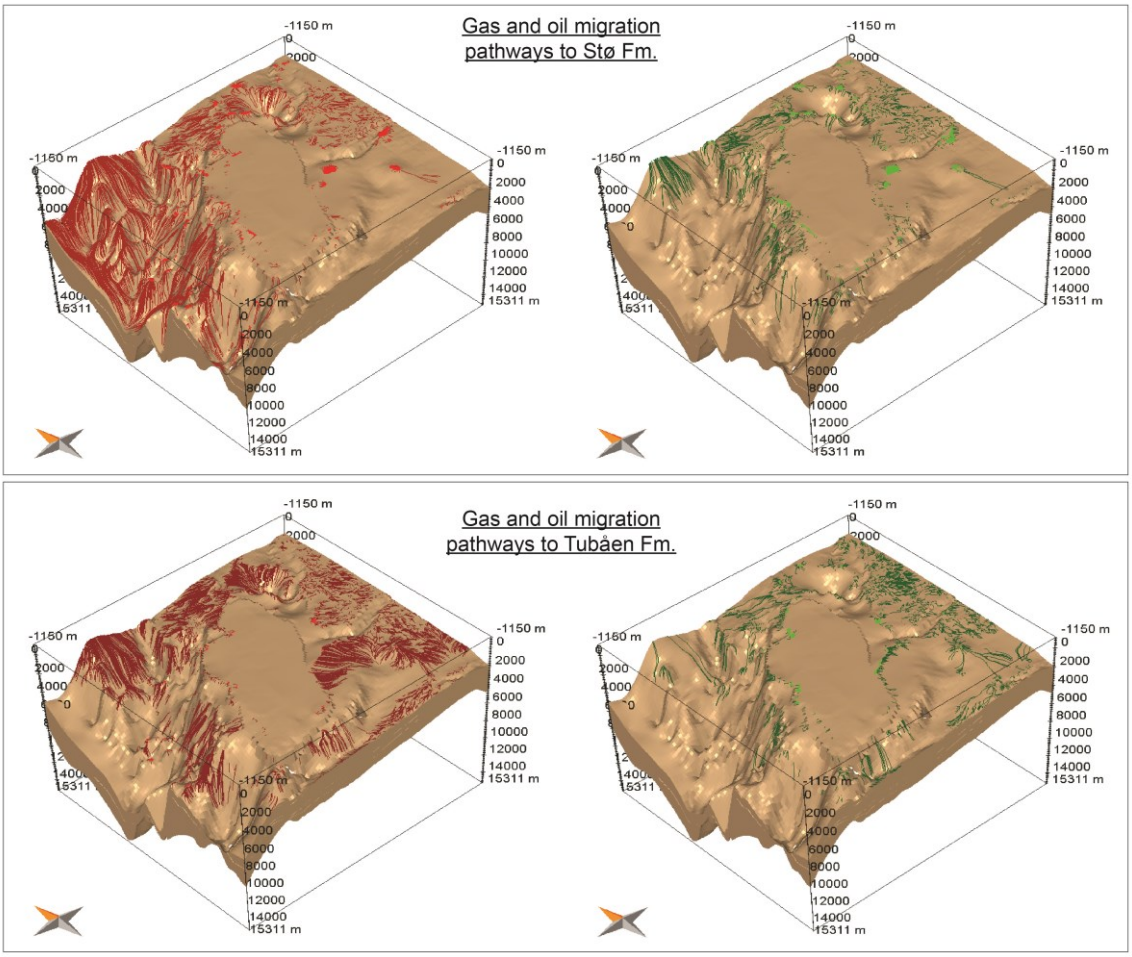

Figure 3.31 Present–day migration pathways of gas (red) and oil (green) for the two reservoir units: the Stø and Tubåen formations.

As discussed in paper 1 (Rodrigues Duran et al., 2013), the glaciations have played an important role in the development of the petroleum systems in the Southwestern Barents Sea, especially in relation with the redistribution or re–migration of hydrocarbons. In order to visualize the possible effect that glaciations could have played precisely in the distribution of hydrocarbons and their migration in this new modelled area, a control of the drainage areas and the hydrocarbon accumulations was done for three locations, which correspond to three key locations where recent discoveries have been made in the

Southwestern Barents Sea (Figure 3.32). The first location corresponds to the southwestern part of the modeled area where the discovery in well 7120/1–3 (close to well 7120/1–1) is found; the second location is to the west of the Loppa High in the Ringvassøy–Loppa Fault Complex and includes the wells of the recent discovery/field named Johan Castberg; the third location is in the northeast part of the modelled area, where the Maud Basin is located close to which the discovery in well 7324/8–1 was made.

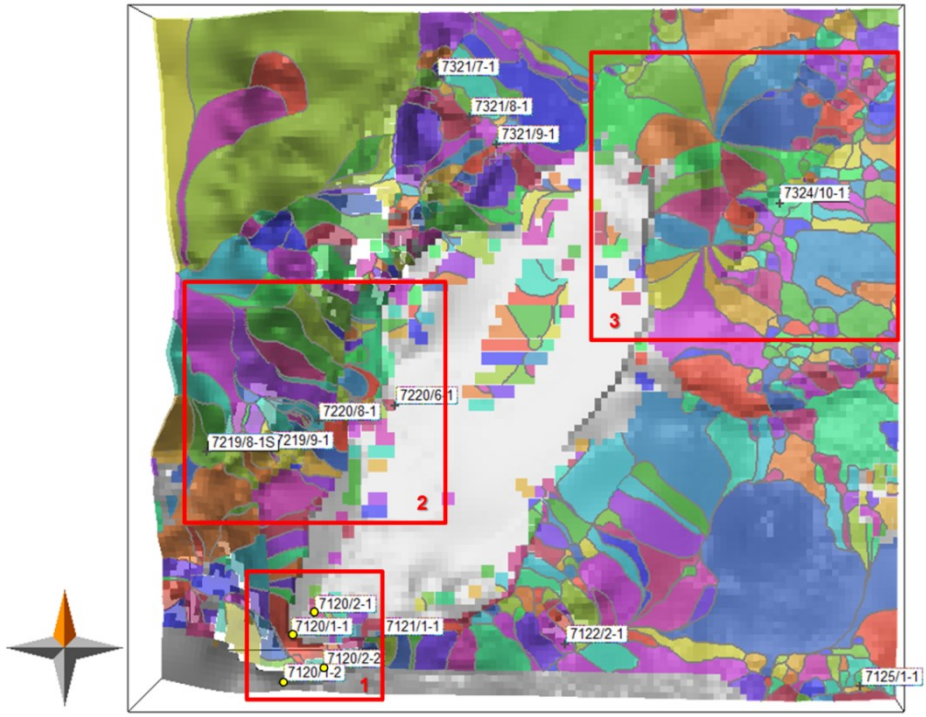

Figure 3.32 Aerial model view with the drainage areas and the location of the three zones selected for further detailed analysis in Figure 3.33 to Figure **3.35**.

At the same time the drainage areas were checked for four specific stages in the glacial cycles, three of them represent a full glacial cycle (glacial growth, retreat and interglacial) and the fourth one corresponding to the present–day situation (Figure 3.33, Figure 3.34 and Figure 3.35). For the first location it is possible to see based on the drainage areas that migration into the southern Loppa High occurred mainly from the west and also from the northern part of the Hammerfest Basin (Figure 3.33). In the second location along the western flank of the Loppa High migration is mainly from the west as expected and also as proven by the migration pathways shown previously

(Figure 3.31 and Figure 3.34). In the case of the third location, in the flank of the Maud basin, the drainage areas are mainly focused towards the Maud Basin, indicating that migration is from the deepest parts of this basin towards the flanks; several and small drainage areas are also observed towards the east of this area (Figure 3.35).

In general no major changes are observed in the drainage areas distribution or pattern for the three locations during the glacial episodes, the main changes observed in some of the patterns are mainly related to the period of glacial growth or maximum glaciation and also at present–day. In location one (Figure 3.33) one of the main changes is observed in the drainage areas connected to the accumulation close to well 7120/1–1, which probably corresponds to the new discovery made in well 7120/1–3. Here when maximum glaciation occurs the accumulation is connected to two drainage areas; while during the interglacial these areas are merged into a single drainage area. At present–day the area is larger and some other changes in the pattern are observed to the east. In the second location (Figure 3.34) fewer changes are observed in the drainage areas, which are mainly observed to the south of wells 7219/8–1S and 7219/9–1 and to the northwest of well 7220/8–1. In location three (Figure 3.35), also few changes are observed, mainly to southwest of well 7324/10–1. The changes in the drainages areas previously described are in accordance with the distribution and changes in the hydrocarbon accumulations. Regarding the hydrocarbon phases, it seems that the accumulations are enriched in gaseous hydrocarbons (gas cap) during the interglacials when the ice–sheet is not present; while during the maximum glacial loading smaller gas caps are observed. Different hydrocarbon distribution is observed at present–day for the three locations, with the tendency to have less volume in the predicted accumulations. This can be an indication of leakage of hydrocarbons due to the development of glaciations, as established in the Hammerfest Basin model (Rodrigues Duran et al., 2013). In location two, a linear trend with accumulations is predicted to the east of well 7220/8–1. This can represent the Johan Castberg discovery. However our model did not reproduce the exact location, due to the fact that the surfaces were coarsely gridded and therefore the structures were not well reproduced and also to the fact that a proper structural pattern, related with the faulting pattern, was not included and this plays a fundamental roll for the accumulation in this discovery.

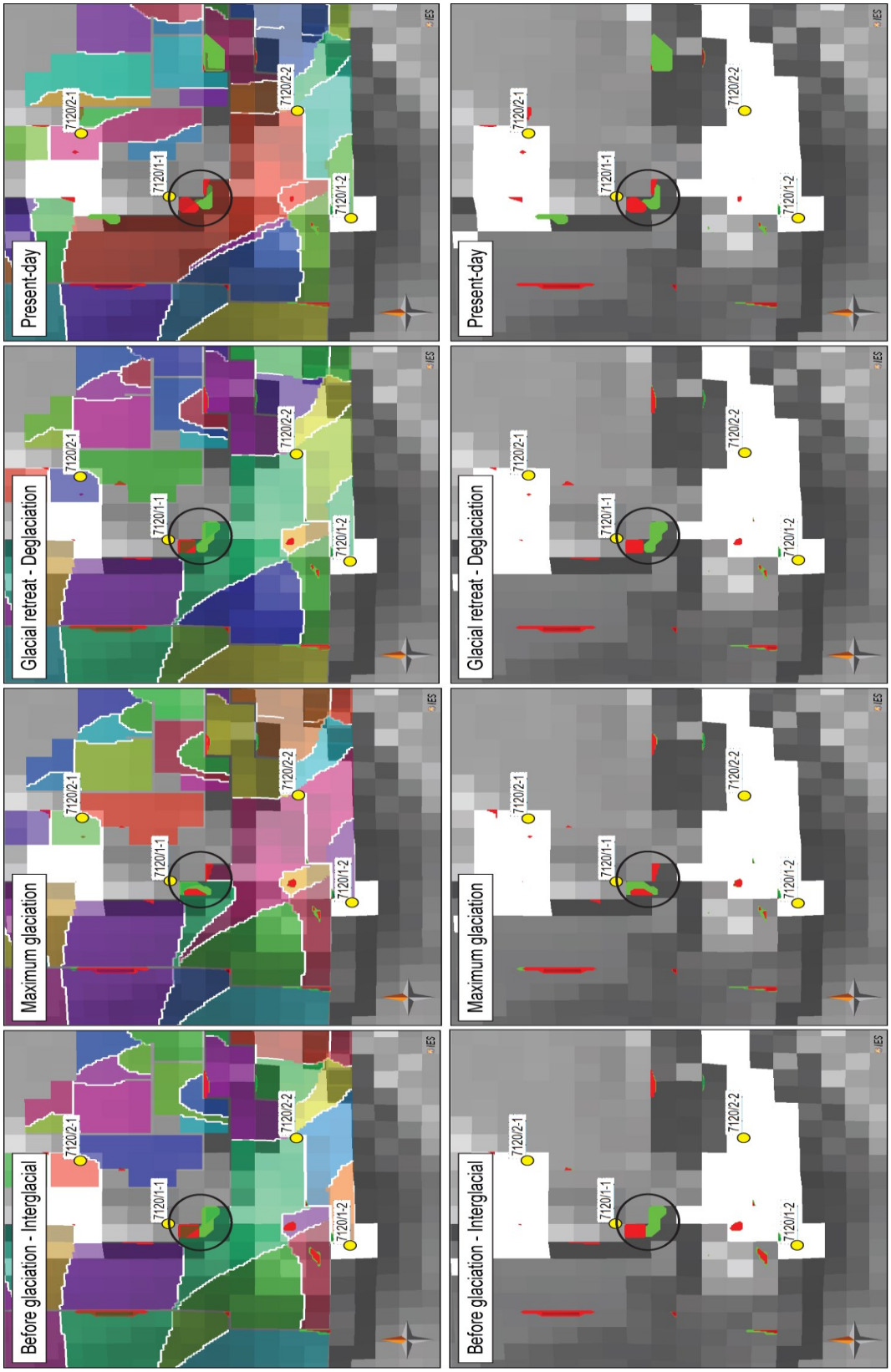

Figure 3.33 Drainage areas and hydrocarbon accumulations in the southwestern part of the modelled area (see Figure 3.32 for reference) for the interglacial period, the maximum glaciation, the glacial retreat or deglaciation and the present–day.

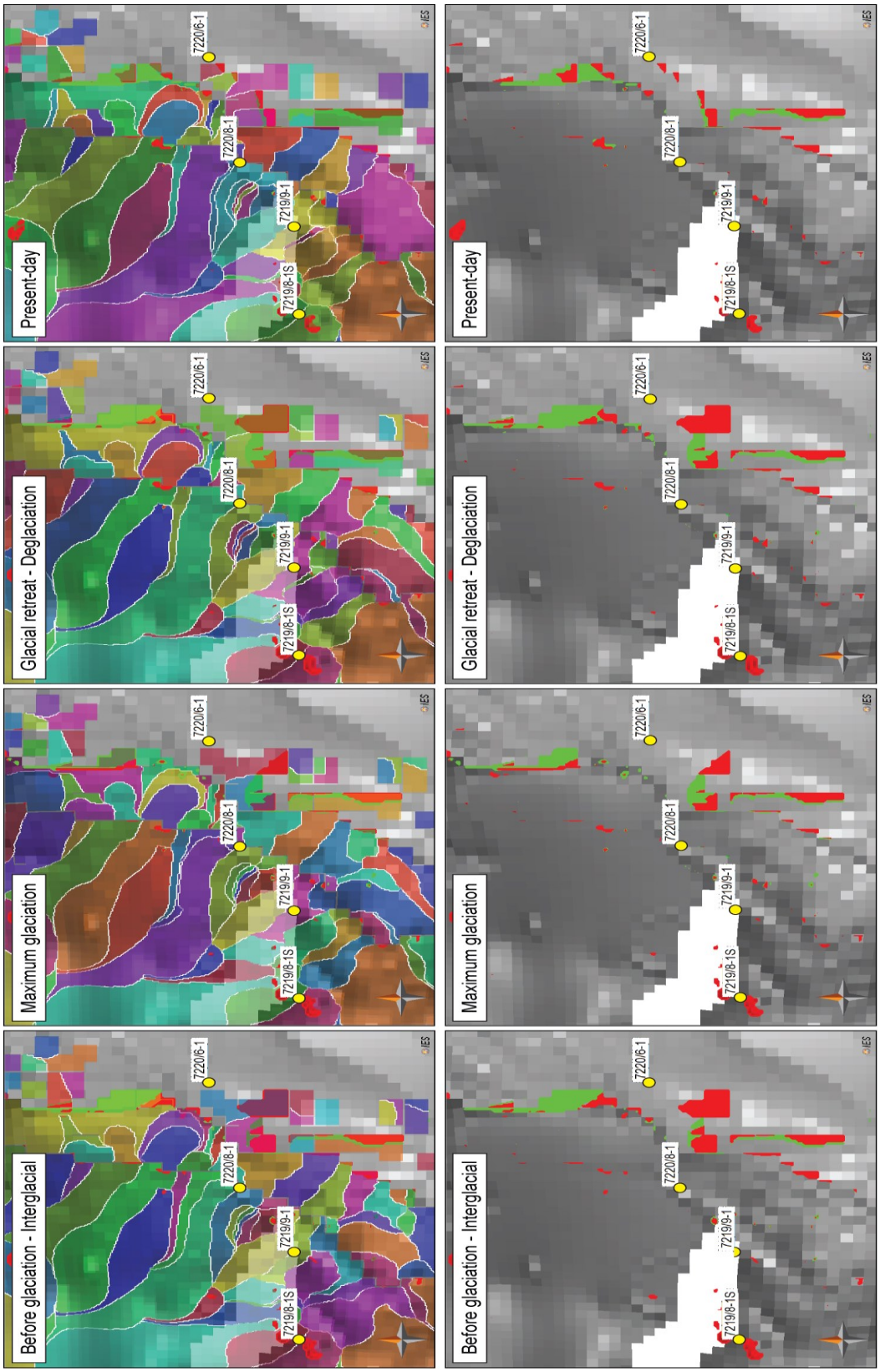

Figure 3.34 Drainage areas and hydrocarbon accumulations in the western part of the modelled area (see Figure 3.32 for reference) for the interglacial period, the maximum glaciation, the glacial retreat or deglaciation and the present–day.

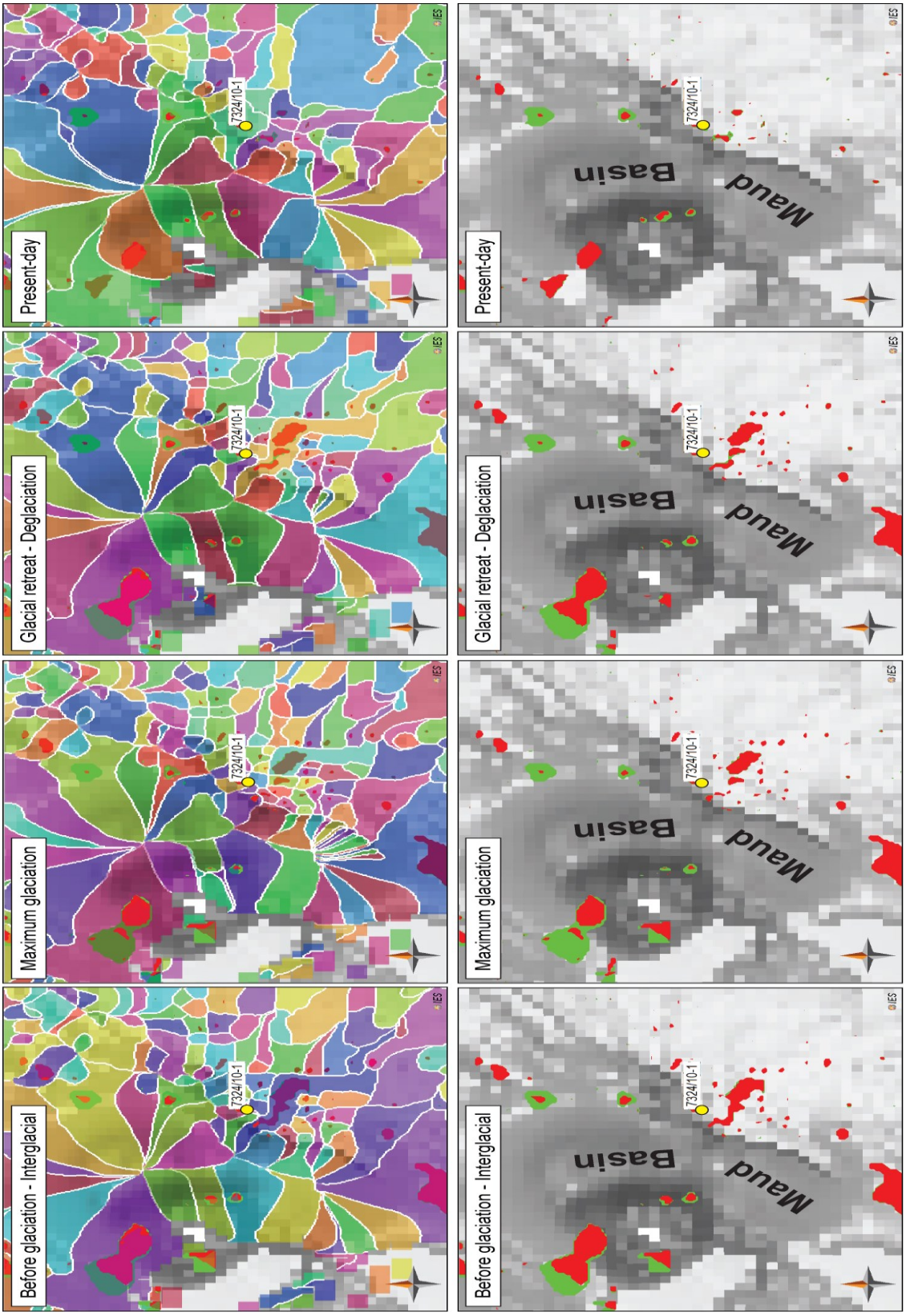

Figure 3.35 Drainage areas and hydrocarbon accumulations in the northeastern part of the modelled area (see Figure 3.32 for reference) for the interglacial period, the maximum glaciation, the glacial retreat or deglaciation and the present–day.

3.2.3 Main discussion from basin modelling in the Loppa High

These new results from basin modelling in the Loppa High area confirm that the Southwestern Barents Sea is a very prolific area for petroleum exploration, with the presence of mature source rocks in large areas. The focus just on the Triassic and Jurassic source rocks represented by the Kobbe, Snadd and Hekkingen formations, limits the results of this work to the two most important petroleum plays in the study area. As previously discussed, these source rocks are overmature in the entire western margin were the Bjørnøya and Tromsø Basins are located. High maturity levels are also observed for the three source rocks in the Fingerdjupet Sub–basin and in the Maud and Hammerfest basins. The Triassic source rocks are as well mature in the Bjarmeland Platform.

The most interesting results of the last part of this PhD study related to the basin modelling of the Loppa High area in the Southwestern Barents Sea are related to the inferences regarding source rock maturity, timing of petroleum generation as well as migration. One of the important aspects is the possibility to corroborate by using petroleum system basin modelling that in those areas of the Southwestern Barents Sea influenced by the recent Cenozoic erosion, a maximum petroleum generation took place at the time of maximum burial, which occurred during the Oligocene–Miocene. At the same time in the areas not affected by these erosion events, a continuous burial is still going on and, therefore, continuous maturation up to the present day. Such areas include, for instance, the Tromsø and Bjørnøya Basins, as well as the Veslemøy High. However, in these deep basins the modelled source rocks are mostly overmature, only the western margin of the Loppa High still has generative source rocks along the Ringvassøy–Loppa and Bjørnøyrenna Fault Complexes. A very important and/or determinant aspect from the 3D model here presented is the fact that in the fault complexes areas previously mentioned, and where wells 7219/8–1S, 7219/9–1 and 7220/8–1 are located, no erosion was assumed, following the observations made by Nardin and Røssland (1993). This assumption was supported by the good calibration of model predictions against temperature and vitrinite reflectance data. An obvious conclusion from these results is that the lack of significant erosion results, as already mentioned, in ongoing petroleum generation from the Hekkingen and Triassic sources

along the basin margin and additionally this enhanced the preservation of the accumulation by reducing losses through inversion related to fault re–activation and leakage. In this sense, it is very important to have the exact location of the erosion boundaries since this will be crucial for defining subsurface prospectivity in the South western Barents Sea.

As already discussed in paper 1 (Rodrigues Duran et al., 2013), in areas subjected to erosion the preservation of earlier accumulated petroleum is the key risk. An assessment of preservation risk is not 100% possible with the semi–regional model that was built in this second part, due to the fact that detailed structural information and fault properties were not integrated into the model. However, the investigation of leakage pathways, like the one performed for the Snøhvit field by Ostanin et al. (2013), indicates that faults reactivated during basin inversion, especially during the glacial period, are the most likely leakage sites in fault–bounded traps.

The drainage area analysis as presented for a few exemplary positions in the Loppa High model shows that the main drainage directions do not change drastically during the development of glaciation. Thus the conventional assessment of drainage areas for available petroleum volumes is still valid for the Barents Sea, at least within the error margin dictated by the assumptions made regarding erosion magnitudes. However, while this model has to consider an ice loading and unloading as almost instantaneous events; the geologic reality is that ice growth occurred gradually, such that effects on the subsurface geometry related to ice growth, retreat, as well as erosion were also gradual. This is of relevance for the Barents Sea since a gradual growth, thickening and retreat of ice–sheets very probably induced a tilting of the subsurface structures resulting in spilling and remigration of oil and gas. These effects are visible in our model as reflected by changing sizes of the oil vs. gas quantities in the modelled accumulations. The limitations of the modelling efforts are not only restricted to the temporal definition of the events, but also include very simplified paleo–water depth definitions (i.e. constant for most events). The relevance of this boundary condition is evident in the strongest change in drainage area definition between the deglaciation event and the present–day situation where an accurate bathymetry was used. Therefore,

it can accordingly be assumed that paleo–drainage areas were likely more strongly affected than what the model predicts. Changing proportions of oil vs. gas in the modelled reservoirs during the glacial loading and unloading cycles can also be attributed to the effects of pressure fluctuations related to the glacial loading on the reservoir fluid composition. As discussed in paper 1 by (Rodrigues Duran et al., 2013), transient effects in the pore and hydrostatic pressure distributions of the modelled reservoir sequences were observed, which indicate the development of an overpressured system. Such pressure oscillations obviously affect the petroleum accumulated in the reservoir, especially the highly compressible gas phase.

4 Conclusions

The petroleum systems represented by the Upper Jurassic Hekkingen Formation and the Triassic Snadd and Kobbe formations as source rocks; the Lower–Middle Jurassic Stø Formation as the main reservoir and the Hekkingen and Fuglen formations as the seals, were successfully reproduced in the Hammerfest Basin model. The source rocks are represented by both, an oil–prone source rock in the case of the Hekkingen Formation and a gas–prone source rock in the case of the Snadd and Kobbe formations. The kitchen area is located to the western and northwestern margins of the basin where high maturity levels have been reached by the three source rocks.

The model reproduced quite well the hydrocarbon accumulations equivalent to the main fields currently known in the Hammerfest Basin (Snøhvit, Albatross, Askeladd, and Goliat). The hydrocarbon phases have also been reproduced, being represented mainly by gas fields with oil legs. Goliat field has been modeled as an oil field with a gas cap.

The 3D petroleum system modelling of the Hammerfest Basin indicates two episodes of reservoir fluid redistribution, both related to erosion events: the Oligocene–Miocene erosion resulted in a significant phase of oil redistribution due to spill from the reservoirs, while the main gas loss from the basin and the associated leakage to the surface occurred in the recent geologic past, linked to the glacial loading–unloading and erosion of the basin. Therefore, the structural tilting and the changes in the temperature and pressure conditions in the reservoir as a consequence of the uplift and erosion dominantly control the leakage dynamics from the accumulations.

The modeling results indicate a loss of *ca.* 0.247 Gt of gaseous hydrocarbons predominantly during the transitions from glacial to interglacial periods. It is important to note that the modeled area represents only a fraction of the glacially influenced Barents Sea. In this sense, it is possible to say that similar amounts of gas may have leaked from other areas in the Barents Sea or even in the entire Arctic region, with a similar architecture and geologic evolution.

The integration of 3D basin modelling and geochemical data, done as part of the second paper allows developing a better understanding of the possible contributions from individual source rocks to the petroleum accumulations of the Hammerfest Basin. Basin modelling indicates that the main gas sourcing was from the Triassic source rocks, while the oil sourcing was from both the Jurassic Hekkingen Formation and the Triassic Snadd and Kobbe formations.

The modelled drainage areas suggest a relatively local sourcing from the west and north to the Askeladd, Albatross and Snøhvit fields, while a combination of a local source contribution as well as long–distance migration and sourcing can be proposed for the Goliat field and the Tornerose discovery.

The organic geochemical data interpretation supports in general the results from basin modelling. However, age–related biomarkers suggest that hydrocarbons present in the main accumulations of the Hammerfest Basin do not have a clear tendency regarding their origin from Triassic or Jurassic source rocks. Gas analysis indicates a maturity gradient from west to east. Light hydrocarbons support long–range migration routes to Tornerose and Goliat, and also support the biodegradation of the oils in the Goliat field. Finally biomarkers indicate the possible contribution of two source rock facies types to the oil fraction of the petroleum accumulations hosted in the Hammerfest Basin.
The integration of 3D petroleum system modelling with geochemical data is a powerful combination that results in a relatively good match of predictions and observations, especially with respect to maturity of the oils and their respective kitchen areas, and provides indications of the processes controlling the observed variability. The long–range migration, biodegradation and petroleum mixing stand out as the main processes which result from the complex geologic history of the basin and make it difficult to pinpoint specific source rock contributions, i.e. Triassic vs. Jurassic.

The 3D petroleum system basin modelling of the Southwestern Barents Sea in the Loppa High indicates high maturity levels for the three main source rocks; the Triassic Snadd and Kobbe formations and the Jurassic Hekkingen Formation. This proves the

effective presence of at least two petroleum plays in the area, which correspond to the Triassic and Lower–Middle Jurassic plays.

The highest maturities were reconstructed in the western part of the area with the three source rocks having reached overmature conditions in the deepest parts. Towards the margins of the Tromsø and Bjørnøya basins, as well as the Veslemøy High the maturities are lower, especially for the Hekkingen Formation. These areas are also characterized by continuous burial and maturation, and likely represent the only positions in the study area where petroleum generation may still ongoing. In the eastern part of the modeled area, where the Bjarmeland Platform is located, the Hekkingen Formation is immature, whereas the Snadd and Kobbe formations have reached oil window maturities. In the Maud Basin all three source rocks modelled are mature.

Regarding petroleum migration our results indicate that ice–sheet growth, subglacial erosion and ice–sheet retreat influenced the migration patterns in the subsurface, causing changes in drainage areas, as well as the spilling and re–migration of the accumulated petroleum. The glacial dynamics play accordingly a very important role with respect to the petroleum prospectivity of the Southwestern Barents Sea.

5 Summary and future work

Summary

The Barents Sea is composed by basins and highs which are considered of exploration interest and which converted the area into a proliferous petroleum province. Among them stand out the Loppa High, the Stappen High, the Bjørnøya Basin, the Tromsø Basin, the Nordkapp Basin and the Hammerfest Basin. Up to date several discoveries have been made (most of them in the Hammerfest Basin), which are mainly dominated by gas and oil legs (Johansen et al., 1993; Larsen et al., 1993; Doré, 1995). These hydrocarbon accumulations correspond to several petroleum systems and/or plays that have been identified in the area, two of the most important the Jurassic and Triassic plays (Johansen et al., 1993; Henriksen et al., 2011b; Norwegian Petroleum Directorate, 2011).

Petroleum systems of the Southwestern Barents Sea

The source rocks for the two petroleum systems considered in this study correspond to the Upper Jurassic Hekkingen Formation and the Triassic Snadd and Kobbe formations. However, some other source rocks intervals have been identified and proven in the Barents Sea. For instance, the Silurian–Late Devonian source rock represented by the Domanik Formation (common in the eastern Barents Sea); a Carboniferous shale; the Lower Permian evaporites of the Ørn Formation in the Nordkapp Basin; the Late Permian Ørret Formation mainly in the Nordkapp and Maud Basins; and Cretaceous shales (Johansen et al., 1993; Henriksen et al., 2011b).

Two stratigraphic units have been assigned as reservoir rocks which correspond to the Lower–Middle Jurassic sandstones of the Stø Formation, identified as the main reservoir in the Barents Sea, and the Tubåen Formation. The seal rocks are represented by the shales in the Fuglen and Hekkingen formations.

Petroleum generation, migration, accumulation and leakage

Hammerfest Basin case study

The kitchen area for the Hekkingen Formation is located in western and northwestern margin of the Hammerfest Basin; here this source rock has a present–day maturity in the oil window–early gas maturity. In the central, southern and eastern parts of the basin the formation is thermally immature. The Triassic Snadd and Kobbe formations source rocks have developed up to the present–day high maturities (gas window maturity) in almost the entire basin, indicating that the biggest proportion of gaseous hydrocarbons found in the Hammerfest Basin might have been generated by these source rocks.

Generation towards the northwestern margin of the basin and at the top of each source rock was initiated during Late Triassic (~215 Ma) for the Kobbe Formation; Early Cretaceous (~125 Ma) for the Snadd Formation and Late Cretaceous (~95 Ma) for the Hekkingen Formation. Maximum burial of the basin occurred at 30 Ma, marking the end of petroleum generation. The total masses of oil and gas generated were calculated and correspond to approximately 76 Gt of oil and around 66 Gt of gas.

The petroleum generated by the Triassic Kobbe Formation, corresponding to the oldest source rock, was predicted to start being expelled at around 120 Ma; meaning that migration in the Hammerfest Basin took place since Early Cretaceous time. The expulsion from the Snadd Formation started during Middle Cretaceous (around 100 Ma) and from the Hekkingen Formation during the Paleogene time at around 50 Ma. The estimated total masses of oil and gas expelled correspond to 30 and 32 Gt, respectively.

The main reservoir unit corresponding to the Stø Formation started to be filled with hydrocarbons from approximately 80 Ma onward, with the main filling pulses taking place at around 55 Ma; when the seal rocks, corresponding to the Fuglen and Hekkingen formations, were already deposited and to a large degree consolidated. The predicted total masses of oil and gas accumulated at present–day in the Stø Formation corresponds to 0.298 and 0.302 Gt, respectively. The natural petroleum accumulations and phases of the main fields that are known at present–day in the basin, such as Snøhvit, Snøhvit–Askeladd, Snøhvit–Albatross and Goliat were quite well predicted.

The first three fields were reproduced mainly as gas fields, with Snøhvit and Snøhvit–Albatross having oil legs. The Snøhvit–Askeladd field was reproduced as a pure gas accumulation. The Goliat field was predicted as an accumulation dominated by oil with a small gas cap. The observed drainage areas suggest then that the Askeladd and Snøhvit fields were mainly sourced from the western and northern margins, respectively; while the Albatross field was sourced from both areas. The Goliat field and the Tornerose discovery have been sourced mainly from the northern margin of the basin, indicating that long distance migration might have occurred.

Based on the volumetric and the drainage areas, it was predicted that the gas contribution into the petroleum systems of the Hammerfest Basin was mainly from the Triassic Snadd and Kobbe formations. On the other hand, it was observed that the oil contribution was from both the Triassic and Jurassic source rocks. For the Snøhvit field the main contributor was the Jurassic Hekkingen Formation, but for the Albatross and Goliat fields the main oil contribution was from the Triassic source rocks.

Two events of hydrocarbon losses were identified. The first one corresponds to the main loss of oil, which occurred after the Oligocene–Miocene time in connection with the tectonic uplift and erosion of the basin. The second one is related to the main loss of gaseous hydrocarbons and occurred during the Pleistocene time due to the development of glaciations in the Barents Sea. It has been observed that transient effects in the pore and hydrostatic pressure distributions of the reservoir occurred during the glacial growth and retreat cycles. Such pressure oscillations affected the petroleum accumulated in the reservoir, especially the highly compressible gas phase. The total amount of gas loss during the entire glacial period is approximately 0.247 Gt. Peaks of gas outflow are synchronous with the leakage or gas lost from the reservoir, which indicates that the gas leaked from the reservoir have reached the surface or seabed.

Geochemistry of the fluid samples from the Hammerfest Basin main fields and the Tornerose discovery

Based on the gas isotopes and the gas composition, the gas fluids accumulated in the Hammerfest Basin have a dominantly thermogenic origin and correspond to oil– and

condensate–associated gases. A mixed microbial–thermogenic origin is suggested for some of the gases in the Goliat field. Gas maturities based on the isotopic composition are between early oil window and gas window maturity. The gas found in the Stø Formation in the Tornerose discovery shows the lowest maturity (~0.70% VR); this correlates quite well with the model results. Samples from Snøhvit and Albatross fields, as well as some samples from the Goliat field and other from the Tornerose discovery show a maturity range between 0.85 and 1.30% VR. The gas in the Askeladd field shows the highest maturity level (between 1.30 and 1.80% VR). These maturities are also correlated with the modelling results.

The C_7 oil–correlation ratios (Halpern, 1995), calculated using the light hydrocarbons composition, show that the light hydrocarbons fractions of the fluids present in the Hammerfest Basin might belong to the same oil family and/or the same source. The C_7 oil–transformation ratios (Halpern, 1995) indicate that biodegradation process affected the oil in Goliat and that Goliat and Tornerose fluids might have reached the reservoir structures after a long–distance migration. This last point is also suggested from basin modelling results.

The Thompson (1983) parameters corroborate as well the observations made with the Halpern parameters, in relation with the biodegradation and long–distance migration. They also indicate that the light hydrocarbons from the Snøhvit, Albatross and Askeladd fields have approximately the same maturity and an origin more connected to a type II oil–prone source rock; while the light hydrocarbons from the Tornerose discovery have, on the other hand, an origin more connected to a type III gas–prone source rock.

The *n*–alkanes and isoprenoids from the oil fraction indicate, in general, an origin from source rocks with a similar type of organic matter, corresponding to a mix between marine and terrigenous input. On the other hand, the steranes and aromatic data show that the oil fraction of the fluids in Snøhvit, Albatross and Askeladd fields and in the Tornerose discovery (Stø Formation) was mainly sourced from a source rock deposited in a marine environment. A transitional environment (shallow marine to coastal) is

suggested for the source rocks of the oils in the Goliat field and also the oil in the Snadd Formation in the Tornerose discovery.

The maturity–related biomarkers indicate that the Snøhvit, Albatross and Askeladd fields might be represented by two different oil families with different maturities or maybe by a contribution from two different source rocks. Differences are observed as well for the Goliat field and the Tornerose discovery. The oil in Goliat in the Kobbe Formation indicates the possibility of having a different source rock, which could be for this particular case the Kobbe Formation. The variability observed could indicate facies differences, sourcing from different rocks, mixing of hydrocarbons in the reservoirs and/or different maturity levels. Specifically the mono– and tri–aromatic steroids together with the C_{29} *iso*/regular steranes ratios suggest maturity levels between 0.7 and 0.8% VR for almost all the fields with the exception of Goliat, for which maturity levels observed correspond to approximately 0.6 and 0.7% VR.

The extended tricyclic terpane ratio from biomarkers (Holba et al., 2001) indicates that all the oils in the Hammerfest Basin for which data is available should have a Middle or Late Jurassic origin, since all the values are <1.2. The C_{28}/C_{29} steranes ratios (Grantham and Wakefield, 1988), on the other hand, indicate a variable source age which extends from Triassic to Upper Jurassic. This means that a clear source differentiation on age related biomarkers is quite difficult or not possible.

Petroleum system dynamics (generation, migration and accumulation)

Loppa High case study

Maturity results show that the Upper Jurassic Hekkingen Formation and the Triassic Snadd and Kobbe formations have very high maturity levels at present–day to the west in the deep Tromsø and Bjørnøya basins (vitrinite reflectance values over 4% and 100% transformation ratio). The Triassic Kobbe Formation has also high maturity in the Bjarmeland platform, in the Maud Basin and in the northern part of the Hammerfest Basin (vitrinite reflectance between 1 and 2.5% and transformation ratio between 70 and 100%). To the east, the Snadd and Hekkingen formations show relatively high

maturity levels (between 1.4 and 1.6% vitrinite reflectance and 80–90% transformation ratio) just in the deepest part of the Maud Basin.

Generation of hydrocarbons in the west (around Ringvassøy–Loppa Fault complex) started between 140 and 160 Ma for the Triassic source rocks; while the Jurassic Hekkingen Formation began to generate at approximately 60 to 50 Ma. In the centre of the Bjørnøya Basin the onset of generation took place at around 210 Ma for the Kobbe Formation, around 170 Ma for the Snadd Formation and around 130 Ma for the Hekkingen Formation (Figure 3.28). At the margin of the Maud Basin the deepest Kobbe Formation started to generate at around 230 Ma and the Snadd Formation at around 100–110 Ma with the main generation pulse between 40 and 30 Ma. At this location the Hekkingen Formation has very low maturity (below 5% transformation ratio). Timing of generation in the Bjarmeland Platform is the same as the timing predicted in the Maud Basin. Petroleum generation has stopped at around 30 Ma with the maximum burial in the areas where uplift and erosion took place afterwards; the areas to the west which were not affected by severe erosion are still being buried and therefore the source rocks still generating. In the western margin it is corroborated the possible existence of a younger petroleum system that has as a source the Cretaceous Kolmule Formation. Maturity for this formation is very high in the deepest parts of the basin, but in the rims of the basinal areas or at shallower depths, this source rock has low maturities.

A general expulsion pattern was observed for all source rocks, which indicates an old expulsion in the west where the deep Bjørnøya and Tromsø basins are located, and becomes younger towards the eastern basin flanks. The expulsion from the deepest Kobbe Formation source rock began first and almost synchronously with the Snadd Formation during Early Cretaceous, whereas the Hekkingen Formation started later during the Late Cretaceous time. A more recent expulsion is predicted for the Kobbe Formation in the Bjarmeland Platform and the Maud Basin. The Snadd and Hekkingen formations show a recent expulsion just in the Maud Basin.

The predicted migration pathways show the typical trend or pattern, which is migration from the deepest part of the basinal areas up to the margins of the basins where the boundaries with the structural highs are present. The drainage areas indicate that migration into the southern part of the Loppa High occurred from the west and also from the northern margin of the Hammerfest Basin. Along the western flank of the Loppa High migration is mainly from the west. In the Maud basin, the drainage areas are mainly orientated towards the deepest part of the basin. Several and small drainage areas are also observed towards the east of this area of the Maud Basin. No major changes were predicted in the drainage areas pattern during the glacial episodes. Several accumulations were reproduced in the entire area, which are enriched in gaseous hydrocarbons during the interglacials when the ice–sheet was not present; while during the maximum glacial loading smaller gas caps are observed. This can be an indication of leakage of hydrocarbons due to the development of glaciations, as established in the Hammerfest Basin model.

Future work

As initially stated this PhD work began as part of the efforts of a research group, named Methane on the Move (MOM), that try to investigate in general the Earth's methane cycle and the possible impact that methane produced and released from petroliferous sedimentary basins could have in past, recent and future climate change. One of the targets areas for this investigation corresponds to the area of interest of this PhD study, the Southwestern Barents Sea, since it is classified as an area of great interest for petroleum exploration and therefore an area where certainly methane generation has occurred. On the other hand, this is also an interesting area in a geological point of view due to the fact that it has been affected by severe uplift and erosion and intense glaciations that may have acted as mechanisms for methane release. The results of this work covered several important aspects as already mentioned throughout the entire manuscript, and also in the summary previously presented. However, there are still a few more points of scientific interest that can be covered in future investigations in order to further unravel the topics related to this work and therefore achieve a better understanding of the methane cycle in the glacially influenced Barents Sea.

It is also important to mention that since this is an area of interest for petroleum exploration, this and further scientific contributions will certainly be of great benefit for the development of the Barents Sea as a petroleum province, aiding in the discovery and the production of petroleum resources. Leaving industry interest aside, the increasing understanding of the methane cycle will surely aid in addressing ongoing or possible future methane leakage from the geologic system to the hydro– and atmosphere, in order to better predict and understand climate impacts. Evidence of enhanced methane leakage has been reported from arctic areas worldwide (Westbrook et al., 2009; Shakhova et al., 2010; Walter Anthony et al., 2012), many of which are apparently linked to the dissociation of methane hydrates potentially sourced by thermogenic gas.

Potential key topics that should be addressed in future research are listed below:

- Additional 3D basin models should be constructed covering areas that have not been included in this study in order to corroborate and expand the database and information, as obtained for this study, for other areas in the Barents Sea. Such areas could include, for instance, the Nordkapp Basin, the entire Bjarmeland Platform and Tromsø Basin, the frontier Sørvestsnaget Basin, the Stappen High and the Finnmark Platform East. Finally a compilation and integration of all the model results, including the two built during this PhD should be done so that the entire Southwestern Barents Sea is covered and a regional model is available.

- From petroleum exploration perspectives such models would be useful in considering other younger or older petroleum plays. As observed in the second model a younger petroleum system with the Albian–Aptian Kolmule Formation shales could be of importance towards the west, where the Triassic and even the Jurassic source rocks have been deeply buried and are cooked out. In these westernmost areas of the Southwestern Barents Sea an even younger source rock, potentially contributing to the Paleocene–Eocene petroleum plays, should be evaluated. Even though these plays have not been proven, there are recent studies that demonstrate the sedimentation of organic matter during Eocene time, for instance the study of Brinkhuis et al. (2006). They have corroborated the massive growth and reproduction of the fern Azolla in the Arctic Ocean at

the onset of the Middle Eocene. On the other hand, older petroleum systems should be considered in areas where severe uplift and erosion has occurred and the remaining source rocks are of Permian/Carboniferous age. These areas could be for instance the Loppa High and the Bjarmeland and Finnmark Platforms.

- The details on the volumetric estimates in terms of masses of petroleum generated, expelled and accumulated as performed for the first model in the Hammerfest Basin should be developed for the second model on the Loppa High (from this study), as well as for future models. In addition, a sensitivity analysis in which several source rock thicknesses and properties are considered should be performed. The most important point when estimating the petroleum volumetric is probably related to the estimation of total methane generated, accumulated and leaked from the reservoir to the surface, with the implications related to climate change.

- The regional 3D models constructed in this study generally assumed constant properties for most sedimentary layers. They could surely be improved by adding more detailed information, for example: definition of a more detailed vertical and horizontal facies differentiation mainly in the source, reservoir and seal rocks intervals; inclusion of structural elements like faults, which are very determinant for the migration and leakage of hydrocarbons and for the trapping of petroleum in the case of fault dependent reservoirs/prospects; improvement of the individual erosional patterns and magnitudes; among other aspects.

- The correlation of geochemical data (if available) and basin modelling results as performed for the second stage of this PhD in the Hammerfest Basin should also be extended to the Loppa High area, as well as to any other area where basin modelling has been performed. Even though, as observed from this study, there are several limitations when doing this type of correlation, mainly due to differences in scales, the results contribute significantly to a better understanding of the petroleum systems.

- This PhD study, which covers the investigation of methane emissions in the Barents Sea as part of the MOM project, was done together with other two PhD projects that focused on seismic interpretation of structural features for gas leakage, and the biogeochemistry of gas emissions at the seabed. The combination of these three disciplines resulted in excellent interactions and conclusions. Therefore, an effort should be placed on trying to establish this type of interdisciplinary approach for future investigations in other study areas.

- The final suggestion is more directed towards estimating the impact of thermogenic methane leakage on global climate. As observed from the Hammerfest Basin study, thermogenic methane leakage has likely occurred in the recent past associated to the development of glaciations. If prediction of methane leakage can be done for the entire Southwestern Barents Sea as well as the estimation of the total amount/mass leaked from the reservoir to the surface, then it will be possible to have an idea of the total amount at least released to the hydrosphere. At the same time an estimation of the total amount of methane converted to carbon dioxide and the total amount release from the hydrosphere to the atmosphere should be performed, e.g. based on present knowledge of methane dissolution rates in water and metabolization in the shallow sediments and in the water column. This will give a total greenhouse gas contribution to the atmosphere, which can be compared to atmospheric compositional records and which can finally be used to estimate the real impact such processes can have on global climate and climate change.

6 References

Aali, J., Rahimpour-Bonab, H., Kamali, M. R. (2006). Geochemistry and origin of the world's largest gas field from Persian Gulf, Iran. *Journal of Petroleum Science and Engineering*, 50. 161-175.

Al-Hajeri, M. M., Al Saeed, M., Derks, J., Fuchs, T., Hantschel, T., Kauerauf, A. I., Neumaier, M., Schenk, O., Swientek, O., Tessen, N., Welte, D., Wygrala, B., Kornpihl, D., Peters, K. (2009). Basin and petroleum system modeling. *Oilfield Review*, 21. 14-29.

Allen, P. A., Allen, J. R. (2005). Basin Analysis. 2nd Edition, Great Britain, Blackwell Science Publishing, 549 pp.

Archer, D. (2005). Fate of fossil fuel CO2 in geologic time. *Journal of Geophysical Research*, 110. C09S05.

Archer, D. (2007). Methane hydrate stability and anthropogenic climate change. *Biogeosciences* 4. 521-544.

Archer, D., Brovkin, V. (2008). The millennial atmospheric lifetime of anthropogenic CO2. *Climatic Change*, 90. 283-297.

Archer, D., Buffett, B., Brovkin, V. (2009). Ocean methane hydrates as a slow tipping point in the global carbon cycle. *Proceedings of the National Academy of Sciences of the United States of America*, 106. 20596-20601.

Archer, D., Martin, P., Buffett, B., Brovkin, V., Rahmstorf, S., Ganopolski, A. (2004). The importance of ocean temperature to global biogeochemistry. *Earth and Planetary Science Letters*, 222. 333-348.

Behar, F., Vandenbroucke, M. (1987). Chemical modelling of kerogens. *Organic Geochemistry*, 11. 15-24.

Benn, D. I., Evans, D. J. A. (2010). Glaciers & Glaciation. 2nd Edition., London & New York, Routledge, 712 pp.

Berbesi, L. A., di Primio, R., Anka, Z., Horsfield, B., Wilkes, H. (2014). Methane leakage from evolving petroleum systems: Masses, rates and inferences for climate feedback. *Earth and Planetary Science Letters*, 387. 219-228.

Berglund, L. T., Augustson, J., Færseth, R., Gjelberg, J., Ramberg-Moe, H. (1986). The evolution of the Hammerfest Basin, *in:* Spencer, A. M., Holter, E., Campbell, C. J., Hanslien, S. H., Nelson, P. H. H., Nysæther, E., and Ormaasen, E. G., eds., Habitat of Hydrocarbons on the Norwegian Continental Shelf: London, Graham & Trotman, p. 319-338.

Bernard, B. B., Brooks, J. M., Sackett, W. M. (1978). Light Hydrocarbons in Recent Texas Continental Shelf and Slope Sediments. *Journal of Geophysical Research*, 83. 4053-4061.

Berner, U., Faber, E. (1988). Maturity related mixing model for methane, ethane and propane, based on carbon isotopes. *Organic Geochemistry*, 13. 67-72.

Biddle, K. T., Wielchowsky, C. C. (1994). Hydrocarbon Traps. *AAPG Memoir*, 60. 219-235.

Blunier, T., Chappellaz, J., Schwander, J., Stauffer, B., Raynaud, D. (1995). Variations in atmospheric methane concentration during the Holocene epoch. *Nature*, 374. 46-49.

Boulton, G. S., Caban, P. E., Van Gijssel, K. (1995). Groundwater flow beneath ice sheets: Part I — Large scale patterns. *Quaternary Science Reviews*, 14. 545-562.

Boulton, G. S., Slot, T., Blessing, K., Glasbergen, P., Leijnse, T., van Gijssel, K. (1993). Deep circulation of groundwater in overpressured subglacial aquifers and its geological consequences. *Quaternary Science Reviews*, 12. 739-745.

References

Brinkhuis, H., Schouten, S., Collinson, M. E., Sluijs, A., Sinninghe Damsté, J. S., Dickens, G. R., Huber, M., Cronin, T. M., Onodera, J., Takahashi, K., Bujak, J. P., Stein, R., van der Burgh, J., Eldrett, J. S., Harding, I. C., Lotter, A. F., Sangiorgi, F., van Konijnenburg-van Cittert, H., de Leeuw, J. W., Matthiessen, J., Backman, J., Moran, K. (2006). Episodic fresh surface waters in the Eocene Arctic Ocean. *Nature*, 441. 606-609.

Broecker, W. S., Denton, G. H. (1990). The role of ocean-atmosphere reorganizations in glacial cycles. *Quaternary Science Reviews*, 9. 305-341.

Cavanagh, A. J., di Primio, R., Scheck-Wenderoth, M., Horsfield, B. (2006). Severity and timing of Cenozoic exhumation in the southwestern Barents Sea. *Journal of the Geological Society*, 163. 761-774.

Clark, P. U., Mix, A. C. (2002). Ice sheets and sea level of the Last Glacial Maximum. *Quaternary Science Reviews*, 21. 1-7.

Clayton, C. J., Hay, S. J. (1994). Gas migration mechanisms from accumulation to surface. *Bulletin of the Geological Society of Denmark*, 41. 12-23.

Corcoran, D. V., Doré, A. G. (2002). Top seal assessment in exhumed basin settings - some insights from Atlantic margin and borderland basins, *in:* Koestler, A. G., and Hunsdale, R., eds., Hydrocarbon Seal Quantification, Volume 11, Norwegian Petroleum Society, p. 89-109.

Dalland, A., Worsley, D., Ofstad, K. (1988). A lithostratigraphic scheme for the Mezosoic and Cenozoic succesion offshore mid- and northern Norway. *Norwegian Petroleum Directorate Bulletin*, 4. 1-65.

Demaison, G. J., Moore, J. T. (1980). Anoxic environments and oil source bed genesis. *Organic Geochemistry*, 2. 9-31.

Dengo, C. A., Røssland, K. G. (1992). Extensional tectonic history of the western Barents Sea, *in:* Larsen, R. M., Brekke, H., Larsen, B. T., and Talleraas, E., eds., Structural and Tectonic Modelling and its Application to Petroleum Geology, Volume 1, Norwegian Petroleum Society, p. 91-107.

di Primio, R., Dieckmann, V., Mills, N. (1998). PVT and phase behaviour analysis in petroleum exploration. *Organic Geochemistry*, 29. 207-222.

di Primio, R., Horsfield, B. (2006). From petroleum-type organofacies to hydrocarbon phase prediction. *AAPG Bulletin*, 90. 1031-1058.

di Primio, R., Lehne, E., Kuhn, P., Baur, F., Horsfield, B., Petroleum quality prediction in basin modelling (Oral presentation), *in* Proceedings International Meeting on Organic Geochemistry, Interlaken-Switzerland, 18-23 September 2011.

Dickinson, W. R. (1993). Basin geodynamics. *Basin Research*, 5. 195-196.

Dieckmann, V., Schenk, H. J., Horsfield, B., Welte, D. H. (1998). Kinetics of petroleum generation and cracking by programmed-temperature closed-system pyrolysis of Toarcian Shales. *Fuel*, 77. 23-31.

Dimakis, P., Braathen, B. I., Faleide, J. I., Elverhøi, A., Gudlaugsson, S. T. (1998). Cenozoic erosion and the preglacial uplift of the Svalbard-Barents Sea region. *Tectonophysics*, 300. 311-327.

Doré, A. G. (1995). Barents Sea geology, petroleum resources and commercial potential. *Arctic*, 48. 207-221.

Dow, W. G. (1974). Application of oil correlation and source rock data to exploration in Williston basin. *AAPG Bulletin*, 58. 1253-1262.

Dow, W. G. (1977). Kerogen studies and geological interpretations. *Journal of Geochemical Exploration*, 7. 79-99.

Durand, B. (1980). Sedimentary organic matter and kerogen. Definition and quantitative importance of kerogen, Paris-France, Éditions Technip, Kerogen: Insoluble Organic Matter from Sedimentary Rocks, 525 pp.

Durand, B., Espitalié, J. (1976). Geochemical studies on the organic matter from the Douala Basin (Cameroon) -- II. Evolution of kerogen. *Geochimica et Cosmochimica Acta*, 40. 801-808.

Eidvin, T., Jansen, E., Riis, F. (1993). Chronology of Tertiary fan deposits off the western Barents Sea: Implications for the uplift and erosion history of the Barents Shelf. *Marine Geology*, 112. 109-131.

Elverhøi, A., Fjeldskaar, W., Solheim, A., Nyland-Berg, M., Russwurm, L. (1993). The Barents Sea ice sheet - a model of its growth and decay during the last ice maximum. *Quaternary Science Reviews*, 12. 863-873.

England, W. A., Mackenzie, A. S., Mann, D. M., Quigley, T. M. (1987). The movement and entrapment of petroleum fluids in the subsurface. *Journal of the Geological Society*, 144. 327-347.

England, W. A., Mann, A. L., Mann, D. M. (1991). Migration from source to trap, *in:* Merril, R. K., ed., Treatise of Petroleum Geology Handbook of Petroleum Geology: Tulsa, Oklahoma, U.S.A., The American Association of Petroleum Geologists, p. 23-46.

Espitalié, J., Ungerer, P., Irwin, I., Marquis, F. (1988). Primary cracking of kerogens. Experimenting and modelling C1, C2–C5, C6–C15 and C15+ classes of hydrocarbons formed. *Organic Geochemistry*, 13. 893-899.

Etiope, G. (2012). Methane uncovered. *Nature Geoscience*, 5. 373-374.

Etiope, G., Klusman, R. W. (2002). Geologic emissions of methane to the atmosphere. *Chemosphere*, 49. 777-789.

Etiope, G., Klusman, R. W. (2010). Microseepage in drylands: Flux and implications in the global atmospheric source/sink budget of methane. *Global and Planetary Change*, 72. 265-274.

Etiope, G., Lassey, K. R., Klusman, R. W., Boschi, E. (2008a). Reappraisal of the fossil methane budget and related emission from geologic sources. *Geophysical Research Letters*, 35.

Etiope, G., Milkov, A. V., Derbyshire, E. (2008b). Did geologic emissions of methane play any role in Quaternary climate change? *Global and Planetary Change*, 61. 79-88.

Faleide, J. I., Gudlaugsson, S. T., Jacquart, G. (1984). Evolution of the western Barents Sea. *Marine and Petroleum Geology*, 1. 123-150.

Faleide, J. I., Solheim, A., Fiedler, A., Hjelstuen, B. O., Andersen, E. S., Vanneste, K. (1996). Late Cenozoic evolution of the western Barents Sea-Svalbard continental margin. *Global and Planetary Change*, 12. 53-74.

Faleide, J. I., Tsikalas, F., Breivik, A. J., Mjelde, R., Ritzmann, O., Engen, Ø., Wilson, J., Eldholm, O. (2008). Structure and evolution of the continental margin off Norway and the Barents Sea. *Episodes*, 31. 82-91.

Fjeldskaar, W., Lindholm, C., Dehls, J. F., Fjeldskaar, I. (2000). Postglacial uplift, neotectonics and seismicity in Fennoscandia. *Quaternary Science Reviews*, 19. 1413-1422.

Forsman, J. P., Hunt, J. M. (1958). Insoluble organic matter (kerogen) in sedimentary rocks. *Geochimica et Cosmochimica Acta*, 15. 170-182.

Gabrielsen, R. H., Færseth, R. B., Jensen, L. N., Kalheim, J. E., Riis, F. (1990). Structural elements of the Norwegian continental shelf. Part I: The Barents Sea Region. *Norwegian Petroleum Directorate Bulletin*, 6. 47.

Gluyas, J., Swarbrick, R. (2004). Petroleum Geoscience, Malden-USA, Oxford-UK, Victoria-Australia, Blackwell Publishing.

Goa, R., Bjørøen, A. (2013). CO2 Storage Atlas Barents Sea. Norwegian Petroleum Directorate, Stavanger-Norway. 74 pp.

Gradstein, F. M., Ogg, J. G., Smith, A. G. (2005). A Geologic Time Scale 2004, Cambridge, Cambridge University Press.

Grantham, P. J., Wakefield, L. L. (1988). Variations in the sterane carbon number distributions of marine source rock derived crude oils through geological time. *Organic Geochemistry*, 12. 61-73.

Halpern, H. I. (1995). Development and applications of light-hydrocarbon-based star diagrams. *AAPG Bulletin*, 79. 801-815.

Hambrey, M. (1994). Glacial Environment United States of America, CRC Press.

Hambrey, M., Alean, J. (2004). Glaciers. 2nd Edition, Cambridge, Cambridge University Press.

Hantschel, T., Kauerauf, A. I. (2009). Fundamentals of Basin and Petroleum Systems Modeling, Berlin-Heidilberg, Germany, Springer-Verlag.

Hantschel, T., Kauerauf, A. I., Wygrala, B. (2000). Finite element analysis and ray tracing modeling of petroleum migration. *Marine and Petroleum Geology*, 17. 815-820.

Henrich, R., Baumann, K. H. (1994). Evolution of the Norwegian Current and the Scandinavian Ice Sheets during the past 2.6 m.y.: evidence from ODP Leg 104 biogenic carbonate and terrigenous records. *Palaeogeography, Palaeoclimatology, Palaeoecology*, 108. 75-94.

Henriksen, E., Bjørnseth, H. M., Hals, T. K., Heide, T., Kiryukhina, T., Kløvjan, O. S., Larssen, G. B., Ryseth, A. E., Rønning, K., Sollid, K., Stoupakova, A. (2011a). Uplift and erosion of the greater Barents Sea: impact on prospectivity and petroleum systems, *in:* Spencer, A. M., Embry, A. F., Gautier, D. L., Stoupakova, A. V., and Sørensen, K., eds., Arctic Petroleum Geology, Volume 35: London, Geological Society of London, p. 271-281.

Henriksen, E., Ryseth, A. E., Larssen, G. B., Heide, T., Rønning, K., Sollid, K., Stoupakova, A. V. (2011b). Tectonostratigraphy of the greater Barents Sea: implications for petroleum systems, *in:* Spencer, A. M., Embry, A. F., Gautier, D. L., Stoupakova, A. V., and Sørensen, K., eds., Arctic Petroleum Geology, Volume 35: London, Geological Society of London, p. 163-195.

Holba, A. G., Ellis, L., Dzou, I. L., Hallam, A., Masterson, W. D., Francu, J., Fincannon, A. L., 2001, Extended tricyclic terpanes as age discriminators between Triassic, Early Jurassic, and Middle–Late Jurassic oils, 20th International Meeting on Organic Geochemistry, Volume 1: Nancy-France, p. 464.

Hood A., G. C. C. M., Heacock, R. L. (1975). Organic Metamorphism and the Generation of Petroleum. *AAPG Bulletin*, 59. 986-996.

Horsfield, B. (1997). The bulk composition of first-formed petroleum in source rocks, Berlin-Germany, Springer-Verlag, Petroleum and Basin Evolution.

Hovland, M., Judd, A. G. (1988). Seabed Pockmarks and Seepages, London, Graham and Trotman, 293 pp.

Hovland, M., Svensen, H., Forsberg, C. F., Johansen, H., Fichler, C., Fosså, J. H., Jonsson, R., Rueslåtten, H. (2005). Complex pockmarks with carbonate-ridges off mid-Norway: Products of sediment degassing. *Marine Geology*, 218. 191-206.

Hunt, J. M. (1996). Petroleum Geochemistry and Geology, San Francisco-USA, W.H. Freeman & Company.

Ingólfsson, Ó., Landvik, J. Y. (2013). The Svalbard–Barents Sea ice-sheet – historical, current and future perspectives. *Quaternary Science Reviews*, 64. 33-60.

International Commision on Stratigraphy (2010). International Stratigraphic Chart. Available from: http://www.stratigraphy.org/index.php/ics-chart-timescale. (date accessed: January, 2010).

Jacobson, S. R. (1991). Petroleum source rocks and organic facies, *in:* Merril, R. K., ed., Treatise of Petroleum Geology Handbook of Petroleum Geology: Tulsa, Oklahoma, U.S.A., The American Association of Petroleum Geologists, p. 3-12.

Jansen, E., Sjoholm, J. (1991). Reconstruction of glaciation over the past 6 Myr from ice-borne deposits in the Norwegian Sea. *Nature*, 349. 600-603.

Johansen, S. E., Ostisty, B. K., Birkeland, Ø., Fedorovsky, Y. F., Martirosjan, V. N., Bruun Christensen, O., Cheredeev, S. I., Ignatenko, E. A., Margulis, L. S. (1993). Hydrocarbon potential in the Barents Sea region: play distribution and Potential, *in:* Vorren, T. O., Bergsager, E., Dahl-Stamnes, Ø. A., Holter, E., Johansen, B., Lie, E., and Lund, T. B., eds., Arctic Geology and Petroleum Potential, Volume 2, Norwegian Petroleum Society, p. 273-320.

Karlsen, D. A., Skeie, J. E. (2006). Petroleum migration, faults and overpressure, part 1: Calibrating basin modelling using petroleum in traps - A review. *Journal of Petroleum Geology*, 29. 227-256.

Kennett, J. P., Cannariato, K. G., Hendy, I. L., Behl, R. J. (2000). Carbon isotopic evidence for methane hydrate instability during Quaternary interstadials. *Science*, 288. 128-133.

Killops, S. D., Killops, V. J. (1993). An Introduction to Organic Gochemistry, New York-U.S.A., Longman Scientific and Technical Essex, UK and John Wiley & Sons.

Knies, J., Matthiessen, J., Vogt, C., Laberg, J. S., Hjelstuen, B. O., Smelror, M., Larsen, E., Andreassen, K., Eidvin, T., Vorren, T. O. (2009). The Plio-Pleistocene glaciation of the Barents Sea-Svalbard region: a new model based on revised chronostratigraphy. *Quaternary Science Reviews*, 28. 812-829.

Knight, P. G. (1999). Glaciers, Cheltenham, United Kingdom, Stanley Thornes Ltd., 263 pp.

Knutsen, S.-M., Richardsen, G., Vorren, T. O. (1993). Late Miocene-Pleistocene sequence stratigraphy and mass-movements on the western Barents Sea margin, *in:* Vorren, T. O., Bergsager, E., Dahl-Stamnes, Ø. A., Holter, E., Johansen, B., Lie, E., and Lund, T. B., eds., Arctic Geology and Petroleum Potential, Volume 2, Norwegian Petroleum Society, p. 573-606.

Kroeger, K. F., di Primio, R., Horsfield, B. (2011). Atmospheric methane from organic carbon mobilization in sedimentary basins — The sleeping giant? *Earth Science Reviews*, 107. 423-442.

Krooss, B. M., Leythaeuser, D. (1996). Molecular difussion of light hydrocarbons in sedimentary rocks and its role in migration and dissipation of natural gas. *AAPG Memoir*, 66. 173-183.

Kukla, G., Cílek, V. (1996). Plio-Pleistocene megacycles: record of climate and tectonics. *Palaeogeography, Palaeoclimatology, Palaeoecology*, 120. 171-194.

Kvenvolden, K. A., Rogers, B. W. (2005). Gaia's breath—global methane exhalations. *Marine and Petroleum Geology*, 22. 579-590.

Lammers, S., Suess, E., Hovland, M. (1995). A large methane plume east of Bear Island (Barents Sea): implications for the marine methane cycle. *Geologische Rundschau*, 84. 59-66.

Larsen, G., Chilingar, G. V. (1967). Chapter 1 - Introduction, *in:* Larsen, G., and Chilingar, G. V., eds., Developments in Sedimentology, Volume 8: Amsterdam-The Netherlands, London-UK, New York-U.S.A., Elsevier, p. 1-17.

Larsen, R. M., Fjæran, T., Skarpnes, O. (1993). Hydrocarbon potential of the Norwegian Barents Sea based on recent well results, *in:* Vorren, T. O., Bergsager, E., Dahl-Stamnes, Ø. A., Holter, E., Johansen, B., Lie, E., and Lund, T. B., eds., Arctic Geology and Petroleum Potential, Volume 2, Norwegian Petroleum Society, p. 321-331.

Larter, S., di Primio, R. (2005). Effects of biodegradation on oil and gas field PVT properties and the origin of oil rimmed gas accumulations. *Organic Geochemistry*, 36. 299-310.

Linjordet, A., Grung-Olsen, R. (1992). The Jurassic Snøhvit Gas Field, Hammerfest Basin, offshore northern Norway. *AAPG Memoir*, 54. 349-370.

Loeng, H. (1991). Features of the physical oceanographic conditions of the Barents Sea. *Polar Research*, 10. 5-18.

Mackenzie, F. T. (2005). Sediments, Diagenesis, and Sedimentary Rocks. Treatise on Geochemitsry, Elsevier, 2nd. Edition, 446 pp.

Magoon, L. B. (1987). The petroleum system – a classification scheme for research, exploration, and resource assessment. *U.S. Geological Survey Bulletin*, 1870. 2-15.

Magoon, L. B., Beaumont, E. A. (2000). Petroleum Systems. Chapter 3, *in:* Beaumont, E. A., and Foster, N. H., eds., Exploring for Oil and Gas Traps, AAPG, p. 34.

Magoon, L. B., Dow, W. G. (1994). The Petroleum System. *AAPG Memoir*, 60. 3-24.

Mangerud, J., Dokken, T., Hebbeln, D., Heggen, B., Ingólfsson, O., Landvik, J. Y., Mejdahl, V., Svendsen, J. I., Vorren, T. O. (1998). Fluctuations of the Svalbard-Barents Sea Ice Sheet during the last 150 000 years. *Quaternary Science Reviews*, 17. 11-42.

Mangerud, J., Jansen, E., Landvik, J. Y. (1996). Late Cenozoic history of the Scandinavian and Barents Sea ice sheets. *Global and Planetary Change*, 12. 11-26.

Mann, D. M., Mackenzie, A. S. (1990). Prediction of pore fluid pressures in sedimentary basins. *Marine and Petroleum Geology*, 7. 55-65.

Mareschal, J.-C. (1987). Subsidence and Heat Flow in Intracontinental Basins and Passive Margins. *AAPG Memoir*, 12. 519-527.

McCarthy, K., Rojas, K., Niemann, M., Palmowski, D., Peters, K., Stankiewicz, A. (2011). Basin petroleum geochemistry for source rock evaluation. *Oilfield Review*, 23. 32-43.

Mienert, J., Vanneste, M., Bünz, S., Andreassen, K., Haflidason, H., Sejrup, H. P. (2005). Ocean warming and gas hydrate stability on the mid-Norwegian margin at the Storegga Slide. *Marine and Petroleum Geology*, 22. 233-244.

Milkov, A. V. (2000). Worldwide distribution of submarine mud volcanoes and associated gas hydrates. *Marine Geology*, 167. 29-42.

Milkov, A. V. (2004). Global estimates of hydrate-bound gas in marine sediments: how much is really out there? *Earth Science Reviews*, 66. 183-197.

Milkov, A. V. (2005). Molecular and stable isotope compositions of natural gas hydrates: A revised global dataset and basic interpretations in the context of geological settings. *Organic Geochemistry*, 36. 681-702.

Molnia, B. F. (2014). Glossary of Glacier Terminology: A glossary providing the vocabulary necessary to understand the modern glacier environment. U.S. Geological Survey. Open-File Report. Available from: http://pubs.usgs.gov/of/2004/1216/g/g.html. (date accessed: May, 2014).

Mørk, B. E., Duncan, R. A. (1993). Late Pliocene basaltic volcanism on the Western Barents Shelf margin: implications from petrology and 40Ar-39Ar dating of volcaniclastic debris from a shallow drill core. *Norsk Geologisk Tidsskrift*, 73. 209-225.

Nardin, T. R., Røssland, K. G. (1993). Restoration of the eroded section in the western Barents Sea, *in:* Vorren, T. O., Bergsager, E., Dahl-Stamnes, Ø. A., Holter, E., Johansen, B., Lie, E., and Lund, T. B., eds., Arctic Geology and Petroleum Potentail, Volume 2, Norwegian Petroleum Society, p. 607-618.

National Oceanographic Data Center (2011). Annual temperature (°C) at 300 m depth Available from: http://www.nodc.noaa.gov/cgi-bin/OC5/SELECT/woaselect.pl. (date accessed: October, 2011).

Norwegian Petroleum Directorate (2009). The Norwegian Petroleum Directorate fact-pages of exploration wellbores. Available from: http://factpages.npd.no/factpages/Default.aspx?culture=en. (date accessed: December, 2009).

Norwegian Petroleum Directorate (2010a). The Norwegian Petroleum Directorate fact-pages. Goliat field. Available from: http://factpages.npd.no/factpages/Default.aspx?culture=en. (date accessed: January, 2010).

Norwegian Petroleum Directorate (2010b). The Norwegian Petroleum Directorate fact-pages. Snøhvit field. Available from: http://factpages.npd.no/factpages/Default.aspx?culture=en. (date accessed: January, 2010).

Norwegian Petroleum Directorate (2011). The Norwegian Petroleum Directorate: Geological plays. Available from: http://www.npd.no/en/Topics/Geology/Geological-plays/. (date accessed: August, 2011).

Norwegian Petroleum Directorate (2012). The Norwegian Petroleum Directorate fact-pages of fields and discoveries. Available from: http://factpages.npd.no/factpages/Default.aspx?culture=en. (date accessed: January, 2012).

Norwegian Petroleum Directorate (2013). Petroleum Resources on the Norwegian Continental Shelf 2013. Norwegian Petroleum Directorate, Stavanger-Norway. 32 pp.

Nyland, B., Jensen, L. N., Skagen, J., Skarpnes, O., Vorren, T. (1992). Tertiary uplift and erosion in the Barents Sea: Magnitude, timing and consequences, *in:* Larsen, R. M., Brekke, H., Larsen, B. T., and Talleraas, E., eds., Structural and Tectonic Modelling and its Application to Petroleum Geology, Volume 1, Norwegian Petroleum Society, p. 153-162.

Nøttvedt, A., Cecchi, M., Gjelberg, J. G., Kristensen, S. E., Lønøy, A., Rasmussen, A., Rasmussen, E., Skott, P. H., van Veen, P. M. (1993). Svalbard-Barents Sea correlation: a short review, *in:* Vorren, T. O., Bergsager, E., Dahl-Stamnes, Ø. A., Holter, E., Johansen, B., Lie, E., and Lund, T. B., eds., Arctic Geology and Petroleum Potential, Volume 2, Norwegian Petroleum Society, p. 363-375.

O'Connor, F. M., Boucher, O., Gedney, N., Jones, C. D., Folberth, G. A., Coppell, R., Friedlingstein, P., Collins, W. J., Chappellaz, J., Ridley, J., Johnson, C. E.

(2010). Possible role of wetlands, permafrost, and methane hydrates in the methane cycle under future climate change: a review. *Reviews of Geophysics*, 48. 1-33.

Ogg, J. G., Ogg, G., Gradstein, F. M. (2008). The Concise Geologic Time Scale, Cambridge, Cambridge University Press.

Ohm, S. E., Karlsen, D. A., Austin, T. J. F. (2008). Geochemically driven exploration models in uplifted areas: Examples from the Norwegian Barents Sea. *AAPG Bulletin*, 92. 1191-1223.

Orr, W. L. (1986). Kerogen/asphaltene/sulphur relationships in sulphur-rich Monterey oils. *Organic Geochemistry*, 10. 499-516.

Osborne, M. J., Swarbrick, R. E. (1997). Mechanisms for generating overpressure in sedimentary basins: A reevaluation. *AAPG Bulletin*, 81. 1023-1041.

Ostanin, I., Anka, Z., di Primio, R. (2013). Hydrocarbon plumbing systems above the Snøhvit gas field: structural control and implications for thermogenic methane leakage in the Hammerfest Basin, SW Barents Sea. *Marine and Petroleum Geology*, 43. 127-146.

Ostanin, I., Anka, Z., di Primio, R., Bernal, A. (2012). Hydrocarbon leakage above the Snøhvit gas field, Hammerfest Basin SW Barents Sea. *First Break*, 30. 55-60.

Palciauskas, V. V. (1991). Primary migration of petroleum, *in:* Merril, R. K., ed., Treatise of Petroleum Geology Handbook of Petroleum Geology: Tulsa, Oklahoma, U.S.A., The American Association of Petroleum Geologists, p. 13-22.

Pepper, A. S., Corvi, P. J. (1995a). Simple kinetic models of petroleum formation. Part I: Oil and gas generation from kerogen. *Marine and Petroleum Geology*, 12. 291-319.

Pepper, A. S., Corvi, P. J. (1995b). Simple kinetic models of petroleum formation. Part III: Modelling an open system. *Marine and Petroleum Geology*, 12. 417-452.

Pepper, A. S., Dodd, T. A. (1995). Simple kinetic models of petroleum formation. Part II: oil-gas cracking. *Marine and Petroleum Geology*, 12. 321-340.

Perrodon, A. (1992). Petroleum systems: Models and applications. *Journal of Petroleum Geology*, 15. 319-326.

Peters, K. E., Walters, C. C., Moldowan, J. M. (2005). The Biomarker Guide. Biomarkers and Isotopes in Petroleum Exploration and Earth History, Cambridge-United Kingdom, Cambridge University, 1155 pp.

Petit, J. R., Jouzel, J., Raynaud, D., Barkov, N. I., Barnola, J. M., Basile, I., Bender, M., Chappellaz, J., Davis, M., Delaygue, G., Delmotte, M., Kotlyakov, V. M., Legrand, M., Lipenkov, V. Y., Lorius, C., Pepin, L., Ritz, C., Saltzman, E., Stievenard, M. (1999). Climate and atmospheric history of the past 420,000 years from the Vostok ice core, Antarctica. *Nature*, 399. 429-436.

Plaza-Faverola, A., Bünz, S., Mienert, J. (2011). Repeated fluid expulsion through sub-seabed chimneys offshore Norway in response to glacial cycles. *Earth and Planetary Science Letters*, 305. 297-308.

Raynaud, D., Barnola, J. M., Chappellaz, J., Blunier, T., Indermühle, A., Stauffer, B. (2000). The ice record of greenhouse gases: a view in the context of future changes. *Quaternary Science Reviews*, 19. 9-17.

Raynaud, D., Chappellaz, J., Blünier, T. (1998). Ice-core record of atmospheric methane changes: relevance to climatic changes and possible gas hydrate sources. *Geological Society, London, Special Publications*, 137. 327-331.

Red Orbit - Your universe online (2011). "Arctic Report Car" Finds Temps Rising, Glacier Mass Decreasing. Available from:

http://www.redorbit.com/news/science/1112433671/arctic-report-card-finds-temps-rising-glacier-mass-decreasing/. (date accessed: August, 2014).

Reemst, P., Cloetingh, S., Fanavoll, S. (1994). Tectonostratigraphic modelling of Cenozoic uplift and erosion in the south-western Barents Sea. *Marine and Petroleum Geology*, 11. 478-490.

Rice, D. D., Claypool, G. E. (1981). Generation, accumulation and resource potential of biogenic gas. *AAPG Bulletin*, 65. 5-25.

Richardsen, G., Knutsen, S.-M., Vail, P. R., Vorren, T. O. (1993). Mid-Late Miocene sedimentation on the southwestern Barents Shelf margin, *in:* Vorren, T. O., Bergsager, E., Dahl-Stamnes, Ø. A., Holter, E., Johansen, B., Lie, E., and Lund, T. B., eds., Arctic Geology and Petroleum Potential, Volume 2, Norwegian Petroleum Society, p. 539-571.

Riis, F. (1992). Dating and measuring of erosion, uplift and subsidence in Norway and the norwegian shelf in glacial periods. *Norsk Geologisk Tidsskrift*, 72. 325-331.

Riis, F., Fjeldskaar, W. (1992). On the magnitude of the Late Tertiary and Quaternary erosion and its significance fro the uplift of Scandinavia and the Barents Sea, *in:* Larsen, R. M., Brekke, H., Larsen, B. T., and Talleraas, E., eds., Structural and Tectonic Modelling and its Application to Petroleum Geology, Volume 1, Norwegian Petroleum Society, p. 163-185.

Rodrigues Duran, E., di Primio, R., Anka, A., Stoddart, D., Horsfield, B. (2013). 3D-basin modelling of the Hammerfest Basin (southwestern Barents Sea): A quantitative assessment of petroleum generation, migration and leakage. *Marine and Petroleum Geology*, 45. 281-303.

Schenk, H. J., di Primio, R., Horsfield, B. (1997a). The conversion of oil into gas in petroleum reservoirs. Part 1, comparative kinetic investigation of gas generation

from crude oils of lacustrine, marine and fluviodeltaic origin by programmed-temperature closed-system pyrolysis. *Organic Geochemistry*, 26. 467–481.

Schenk, H. J., Horsfield, B., Krooss, B., Schaefer, R. G., Schwochau, K. (1997b). Kinetics of Petroleum Formation and Cracking, *in:* Welte, D. H., Horsfield, B., and Baker, D. R., eds., Petroleum and Basin Evolution: Berlin-Heidelberg, Germany, Springer-Verlag, p. 231-270.

Schlumberger (2009). PetroMod 3D Basic Tutorial Rev. A, software version 11, Aachen, Germany. 98 pp.

Schlumberger (2014). Trap - Oilfield glossary. Available from: http://www.glossary.oilfield.slb.com/en/Terms/t/trap.aspx. (date accessed: May, 2014).

Selley, R. C. (1985). Elements of Petroleum Geology, New York-U.S.A., W.H. Freeman & Company.

Shakhova, N., Semiletov, I., Salyuk, A., Yusupov, V., Kosmach, D., Gustafsson, Ö. (2010). Extensive Methane Venting to the Atmosphere from Sediments of the East Siberian Arctic Shelf. *Science*, 327. 1246-1250.

Siegert, M. J., Dowdeswell, J. A., Hald, M., Svendsen, J.-I. (2001). Modelling the Eurasian Ice Sheet through a full (Weichselian) glacial cycle. *Global and Planetary Change*, 31. 367-385.

Siegert, M. J., Dowdeswell, J. A., Melles, M. (1999). Late Weichselian Glaciation of the Russian High Arctic. *Quaternary Research*, 52. 273-285.

Siegert, M. J., Marsiat, I. (2001). Numerical reconstructions of LGM climate across the Eurasian Arctic. *Quaternary Science Reviews*, 20. 1595-1605.

Skogseid, J., Planke, S., Faleide, J. I., Pedersen, T., Eldholm, O., Neverdal, F. (2000). NE Atlantic continental rifting and volcanic margin formation, *in:* Nøttvedt, A., Larsen, B. T., Olaussen, S., Tørudbakken, B., Skogseid, J., Gabrielsen, R. H., Brekke, H., and Birkeland, Ø., eds., Dynamics of the Norwegian Margin, Volume 167: London, Geological Society of London, p. 295-326.

Solheim, A., Riis, F., Elverhøi, A., Faleide, J. I., Jensen, L. N., Cloetingh, S. (1996). Impact of glaciations on basin evolution: data and models from the Norwegian margin and adjacent areas - introduction and summary. *Global and Planetary Change*, 12. 1-9.

Sundvor, E., Eldholm, O. (1992). Norway Offshore and North-East Atlantic, *in:* Hurtig, E., Cermak, V., Haenel, R., and Zui, V., eds., Geothermal Atlas of Europe, Volume 1, Potsdam: GeoForschungZentrum Publications, p. 63-66.

Sundvor, E., Eldholm, O., Gladczenko, T. P., and Planke, S. (2000). Norwegian-Greenland Sea thermal field, *in:* Nøttvedt, A., Larsen, B. T., Olaussen, S., Tørudbakken, B., Skogseid, J., Gabrielsen, R. H., Brekke, H., and Birkeland, Ø., eds., Dynamics of the Norwegian Margin, Volume 167: London, Geological Society of London, p. 397-410.

Svendsen, J. I., Alexanderson, H., Astakhov, V. I., Demidov, I., Dowdeswell, J. A., Funder, S., Gataullin, V., Henriksen, M., Hjort, C., Houmark-Nielsen, M., Hubberten, H. W., Ingólfsson, Ó., Jakobsson, M., Kjær, K. H., Larsen, E., Lokrantz, H., Lunkka, J. P., Lyså, A., Mangerud, J., Matiouchkov, A., Murray, A., Möller, P., Niessen, F., Nikolskaya, O., Polyak, L., Saarnisto, M., Siegert, C., Siegert, M. J., Spielhagen, R. F., Stein, R. (2004). Late Quaternary ice sheet history of northern Eurasia. *Quaternary Science Reviews*, 23. 1229-1271.

Svendsen, J. I., Astakhov, V. I., Bolshiyanov, D. Y., Demidov, I., Dowdeswell, J. A., Gataullin, V., Hjort, C., Hubberten, H. W., Larsen, E., Mangerud, J. A. N., Melles, M., Möller, P. E. R., Saarnisto, M., Siegert, M. J. (1999). Maximum

extent of the Eurasian ice sheets in the Barents and Kara Sea region during the Weichselian. *Boreas*, 28. 234-242.

Sweeney, J. J., Braun, R. L., Burnham, A. K. (1995). Chemical kinetic model of hydrocarbon generation, expulsion, and destruction applied to the Maracaibo basin, Venezuela. *AAPG Bulletin*, 79. 1515-1532.

Sættem, J., Bugge, T., Fanavoll, S., Goll, R. M., Mørk, A., Mørk, M. B. E., Smelror, M., Verdenius, J. G. (1994). Cenozoic margin development and erosion of the Barents Sea: Core evidence from southwest of Bjørnøya. *Marine Geology*, 118. 257-281.

Thompson, K. F. M. (1983). Classification and thermal history of petroleum based on light hydrocarbons. *Geochimica et Cosmochimica Acta*, 47. 303-316.

Tissot, B. (1969). Premieres donnees sur les mecanismes et la cinetique de la formation du petrole dans les sediments; simulation d'un schema reactionnel sur ordinateur. *Revue de l'Institut Francais du Petrole*, 24. 470-501.

Tissot, B., Durand, B., Espitalié, J., Combaz, A. (1974). Influence of the nature and diagenesis of organic matter in the formation of petoleum. *AAPG Bulletin*, 58. 499-506.

Tissot, B., Welte, D. (1984). Petroleum Formation and Occurrence, Berlin, Heidelberg, New York, Tokyo, Springer-Verlag.

Ungerer, P., Pelet, R. (1987). Extrapolation of the kientics of oil and gas formation from laboratory experiments to sedimentary basins. *Nature*, 327. 52-54.

USGS (2014). Wolverine Glacier, Alaska. Available from: http://ak.water.usgs.gov/glaciology/wolverine/. (date accessed: August, 2014).

van Weert, F. H. A., van Gijssel, K., Leijnse, A., Boulton, G. S. (1997). The effects of Pleistocene glaciations on the geohydrological system of Northwest Europe. *Journal of Hydrology*, 195. 137-159.

Vandenbroucke, M., Largeau, C. (2007). Kerogen origin, evolution and structure. *Organic Geochemistry*, 38. 719-833.

Vorren, T. O., Richardsen, G., Knutsen, S.-M., Henriksen, E. (1991). Cenozoic erosion and sedimentation in the western Barents Sea. *Marine and Petroleum Geology*, 8. 317-340.

Walter Anthony, K. M., Anthony, P., Grosse, G., Chanton, J. (2012). Geologic methane seeps along boundaries of Arctic permafrost thaw and melting glaciers: Nature Geoscience, 5. 419-426. *Nature Geoscience*, 5.

Weiss, H. M., Wilhelms, A., Mills, N., Scotchmer, J., Hall, P. B., Lind, K., Brekke, T. (2000). NIGOGA – The Norwegian Industry Guide to Organic Geochemical Analyses. Edition 4.0 Published by Norsk Hydro, Statoil, Geolab Nor, SINTEF Petroleum Research and the Norwegian Petroleum Directorate. Available from: http://www.npd.no/engelsk/nigoga/default.htm. (date accessed: June, 2013).

Weissert, H. (2000). Global change: Deciphering methane's fingerprint. *Nature*, 406. 356-357.

Welte , D. H., Yukler, M. A. (1981). Petroleum origin and accumulation in basin evolution – A quantitative model. *AAPG Bulletin*, 65. 1387-1396.

Westbrook, G. K., Thatcher, K. E., Rohling, E. J., Piotrowski, A. M., Pälike, H., Osborne, A. H., Nisbet, E. G., Minshull, T. A., Lanoisellé, M., James, R. H., Hühnerbach, V., Green, D., Fisher, R. E., Crocker, A. J., Chabert, A., Bolton, C., Beszczynska-Möller, A., Berndt, C., Aquilina, A. (2009). Escape of methane gas from the seabed along the West Spitsbergen continental margin. *Geophysical Research Letters*, 36. L15608.

Whiticar, M. J. (1994). Correlation of Natural Gases with Their Sources, *in:* Magoon, L. B., and Dow, W. G., eds., The Petroleum System - from Source to Trap, Volume 60, AAPG Memoir.

Wygrala, B. P. (1989). Integrated study of an oil field in the southern Po Basin, northern Italy. [PhD]: University of Cologne.

Yalçın, M. N., Littke, R., Sachsenhofer, R. F. (1997). Thermal History of Sedimentary Basins, *in:* Welte, D. H., Horsfield, B., and Baker, D. R., eds., Petroleum and Basin Evolution. Insights from Petroleum Geochemistry, Geology and Basin Modelling: Berlin, Springer-Verlag, p. 535.

Appendices

Appendix I – Additional figures

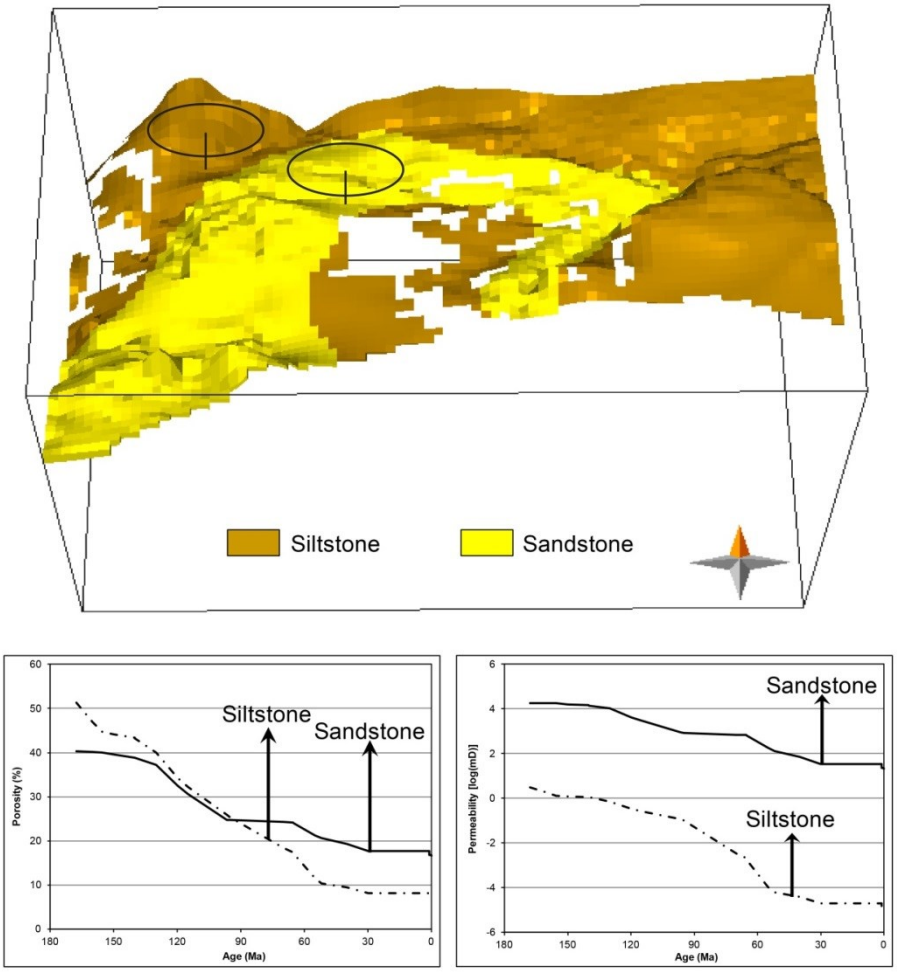

Figure I.1 Lateral facies variation of the Stø Formation unit. The two plots at the bottom correspond to the porosity (bottom left) and permeability (bottom right) behavior through time for the two main facies in two different locations of the basin (ellipses outline positions of the respective data).

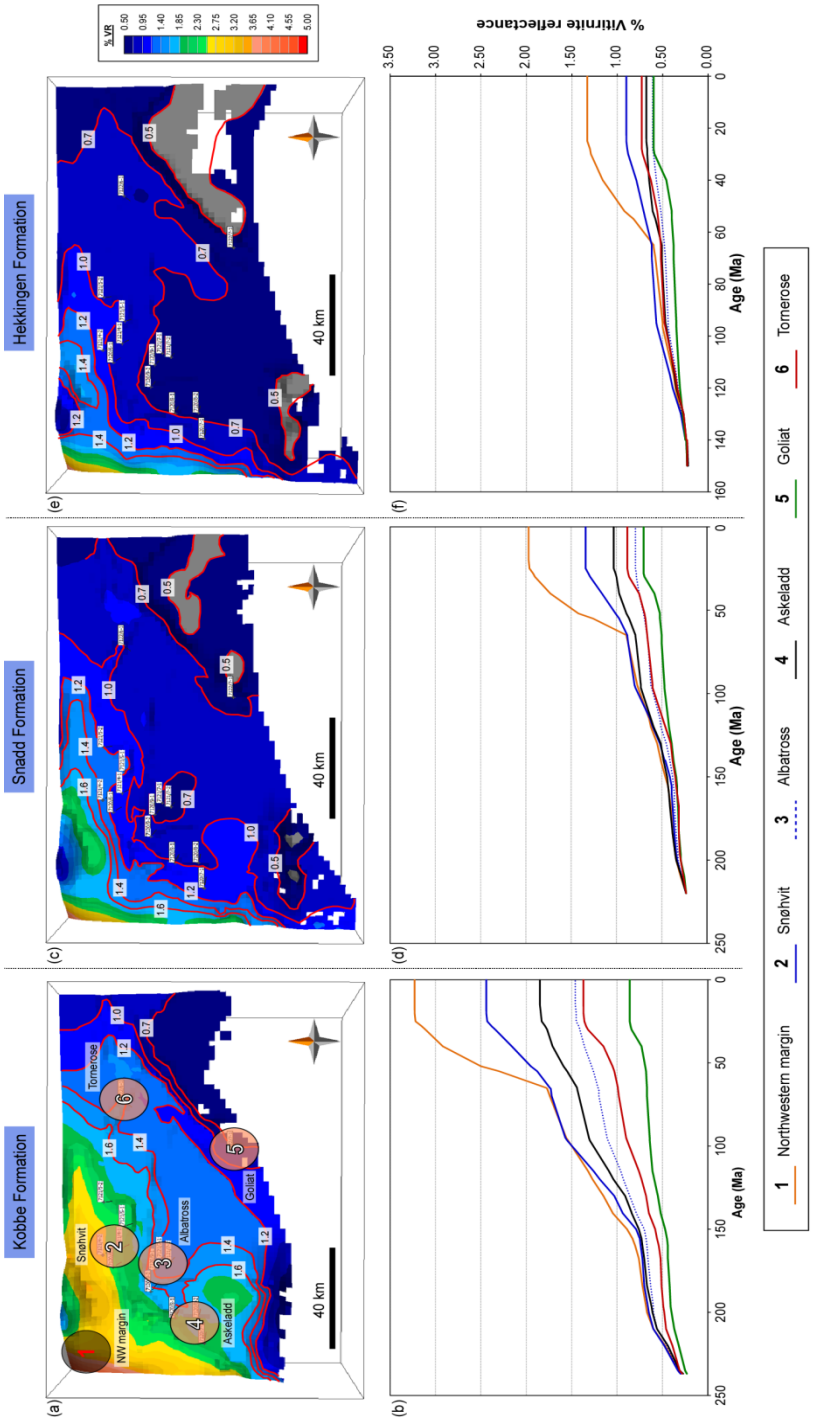

Figure I.2 Maturity level of the Hekkingen, Snadd and Kobbe formations. a, c, e) Maturity maps in terms of vitrinite reflectance (VR) at present-day, red lines in the maps represent the VR isolines. b, d, f) Maturity history for six different pseudo-wells located in different areas of the Hammerfest Basin, specially where the maximum maturity level was reached and where the main fields and discoveries are located. The circles showed in "a" represent the six areas.

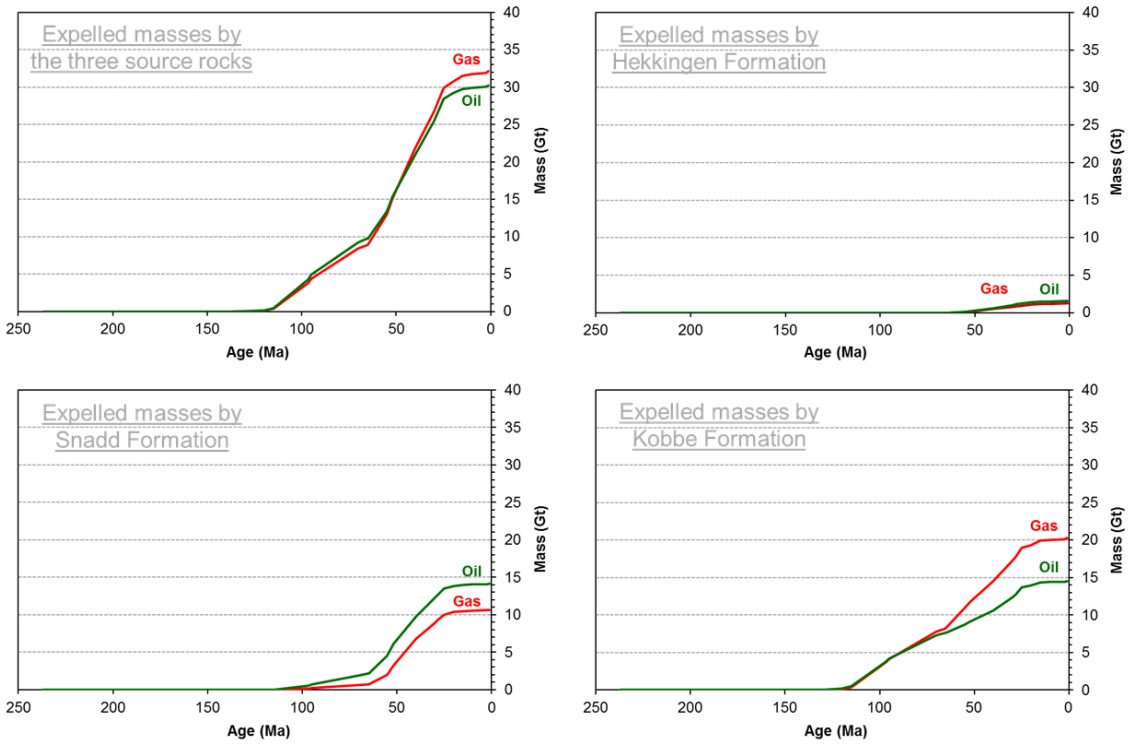

Figure I.3 Total cumulative mass (in Gigatonnes) of oil and gas expelled by the three source rocks considered in this model together (top left), and separately (top right and bottom).

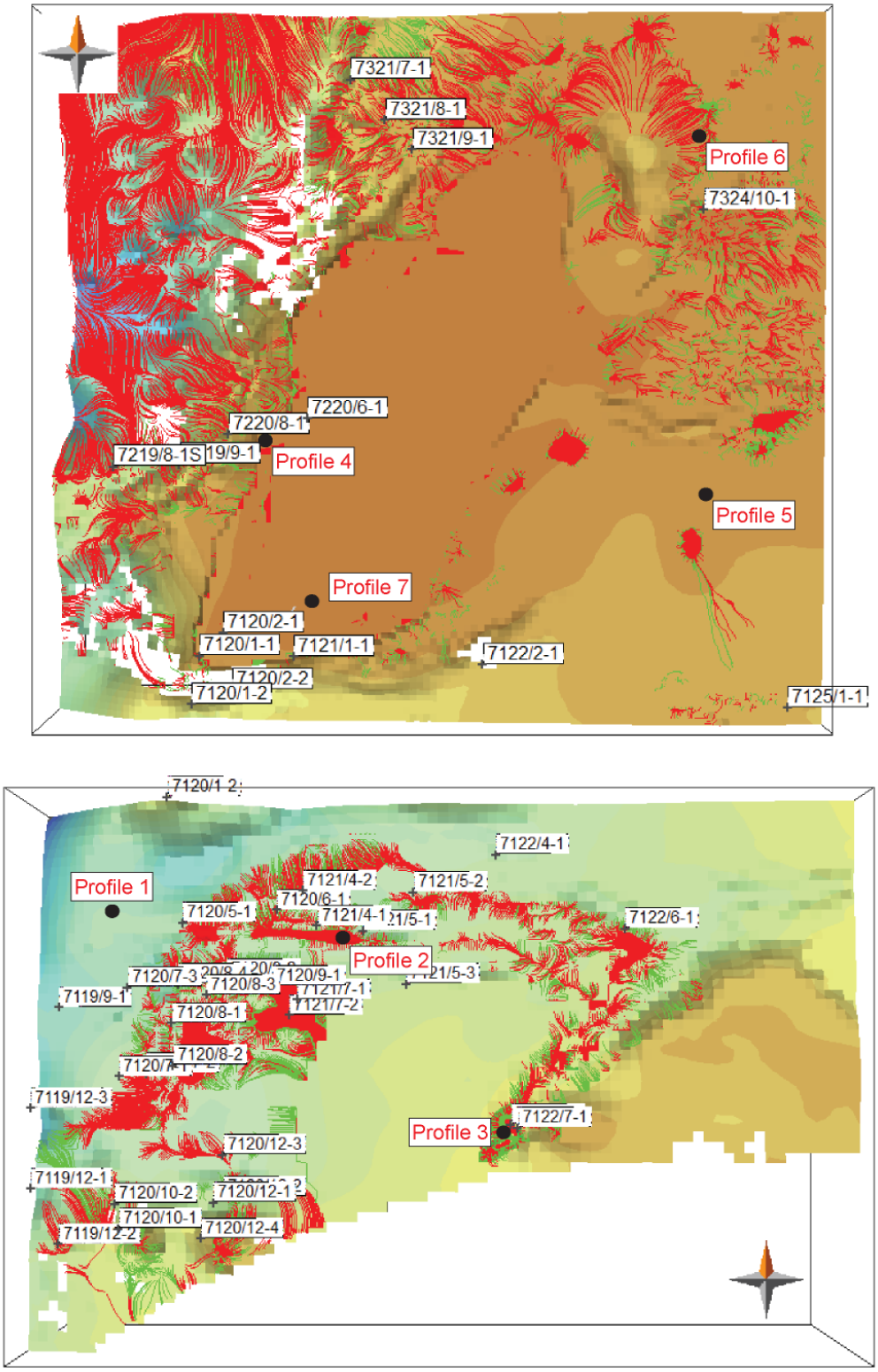

Figure I.4 Map view of the two modeled areas, Loppa High (top) and Hammerfest Basin (bottom), showing the location of seven areas (profile X) where pseudo wells were taken to have a detailed view of the burial history and the lithostratigraphy in these locations, the depth map of the Snadd Formation is only used as background, no scale is shown since the idea of the map is just to show the location of the areas.

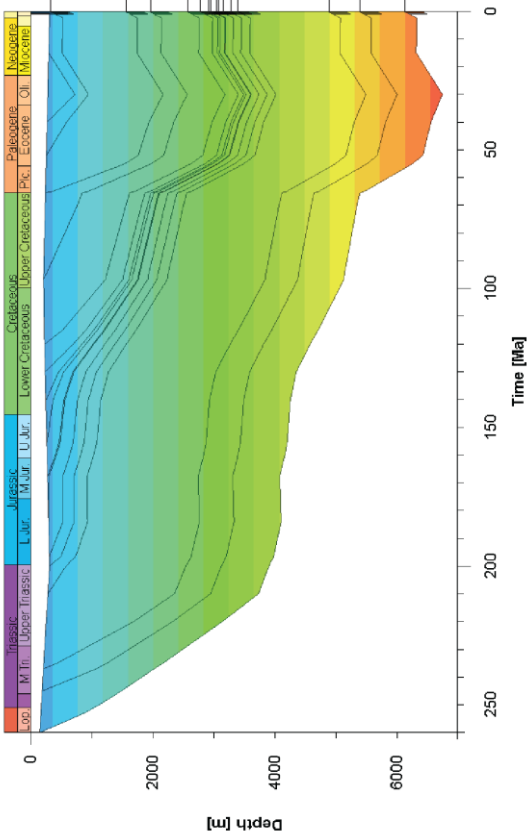

Name	Lithology	Mechanical properties		Permeability
		Density (kg/m^3)	Initial porosity (%)	[log(mD)]
Nordland Gp.	Siltstone (organic lean)	2720	55	0.71
Torsk Fm.	Shale (organic lean, typical)	2700	70	-1.00
Kvelte-Kviting fms.	Siltstone (organic lean)	2720	55	0.71
Kolmule Fm.	Shale (organic lean, silty)	2700	67	0.50
Kolje Fm.	Shale (typical)	2700	70	-1.00
Knurr Fm.	Shale (typical)	2700	70	-1.00
Hekkingen Fm.	Shale (organic rich, 8% TOC)	2500	70	-1.00
Fuglen Fm.	Shale (organic lean, siliceous, typical)	2710	70	1.30
Stø Fm. 02	Siltstone (organic lean)	2720	55	0.71
Nordmela Fm.	Siltstone (organic lean)	2720	55	0.71
Tubåen Fm.	Sandstone (clay poor)	2700	42	4.84
Fruholmen Fm.	Siltstone (organic rich, 2-3% TOC)	2700	55	0.71
Snadd Fm.	Siltstone (organic rich, 2-3% TOC)	2700	55	0.71
Kobbe Fm.	Siltstone (organic rich, 2-3% TOC)	2700	55	0.71
Havert-Klappmys fms.	Shale (organic lean, silty)	2700	67	0.50

Figure I.5 Burial history of zone 1 (profile 1) identified in previous Figure I.4 and lithostratigraphy for this particular well position. Other details regarding the lithology characteristics are specified in Table 2.2.

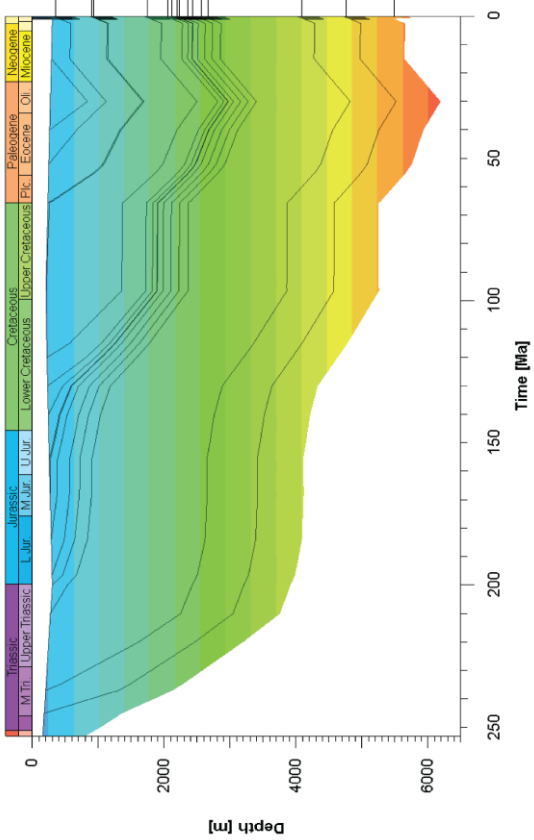

Name	Lithology	Mechanical properties		Permeability
		Density (kg/m^3)	Initial porosity (%)	[log(mD)]
Nordland Gp.	Siltstone (organic lean)	2720	55	0.71
Torsk Fm.	Shale (organic lean, typical)	2700	70	-1.00
Kvelte-Kviting fms.	Siltstone (organic lean)	2720	55	0.71
Kolmule Fm.	Shale (organic lean, silty)	2700	67	0.50
Kolje Fm.	Shale (typical)	2700	70	-1.00
Knurr Fm.	Shale (typical)	2700	70	-1.00
Hekkingen Fm.	Shale (organic rich, 8% TOC)	2500	70	-1.00
Fuglen Fm.	Shale (organic lean, siliceous, typical)	2710	70	1.30
Stø Fm. 01	Sandstone (typical)	2720	41	4.33
Nordmela Fm.	Siltstone (organic lean)	2720	55	0.71
Tubåen Fm.	Sandstone (clay poor)	2700	42	4.84
Fruholmen Fm.	Siltstone (organic rich, 2-3% TOC)	2700	55	0.71
Snadd Fm.	Siltstone (organic rich, 2-3% TOC)	2700	55	0.71
Kobbe Fm.	Siltstone (organic rich, 2-3% TOC)	2700	55	0.71
Havert-Klappmys fms.	Shale (organic lean, silty)	2700	67	0.50

Figure I.6 Burial history of zone 2 (profile 2) identified in previous Figure I.4 and lithostratigraphy for this particular well position. Other details regarding the lithology characteristics are specified in Table 2.2.

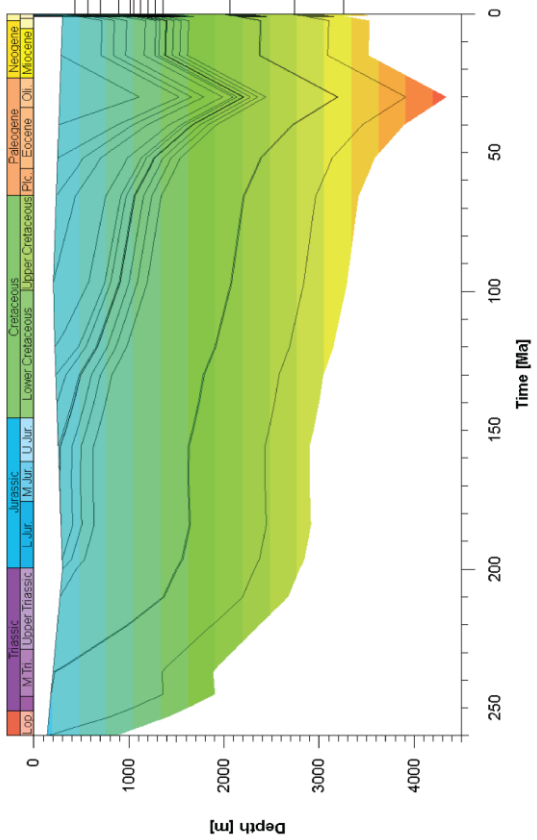

Name	Lithology	Mechanical properties		Permeability
		Density (kg/m^3)	Initial porosity (%)	[log(mD)]
Nordland Gp.	Siltstone (organic lean)	2720	55	0.71
Torsk Fm.	Shale (organic lean, typical)	2700	70	-1.00
Kvelte-Kviting fms.	Siltstone (organic lean)	2720	55	0.71
Kolmule Fm.	Shale (organic lean, silty)	2700	67	0.50
Kolje Fm.	Shale (typical)	2700	70	-1.00
Knurr Fm.	Shale (typical)	2700	70	-1.00
Hekkingen Fm.	Shale (organic rich, 8% TOC)	2500	70	-1.00
Fuglen Fm.	Shale (organic lean, siliceous, typical)	2710	70	1.30
Stø Fm. 01	Sandstone (typical)	2720	41	4.33
Nordmela Fm.	Siltstone (organic lean)	2720	55	0.71
Tubåen Fm.	Sandstone (clay poor)	2700	42	4.84
Fruholmen Fm.	Siltstone (organic rich, 2-3% TOC)	2700	55	0.71
Snadd Fm.	Siltstone (organic rich, 2-3% TOC)	2700	55	0.71
Kobbe Fm.	Siltstone (organic rich, 2-3% TOC)	2700	55	0.71
Havert-Klappmys fms.	Shale (organic lean, silty)	2700	67	0.50
Ørret Fm.	Siltstone (organic lean)	2720	55	0.71

Figure I.7 Burial history of zone 3 (profile 3) identified in previous Figure I.4 and lithostratigraphy for this particular well position. Other details regarding the lithology characteristics are specified in Table 2.2.

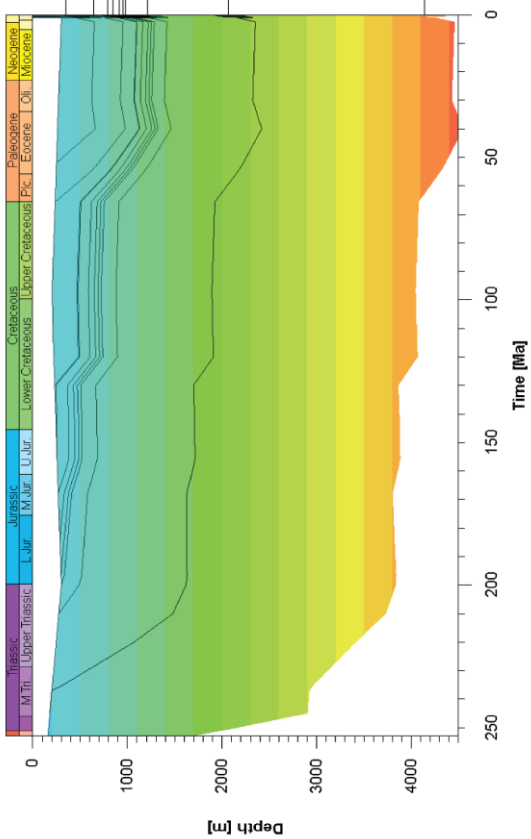

Name	Lithology	Mechanical properties		Permeability
		Density (kg/m^3)	Initial porosity (%)	[log(mD)]
Nordland Gp.	Siltstone (organic lean)	2720	55	0.71
Torsk Fm.	Shale (organic lean, typical)	2700	70	-1.00
Kolje Fm.	Shale (typical)	2700	70	-1.00
Hekkingen Fm.	Shale (organic rich, 8% TOC)	2500	70	-1.00
Fuglen Fm.	Shale (organic lean, siliceous, typical)	2710	70	1.30
Stø Fm. 01	Sandstone (typical)	2720	41	4.33
Nordmela Fm.	Siltstone (organic lean)	2720	55	0.71
Tubåen Fm.	Sandstone (clay poor)	2700	42	4.84
Fruholmen Fm.	Siltstone (organic rich, 2-3% TOC)	2700	55	0.71
Snadd Fm.	Siltstone (organic rich, 2-3% TOC)	2700	55	0.71
Havert-Klappmys fms.	Shale (organic lean, silty)	2700	67	0.50

Figure I.8 Burial history of zone 4 (profile 4) identified in previous Figure I.4 and lithostratigraphy for this particular well position. Other details regarding the lithology characteristics are specified in Table 2.2.

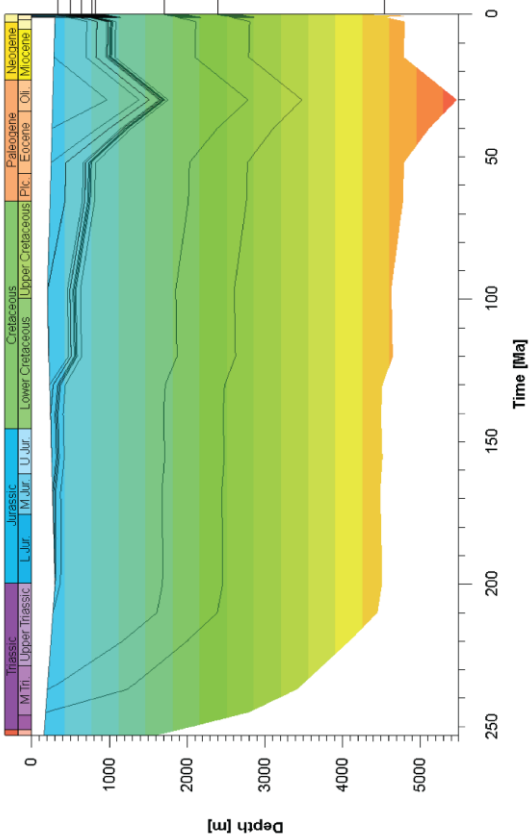

Name	Lithology	Mechanical properties		Permeability
		Density (kg/m^3)	Initial porosity (%)	[log(mD)]
Nordland Gp.	Siltstone (organic lean)	2720	55	0.71
Kveite-Kviting fms.	Siltstone (organic lean)	2720	55	0.71
Kolmule Fm.	Shale (organic lean, silty)	2700	67	0.50
Kolje Fm.	Shale (typical)	2700	70	-1.00
Knurr Fm.	Shale (typical)	2700	70	-1.00
Hekkingen Fm.	Shale (organic rich, 8% TOC)	2500	70	-1.00
Fuglen Fm.	Shale (organic lean, siliceous, typical)	2710	70	1.30
Stø Fm. 01	Sandstone (typical)	2720	41	4.33
Nordmela Fm.	Siltstone (organic lean)	2720	55	0.71
Tubåen Fm.	Sandstone (clay poor)	2700	42	4.84
Fruholmen Fm.	Siltstone (organic rich, 2-3% TOC)	2700	55	0.71
Snadd Fm.	Siltstone (organic rich, 2-3% TOC)	2700	55	0.71
Kobbe Fm.	Siltstone (organic rich, 2-3% TOC)	2700	55	0.71
Havert-Klappmys fms.	Shale (organic lean, silty)	2700	67	0.50

Figure I.9 Burial history of zone 5 (profile 5) identified in previous Figure I.4 and lithostratigraphy for this particular well position. Other details regarding the lithology characteristics are specified in Table 2.2.

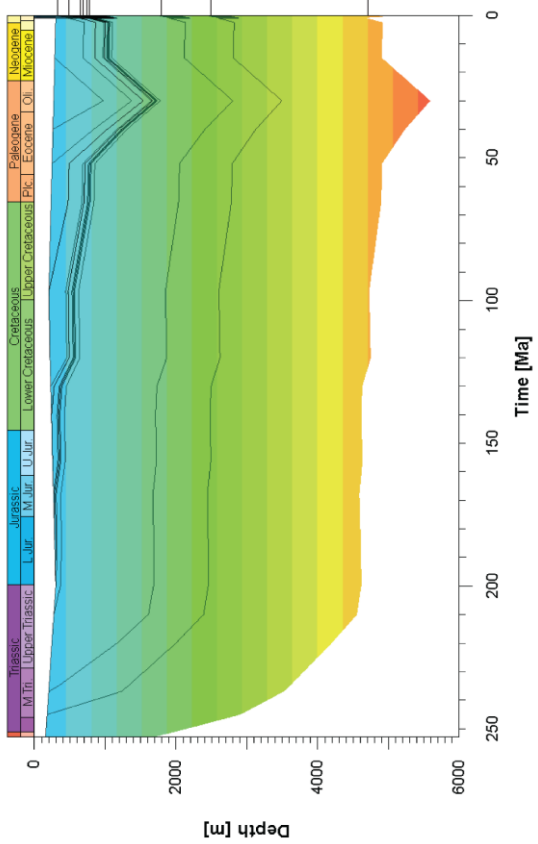

Name	Lithology	Mechanical properties		Permeability
		Density (kg/m^3)	Initial porosity (%)	[log(mD)]
Nordland Gp.	Siltstone (organic lean)	2720	55	0.71
Kveite-Kviting fms.	Siltstone (organic lean)	2720	55	0.71
Kolmule Fm.	Shale (organic lean, silty)	2700	67	0.50
Kolje Fm.	Shale (typical)	2700	70	-1.00
Knurr Fm.	Shale (typical)	2700	70	-1.00
Hekkingen Fm.	Shale (organic rich, 8% TOC)	2500	70	-1.00
Fuglen Fm.	Shale (organic lean, siliceous, typical)	2710	70	1.30
Stø Fm. 01	Sandstone (typical)	2720	41	4.33
Nordmela Fm.	Siltstone (organic lean)	2720	55	0.71
Tubåen Fm.	Sandstone (clay poor)	2700	42	4.84
Fruholmen Fm.	Siltstone (organic rich, 2-3% TOC)	2700	55	0.71
Snadd Fm.	Siltstone (organic rich, 2-3% TOC)	2700	55	0.71
Kobbe Fm.	Siltstone (organic rich, 2-3% TOC)	2700	55	0.71
Havert-Klappmys fms.	Shale (organic lean, silty)	2700	67	0.50

Figure I.10 Burial history of zone 6 (profile 6) identified in previous Figure I.4 and lithostratigraphy for this particular well position. Other details regarding the lithology characteristics are specified in Table 2.2.

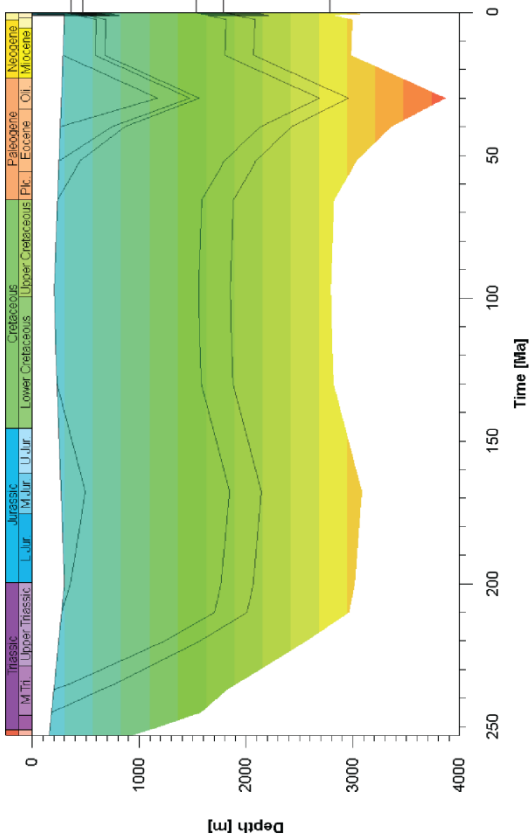

Name	Lithology	Mechanical properties		Permeability
		Density (kg/m^3)	Initial porosity (%)	[log(mD)]
Nordland Gp.	Siltstone (organic lean)	2720	55	0.71
Torsk Fm.	Shale (organic lean, typical)	2700	70	-1.00
Snadd Fm.	Siltstone (organic rich, 2-3% TOC)	2700	55	0.71
Kobbe Fm.	Siltstone (organic rich, 2-3% TOC)	2700	55	0.71
Havert-Klappmys fms.	Shale (organic lean, silty)	2700	67	0.50

Figure I.11 Burial history of zone 7 (profile 7) identified in previous Figure I.4 and lithostratigraphy for this particular well position. Other details regarding the lithology characteristics are specified in Table 2.2.

Appendix II – Additional tables

Table II.1 Well data for the wells used for calibration in the Hammerfest Basin model. Data collected from the Norwegian Petroleum Directorate website.

Well	UTM Coordinates		Zone	Total depth	Elevation	Water depth	Wellbore contents	Field
	mE	mN		(m)	(m)	(m)		
7119/9-1	458333.92	7924275.60	34	3248.00	25	201	**Dry**	
7119/12-1	456424.42	7889443.98	34	3088.00	25	200	**Oil shows**	
7119/12-2	462689.20	7879530.38	34	1902.00	25	180	**Shows**	
7119/12-3	454909.86	7904727.31	34	3314.00	29	211	**Gas/Condensate**	Not yet developed
7120/1-2	474839.56	7966032.04	34	2630.00	24	305	**Oil**	Not yet developed
7120/5-1	480135.74	7942513.53	34	2700.00	22	296	**Shows**	
7120/6-1	497650.92	7946756.85	34	2820.00	23	314	**Oil/Gas**	Snøhvit
7120/7-1	471011.63	7912388.54	34	2839.00	25	234	**Gas**	Snøhvit/Askeladd
7120/7-2	476011.92	7913417.99	34	2523.00	22	241	**Gas/Condensate**	Snøhvit/Askeladd
7120/7-3	470886.27	7929340.44	34	3062.00	22	256	**Shows**	
7120/8-1	479897.51	7923384.58	34	2610.00	25	270	**Gas/Condensate**	Snøhvit/Askeladd
7120/8-2	480927.89	7915359.17	34	2590.00	25	245	**Gas**	Snøhvit/Askeladd
7120/8-3	485899.85	7929358.33	34	2335.00	22	281	**Shows**	Snøhvit/Askeladd
7120/8-4	480342.17	7930889.05	34	2697.00	23	275	**Dry**	
7120/9-1	498124.67	7932342.99	34	2300.00	23	320	**Gas**	Snøhvit/Albatross
7120/9-2	489425.03	7932809.50	34	5072.00	23	293	**Gas**	Snøhvit/Albatross
7120/10-1	473722.27	7883536.50	34	2000.00	25	183	**Dry**	
7120/10-2	472556.90	7888153.58	34	2500.00	25	186	**Dry**	
7120/12-1	491169.71	7890289.38	34	3573.00	25	167	**Shows**	
7120/12-2	492968.97	7891571.43	34	4680.00	25	164	**Gas/Condensate**	Not yet developed
7120/12-3	492041.76	7899413.56	34	2523.00	23	185	**Gas**	Not yet developed
7120/12-4	489450.11	7883245.96	34	2199.00	23	152	**Dry**	
7121/4-1	505507.86	7944529.35	34	2609.00	22	335	**Oil/Gas**	Snøhvit
7121/4-2	502204.76	7950918.80	34	2800.00	22	317	**Gas/Condensate**	Snøhvit
7121/5-1	514306.93	7944421.61	34	3200.00	22	336	**Oil/Gas**	Snøhvit
7121/5-2	523051.48	7952737.91	34	2543.00	22	328	**Oil/Gas**	Snøhvit
7121/5-3	523420.77	7935226.77	34	2265.00	24	345	**Oil/Gas Shows**	
7121/7-1	503105.18	7930306.01	34	2160.00	22	329	**Gas/Condensate**	Snøhvit/Albatross
7121/7-2	501987.36	7927117.40	34	2156.00	22	325	**Gas**	Snøhvit/Albatross
7122/4-1	537933.23	7961309.50	34	3015.00	24	345	**Shows**	
7122/6-1	563698.43	7949804.84	34	2707.00	23	401	**Gas/Condensate**	Not yet developed
7122/7-1	547217.44	7910064.25	34	1524.00	24	381	**Oil**	Goliat
7122/7-2	545915.01	7910579.51	34	1418.00	18	377	**Oil**	Goliat

Table II.2 Well data for the wells used for calibration in the Loppa High model. Data collected from the Norwegian Petroleum Directorate website.

Well	UTM Coordinates		Zone	Total depth	Elevation	Water depth	Wellbore contents	Field
	mE	mN		(m)	(m)	(m)		
7120/1-1	475816.85	7980020.26	34	2569.00	25	342	**Oil/Gas Shows**	Not yet developed
7120/1-2	474839.56	7966032.04	34	2630.00	24	305	**Oil**	Not yet developed
7120/2-1	481923.84	7987305.65	34	3502.00	23	387	**Oil Shows**	
7120/2-2	486119.44	7971348.28	34	2794.00	23	337	**Oil Shows**	
7121/1-1	502657.85	7982512.86	34	916.00	27	369	**Dry**	
7122/2-1	556833.38	7985596.37	34	2120.00	23	363	**Dry**	
7125/1-1	437126.92	7977833.23	35	2200.00	24	252	**Oil/Gas**	Not yet developed
7219/8-1S	648406.81	8036356.27	33	4611.00	24	369	**Dry**	
7219/9-1	667003.56	8040679.94	33	4300.00	23	356	**Shows**	
7220/6-1	700186.92	8060886.89	33	1540.00	25	368	**Oil shows**	
7220/8-1	678908.52	8051910.71	33	2222.00	23	374	**Oil/Gas**	Johan Castberg
7321/7-1	311704.77	8158249.22	35	3550.00	24	475	**Gas Shows**	
7321/8-1	321501.02	8146601.96	35	3482.00	23	468	**Shows**	
7321/9-1	329361.05	8138267.66	35	1800.00	24	459	**Shows**	
7324/10-1	413162.08	8120918.38	35	2919.00	23	408	**Shows**	

Table II.3 Ice sheet periodicity used as input for the 3D basin model. The thickness for each glaciation is shown, together with the different events considered in each megacycle and the duration. MC = Megacycle.

Name	Ice MC	Thickness (m)	Age growth (Ma)	Duration (Ma)	Age stable (Ma)	Duration (Ma)	Ice decay (Ma)	Duration (Ma)	Interglacial (Ma)	Duration (Ma)
Ice I	MC5	1500	1.10-1.05	0.05	1.05-1.00	0.05	1.00-0.95	0.05	0.95-0.90	0.05
Ice II	MC4	1500	0.90-0.85	0.05	0.85-0.80	0.05	0.80-0.75	0.05	0.75-0.70	0.05
Ice III	MC3	1500	0.70-0.65	0.05	0.65-0.60	0.05	0.60-0.55	0.05	0.55-0.50	0.05
Ice IV	MC2	1500	0.50-0.42	0.08	0.42-0.34	0.08	0.34-0.26	0.08	0.26-0.18	0.08
Ice V	MC1	1500	0.18-0.16	0.02	0.16-0.15	0.01	0.15-0.13	0.02	0.13-0.12	0.01
Ice VIa	MC1	480	0.12-0.11	0.01	-	-	0.11-0.10	0.01	-	-
Ice VIb	MC1	750	0.10-0.09	0.01	-	-	0.09-0.08	0.01	-	-
Ice VIc	MC1	550	0.08-0.07	0.01	0.07-0.02	0.05	0.02-0.01	0.01	0.01 to present-day	-
Ice VId	MC1	1250	0.07-0.06	0.01	-	-	0.06-0.05	0.01	-	-
Ice VIe	MC1	1750	0.03-0.02	0.01	-	-	0.02-0.01	0.01	0.01 to present-day	-

Table II.4 Detailed heat flow data corresponding for the two trends (a=orange trend/color; b=blue trend/color in Figure 2.4, bottom) used in the Hammerfest Basin model. The numbers 1, 2, 3 correspond to the minimun, medium and maximum scenarios used for sensitiviy, respectively.

1	a	b
Age (Ma)	HF (mW/m^2)	HF (mW/m^2)
0	50	45
10	50	45
20	52	47
25	55	50
28	52	47
30	50	45
55	51	46
65	52	47
95	52	47
115	53	48
130	55	50
140	57	52
150	53	48
160	50	45
220	50	45
235	57	52
250	67	62
253	50	45
270	50	45

2	a	b
Age (Ma)	HF (mW/m^2)	HF (mW/m^2)
0	58	53
10	58	53
20	60	55
25	63	58
28	60	55
30	58	53
55	59	54
65	60	55
95	60	55
115	61	56
130	63	58
140	65	60
150	61	56
160	58	53
220	58	53
235	65	60
250	75	70
253	58	53
270	58	53

3	a	b
Age (Ma)	HF (mW/m^2)	HF (mW/m^2)
0	66	61
10	66	61
20	68	63
25	71	66
28	68	63
30	66	61
55	67	62
65	68	63
95	68	63
115	69	64
130	71	66
140	73	68
150	69	64
160	66	61
220	66	61
235	73	68
250	83	78
253	66	61
270	66	61

Table II.5 Detailed heat flow data corresponding for the three trends (a=orange trend/color; b=light blue trend/color; c=dark blue trend/color in Figure 2.4 top) used in the Loppa High model. The numbers 1, 2, 3 correspond to the minimun, medium and maximum scenarios used for sensitiviy, respectively.

1	a	b	c
Age (Ma)	HF (mW/m^2)	HF (mW/m^2)	HF (mW/m^2)
0	65	48	43
10	65	48	43
20	67	50	45
25	70	53	48
28	67	50	45
30	65	48	43
55	66	49	44
65	67	50	45
95	67	50	45
115	68	51	46
130	70	53	48
140	72	55	50
150	68	51	46
160	65	48	43
220	65	48	43
235	72	55	50
250	82	65	60
253	65	48	43
270	65	48	43

2	a	b	c
Age (Ma)	HF (mW/m^2)	HF (mW/m^2)	HF (mW/m^2)
0	75	58	53
10	75	58	53
20	77	60	55
25	80	63	58
28	77	60	55
30	75	58	53
55	76	59	54
65	77	60	55
95	77	60	55
115	78	61	56
130	80	63	58
140	82	65	60
150	78	61	56
160	75	58	53
220	75	58	53
235	82	65	60
250	92	75	70
253	75	58	53
270	75	58	53

3	a	b	c
Age (Ma)	HF (mW/m^2)	HF (mW/m^2)	HF (mW/m^2)
0	85	68	63
10	85	68	63
20	87	70	65
25	90	73	68
28	87	70	65
30	85	68	63
55	86	69	64
65	87	70	65
95	87	70	65
115	88	71	66
130	90	73	68
140	92	75	70
150	88	71	66
160	85	68	63
220	85	68	63
235	92	75	70
250	102	85	80
253	85	68	63
270	85	68	63